THESIS
4
2007
V.1

LIBRARY
Michigan State
University

This is to certify that the
dissertation entitled

EXFOLIATED GRAPHITE NANOPLATELETS AS
REINFORCEMENT FOR MULTIFUNCTIONAL
POLYPROPYLENE NANOCOMPOSITES

presented by

KYRIAKI KALAITZIDOU

has been accepted towards fulfillment
of the requirements for the

Ph.D. degree in Chemical Engineering and Materials science

Lawrence T. Drzal
Major Professor's Signature

February 14, 2006
Date

MSU is an Affirmative Action/Equal Opportunity Institution

PLACE IN RETURN BOX to remove this checkout from your record.
TO AVOID FINES return on or before date due.
MAY BE RECALLED with earlier due date if requested.

DATE DUE	DATE DUE	DATE DUE
MAY 1 3 2008		
111808		
AUG 2 9 2009 08 08 12		
08 28 12		

2/05 p:/CIRC/DateDue.indd-p.1

EXFOLIATED GRAPHITE NANOPLATELETS AS REINFORCEMENT FOR MULTIFUNCTIONAL POLYPROPYLENE NANOCOMPOSITES

VOLUME I

By

Kyriaki Kalaitzidou

A DISSERTATION

Submitted to
Michigan State University
In partial fulfillment of the requirements
for the degree of

DOCTOR OF PHILOSOPHY

Department of Chemical Engineering and Materials Science

2006

ABSTRACT

EXFOLIATED GRAPHITE NANOPLATELETS AS REINFORCEMENT FOR MULTIFUNCTIONAL POLYPROPYLENE NANOCOMPOSITES

By

Kyriaki Kalaitzidou

The focus of this research is to investigate the interactions between exfoliated graphite nanoplatelets (graphene sheets ~10nm thickness, ~1um diameter), a new nano-material developed by Drzal's group, with polyolefin based thermoplastics. The goal is: (i) to fabricate exfoliated graphite nanoplatelet (xGnP) polypropylene nanocomposites and determine properties and (ii) to elucidate the fundamental interfacial (i.e. adhesion and dispersion), processing and property mechanisms in polyolefin thermoplastics.

This research provides an understanding about how the fabrication method and processing conditions used, which were optimized using factorial design of experiments, affect the properties of these xGnP/PP nanocomposites and therefore can lead to materials with desired properties. A significant development is a new compounding method, i.e., premixing of xGnP and PP powder in isopropyl alcohol using sonication to disperse the xGnP by coating individual PP powder particles. The premixing method is more effective than the solution method widely used, in terms of lowering the percolation threshold of thermoplastic nanocomposites, and enhancing the probability that the large platelet morphology of xGnP can be preserved in the final composite. The feasibility of using xGnP-PP nanocomposites was investigated by evaluating the properties of this

system and comparing the xGnP-PP with composites made with commercial available reinforcements.

It was found that xGnP can be used at very low concentrations as a nucleating agent for the β-form of PP crystals which have higher impact strength and toughness compared to the most common occurring α-form. The aspect ratio and concentration of xGnP combined with the crystallization conditions can also affect the population and size distribution of PP spherulites, which were found to nucleate and grow on the xGnP surface, are closely related to the mechanical and barrier properties.

In addition, the crystal structure of the polymer was also found to affect the percolation threshold. The presence of many small spherulites nucleated by the xGnP disrupts the continuous network formed by the conductive particles and thus increases the percolation threshold. Other factors such as the shape and aspect ratio of the conductive filler, its morphology, distribution and orientation which affect the percolation threshold and conductivity of composites were also explored and evaluated.

The morphological investigation of the PP nanocomposites indicated the presence of particle agglomerates and poor dispersion especially in the case of high aspect ratio xGnP and clays. The plateau observed at the flexural strength-xGnP loading curve points toward weak adhesion along the xGnPP-PP interface. The problem of agglomeration was partially solved by using the premixing compounding method. Oxidation of xGnP followed by silane treatment was employed to address the weak adhesion problem. As a result, this crystallization study provides a fundamental understanding of how the xGnP affects the crystallization behavior of PP and allows fabrication of xGnP-PP nanocomposites with engineered crystal structure.

Copyright by
Kyriaki Kalaitzidou
2006

TO MY PARENTS

DESPINA KALAITZIDOU
&
KONSTANTINOS KALAITZIDIS

ACKNOWLEDGEMENT

The last four and half years have been very challenging and essential for my professional progress and development as an individual. Most of the credit should be given to my advisor Prof. Lawrence T. Drzal for providing me with the creative freedom and intellectual guidance that fostered my growth as a scientist, for exposing me in the academic world through writing of papers and participating in conferences. I thank him for his patience and assistance. His enthusiasm and positive attitude have been a great inspiration for me. I will always cherish my association with him.

Special thanks to my committee members Prof. Gregory Baker, Prof. Phillip Duxbury, Prof. Krishnamurthy Jayaraman and Prof. Andre Lee for reviewing my dissertation and providing valuable advices and comments.

The Center for Composite Materials and Structures has been my home and the people in CMSC my second family. I am thankful to Dr. Per Askeland for his valuable friendship, Inhwan, Mike, Brian, and Kelby and my fellow graduate students in EB 1105 for their help and support. It was fun to work with them. Special thanks to Dr Hiroyuki Fukushima for his guidance and the endless discussions that often created more questions than answers. His professional commitment and dedication was very inspiring and my research project would not have been the same without him.

Part of the reason I came to MSU is the encouragement I had from Prof. Sutherland, Prof. Milligan and Dr. Mengeloglu during the difficult times in MTU.

My parents Kostas and Despina, my brother Giorgos and my fiancé Kostas have been an endless source of support and love. Their catalytic presence in my life even when they are far away is priceless and greatly appreciated.

TABLE OF CONTENTS

CHAPTER 1
INTRODUCTION-LITERATURE REVIEW

CHAPTER 2
MATERIALS USED AND PROCESSING OF NANOCOMPOSITES

CHAPTER 3
DETERMINATION OF OPTIMIZED CONDITIONS DURING MELT-MIXING AND INJECTION MOLDING OF NANOCOMPOSITES USING FACTORIAL DESIGN OF EXPERIMENTS

CHAPTER 4
MECHANICAL PROPERTIES AND MORPHOLOGICAL CHARACTERIZATION OF EXFOLIATED GRAPHITE POLYPROPYLENE NANOCOMPOSITES

CHAPTER 5
THERMAL, VISCOELASTIC AND BARRIER PROPERTIES OF EXFOLIATED GRAPHITE POLYPROPYLENE NANOCOMPOSITES

CHAPTER 6
EXPERIMENTAL STUDY OF THE FACTORS AFFECTING THE ELECTRICAL CONDUCTIVITY AND PERCOLATION THRESHOLD OF CONDUCTIVE POLYMER NANOCOMPOSITES

CHAPTER 7
EFFECT OF EXFOLIATED GRAPHITE NANOPLATELETS ON THE CRYSTALLIZATION BEHAVIOR OF POLYPROPYLENE

CHAPTER 8
SURFACE TREATMENT OF EXFOLIATED GRAPHITE NANOPLATELETS

LIST OF TABLES

LIST OF FIGURES

CHAPTER 1

INTRODUCTION-LITERATURE REVIEW

1.1 Introduction

In recent years researchers both in industry and in academia have focused their interest on polymeric nanocomposites, which represent a radical alternative to conventional filled polymers or polymer blends. In contrast to conventional systems, the reinforcement in the nanocomposites has at least one dimension in the nanometer range. This characteristic enables the nanoreinforcements whether inorganic i.e., clays or organic i.e., carbon nanotubes, to enhance overall material performance by synergistically producing unique material properties resulting from phenomena that occur only when the morphology and the physics coincide at the nanoscale [1,2].

In 1987 a research group at Toyota was the first to report the fabrication of a nylon 6-clay hybrid composite where individual silicate layers were homogeneously dispersed in a continuous polymer matrix [3,4]. Since then nanocomposites research has flourished and a plethora of studies that cover the design and fabrication, the characterization, the properties and the potential applications of the nanocomposites from both an experimental and theoretical perspective can be found in the literature. A wide range of polymer resins have been investigated as matrices such as polystyrene, polyolefins, nylon, as well as, thermosets i.e., epoxies. The most commonly studied nanoreinforcement is exfoliated clay, however, there is an increased interest in using other materials such as carbon nanotubes and graphite as reinforcements for polymers due to their superior thermal and electrical properties in addition to their mechanical properties.

Research on polymer nanocomposites is part of the wide area of nanotechnology, the process of manipulating matter at the nanoscale. However, nanomaterials defined as materials that have at least one dimension in the nanoscale (<100nm) are not new. Ancient craftsmen utilized nanoscale particles in glazes to create unique colors that change with incident lighting [5]. The roots of modern nanotechnology and nanomaterials can be traced in Feynman's now-famous presentation "plenty of room at the bottom" given at a meeting of the American Physical Society in 1959 [6]. Later, in the mid-1980s the work on buckeyballs by Smalley [7], which led to the discovery of carbon nanotubes and Drexler's publication of the "Engines of Creation" [8], awoke the scientific community to the potential technological benefits of nanotechnology.

The question that arises is what are the unique characteristics that differentiate nanomaterials from their conventional counterparts. The fundamental difference is that in nanomaterials the majority of the atoms are located on the surface of the particles. The surface atoms, compared to the bulk ones, are exposed to a different environment that gives rise to high surface area materials that have novel intrinsic properties, interact differently with their external environments and thus they are ideal candidates for many applications. In summary, the dominant effects at the nanoscale are [9]: (i) small size effect, (ii) surface-interface effect and (iii) classical and quantum confinement effect.

1.1.1 Small Size Effect

The small size, which approaches the length scale of physical interaction with energy, is responsible for the unique electronic, magnetic and optical behavior of particles. In addition, the small size results in enhanced mechanical properties as reported first by Griffith in 1920's. He found that the strength of glass fibers depends on their size and concluded that the smaller the material is, the stronger it becomes [10]. He proposed that the failure of macroscopic specimens is due to the existence of defects i.e., cracks. Based on the assumption that the necessary energy for the nucleation and propagation of a crack equals the strain energy released during the material's relaxation, he proposed that for any material at any given stress condition there is a critical crack length [11] given by Equation (1.1).

$$\alpha = \frac{2E\gamma}{\pi\sigma^2} \tag{1.1}$$

where α is half of the crack length, E is the Young's Modulus, γ is the surface tension and σ is the applied stress. Materials with cracks longer than the critical length will fail whereas materials that are smaller than the critical crack length are able to reach their theoretical maximum strength.

Griffith's observation was also confirmed by Weibull in the 1950's who reached the same conclusion: the smaller a material is, the stronger it becomes. Weibull proposed a statistical analysis in order to estimate the probability of failure of fibers due to random distribution of defects [12]. This probability is given by Equation (1.2)

$$P_V = 1 - \exp\left[-\left(\frac{\sigma - \sigma_u}{\sigma_o} \right)^m V \right] \tag{1.2}$$

where σ is the applied stress, σ_u is the critical stress above which failure occurs in a material, σ_o is constant related to the density and the flaw size distribution of the material, and m is obtained empirically and called the Weibull modulus or Weibull shape parameter. Applying Equation (1.2) for two specimens of the same material but with different volumes V_1 and V_2, and assuming that the material has a zero critical stress, σ_u, and the median failure stresses (stress at which 50% of the material fails which means P_V=0.5) for the two specimens are σ_1 and σ_2 respectively, Weibull concluded that

$$\frac{V_2}{V_1} = \left(\frac{\sigma_1}{\sigma_2}\right)^m \tag{1.3}$$

Based on Equation (1.3) the larger material i.e., the specimen with V_1 where $V_1>V_2$ will fail at lower stress $\sigma_1 < \sigma_2$ which is a clear indication that in terms of strength, smaller materials can be better reinforcements in composite systems.

Piggott [13] took into consideration that the smaller a material gets, the stronger it becomes and proposed that the critical volume fraction of the filler (amount necessary to enhance the properties) decreases when stronger materials are used. Therefore, the following conclusion can be reached: Nanomaterials are more effective reinforcements than their conventional counterparts i.e., low concentrations of nanomaterials cause a larger improvement in the matrix properties leading to lightweight composites at lower cost.

The nanoscale size not only enhances the mechanical strength of materials but it also decreases the average dispersion distance of particles in the matrix, which means that the composite system can achieve a lower percolation threshold (filler content above which a step transition in materials behavior occurs i.e., a polymer based composite becomes electrically conductive above the percolation threshold).

1.1.2 Surface-Interface Effect

In nanomaterials most of the atoms are in the surface. Atoms that are located in the grain boundaries (metals) or at the edges of the nanoparticles (organic materials) are unsaturated in chemical bonding, disordered in the lattice and have an irregular crystalline structure [9]. These characteristics combined with the large interfacial area per unit volume, i.e., $700m^2/cm^3$ for layered silicates in polymers which is comparable to a football field within a raindrop [1], result in materials with enhanced chemical reactivity that can be used as catalyst supports, for storage of small molecules and for gas absorption applications to mention just a few.

1.1.3 Quantum Confinement Effect

In nanomaterials electrons are confined to a small domain and thus they have discrete electronic energy levels that alter their electrical and optical properties. In particular, altering the size of a particle can change the associated energy and wavelength of absorbed light [5]. The quantum effect is also responsible for the non-linear dependence of electrical conductivity on electric field and can produce electron-tunneling characteristics. Quantum interference between separate paths an electron may follow through a material can strongly enhance or suppress electrical conductivity.

1.1.4 Nanoreinforcements

Materials that can be used as nanoreinforcements can be oxides i.e., SiO_2, metals i.e., Ni, Pt, inorganic minerals i.e. clays and organic i.e., carbon nanotubes and graphite. The first reported application of nanocomposites is the use of carbon black in car tires in order to increase their lifetime in the early 1900s. Fumed silica, used as a component of silicon rubber, coatings, sealants and adhesives, is also a nanomaterial that is commercially available since the 1940s [14]. Clays are the first nanoreinforcement used in polymeric matrices that have been studied systematically since the 1980's. Recently, there is an increased interest in using organic materials such as carbon black, carbon fibers and nanotubes, as well as, graphite as reinforcements for polymers due mainly to their superior thermal and electrical properties.

1.1.4.1 Clays: Layered Silicates

Layered silicates, a family of phylosilicates, are the most commonly used inorganic nanoreinforcement in the polymer nanocomposites research. They possess the same structural characteristics as the well-known minerals talc and mica [1] i.e., closely stacked layered structures comprising of silica and aluminum or magnesium sheets joined together. Their structure and high aspect ratio, as well as, their good mechanical properties make them ideal reinforcements for polymers. The challenges to overcome are (i) their intrinsic tendency to stack together forming tactoids and (ii) their hydrophilicity that makes them incompatible with most of the engineering polymers. These two properties make the exfoliation of clays and their dispersion in polymer matrices very difficult.

1.1.4.2 Carbon Black

Carbon black is a nanomaterial used in many applications such as pigment in black ink, for toners in copy machines and printers, and as additive to rubber in order to enhance the tear strength and improve wear characteristics. Recently, it is also used to impart electrical conductivity in polymeric composites aiming to applications where electrostatic dissipation is required. Carbon black consists mainly of elemental carbon and is available in the form of spherical particles that have been fused together forming aggregates of an average size 30-100nm. Carbon black is produced by (i) a thermal-oxidative process, where natural gas is combusted in air and then mixed with feedstocks such as coal tar or crude oil and (ii) by thermal decomposition of acetylene in the absence of oxygen [15] that results in carbon black with a high degree of crystallinity and large surface area agglomerates with very low density and increased electrical conductivity.

1.1.4.3 Vapor Grown Carbon Fibers

The earliest reference to macroscopic vapor grown carbon fibers (VGCF) was made in a patent by Hughes and Chambers in 1889 [16]. This patent described the growth of "hair-like" carbon filaments produced from a feedstock of hydrogen and methane in sealed iron crucible. The next milestone in the history of VGCF is in 1970's when high-yield production of VGCF by thermal decomposition of benzene or methane at 1200 °C was demonstrated [17]. Since then, impressive progress has been made on the growth processes for these fibers; however, the large production cost still limits their applications. This problem was partly overcome in the early 1990's by using methods that can produce high volumes of VGCF at low cost using natural gas or coal as feedstock [18]. However, their cost is still in the ~$100 per pound range.

Carbon nanofibers can be produced in a relative large scale by the catalytic decomposition of certain hydrocarbons on small metal particles [19]. The diameter of the nanofibers is governed by that of the catalyst particles responsible for their growth. Typical values are 50-200nm for the inner diameters or 30-90nm for hollow cores and 50-100um for the length. An advantage of using VGCF in composites is that many surface treatment methods are available that can modify their surface area, energy and reactivity and make VGCF more compatible with the polymer matrix i.e., air etching or CO_2 oxidization [20].

1.1.4.4 Carbon Nanotubes

Carbon nanotubes (CNTs) were discovered in 1991 by Iijima of the NEC Laboratory in Japan, who observed them using high-resolution transmission electron microscopy [21]. CNTs have probably been around for much longer and may have been formed during carbon vapor deposition but due to lack of characterization tools able to distinguish them from other types of tubes, their discovery was delayed [14]. Carbon nanotubes are unique nanostructures with remarkable electronic and mechanical properties. When made exclusively from carbon, they are chemically inert, about 100 times stronger than steel, and offer a full range of electrical and thermal conductivity possibilities [22, 23].

An ideal nanotube can be thought of as a network of hexagonal rings of carbon atoms that has been rolled up to make a seamless cylinder. Nanotubes come in a variety of diameters and lengths. They can also differ in size of the surface cavities or the end cups, which are half fullerene balls [14]. Carbon nanotubes are divided in single-walled nanotubes (SWNT) and multi-walled nanotubes (MWNT) based on the number of graphite tubes they consist of. The structure of the nanotube affects its properties, including mechanical strength and modulus, density, thermal and electrical conductivity.

Carbon nanotubes can be produced by plasma arching that involves evaporation of one electrode (the anode) as cations followed by deposition at the other electrode [24, 25], and by laser vaporization of graphite rods [26]. Both methods suffer from some drawbacks such as the difficulty of scaling up nanotube production and that the produced nanotubes are entangled and contain many impurities. Alternative methods for production of nanotubes are: chemical vapor deposition (CVD) of hydrocarbons over metal catalysts that result in aligned nanotube bundles [27], ball milling with subsequent annealing [28], and less common but more promising diffusion flame synthesis, electrolysis, heat treatment of a polymer and low temperature solid pyrolysis [14].

The most important properties of nanotubes are electrical conductivity [29], which is a function of their diameter, high stiffness and Young's modulus [30]. However, their high cost [31] due to the lack of a large-scale production method and the presence of impurities limits their use especially as nanoreinforcements. Other applications of carbon nanotubes are in electronics i.e., in displays, sensors and nanosize circuits.

1.1.4.5 Graphite

Graphite can be found in three main types [32]: (i) natural graphite, that contains many impurities and its appearance and structure varies depending on its geochemical origin; (ii) kish graphite, which is produced during the manufacture of cast iron and (iii) synthetic graphite, which is formed by progressive dehydrogenation and polymerization of hydrocarbon materials.

Graphite is the most stable allotrope of carbon in environmental conditions. It's a material with a well-developed layered structure in which the atoms are arranged in open hexagons and the layers show some order in stacking sequence. Due to Van der Waals forces the distance between the layers, along the c-axis of the crystallographic unit cell, is 0.335nm [33]. The lattice constants are α_o=0.2462nm and c_o= 0.6707nm at room temperature resulting in an in-plane bond length of 0.142nm [34]. Thus, the bond strength is higher within the layers than perpendicular to them giving rise to the anisotropic behavior of graphite, its easy cleaving and its morphology i.e., flakes and platelets [35].

The exfoliated graphite nanoplatelets (xGnP) used as nanoreinforcement is mainly produced in a two-step process (i) intercalation, which is defined as insertion of atoms and molecules between the graphite layers and (ii) exfoliation, which means separating the individual layers in order to remove all the interplanar interactions resulting in platelets with a thickness of few nanometers.

The intercalation can be achieved by electrochemical means, in which the carbon layers function as macro-cations. The compounds used for direct addition can be either electron-donor reagents i.e., alkali metal atoms or electron acceptors i.e., halogens [32]. Thus, a wide range of graphite intercalated compounds (GIC) can be prepared. All GIC share some common features such as, they maintain the aromatic character and planar structure of graphite, and they are characterized by a parameter called stage of GIC, which is the number of carbon layers separating two successive layers of intercalate [35].

The exfoliation of graphite is accomplished by applying a thermal shock to GIC. The heating shock can be carried out by conventional i.e., flame or non conventional i.e., microwave as first proposed by Fukushima [36], infrared, laser or even solar furnace heating sources [35]. The rapid heating results in vaporization of the intercalated species, giving rise to a significant expansion of graphite along the c-axis, i.e., increasing the volume by a factor of 500 [36].

Any type of GIC can theoretically be used for exfoliation but due to economical concerns graphite bisulphate is most commonly used. This is a sulphuric acid-based GIC precursor produced by electrochemical oxidation of graphitic carbon with strong sulphuric acid in presence of a strong oxidizing agent i.e., nitric or chromic acid. This reaction was first described by Schaufhault in 1841 and was further studied by Brodie in 1859 as reported in [32]. A change in the color from black to blue indicates the completion of the reaction, i.e. complete intercalation.

Graphite is used as fire extinguisher or flame retardant and for thermal insulation in steel industry [37] due to its ability to absorb heat by expansion. It is also used (i) as a constituent in various solid lubricants due to the ability of graphite sheets, which are stack on top of one another, to easily slide past each other making graphite act as a grease [14]; and (ii) in batteries, where it lowers the threshold and has higher conductivity than carbon black, which is currently used in batteries, due its flaky shape [35].

Exfoliated graphite nanoplatelets are very promising nanoreinforcements that combine the layered structure of clays with the superior thermal and electrical properties of carbon nanotubes. Thus, the graphite nanocomposites can be used not only for structural applications but also for electrostatic dissipation, electromagnetic and radio frequency interference shielding, and heat dissipation.

The challenges are, as in the case of all nanoreinforcements, to modify the surface of graphite in order to improve adhesion with the polymer matrix and avoid particle agglomeration resulting in a well-dispersed system. Good adhesion is necessary for effective stress transfer from the matrix to the reinforcements and results in improved performance of the composite system. For a given system the interactions at the matrix-reinforcement interface and thus the surface condition have to be optimized since very strong interactions can lead to a stiff and brittle interface degrading the composite's performance.

In order to understand the bonding and interactions that are present between reinforcements and matrix, it is necessary to know the type, quantity and reactivity of the functional groups on the surface of the reinforcements. The exfoliated graphite used in this research is highly crystalline and contains up to 6% (atomic concentration) of oxygen as determined by XRD and XPS respectively [36]. No residuals of sulfur or nitrogen are detected which indicates that the sulfuric and nitric acids contained in the as-received acid intercalated graphite flakes have been removed during exfoliation. More details on the chemistry of the graphite surface will be presented in Chapter 8.

1.2 Processing of Nanocomposites

Nanocomposites are defined as composite materials where the reinforcement has at least one dimension in the range of 1-100nm. As in the case of conventional reinforcements, the matrices may be ceramic, metallic or organic materials. This research focuses on organic i.e., polymeric matrices and organic i.e., graphite, carbon black and carbon fibers, reinforcements. As expected, the possible property improvements differ for each matrix-filler system but what is more interesting is to explore how changing the processing method or conditions affects the properties of the same matrix-filler system. Such knowledge is necessary to allow fabrication of nanocomposites with desired properties necessary for the application under consideration, by controlling the processing conditions.

1.2.1 Clay Nanocomposites

In the case of clay nanocomposites a variety of fabrication methods have been proposed. The basic ones are:

(i) *In situ* polymerization, the monomer is polymerized inside the clay galleries and clays are exfoliated during polymerization. This is a two-step method where initially the clay cations are substituted by alkylammonium ions via an ion exchange reaction and then the polar monomers are intercalated and polymerized by heating. The obtained composites can be either intercalated (insufficient polymer penetration inside the galleries to separate the clay layers) or exfoliated (extensive polymer penetration and delamination of the silicate layers) depending on the type of monomers used and the polymerization conditions. Some of the monomers used are ε-caprolactam [3, 4, 38, 39, 40]; ε-caprolactone [41, 42]; and epoxy resins [43, 44, 45].

(ii) Polymer intercalation from solution [46-48]. In this method a solvent is used to dissolve the polymer, the reinforcement is dispersed in the solution and finally, the polymer resolidifies as the solvent is removed.

(iii) Polymer melt intercalation. This is a solventless, versatile and environmentally benign synthesis in which the layered silicate is mixed with the polymer in solid state and then the mixture is heated above the softening point of the polymer. Compatibility with various polymers can be accomplished by derivatizing the silicates with alkylammonium cations and nanodispersion can be achieved by fine-tuning of the surface characteristics [49]. Polymers that have been used to make nanocomposites with this method are polyimide [50], poly(ethylene oxide) [51], polystyrene [52], and acrylonitrile-butadiene rubber [53]. Melt intercalation may be adaptabed to existing processing techniques like roll milling, extrusion and molding.

There are various modified versions of the polymer melt intercalation method that aim to improve intercalation and lead to exfoliated and well-dispersed systems. For example, surface modification of clays or use of compatibilizer or combination of both [54] is used with a non-polar polymer i.e., polypropylene [54-56]. A compatibilizer can be a functionalized oligomer or copolymer whose polar segments will enter in the clay galleries while the non-polar sections will interact with the matrix.

Another alternative method is to introduce supercritical carbon dioxide (scCO_2) in a conventional melt mixing system [57]. Because of the high compressibility of scCO_2, its solvent properties can be controlled by small changes in processing conditions, acting as "reversible plasticizer" that can be easily removed from the system. Preliminary results [57] show that introduction of $scCO_2$ in HDPE-clay system increases the basal spacing of the clay.

It has also been proposed that the degree of exfoliation obtained by a regular polymer melt intercalation method can be improved through the aid of conventional shear devices such as extruders, mixers, ultrasonicators, etc. [58]. An example is use of a three-roll mill to fabricate clay-epoxy nanocomposites. The technique is environmentally friendly and is found to be highly efficient in achieving high levels of exfoliation and dispersion within a short period of time [59].

1.2.2 Carbon Nanotube Nanocomposites

The same processing techniques can be used to fabricate carbon nanotube reinforced polymer nanocomposites. Although they have a very high aspect ratio they are still short enough to flow through conventional polymer processing equipment [60]. The challenge is to achieve a well-dispersed system with controlled orientation in order to utilize the unique properties of nanotubes. Promising results obtained by melt processing of isotactic polypropylene with nanotubes using extrusion followed by stretching of the melt i.e., melt spinning and subsequent melting of the solidified material i.e., drawing the composite in the form of fibers or sheet along a series of rollers [61]. Another approach is the functionalization of CN that enables uniform dispersion in different solvents, polymers and epoxy materials without degrading their properties [62]. An example is poly(vinyl alcohol) composites film were carbon nanotubes covered by surfactants were used [63].

Functionalized or not the carbon nanotubes are usually dissolved in a solvent using sonication and the polymer is added to the solution. A loose composite powder is obtained after the solvent evaporates that is used for further processing. Nanocomposites made using the solvent approach, which is similar to the solvent intercalation method used in clays, are MWCN-PS [64,65], CN-PP [66] and SWCN-PAN [67].

In-situ polymerization has also been used for fabrication of CN reinforced composites. Some of the monomers used are methyl methacrylate [68] and poly(amic acid) [69]. Finally, melt mixing can also be employed i.e, in case of HDPE [70] and nylon 6 [71]. Different compounding methods such as ball milling, high shear mixing in the melt and extrusion using twin screw extruders have been used to improve dispersion of CN in the polymer matrix [72].

In case of VGCF, in theory, nanocomposites can be fabricated using all the above processing methods, however, in practice only melt mixing is used. The reason is that there is no need to use the solvent approach or *in situ* polymerization in order to obtain a well-dispersed system. Surface modification of the VGCF fibers [20], which is a well-established technique, can lead to satisfactory results.

1.2.3 Exfoliated Graphite Nanocomposites

EG was developed and proposed by Aylsworth [73, 74] as reinforcement of polymers, phenolic resins in particular, in 1910's. The incorporation of intercalated graphite into an organic using conventional processing techniques such as extrusion, lay-up, injection molding and pressing, was proposed by Lincoln [75] in 1980's. Since that time, research has been conducted on exfoliated graphite reinforced polymers using graphite particles of various dimensions and a wide range of polymers. In all the cases the objective is to find the optimum processing method that will utilize graphite's superior properties and lead to nanocomposites with the desired properties.

The processing methods used for graphite-polymer nanocomposites are similar to the ones used for clays since both materials have a layered structure. However, because they are chemically different some modifications are required. Once the graphite is exfoliated (ex-situ process) then the nanocomposites can be made by:

(i) Direct mixing, often used in case of low viscosity thermoset matrices [36, 76]

(ii) Melt compounding, a method used mainly with polyolefins i.e., HDPE [77], PE-exfoliated graphite and PS-graphite using a Brabender mixer [78], HDPE-graphite using a Haake mixer and twin screw extruder [79], nylon 6,6-graphite and polycarbonate-graphite, using a twin screw extruder [80] and HDPE-graphite nanocomposites made using a two-roll mill [81].

(iii)Solution intercalation, a method utilizing a solvent to dissolve the polymer and disperse the graphite. The solvent is evaporated once the mixing is completed. Nanocomposites made by the solution approach are PMMA/graphite using chloroform as solvent [82, 83], and maleic anhydride grafted polypropylene/graphite in the presence of xylene [84]. This processing method results in nanocomposites with higher electrical conductivity and lower percolation threshold compared to nanocomposites made from the exactly same materials using the melt mixing technique [84].

(iv)*In-situ* polymerization where the monomer is polymerized in the presence of graphite nanosheets. Examples of some composite systems made using this method are nylon 6/graphite nanocomposites via intercalation polymerization of e-caprolactam in the presence of expanded graphite [85], graphite-polystyrene starting with styrene-graphite-benzoyl peroxide mixture [86, 87, 88], and graphite-polyacrylonitrile nanocomposites [89].

(v) Electrospinning of nanoscale fibers using polymer solution and melts at ambient conditions. The nanofibers are created by applying electric field between the polymer reservoir and a collection plate that is oppositely charged. The polymer fluid,is ejected through a capillary tip of a glass syringe, and is stretched toward a collection screen, the electrode. The method was initially used to produce exfoliated montmorillonite-nylon 6 nanofibers from hexafluoroisopropanol solution but there were dispersion issues [90]. Recently, the method was used to make graphite nanofibers starting from xGnP dispersed in (PAN)/N,N DMF solution [91].

If the graphite is not exfoliated prior to fabricating the composite, then an in-situ exfoliation process can be used such as:

(vi) Polymerization filling technique, where *in situ* polymerization occurs in the presence of initiator-intercalated graphite. It is known that organic molecules such as benzene ethylene or acetylene can easily, with the assistance of alkali metal, be intercalated into graphite layers forming oligomers. A review on the subject is given by Fukushima [36]. Using this approach a variety of graphite composites has been fabricated i.e. intercalated graphite was mixed with an epoxy resin and exfoliated *in-situ* during the curing process [92], and starting from styrene and graphite dispersed in BPO polystyrene grafted graphite was obtained [93]. The obtained composite had better properties compared to composites made by melt mixing of polystryrene with expanded graphite.

In summary, composites made by in-situ processing have better mechanical properties compared to composites made by melt-mixing or other ex-situ fabrication methods due to better dispersion, prevention of agglomeration and stronger interactions between the reinforcement and the polymer. In-situ exfoliation can also be achieved during melt mixing, however since the temperature required for exfoliation is ~230°C only polymers which can be processed without being degraded can be used for in-situ fabrication of nanocomposites.

1.3 Characterization Techniques and Tools

It is necessary to characterize the nanomaterials and determine their properties and performance. The most common techniques and tools used are:

(i) Atomic Force and Scanning Tunneling Microscopy (AFM and STM), they are closely related microscopic techniques that can provide atomic resolution images with a minimum sample preparation. In both instruments a probe scanned across the sample surface is used to detect changes in surface structure and topology on the atomic scale. Their difference is that AFM provides the information based on the interaction forces between the probe and the sample whereas; STM measures the surface electron density and thus requires electrically conductive samples [94]. Since this method interrogates the surface, care must be taken not to introduce artifacts during sample preparation.

(ii) X-Ray Diffraction (XRD), a technique that provides structural information based on the scattering of the incident X-ray due to Bragg interactions with the sample. For crystalline or samples with an ordered structure, the scattered radiation is recorded and represented as a peak at a particular angle in the diffraction pattern [95]. The position of the peak as well as, the peak area, provide information about the size of the reinforcement, the dispersion state within the polymer matrix, and the exfoliation degree by measuring the basal distance between individual platelets in case of clay or graphite composites.

(iii) Transmission Electron Microscopy (TEM), used mainly to provide information about the average size, dispersion and orientation of the nanoreinforcements. Visual images of the sample's surface which reveal the morphology and structure can be obtained at very high resolution and magnification (~2nm) but the technique requires extensive sample preparation of very thin section by microtomy and probes a very small area of the sample allowing thus for qualitative analysis only.

(iv) X-ray photoelectron spectroscopy (XPS) is one of the most powerful analytical techniques that provides qualitative and quantitative information about the chemistry, organization and composition of a surface. It can detect all the elements with atomic number $z>3$ and identify their molecular environment by collecting and counting the core electrons emitted by surface atoms when these atoms are excited due to bombardment of the surface by Xray photons [94]. This surface technique is mainly used in this research to characterize the surface of graphite and evaluate the various surface modification approaches that will be employed to treat graphite.

More conventional equipment was also used during the course of this research in order to determine the mechanical, thermal, electrical and barrier properties of the nanocomposites. Details can be found in Chapter 4.

1.4 Properties of Nanocomposites

As proposed by Griffith and also confirmed by Weibull [12] the smaller a material is, the stronger it becomes. Also Piggott [13] explained that the critical volume fraction (amount necessary to enhance the properties) of the filler is decreased when stronger materials are used. It is concluded that nanocomposites can combine desired performance with low cost and simple processability. However, their novel properties cannot be understood by simply scaling the existing continuum mechanics theories since such theories do not take into account the basic characteristic of the nanocomposites: the large internal interfacial surface.

1.4.1 Clay nanocomposites

Clay nanocomposites show enhanced mechanical properties such as strength and modulus accompanied by an increase in impact strength. In addition, the heat distortion temperature increases and there is significant reduction of water adsorption as demonstrated in clay/nylon 6 systems by the Toyota research center [39, 96, 97]. Similar improvement in mechanical properties has been reported by Giannelis group [44] who found that nanocomposites containing only 4 vol% silicate shows 60% and 450% increase in storage modulus in the glassy and rubbery region respectively, compared to the unfilled epoxy. Pinnavaia and co-workers [45] have also reported that clay/epoxy nanocomposites show more than 10-fold improvement of the modulus and strength, which is attributed to possible strain induced alignment of the silicate layers in the rubbery phase.

Besides the superior mechanical properties, clay nanocomposites also show improved barrier properties i.e., water permeability decreases dramatically as the silicate content is increased [42, 50]. As explained by the Giannelis group [42] this is due the presence of well dispersed large aspect ratio silicate layers in the polymer matrix which is impermeable to water molecules. Thus, the solutes have to follow a tortuous path that increases the effective path length for diffusion.

Additionally, clay nanocomposites display a significant increase in heat resistance and thermal stability and self-distinguishing characteristics [49]. Furthermore, silicates act as a nucleating agent for crystallization leading to smaller spherulite size improving thus the impact strength of nanocomposites [98]. Finally, due to the layer orientation polymer-silicate nanocomposites exhibit stiffness, strength and dimensional stability in two dimensions (rather than one as in case of fiber-type reinforcement) if the platelets are randomly distributed in the 2D plane [99]. However, the clay nanocomposites lack electrical and thermal conductivity that limits their potential applications.

1.4.2 Carbon Nanotube Composites

CNTs are potentially ideal nanoreinforcements since they combine high aspect ratio; they are electrically and thermally conductive and have excellent stiffness and strength, and low density [60]. However, their high price makes the nanotube reinforced polymers too costly for most applications. Other problems that need to be solved are the difficulty in dispersing individual nanotubes into the polymer matrix and the poor adhesion at the interface, which does not allow utilization of the novel properties of nanotubes in the fabricated nanocomposites.

Despite the above difficulties, homogeneous distribution of MWNTs in polystyrene by ultrasonic assisted method has been reported [64]. Addition of only 1wt% MWNT significantly increases the mechanical properties i.e., 25% increase of the break stress and ~40% of the elastic modulus. Similar results were reported by the Kearns group [66] who dispersed SWNT into PP via solution processing and melt spinning and observed a 40% increase in tensile strength at a loading of 1wt%. Fiber spinning became difficult at higher loadings. Kumar's group [72, 100, 101 and 102] also used SWNT up to 10wt% in various polymer matrices i.e., PMMA, PP and PAN, to make composite fibers through melt or a gel spinning process. The modulus increased more than 100% and there was improvement of the toughness and compressive strength, however, the elongation at break as well as, the tensile strength decreased especially at higher loadings. In the case of PAN-SWNT composite fibers addition of nanotubes resulted in increase of the glass transition temperature by 40°C, and significant reduction in thermal shrinkage and in polymer solubility.

In addition to the improvement of thermo-mechanical properties CNT composites are electrically conductive even at very low nanotube contents i.e., addition of only 0.05vol% of SWNT in polyimide, fabricated by *in situ* polymerization approach using DMF as solvent [69], results in composites with 10^{-8} S/cm volume conductivity, 10 orders of magnitude higher than the conductivity of the neat polymer. Similar results were reported for SWNT-PMMA nanocomposites prepared by the coagulation method [103] that produced a conductivity of 10^{-8} S/cm at 0.5wt% SWNT loading.

1.4.3 Exfoliated Graphite Platelet Nanocomposites

Besides layered silicate nanoclays and carbon nanotubes, graphite platelets are also among the leading nano-scale fillers in research and development and commercial projects [104]. Although xGnP nanocomposites have not received as much attention as carbon nanotubes, research in the Drzal group has shown that they can be a cost effective alternative to carbon nanotubes and provide excellent competitive functional properties. They combine the layered structure and low price of clays and the superior electrical and thermal properties of nanotubes. There is a wide variation of the properties of the xGnP-polymer nanocomposites depending on the origin (kind of GIC used), form (intercalation or degree of exfoliation), morphology and aspect ratio of graphite used, as well as on the fabrication method.

The challenge in fabricating graphite-polymer nanocomposites is the dispersion of the graphite platelets and adhesion to the polymer matrix. Fukushima [36] was the first to report a surface treatment of graphite, acrylamide grafting on the graphite edges via *in situ* polymerization of acrylamide, that improved adhesion and resulted in graphite-epoxy composites with higher flexural strength (+10% at 3vol%) and modulus of elasticity (+28% at 3vol%) compared to neat epoxy and to untreated-graphite epoxy composites. It was also reported that the treated exfoliated graphite nanoplatelets performed better than commercially available octyldecylamine treated nanoclay and carbon fillers i.e., CB, VGCF and PAN based carbon fibers.

Using two types of graphite, Krupa and Chodak [78] demonstrated that in HDPE-graphite systems, smaller particles with narrower particle size distribution and higher specific surface area cause larger improvement in the mechanical properties.

The differences between expanded (EG) and untreated (UG) graphite on the properties of graphite-HDPE [83] and graphite-PMMA [83] composites were explored by Zheng *et al.* In the case of HDPE the overall improvement in mechanical properties was not impressive; however, their results confirmed the advantages of expanded graphite in enhancing both the electrical conductivity and mechanical strength and stiffness of neat polymer. In the case of PMMA composites, addition of untreated graphite did not affect the storage (G') and loss modulus (G") of neat PMMA, but increased the Tg. Addition of expanded graphite had more dramatic effects. Both G' and G" increased even at low loadings i.e., increase of 20% and 52% respectively at a loading of 2wt%. In addition, there was a shift of Tg to higher temperatures by 10°C, which was ascribed to the restricted segmental movement due to the presence of graphite.

Weng *et al* [81] fabricated xGnP-HDPE nanocomposites by melt mixing using a two-roll mill and reported that tensile strength, elongation at break and impact strength reduced with addition of xGnP even at low contents i.e., 5wt%. They attributed the reduction in mechanical properties on the reduced mobility of HDPE chains due to the presence of the rigid and high modulus graphite particles. Similar results were reported by Pan *et al.* [85] who fabricated nylon 6/graphite nanocomposites via intercalation polymerization and found that addition of graphite up to 2.5vol% results in a slight increase of the flexural modulus and significant decrease of the flexural and impact strength.

In agreement with the above, are the results obtained by Chen's group [87, 88] who reported that addition of graphite increases the tensile strength and modulus of EG-PS nanocomposites made by intercalation polymerization. They also observed a sharp reduction of the impact strength that was attributed to insufficient intercalation, poor dispersion of graphite due to lack of affinity between the non-polar monomer and the polar graphite surface. Finally the same trend i.e., slight increase in tensile strength and a larger increase in tensile modulus with addition of graphite platelets was observed in graphite-epoxy nanocomposites made by direct mixing [105].

1.5 Theories of Nanocomposites

1.5.1 Mechanics of Nanoplatelets

In general, the advantage of using platelet-type reinforcement is that, when properly oriented, they stiffen the material in two dimensions rather than in one, as in the case of aligned fibers. However, due to stronger interactions between nearest neighbor platelets the strength is not as high as expected [99].

A very critical parameter in the case of platelet reinforcements is the aspect ratio as pointed out by Piggot [99]. The analysis assumes square platelets aligned with an edge parallel to the applied stress and with constant thickness. Based on the slip theory there are slip regions near the ends of the platelet due to imperfect bonding between the platelet and the matrix. The stress transfer at the edges parallel to the applied stress is neglected.

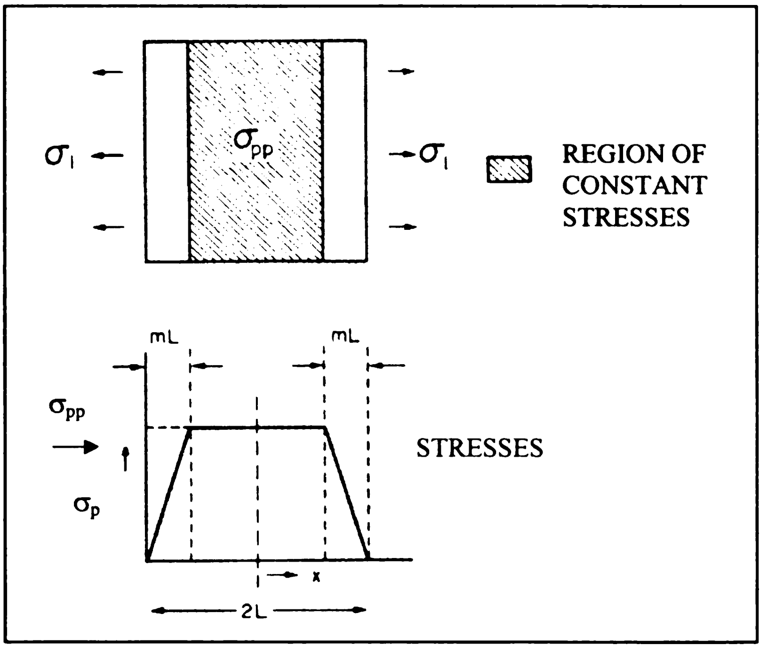

Figure 1.1: Stresses in a single embedded square platelet adapted by Piggot [99]

There are two forces applied in the platelet, the first is due to the interfacial shear stress τ_ι, which operates over an area *2wdx*, where *w* is the width of the platelet, and the second is the force exerted by the platelet stress σ_p acting over the area *tw*, where *t* is the platelet thickness. The two forces must be equal so

$$\frac{d\sigma_p}{dx} = -\frac{2\tau_i}{t} \tag{1.4}$$

Based on the geometry shown in Figure 1.1 and using the boundary condition i.e., $\sigma_p = 0$ *at* $x = L$ the plateau stress is given by Equation (1.5)

$$\sigma_{pp} = \frac{2\tau_i mL}{t} \tag{1.5}$$

Using the definition of aspect ratio given in Equation (1.6)

$$s = 2L/t \tag{1.6}$$

the maximum stress in the center region of the platelet becomes

$$\sigma_{pp} = \tau_i ms \tag{1.7}$$

Finally, based on the fact that the platelet strain in the unslipped region will be equal to the matrix and the composite strain i.e.,

$$\varepsilon_1 = \frac{\sigma_{pp}}{E_p} \tag{1.8}$$

where E_p is the platelet modulus. The parameter *m*, which relates to the extent of slip along the interface can be estimated by combining Equations (1.6-1.8). Consequently,

$$m = \frac{E_p \varepsilon_1}{\tau_i s} \tag{1.9}$$

As shown from the above analysis the platelet aspect ratio has a significant effect on the platelet stress and thus, on the composite strength as well. However, in order to estimate the composite stress the platelet packing arrangement needs to be taken into account. In addition, the stress concentration near the end of a platelet due to adjacent platelets, which is 50% larger than in the case of fiber type reinforcement, should be considered as well, because these stress concentrations are responsible for composite failure at strains $\varepsilon_l < \varepsilon_{pu}$ where ε_l is the composite strain and ε_{pu} is the strain at platelet breaking stress.

Finally it is noted that there is a critical aspect ratio, s_c, defined as the aspect ratio large enough for the matrix to transfer the breaking stress to the platelet and can be estimated using Equation (1.6) with $m=1/2$ and $\sigma_{pp}=\sigma_{pu}/2$. Thus

$$s_c = \frac{\sigma_{pu}}{\tau_i} \tag{1.10}$$

Composites with platelets that have $s < s_c$ will fail by slip rather than by platelet fracture whereas, if the platelets have aspect ratio larger than the critical value, $s > s_c$ will fail at the platelet breaking-stress.

The same analysis applies in case of round or disk shape platelets, which models better the xGnP, with the extra assumptions that the stress transfer within the platelet is neglected, which is true only for very thin platelets. Similarly to the case of square platelets, the stress of composite containing round platelets depends strongly on the aspect ratio and the packing arrangement. Experimental evidence indicated that the platelets do break along their diameters as expected based on the stress distribution provided by Piggott [99].

The existing theoretical models used to estimate the modulus of platelet-reinforced nanocomposites are based on the analysis just presented. In most cases there is a huge discrepancy between theoretical predictions i.e., rule of mixtures or Halpin-Tsai, and experimental data mainly because the models assume perfect bonding between the matrix-reinforcement interface which might be a good approximation for conventional composites but it's not valid for nanocomposites where the interface is much larger; and also because there is a big modulus difference between the matrix and the platelets.

Shia *et al* [106] used a simple interface model to quantify the imperfect interfacial bonding and introduced the concept of effective aspect ratio and effective aspect volume fraction of the platelets. These effective quantities depend on a single material parameter, the constant interfacial shear stress, τ_I which was determined by fitting the theory to experimental data obtained for elastomer-silicate nanocomposites systems by Burnside and Giannelis [107].

The concept of effective aspect ratio and volume fraction is used to account for the fact that an imperfect interface reduces the reinforcing efficiency of the platelet since a greater portion of its width is not fully loaded. The effective quantities are smaller than the actual ones and can be estimated by simple algebraic equations derived for various cases of applied stress [106].

1.5.2 Toughness and Strength

The fracture toughness of composites is the result of a combination of various mechanisms. Energy absorbing mechanisms such as increased plastic deformation of the matrix along the matrix-reinforcement interface, crack branching due to hindrance by reinforcements, shear deformation in the interphase region and creation of voids and crazes at the reinforcement edges have a positive effect on toughness. On the other hand introduction of stress concentration sites decreases the composite toughness.

The strength of composites is the result of the adhesion condition and the stress concentration at the interface. The better the adhesion the more effective the stress transfer from matrix to reinforcements is, which means higher ultimate strength. Factors that affect the stress transfer at the interface are the shape, aspect ratio and geometric arrangement of the reinforcements. The energy absorbing mechanisms described above do not have a positive effect on the strength of composite materials, thus, composites can show higher toughness and lower strength and vice versa.

In case of nanocomposites, the stress transfer from the matrix to the reinforcements should be more efficient due to the increased surface area, assuming good adhesion at the interface. Also, crack propagation length at the interface becomes longer which results to improved strength and toughness.

As the size of the reinforcement decreases the average dispersion distance becomes shorter which means that the stress at the reinforcement edges could be reduced due to the presence of other reinforcements located nearby. Factors that affect the stress condition at the reinforcement edges are the distance between the reinforcements as well as the orientation of the adjacent reinforcements. Based on numerical simulations Fukushima [36] concluded that if the reinforcements are positioned in parallel the stress concentration is reduced due to stress transfer from one edge to another, whereas in case of reinforcements oriented in an edge-to-edge position the stress at the edges could be increases and cause cracks. Thus, orientation of the reinforcement strongly affects the strength and toughness of the composite.

1.5.3 Electrical Conductivity

1.5.3.1 Introduction

The advantage of CNTs and xGnP over clays is that the carbon nanoreinforcements are electrically and thermally conductive opening up new applications. To utilize these materials it is necessary to identify the factors that affect the conductivity of composites, study them independently, and fully understand the mechanisms and interactions or synergistic phenomena at the nanoscale. A simple approach is to use electrical conductivity models that will take into account all the factors affecting the conductivity of the composites and will allow for efficient composite design.

The important properties in electrically conductive composites are i) the electrical conductivity, reported either as bulk conductivity (S/cm) or surface conductivity (S-cm) and ii) the percolation threshold, defined as the minimum volume content of the conductive reinforcement above which the polymer composite becomes electrically conductive.

1.5.3.2 Percolation Theory

At very low concentrations particles are either dispersed in the polymer matrix or form agglomerates and in both cases they are not in contact with each other. At higher filler contents the particles begin to contact each other forming a continuous network through the volume of the sample. The filler content at which this conductive path is formed allowing electrons to travel across the sample is the percolation threshold. The formation of this network is based on the principles of percolation theory [108, 109]. It is desirable for the conductive filler content to be as low as possible in order to achieve good processability, low cost and satisfactory mechanical performance.

The percolation theory has its roots in the theory for the gelation of polymers proposed by Flory in the 1940's. The term percolation was first introduced by Hammersley and Broadbent in 1957 [110] who investigated how the random properties of a "medium" influence the spread of "fluid" through it i.e., passage of a fluid through a network of channels, using geometrical and probabilistic concepts. In the case of composites with conductive reinforcement in an insulating polymer matrix the conductivity or resistivity of the composite can be described as follows

$$\sigma = \sigma_o(\rho - \rho_c)^t \text{ for } \rho > \rho_c \tag{1.11}$$

where σ and σ_0 are the conductivity of the composite and of the conductive reinforcement respectively, ρ is the volume fraction of the conductive phase, ρ_c the percolation threshold and t is called the critical exponent which can be determined using Equation (1.11) and a least-square linear fit of the experimental data in a log-log plot.

1.5.3.3 Factors Affecting Electrical Conductivity

The electrical conductivity and especially the percolation threshold are the result of interactions of various factors with the most important being the volume fraction, distribution, size, shape, orientation and spacing of the filler particles within the polymer matrix as well as the fabrication method of the composite. In addition, the conductivities of the constituents are also important with the conductivity of the filler defining the upper limit for the electrical conductivity of the composite.

For spherical particles, the percolation threshold declines with decreasing their diameter [111, 112]. The reason is that as the particles become smaller, the interparticle distance decreases. For non-spherical particles, as the aspect ratio of the conductive fillers increases, the critical concentration to induce bulk conductivity in the composite reduces significantly [113]. That is, the large aspect ratio particles can still maintain point-to-point contact at low concentrations and allow for electron tunneling. Therefore percolation can take place at lower concentrations than for spherical particles. Electron tunneling is a mechanism explained by quantum mechanics based on which electrons may pass through thin, insulating films at field strengths encountered in the gaps between adjacent conductive particles [111]. Asymmetric filler particles i.e., fibers or flakes, provide an additional advantage in terms of decreasing the interparticle distance [114]. Finally, fillers with broader particle size distributions percolate at lower contents [114, 115].

Other characteristics of the filler that lower the percolation threshold are: highly agglomerated (highly structured) fillers, or fillers with high degree of porosity that allow for polymer penetration and produce a conductive network by occupying a large occluded volume at low concentrations [111].

Another critical factor for the percolation threshold is the fabrication method of the composites. The processing conditions significantly affect the percolation threshold. Extensive mixing i.e., twin screw extruder or long mixing using roll mill, can destroy the conductive network [87, 88, 111] and also reduce the aspect ratio of the fillers [111, 116] in both cases resulting in composites with increased percolation threshold. A demonstration of the above is given by comparing compression to injection-molded composites i.e., aluminum flake reinforced polypropylene percolates at 7.5 vol% when it is compression molded and 14 vol% when injection molding is used [111]; carbon black-polypropylene composites have a percolation threshold of 5 and 10 wt% for compression and injection molded samples respectively [117]. Besides the reduction of the aspect ratio, injection molding introduces alignment of the filler along the flow direction [116] and thus the sample percolates at higher loadings compared to a compression-molded one where the random orientation of the filler facilitates the formation of the conductive network.

Comparison of melt mixing and solution intercalation method used by Chen's group [84, 118] for fabrication of graphite-maleic anhydride grafted polypropylene, (gPP), nanocomposites indicated that solution intercalation lowers the percolation threshold. The explanation provided is that gPP molecules disentangled in the solution, and through physical adsorption into the pores and interplanar spaces of expanded graphite support and fix the graphite-gPP networks and maintain the high aspect ratio of the graphite sheets.

Finally, the crystallinity of the matrix also affects the conductivity of the composites since in a highly crystalline matrix the formation of the continuous conductive path is easier compared to a less crystalline polymer where the higher amorphous portion may result in more homogeneous particle distribution [119]. The surface free energy of both the filler and the polymer matrix is also a critical factor. Using materials with similar surface energies leads to better wetting and improves adhesion and dispersion within the matrix, which means enhancement of the mechanical properties but increase in percolation threshold.

1.5.3.4 Models for Electrical Conductivity

Various models have been proposed in order to predict and describe the electrical conductivity of composites, however, none of them is generally valid since none is taking into consideration all the factors mentioned above that affect the composite's percolation threshold and conductivity. As mentioned by King's group in a review study about evaluation of electrical conductivity models [80], there are four main classes of conductive models reported in literature. These are:

- Statistical, which are using percolation theory and predict the conductivity based on the probability of particle contacts within the composite. The first models of this type were proposed by Kirkpatrick [120] and Zallen [110] and are described by a power-law equation of the following form:

$$\sigma = \sigma_o (V - V_C)^S \tag{1.12}$$

where σ is the conductivity of the composite, σ_o the conductivity of the filler, V the filler volume fraction, V_C the percolation threshold, and S the critical exponent that depends on the dimension of the lattice.

The initial models were not very accurate but became the basis for various modified improved statistical models such us the one proposed by Bueche [121], who used the concept of polymer gelation in order to predict the conductivity of composites, which is described in Equation (1.13):

$$\rho = \frac{\rho_m \rho_f}{(1 - V_f)\rho_f + V_f \omega_g \rho_m} \tag{1.13}$$

where ρ, ρ_m and ρ_f are the resistivities of the mixture, insulator and conductor respectively, and ω_g is the weight fraction of the conductive phase in an infinite cluster, a function of the number of contacts per particle and the probability of contact.

Another modified model proposed by McLachlan [122], is based on a general effective media equation and is described by Equation (1.14).

$$\frac{(1-\phi)\left(\rho_m^{1/t}-\rho_h^{1/t}\right)}{\rho_m^{1/t}+\left(\dfrac{1-\phi_c}{\phi_c}\right)\rho_h^{1/t}}+\frac{\phi\left(\rho_m^{1/t}-\rho_l^{1/t}\right)}{\rho_m^{1/t}+\left(\dfrac{1-\phi_c}{\phi_c}\right)\rho_l^{1/t}}=0 \tag{1.14}$$

where ρ_m, ρ_h and ρ_l are the resistivities of the composite, of the high resistive constituent and the low one respectively, ϕ and ϕ_c are the filler volume fraction and percolation threshold and finally, t is the critical exponent that can be determined either by a calculation of by curve-fitting techniques.

- Thermodynamic models that take into account the filler and polymer surface energies, as well as, the polymer melt viscosity. A representative model of this class is the one proposed by Mamunya *et al* [123] described by Equations (1.15)-(1.18).

$$\log\sigma = \log\sigma_c + (\log\sigma_m - \log\sigma_c)\left(\frac{\phi-\phi_c}{F-\phi_c}\right)^k \tag{1.15}$$

$$k = \frac{K\phi_c}{(\phi-\phi_c)^{0.75}} \quad K = A - B\gamma_{pf} \tag{1.16}$$

where σ is the conductivity of the composite, σ_c the conductivity at the percolation threshold; σ_m the conductivity at F; F is the maximum packing fraction, ϕ the volume fraction, AR is the aspect ratio; ϕ_c the percolation threshold, γ_{pf} the interfacial tension and A and B, are constants. The exponent k depends on the filler volume fraction, percolation threshold and interfacial tension calculated by Fowkes equation:

$$\gamma_{pf} = \gamma_p + \gamma_f - 2(\gamma_p \gamma_f)^{0.5} \tag{1.17}$$

where γ_{pf} is the interfacial tension, γ_p and γ_f are the surface tensions of the polymer and the filler respectively. The maximum packing fraction can be determined using the Equation (1.18):

$$F = \frac{5}{\frac{75}{10 + AR} + AR} \tag{1.18}$$

- Geometrical models which proposed to predict the conductivity of sintered mixtures of conducting and insulating powders. The main parameters used are the diameters of the nonsintered particles or the edge length of the sintered ones.Structure oriented models that take into account structural properties such as aspect ratio and filler orientation, which are a result of the composite processing techniques. One model of this class is the one proposed by Nielsen [124] presented in Equations (1.19)-(1.20).

$$\sigma_c = \sigma_{poly} \frac{1 + AB\phi_f}{1 - B\Psi\phi_f} \tag{1.19}$$

$$B = \frac{\sigma_f / \sigma_{poly} - 1}{\sigma_f / \sigma_{poly} + A}, \quad \Psi = 1 + \left(\frac{1 - \phi_m}{\phi_m^2}\right)\phi_f \tag{1.20}$$

where ϕ_f is the filler volume fraction, σ_c, σ_{poly}, and σ_f the conductivities of the composite, polymer and filler respectively; ϕ_m the maximum packing fraction; and A is a function of aspect ratio.

1.5.4 Thermal Conductivity

Thermal conductivity is another important property of xGnP polymer nanocomposites that enhances their overall attractiveness. Potential mechanisms to enhance thermal conductivity in nanofluids [125], which can also be applicable in case of solid phase nanocomposites are; (i) ordered structures at the interface, i.e., crystalline interface vs amorphous; (ii) ballistic nature of heat transfer i.e., heat carried by phonons through propagating lattice vibrations and (iii) lower interfacial resistance i.e, increase the size of the conductive particles and (iv) clustering effects.

The work of Agari's group [126, 127, 128, 129, 130, 131] on thermal conductivity of carbon filled polymer composites provided basic knowledge about the factors that affect thermal conductivity, same as the factors controlling electrical conductivity; and led to models i.e., a combination of the general Maxwell-Eucken model with a model that takes into account the contribution of the conductive particle chains, that could accurately predict conductivity values for a significant number of systems. Polymer used as matrices are PE, PVC, PS and polyamide and the fillers used are graphite, carbon black and copper and aluminum oxides. The conductivity was measured as a function of filler content and its temperature dependence was determined.

The experimental work reported by King's group [132] on thermally conductive graphite-nylon 6,6 composites show that (i) by increasing the amount of graphite the through plane conductivity increased significantly, (ii) Nielsen's thermal conductivity model (presented above) fits accurately the through-plane thermal conductivity data at lower filler concentrations and (iii) the in-plane thermal conductivity is ~3 times larger than the through plane conductivity due to orientation during injection molding and the anisotropy of the fillers. In another study, King's group [133, 134], determined the synergistic effects and interactions of CB, PAN carbon fibers and graphite on the thermal conductivity of nylon 6,6 and PC composites using factorial design.

Finally, it is reported [135] that the basic heat transfer mechanisms for conductive resins are (i) lattice vibrations (major contribution) and (ii) electron movement. The same study indicated that the factors that affect the thermal conductivity of composites are (i) conductivity of constituents, (ii) bonding between filler-matrix, (iii) crystallinity of the polymer (increasing crystallinity improves conductivity), and (iv) filler size, shape, concentration, dispersion, orientation, i.e., increasing aspect ratio or mixing different fillers due to packing phenomenon increases conductivity.

1.6 Applications of Nanocomposites

Clay nanocomposites offer significant weight reduction due to their high strength-to-weight ratio and they are already used in few commercial applications i.e., in 1991, Toyota motor Company introduced a timing-belt cover made from a nylon-silicate nanocomposites [136], General Motors Corp currently uses a thermoplastic olefin nanocomposite for the step-assist on its Chevy Astro/GMC Safari minivan [137], and GE plastics produced an automotive mirror housing of conductive PPO/nylon alloy [138]. More recently, a PP/nanoclay composite appeared on the body side molding of General Motors' highest-volume car, the 2004 Chevrolet Impala [104]. The latest application is on the 2005 GM Hummer H2 SUT where about seven pounds of molded-in-color nanocomposite parts are used for its center bridge, sail panel, and box-rail protector [104]. Other uses of clay nanocomposites in the automotive industry are in fuel tanks, brake parts, engine components, interior and exterior trim. A very promising market is also packaging i.e., films for food, cosmetics or pharmaceutical products and housing for electronic devices, wire and cable covers.

However, lack of thermal and electrical conductance limits these applications. On the other hand, conductive composites, polymers reinforced with thermal and electrical conductive particles i.e., nanotubes, carbon fibers or graphite, can be used in place of metals when improved properties such as light weight, toughness, versatility in shaping, and corrosion resistance, just to mentioned few, are required.

A thermally conductive material is useful as a heat sink in applications such as lighting ballasts, transformer housings, radiator, and fins [138]. In addition if the reinforcement has aspect ratio greater than 1 then composites can be designed with strategically-oriented fibers/particles to produce desired combinations of thermal conductivity and coefficient of thermal expansion.

An electrically conductive material can be used in static dissipative, slightly electrically conductive (e.g., fuel gages, etc.), or EMI (Electromagnetic Interference)/RFI (Radio Frequency Interference) shielding applications (computer and cellular phone housings, etc), as well as, as aircraft structural materials for protection against lightning. They can also be used as battery components and electric power cables. Finally, they found applications as membranes in fuel cells [139]

Despite the high cost of carbon nanotubes there are already commercial applications of carbon nanotube reinforced polymers i.e., every car produced in the U.S. since the late 1990s contains some carbon nanotubes, typically blended into nylon to protect against static electricity in the fuel system. Static-dissipative compounds containing nanotubes are also protecting computer read/write heads and blends of nanotubes in thermoplastics have been used for electrostatic painting of car body panels by General Electric [104].

1.7 Summary of Introduction

Based on the analysis provided by Griffith [10, 11], Weibull [12] and Piggot [13], the smaller a material gets the stronger it becomes. Therefore the nanomaterials are more effective nanoreinforcements compared to their conventional micro-scale counter parts. Clays are the most common nanoreinforcements used and clay reinforced polymers show superior mechanical and barrier properties. However, clays lack thermal and electrical conductivity that limits their applications.

Recently there is an increased interest in using organic materials such as carbon nanotubes and graphite as reinforcements for polymers due mainly to their superior thermal and electrical properties. The limiting factor in case of carbon nanotubes is their high cost. Exfoliated graphite is the less common nanoreinforcement but gains popularity due to its low cost, high availability and superior thermomechanical, electrical and barrier properties.

The challenge to overcome in order to utilize the advanced properties of nanoreinforcements in polymer composites is the poor dispersion and weak adhesion with the polymer matrix. Pretreatment of the nanoreinforcements, use of coupling agents and special mixing elements or modified processing methods and conditions need to be employed in order to obtain nanocomposites with homogeneous structure, advanced performance and superior properties.

1.8 Motivation and Research Objectives

The current and potential applications of nanocomposites just described combined with the fact that a new nanoreinforcement material (xGnP), developed in the Drzal Group [36] was available, were the motivation for this research. The promising results obtained for the exfoliated graphite-epoxy system was the driving force for this project: using the exfoliated graphite nanoplatelets in thermoplastics. Since the nanocomposites area and the graphite nanocomposites in particular, is a new research field it is clear that there is a lack of fundamental knowledge about the interactions between the nanoplatelets and the polymer matrix and lack of basic understanding about the mechanisms at the nanoscale, which result in materials with novel properties.

The objectives of this research are to:

- Explore the possible fabrication methods and understand the effect of the processing conditions on the various properties of the nanocomposites
- Investigate how addition of xGnP alters the physical properties of the polymer matrix such as crystallinity, (degree of crystallinity, crystallization temperature, structure and size of crystals), melting and glass transition temperature, and viscosity;
- Determine the mechanical (flexural strength and modulus, impact strength, storage and loss modulus), thermal (thermal conductivity and coefficient of thermal expansion) and electrical (electrical conductivity and percolation threshold) properties of the xGnP nanocomposites

- Provide systematic knowledge about the interactions between xGnP and polymer chains by understanding how the nanocomposites properties are related to xGnP's microstructure; state of dispersion, aspect ratio and orientation of the nanoplatelets within the polymer matrix, and
- Propose an appropriate surface treatment for the xGnP, which is a key factor in utilizing the superior properties of graphite, that will improve the adhesion with the polymer matrix and prevent the agglomeration of the xGnP resulting thus in a well dispersed system.

1.9 References

1. R. A. Vaia, "Polymer Nanocomposites Open a New Dimension for Plastics and Composites", The AMPTIAC Newsletter, vol 6 no 1, 17-24 (2003)

2. Polymer Nanocomposites Synthesis, Characterization and Modeling, R. Krishnamoorti, and R. A. Vaia, eds., American Chemical Society, Symposium Series 804, Washington, DC (2001)

3. A. Okada, M. Kawasumi, T. Kurauchu and O. Kamigaito, "Synthesis and Characterization of a Nylon 6-Clay hybrid" *Polymer Prepr.*, **194**, 10 (1987)

4. Y. Fukushima and S. Inagaki, "Synthesis of an Intercalated Compound of Montmorillonite and 6-Polyamide", Journal of Inclusion Phenomena, **5** 475 (1987)

5. R. Lane, B. Craig and W. Babcock, " Materials Engineering with Nature's Building Blocks", The AMPTIAC Newsletter, vol 6 no 1, 31-36 (2003)

6. http://www.zyvex.com/nanotech/feynman.html

7. http://smalley.rice.edu/

8. E.K., Drexler, "Engines Of Creation:The Coming Era of Nanotechnology" Anchor Books (1986)

9. "Handbook of Nanophase and Nanostructured Materials: Materials Systems and Applications (II)", Eds Z. L., Wang, Y. Liu and Z. Zhang, vol 4, pp 74-75 (2003)

10. A.A. Griffith, "The Theory of Rapture" Proceedings of the 1st International Congress on Applied Mechanics 55, (1924)

11. A. A. Griffith, " The phenomena of Rapture and Flaw in Solids" *Phil. Tans. Roy. Soc.*, **A221**, 163 (1920)

12. W. J. Weibull, " A Statistical Distribution Function of Wide Applicability" *J. Appl Mech.*, Sep 293, (1951)

13. M.R. Piggott, "Load Bearing Fibre Composites", Pergamon Press, p100 (1980)

14. M. Wilson, K. Kannangara, G. Smith, M. Simmons and B. Raguse, "Nanotechnology: Basic Science and Emerging Technologies", Eds Chapman and Hall/CRC Press, pp 56-60, (2000)

15. G. Kuhner and M. Voll, "Carbon Black, Science and Technology", eds. J.B.

Donnet, R.C. Bansal and M.J. Wang, Marcel Dekker, Inc; New York; p1 (1993)

16. T.V. Hughes and C.R. Chambers, US Patent No 405,480 (1889)

17. T. Koyoma, "Formation of Carbon Fibers from Benzene", *Carbon* **10**, 757 (1970)

18. W. Tarasen, R. Alig, G. Glasgow and R. Jacobsen, "Pyrograf-III: VGCF Nanofibers for Engineered Composites" Pyrograg Products Inc. report

19. N.M. Rodriguez, "A Review of Catalytically Grown Carbon Nanofibers" *J. Mater. Res.*, **8,** 3233, (1993)

20. G.G. Tibbetts, J.C. Finegan, J.J. McHugh, J.M. Ting, D.G. Glasgow, and M.K. Lake, "Applications Research on Vapor-Grown Carbon Fibers", Science and Application of Nanotubes, eds Tomanek and Enbody, Kluwer Academic, New York, pp 35-51, (2000)

21. S Iijima, "Helical Microtubules of Graphitic Carbon", *Nature*, **354**, 6348, (1991)

22. L.Yarris, "Atom-Sized Electronic Devices Identified Within Carbon Nanotubes", electronic edition of Lawrence Berkeley National Laboratory (http://www.lbl.gov/Science-Articles/Archive/nanotubes.html)

23. http://physicsweb.org/article/world/11/1/9

24. L.S.K. Pang, A.M. Vassallo and M.A. Wilson, "Fullerenes from Coal", *Nature*, **352**, 480 (1991)

25. M.A. Wilson, L.S.K. Pang and A.M. Vassallo, "C_{60} Separation on Coal", *Nature*, **355**, 117, (1992)

26. A. Thess, R. Lee, P. Nikolaev, H.J. Dai, P. Petit, J. Robert, C.H. Xu, Y.H. Lee, S.G. Kim, A.G. Rinzler, D.T. Colbert, G.E. Scuseria, D. Tomanek, J.E. Fischer, and R.E. Smalley, "Crystalline Ropes of Metallic Carbon Nanotubes", *Science*, **263** 383-87 (1996)

27. M.J. Yacaman, M.M. Yoshida, L. Rendon, and J.G. Santiesteban, "Catalytic growth of carbon microtubules with fullerene structure", *Appl. Phys. Lett.*, **62,** 202-204 and 657-59 (1993)

28. R.G., Ding, G.Q. Lu, Z.F. Yan, and M.A. Wilson, *Journal of Nanoscience and Nanotechnology,* **1** 1-23 (2001)

29. R. Saito, M. Fujita, G. Dresselhaus, and M.S. Dresselhaus, " Electronic structure of chiral Graphene Tubules", *Appl. Phys. Lett.* **60** 18, 2204-2206 (1992)

30. M.M.J Treacy, T.W. Ebbesen, and J.M. Gibson, "Exceptionally high Young's Modulus Observed for Individual Carbon Nanotubes", *Nature* **381**, 678-680, (1996)

31. http://www.fuentek.com/technologies/carbon-nantubes.htm

32. A.R. Ubbelhde and F.A. Lewis, "Graphite and its Crystal Compounds", Oxford University Press, pp1-30, (1960)

33. W.N. Reynolds, "Physical Properties of Graphite" Elsevier Publishing Co. Ltd, pp 1 (1968)

34. B.T. Kelly, "Physics of Graphite", Applied Science, London (1981)

35. A. Celzard, J.F. Mareche, and G. Furdin, "Modelling of Exfoliated Graphite", *Progress in Materials Science*, **50**, 93-179 (2005)

36. H. Fukushima, "Graphite Nanoreinforcements in Polymer Nanocomposites", PhD Thesis, Michigan State University, 2003

37. D.D.L. Chung, "Revue. Exfoliation Graphite", *Journal of Materials Science,* **22** 12, 4190-4199, (1987)

38. A. Usuki, Y. Kojima, M. Kawasumi, A. Okada, Y. Fukushima, T. Kurauchi and O. Kamigaito, " Syntesis of Nylon 6-Clay Hydrid", *J. Mater. Res.*, **8**, 1179, (1993)

39. Y. Kojima, A. Usuki, M. Kawasumi, A. Okada, Y.Fukushima, T. Kurauchi, and O. Kamigaito, " Mechanical Properties of Nylon 6-clay hybrid", *J. Mater. Res.*, **8**, 5, 1185 (1993)

40. Y. Kojima, A. Usuki, M. Kawasumi, A. Okada, T. Kurauchi, and O. Kamigaito, "Synthesis of Nylon 6-Clay Hybrid by Montmorillonite Intercalated with e-Caprolactam", *J. Polym. Sci. A: Polym. Chem.*, **31**, 983 (1993)

41. P.B. Messersmith and E.P. Giannelis, "Polymer-Layered Silicate Nanocomposites:In Situ Intercalative Polymerization of e-caprolactone in Layered Silicates" *Chem. Mater.,* **5** 1064 (1993)

42. P.B. Messersmith and E.P. Giannelis, "Synthesis and Barrier Properties of Poly(å-Caprolactone)-Layered Silicate Nanocomposites", *Journal of Polymer Science, Part A:Polymer Chemistry*, **33**, 1047-57 (1995)

43. M.S. Wang and T.J. Pinnavaia, "Clay-Polymer Nanocomposites Formed from Acidic Derivatives of Montmorillonite and an Epoxy Resin" *Chem. Mater.,* **6**, 468 (1994)

44. P.B. Messersmith and E.P. Giannelis, "Synthesis and Characterization of Layered Silicate-Epoxy Nanocomposites", *Chem. Mater*, **6**, 1719 (1994)

45. T. Lan, and T.J. Pinnavaia, "Clay-Reinforced Epoxy Nanocomposites", *Chem. Mater.*, **6**, 2216 (1994)

46. E. Ruiz-Hitzky, and P. Aranda, "Polymer-Salt Intercalation Complexes in Layer Silicates", *Adv. Mater.* **2**, 545-547 (1990)

47. P. Aranda and E. Ruiz-Hitzky, "Poly(ethylene oxide)-silicate intercalation materials", *Chem. Mater.* **4**,1397 (1992)

48. J. Wu and M.M. Lerner, "Structural, Thermal and Electrical Characterization of Layered Nanocomposites Derived from Na-Montmorillonite and Polyethers", *Chem. Mater.* **5**, 835 (1993)

49. E.P. Giannelis, "Polymer Silicate Nanocomposites" *Adv. Mater.* **8**, 29-35, (1996)

50. K. Yano, A. Usuki, A. Okada, T. Kurauchi and O. Kamigaito, "Synthesis and Properties of polyimide-Clay Hybrid", *J. Polym Sci.: Part A:Polym. Chem.*, **31** 2493, (1993)

51. R.A. Vaia, S. Vasdevan, W. Krawiec, L.G. Scanlon and E.P. Giannelis, "New Polymer Electrolyte Nanocomposites-Melt Intercalation of Poly(Ethylene Oxide) in Mica-Type Silicates", *Adv Mater.*, **7**, 2 154 (1995)

52. R.A. Vaia, K.D. Jandt, E.J. Kramer and E.P. Giannelis, "Kinetics of Polymer Melt Intercalation", *Macromolecules*, **28** 8080 (1995)

53. Y. Kojima, K. Fukumori, A. Usuki, A. Okada and T. Kurauchi, "Gas Permeabilities in Rubber-Clay Hybrid", *J. Mater. Sci., Lett.*, **12** 889 (1993)

54. P. Reichert, H.Nitz, S. Klinke, R. Brandsch, R. Thomann, and R. Mulhaupt, "Polypropylene/Organoclay Nanocomposite Formation: Influence of Compatibilizer Functionality and Organocly Modification", *Macromol. Mater. Eng.*, **275**, 8 (2000)

55. M. Kawasumi, N. Hasegawa, M. Kato, A. Usuki and A. Okada, "Preparation and Mechanical Properties of Polypropylene-Clay Hybrids", *Macromolecules* **30**, 6333, (1997)

56. M. Kato, A. Usuki and A. Okada, "Synthesis of Polypropylene Oligomer-Clay Intercalation Compounds", *J. Appl. Polym. Sci.* **66** 1781, (1997)

57. M. Garcia-Leiner and A.J. Lesser, "Polymer-Clay Nanocomposites Prepared in Supercritical Carbon Dioxide", *Polymeric Materials: Science and Engineering,* **88** 92, (2003)

58. R.A. Vaia, K.D. Jandt, E.J. Kramer, and E.P. Giannelis, "Microstructural Evolution of Melt Intercalated Polymer-Organically Modified Layered Silicates Nanocomposites", *Chem. Mater.*, **8**, 2628, (1996)

59. A. Yasmin, J.L. Abot and I.M. Daniel, "Processing of Clay/Epoxy Nanocomposites by Shear Mixing", *Scripta Materialia* **49**, 81, (2003)

60. P. Calvert, "Nanotube Composites: A recipe for Strength", *Nature* **399**, 210 (1999)

61. D. Marc and M. Jacques, "Reinforced Polymers" European Patent Office, EP 1 054 036 A1, (2000)

62. http://www.zyvex.com/

63. X. Zhang, T. Liu, T.V. Sreekumar, S. Kumar, V.C. Moore, R.H. Hauge and R.E. Smalley, "Poly(vinyl alcohol)/SWVN Composite Film" *Nanoletters*, **3**, 9 1285, (2003)

64. D. Qian and E.C. Dickey, "Load Transfer and Deformation Mechanisms in Carbon Nanotube-Polystyrene Composites", *Applied Physics Letters* **76**, 20, 2868 (2000)

65. B. Safadi, R. Andrews and E.A. Grulke, "Multiwalled Carbon Nanotube polymer Composites: Synthesis and Characterization of Thin Films", *J. Appl. Polym. Sci.*, **84**, 14, 2660, (2002)

66. J.C. Kearns, and R.L. Shambaugh, "Polypropylene Fibers Reinforced with Carbon Nanotubes", *Journal of Applied Polymer Science* **86**, 2079, (2002)

67. T. Liu, T.V. Sreekumar, S. Kumar, R.H. Hauge and R.E. Smalley, "SWNT/PAN Composite Film-based Supercapacitors", *Letter to the Editor/Carbon* **41**, 2427 (2003)

68. Z. Jia, Z. Wang, C. Xu, J. Liang, B. Wei, D. Wu and S. Zhu, "Study on Poly(methyl methacrylate)/Carbon Nanotube Composites", *Mater. Sci. Eng. A*, **271**, 395 (1999)

69. C. Park, Z. Ounaies, K.A. Watson, R.E. Crooks, J. Smith Jr., S.E. Lowther, J.W. Connell, E.J. Siochi, J.S. Harrison, and T.L. St.Clair, "Dispersion of single wall carbon nanotubes by in situ polymerization under sonication", *Chem Phys Lett*, **370**, 820 (2003)

70. W. Tang, M. Santare, and S. Advani, "Melt processing and mechanical property characterization of multi-walled carbon nanotube/high density polyethylene (MWNT/HDPE) composite films" *Carbon* **41**, 2779 (2003)

71. T. Liu, I-Y. Phang, L. Shen, S.Y. Chow and W-D. Zhang, "Morphology and Mechanical Properties of Multiwalled Carbon Nanotubes Reinoforced Nylon-6 Composites", *Macromolecules*, (2004)

72. H. Ma, J. Zeng, M-L. Realff, S. Kumar and D.A. Schiraldi, "Processing, Structure, and Properties of Fibers from Polyester/Carbon Nanofiber Composites", *Composites Science and Technology*, **63**, 1617 (2003)

73. J.W. Aylsworth, "Expanded Graphite and Composition Thereof', US Patent 1,137373 (1915)

74. J.W. Aylsworth, "Expanded Graphite" US Patent 1,191,383 (1916)

75. V.F. Lincoln and Z. Claude, "Organic Matrix Composites Reinoforced with Intercalated Graphite" US Patent 4,414,142 (1983)

76. A. Celzard, E. McRae, J.F. Marache, G.Furdin, M, Dufort and C. Deleuze, "Composites based on Micron-Sized Exfoliated Graphite particles: Electrical Conduction, Critical Exponents and Anisotropy", *J. Phys. Chem Solid*, **57** 6-8, 715 (1996)

77. Y.S. Wang, M.A. O'Gurkis and J.T. Lindt, "Electrical Properties of Exfoliated-Graphite Filled Polyethylene Composites", *Polymer Composites*, **7**,5 349 (1996)

78. I. Krupa, I. Chodak, "Physical Properties of Thermoplastic-Graphite Composites", *European Polymer Journal*, **37** 2159 (2001)

79. W. Zheng, X. Lu and S-C. Wong, "Electrical and Mechanical Properties of Expanded Graphite-Reinforced High-Density Polyethylene", *Journal of Applied Polymer Science*, **91** 2781 (2004)

80. M.L. Clingerman, J.A. King, K.H. Schulz and J.D. Meyers, "Evaluation of electrical Conductive models for Conductive polymer Composites", *Journal of Applied Polymer Science*, **83**, 1341 (2002)

81. W-G. Weng, G-H. Chen, D-J. Wu and W-L Yan, "HDPE/Expanded Graphite Electrically Conducting Composite", *Composite Interfaces*, **11**, 2, 131 (2004)

82. W. Zheng, S-C Wong and H-J. Sue, "Transport Behavior of PMMA/Expanded Graphite Nanocomposites", *Polymer*, **73** 6767 (2002)

83. W. Zheng and S-C. Wong, "Electrical Conductivity and Dielectric Properties of PMMA/Expanded Graphite Composites", *Composites Science and Technology,* **63**, 225 (2003)

84. J-W. Shen, X-M. Chen and W-Y. Huang, "Structure and Electrical Properties of Grafted polypropylene/Graphite Nanocomposites Prepared by Solution Intercalation", *Journal of Applied Polymer Science*, **88** 1864 (2003)

85. Y-X, Pan, Z-Z. Yu, Y-C Ou and G-H Hu, "A New Process of Fabricating Electrically Conducting Nylon 6/Graphite Nanocomposites via Intercalation Polymerization", *Journal of Polymer Science:Part B: Polymer Physics*, **38** 1626 (2000)

86. J-F Zou, Z-Z. Yu, Y-X. Pan, X-P Fang and Y-C Ou, "Conductive Mechanism of Polymer/Graphite Conducting Composites with Low Percolation Threshold", *Journal of Applied Polymer Science,* **40** 954, (2002)

87. G-H. Chen, D-J. Wu, W-G Weng, B. He and W-L Yan, "Preparation of Polystyrene-Graphite Conducting Nanocomposites via Intercalation Polymerization", *Polymer International*, **50**, 980 (2001)

88. G-H. Chen, D-J. Wu, W-G Weng, and W-L Yan, "Preparation of Polymer/Graphite Conducting Nanocomposite by Intercalation Polymerization", *Journal of Applied Polymer Science*, **82** 2506, (2001)

89. X.S. Du, M. Xiao and Y.Z. Meng, "Synthesis and Characterization of polyaniline/Graphite Conducting Nanocomposites", *Journal of Polymer Science: Part B: Polymer Physics*, **42**, 1972 (2004)

90. H. Fong, W. Liu, C-S. Wang and R.A. Vaia, "Generation of Electrospun Fibers of Nylon 6 and Nylon 6-Montmorillonite Nanocomposite", *Polymer,* **43** 775 (2002)

91. J. Mack, L. Viculis, R. luoh, R. Kaner, T. Hahn, A. Ali, G. Yang and F. Ko, "Nanocomposite Fibrils From Graphite Nanoplatelets", Proceedings of the 14th International Cdonference on Composite Materials, San Diego, California, July 14-18, (2003)

92. D.D.L. Chung, "Composites of In-situ Exfoliated Graphite", US Patent, 4,946,892 (1990)

93. P. Xiao, M. Xiao and K. Gong, "Preparation of Exfoliated Graphite/Polystyrene Composite by Polymerization-Filling Technique", *Polymer* **42**, 4813 (2001)

94. "Surface Analysis-The principal Techniques" edited by J.C. Vickerman, John Wiley and Sons Ltd, chapter 1, 9, (1997)

95. "Handbook of Nanophase and Nanostructured Materials: Characterization" edited by Z-L Wang, Y.Liu and Z. Zhang, Kluwer Academic/Plenum Publishers, Tsinghua University Press, chapter 1, (2003)

96. Y.Kojima, A.Usuki, M.Kawasumi, A.Okada, T.Kurauchi, and O.Kamigaito, "Sorption of Water in Nylon 6-Clay Hybrid" *Journal of Applied Polymer Science*, **49**, 1259 (1993)

97. A. Usuki, A.Koiwai, Y.Kojima, M.Kawasumi, A.Okada, T.Kurauchi and O.Kamigaito, "Interaction of Nylon 6-Clay Surface and Mechanical Properties of Nylon 6-Clay Hybrid", *Journal of Applied Polymer Science*, 55 119 (1995)

98. P. Svoboda, C. Zeng, H. Wang, L.J. Lee and D.L. Tomasko, "Morphology and Mechanical Properties of Polypropylene/Organoclay Nanocomposites", *Journal of Applied Polymer Science*, **85**, 1562 (2002)

99. M.R. Piggott, "Load Bearing Fibre Composites", Pergamon Press, chapter 8, (1980)

100. S. Kumar, H. Doshi and M. Srinivasarao, J.o. Park and D.A. Schiraldi, "Fibers from Polypropylene/Nano Carbon Fiber Composites", *Polymer,* **43** 1701 (2002)

101. S. Kumar, T.D. Dang, F.E. Arnold, A.R. Bhattacharyya. B.G. Min, X. Zhang, R.A. Vaia, C. Park, W.W. Adams, R.H. Hauge, R.E. Smalley, S. Ramesh, and P.A. Willis, "Synthesis, Structure, and Properties of PBO/SWNT Composites", *Macromolecules,* **35** 9039 (2002)

102. T.V. Sreekumar, T. Liu, B.G. min, H. Gou, S. Kumar, R.H. Hauge and R.E. Smalley, "Polyacrylonitrile Single-Walled Carbon Nanotube Composite Fibers" *Advanced Materials*, **16**, 58 (2004)

103. F. Du, R.C. Scogna, W. Zhou, S. Brand, J.E. Fischer, and K.I. Winey, "Nanotube Networks in polymer Nanocomposites: Rheology and Electrical Conductivity", *Macromolecules* (2004)

104. L. M Sherman, "Chasing Nanocomposites", Plastics Technology, Online Article can be found in http://www.plasticstechnology.com/articles/200411fa2.html

105. A. Yasmin and I. M. Daniel, "Mechanical and Thermal Properties of Graphite Platelet/Epoxy Composites", *Polymer* **45** 8211, (2004)

106. D. Shia, C.Y. Hui, S.D. Burnside and E.P. Giannelis, "An Interface model for the Prediction of Young's Modulus of Layered Silicate-Elastomer Nanocomposites", *Polymer Composites*, **19** 5, 608 (1998)

107. S.D. Burniside and E.P. Giannelis, "Synthesis and properties of new poly(dimethylsiloxane) nanocomposites" ***Chem***. *Mater*., **7** 1597 (1996)

108. S. R. Broadbent and J. M. Hammersley, *Proc. Camb.Phil. Soc.,* **53**, 3, 629 (1957)

109. D. Stauffer, "Introduction of Percolation Theory", Taylor and Francis, London (1985)

110. R. Zallen, In the Physics of Amorphous Solids; Wiley: New York, p135 (1983)

111. P. Banerjee and B.M. Mandal, "Conducting polyaniline Nanoparticle Blends with Extremely Low Percolation Thresholds", *Macromolecules* **28**, 3940, (1995)

112. X. Jing, W. Zhao, and L. Lan, "The Effect of Particle Size on Electric Conducting Percolation Threshold in Polymer/Conducting particle Composites", *Journal of Materials Science Letters* **19**, 377 (2000)

113. D.M. Bigg, "The Effect of Compounding on the Conductive Properties of EMI Shielding Compounds", *Advances in Polymer Technology*, **4**, 255, (1984)

114. H. S. Gokturk, T. J. Fiske, and D. M. Kalyon, "Effects of Particle Shape and Size Distributions on the Electrical and Magnetic Properties of Nickel/Polyethylene composites", *Journal of Applied Polymer Science*, **50**, 1891 (1993)

115. T.J. Fiske, H.S. Gokturk and D.M. Kalyon, "Percolation in Magnetic Composites", *Journal of Materials Science* **32**, 5551, (1997)

116. J. A. Heiser, J.A. King, J. P. Konell and L. L. Sutter, "Electrical Conductivity of carbon Filled Nylon 6,6", *Advances in Polymer Technology*, **23**, 2, 135 (2004)

117. I. Chodak, M. Omastova and J. Pionteck, "Relation Between Electrical and mechanical Properties of Conducting polymer composites", *Journal of Applied Polymer Science*, **82**, 1903, (2001)

118. X-M. Chen, J-W. Shen, W-I. Huang, "Novel Electrically Conductive Polypropylene/Graphite Nanocomposites", *Journal of Materials Science Letters*, **21**, 213 (2002)

119. I. Chodak and I. Krupa, "Percolation Effect and Mechanical Behavior of Carbon Black Filled Polyethylene", *Journal of Materials Science Letters*, **18** 1457, (1999)

120. S. Kirkpatrick, "Percolation and Conduction", *Rev Mod Phys* **45** 574, (1973)

121. F. Bueche, "Electrical resistivity of conducting particles in an insulating matrix", *J Applied Phys* **43** 4837 (1972)

122. D. S. McLachlan, M. Blaszkiewicz, R. E. Newnham, "Electrical Resistivity of Composites", *J. Am Cerm Soc* **73**, 2187 (1990)

123. E. P. Mamunya, V.V. Davidenko, and E. V. Lebedev, "Effect of polymer-filler interface interactions on percolation conductivity of thermoplastics filled with carbon black", *Compos Interf.* **4** 169, (1997

124. L. Nielsen, *Ind Eng Chem Fundam* **13**, 17 (1974)

125. P. Keblinski, S Phillpot, S. Choi and J. Eastman, "Mechanics of heat flow in suspensions of nano-sized particles (nanofluids), *International Journal of Heat and Mass Transfer* **45,** 855-863, (2002)

126. Y. Agari and T. Uno, "Thermal Conductivity of Polymer Filled with Carbon Materials: Effect of Conductive Particle Chains on Thermal Conductivity", *Journal of Applied Polymer Science*, **30** 2225 (1985)

127. Y. Agari, T. Uno, "Estimation on Thermal Conductivities of Filled polymers", *Journal of Applied Polymer Science*, **32** 5705 (1986)

128. Y. Agari, M. Tanaka and S. Nagai, "Thermal Conductivity of a Polymer Composite Filled with Mixtures of Particles", *Journal of Applied Polymer Science*, **34** 1429, (1987)

129. Y. Agari, A. Ueda, M. Tanaka and S. Nagai, "Thermal Conductivity of a Polymer Filled with particles in the Wide Range from Low to Super-High Volume Content", *Journal of Applied Polymer Science*, **40** 929, (1990)

130. Y. Agari, A. Ueda and S. Nagai, "Thermal Conductivities of Composites in Several Types of Dispersion Systems", *Journal of Applied Polymer Science*, **42** 1665, (1991)

131. Y. Agari, A. Ueda and S. Nagai, "Thermal Conductivity of a Polyethylene Filled with Disoriented Short-Cut Carbon Fibers", *Journal of Applied Polymer Science*, **43** 1117 (1991)

132. J. King, K. Tucker, B. Vogt, E. Weber and C. Quan, "Electrically and Thermally Conductive Nylon 6,6", *Polymer Composites* **20**, 5, 643 (1999)

133. J. King, K. Tucker, J. Meyers, E. Weber, M. Clingerman and K. Ambrosius, "Factorial Design Approach to Electrically and Thermally Conductive Nylon 6,6", *Polymer Composites* **22**, 1, 142 (2001)

134. E. Weber, M. Clingerman and J. King, "Thermally Conductive Nylon 6,6 and Polycarbonate Based Resins. I. Synergistic Effects of Carbon Fillers", *Journal of Applied Polymer Science,* **88**, 112 (2003)

135. E. Weber, M. Clingerman and J. King, "Thermally Conductive Nylon 6,6 and Polycarbonate Based Resins. II. Modeling", *Journal of Applied Polymer Science,* **88**, 123 (2003)

136. T. Kurauchi, A.Okada, T.Nomura, T.Nishio, S.Saegusa, and R.Deguchi, *SAE Technical Paper Ser,* 910584 (1991)

137. http://www.plasticstechnology.com/articles/200110fa3.html

138. From applied science http://www.apsci.com/

139. http//www.pittstate.edu/services/nsfreu/ResearchReports2004/dweberfuelcellicce11submit.pdffgh

140. http://www.dow.com/polyolofins/about/pptectr/prime/typical.htm

CHAPTER 2

MATERIALS AND PROCESSING OF NANOCOMPOSITES

2.1 Materials

2.1.1 Matrix-Polypropylene

A polypropylene resin was chosen as the baseline matrix for this research.

Polyolefins and especially polypropylene (PP), are the most widely used thermoplastics due to their well-balanced physical and mechanical properties, easy processing and recycle characteristics which combined with their low cost makes them a versatile material [1].

In addition, PP has a lower density, in comparison to other engineering thermoplastics, allowing for potential weight reductions. PP also has very good heat resistance and high resistance to solvents and other chemicals and can be used in very harsh environments. Due to its higher crystallinity, polypropylene has excellent moisture barrier properties and good optical properties [2].

Finally, PP can be used as a model to provide insight into the interaction between xGnP and other semi-crystalline polymers. The polymer used in this research is polypropylene powder with the trade name Pro-fax 6301 (melt flow index 12 g/10min, ASTM D1238) which was kindly supplied by Basell [3].

2.1.2 Exfoliated Graphite Nanoplatelets

The exfoliated graphite nanoflakes are produced as follows: First, a sulfuric acid-based intercalated graphite, in this case obtained from UCAR International Inc, in the form of a thick platelets as shown in Figure 2.1, is heated in a microwave oven. This results in a cost and time effective exfoliation process as initially proposed by Fukushima [4]. The graphite rapidly heats and the entrapped intercalants vaporize as a result of the coupling of the conductive graphite to the microwave radiation and the graphite flake particles undergo significant expansion (~500 times). The result of this exfoliation process is a worm-like or accordion-like expanded structure as shown in Figure 2.2

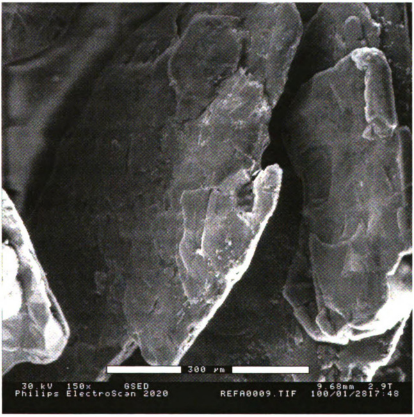

Figure 2.1. ESEM micrograph of as received acid intercalated graphite (scale bar 300µm)

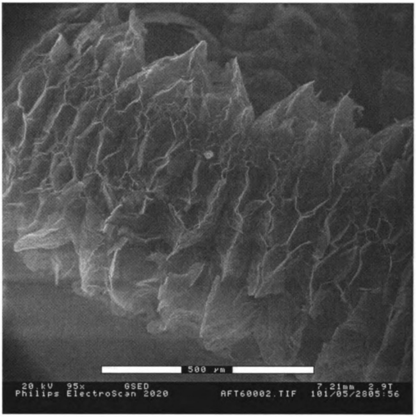

Figure 2.2:ESEM micrograph of microwave expanded graphite (scale bar 500μm)

The next step is to break down the worm-like structure in order to obtain individual graphite sheets. This is done by pulverization using an ultrasonic processor which results in graphite nanoflakes that are less than 10nm thick and have a diameter of ~15um. Their diameter can be further reduced by milling using a vibratory mill, resulting thus in nanoflakes with the same thickness but with diameter less than 1um. In this way, two types of graphite nanoflakes are produced which differ in their aspect ratio. Figures 2.3 and 2.4 show the 15μm (xGnP-15) and 1μm (xGnP-1) exfoliated graphite nanoplatelets respectively.

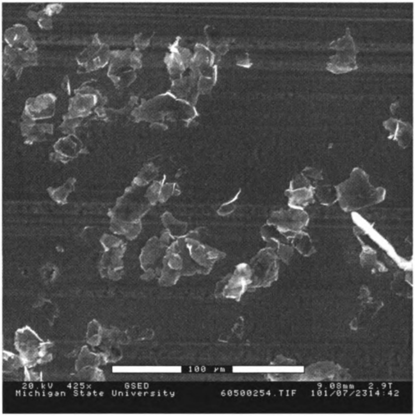

Figure 2.3. ESEM micrographs of exfoliated graphite nanoflakes 15µm, xGnP-15

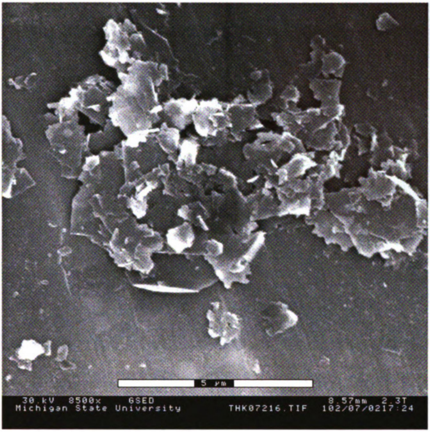

Figure 2.4. ESEM micrographs of milled graphite nanoflakes 1μm, xGnP-1

The thickness of the nanoflakes was determined using TEM and it is shown in Figure 2.5 and 2.6. As indicated in Figure 2.6, which shows two adjacent nanoflakes, each nanoplatelet consists of more than 10 graphene sheets. Taking into account that the basal plane distance of graphite is 0.335nm [5] it is estimated that the average thickness of the graphite nanoflakes is ~5nm with a distribution of platelets having thicknesses in the nanometer range expected.

Figure 2.5: TEM images of xGnP-1, the scale bar is 50nm

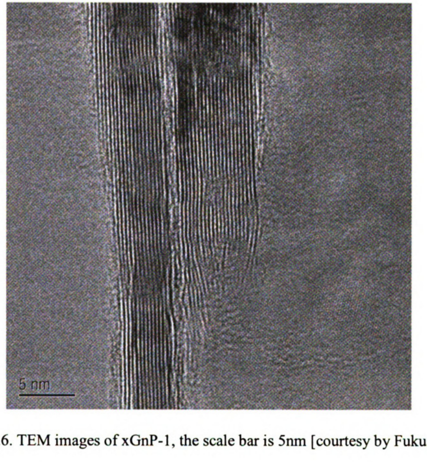

Figure 2.6. TEM images of xGnP-1, the scale bar is 5nm [courtesy by Fukushima]

2.1.3 Carbon Reinforcements and Clays

The control carbon materials used for comparison with the xGnP were (i) PAN based carbon fiber (PANEX 33 MC Milled Carbon Fibers, Zoltek Co), (ii) VGCF (Pyrograf III, PR-19 PS grade, Pyrograf Products, Inc.) and (iii) nanosize High Structure carbon black (KETJENBLACK EC-600 JD, Akzo Novel Polymer Chemicals LLC). It is noted that this is a special highly conductive carbon black. The clays used are Octadecyl amine (ODA) modified montmorillonite (Nanomer I.30P from Nanocor). The geometrical and surface characteristics of all the reinforcements used are given in Table 2.1. ESEM micrographs of these materials are shown in Figures 2.7-2.9.

Table 2.1: Geometrical and surface characteristics of conductive fillers

Material	Length (μm)	Diameter (μm)	Aspect Ratio	Surface Area (m^2/g)	Density (g/cm^3)	Cost ($/lb)
xGnP-1	<0.01	<1	<100	100	2	<5
xGnP-15	<0.01	15	~1500	100	2	<5
PAN CF	175	7.2	~24	16	1.81	5-6
VGCF	50-100	0.15	300-700	25	2	40-50
Carbon Black	0.4-0.5	0.4-0.5	1	1400	1.8	12
Clays	0.05	10-25	300		2.85	

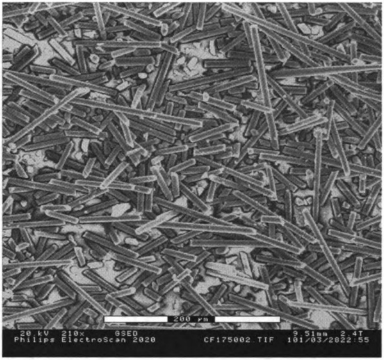

Figure 2.7: ESEM images of chopped carbon fiber (scale bar 200µm)

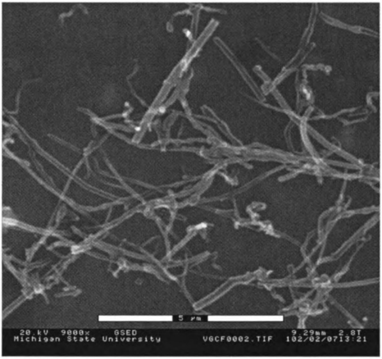

Figure 2.8: ESEM images milled VGCF (scale bar 5µm)

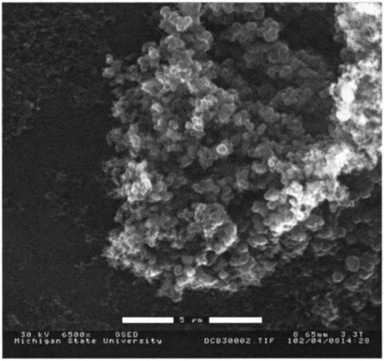

Figure 2.9: ESEM image of nano-size carbon black (scale bar 5μm)

2.2 Processing of Nanocomposites

2.2.1 Melt-mixing and Injection Molding

The basic fabrication method used in this project is melt-mixing due to its simplicity and compatibility with existing polymer processing techniques such as extrusion, injection molding and compression molding.

The nanocomposites were fabricated by melt mixing in a DSM Micro 15cc Compounder, (vertical, co-rotating twin-screw microextruder), at 180 °C for 3 minutes at a screw speed of 200rpm, which is shown in Figure 2.10. The injection-molded samples were made using a Daca Micro Injector. The cylinder temperature was 180 ^{0}C and the mold temperature used was 80 ^{0}C. An injection pressure of 160 psi was used. The injection molder and the molds used are shown in Figure 2.11a and 2.11b respectively.

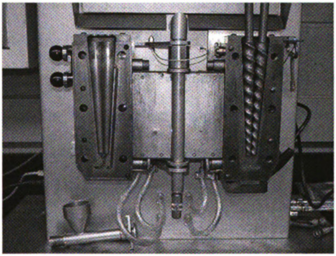

Figure 2.10: DSM twin-screw microextruder (10g capacity) and feeder

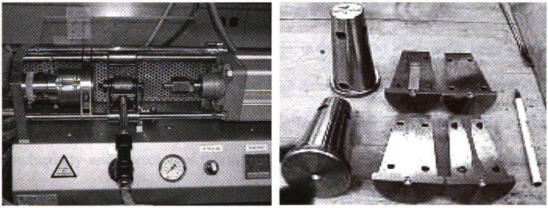

Figure 2.11. a) DSM injection molder and b) tensile and flex molds

It is noted that the DSM equipment used is sufficient for screening experiments but has limitations when trying to relate this to a larger scale extruder-injection molder system. For instance, the maximum allowable packing pressure during injection molding is 160psi, which is much lower than the pressure used normally with large size injection molding systems. This means that the degree of orientation and alignment of the reinforcements in the DSM composites is smaller indicating that the performance of nanocomposites made using DSM may be limited by this processing system.

In an effort to identify the operating conditions of the DSM system that maximize the flex strength of the graphite-polypropylene nanocomposites a 2^3 factorial experimental design was used. The conditions that were optimized were (i) mixing time, (ii) barrel temperature and (iii) temperature of the mold. These conditions were optimized with respect to the flexural strength and modulus of the neat polymer as well as of 3 vol% xGnP-1/PP nanocomposites. The conditions mentioned above resulted from the factorial analysis presented in Chapter 3.

2.2.2 Solution Processing of Nanocomposites

The solution approach, while feasible, in the case of PP requires large amounts of solvents such as toluene or xylene and high temperatures that are neither practical nor safe. However, in order to understand the effect of fabrication method on the electrical conductivity and percolation threshold of xGnP-PP composites, a limited number of samples were also fabricated using the solution approach, a modified version of the one proposed by Shen *et al* [6]. The xGnP were dispersed in xylene using sonication for 2hrs and the PP was dissolved in refluxing xylene at 130 °C for 0.5 hrs. The graphite suspension was added drop wise to the PP solution and after refluxing for 1.5hrs it was filtered. When the temperature dropped to about 70 °C the solution precipitated by addition of acetone, filtered, and dried in vacuum oven. The resulting composite powder was used for compression and injection molding.

2.2.3 Processing by Premixing by Coating of Polypropylene with Graphite

Premixing of graphite and polypropylene in presence of isopropyl alcohol is a new compounding method developed in our lab. The xGnP is dispersed in isopropyl alcohol (IPA) by sonication for 1 hour at room temperature. The PP powder is added to the solution and sonication is continued for 0.5 hrs. Finally, the solvent is evaporated at 80°C resulting in complete coverage of the powder particles with the xGnP. Alternatively, the isopropyl alcohol can be recycled by using filtration and reused. Thus, this new premixing method can be environmental friendly and more cost and time effective compared to the solution approach. The main advantage of this method is that sonication breaks down the xGnP agglomerates and the thick xGnP-IPA solution covers the PP particles very efficiently resulting in a homogeneous xGnP coated PP powder that is used for compression molding. Micrographs of the uncompressed neat polymer powder and xGnP-15 coated PP at 0.2 wt% are shown in Figures 2.12 to 2.13.

2.2.4 Compression Molding

The compression-molded samples were made using the composite pellets or powder obtained by the melt mixing or solution and premixing method. The conditions used are at 200 °C for 20 minutes with no pressure applied and 200 °C for 20 minutes under pressure ~35000 psi. During the compression molding vacuum was applied to remove any trapped air.

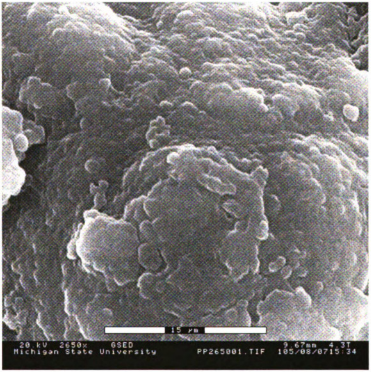

Figure 2.12. ESEM image of polypropylene particle (scale bar 15μm)

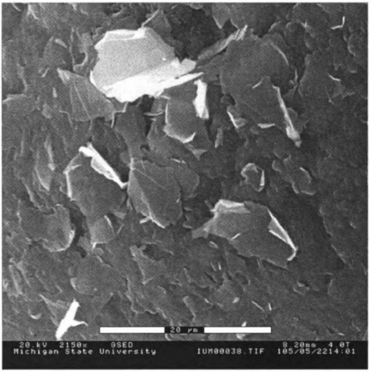

Figure 2.13. ESEM image of 0.2wt% xGnP-15 coated PP (scale bar 20μm)

As mentioned, the basic fabrication method used in this research is melt mixing through a twin-screw extruder followed by injection molding. The processing conditions used such as the temperature of the barrel, the screw speed, the processing time and the temperature of the mold were optimized using factorial design of experiments which is presented in Chapter 3.

The mechanical properties and morphological characterization of the polypropylene based nanocomposites are presented Chapter 4, followed by the thermal, barrier and rheological properties of xGnP/PP shown in Chapter 5. The electrical conductivity and percolation threshold of xGnP/PP nanocomposites are discussed in Chapter 6 whereas the effect of xGnP on the PP crrystallinity is presented in Chapter 7. Finally, a study on the improvement of the xGnP-PP interfacial adhesion is presented in Chapter 8.

2.3 References

1. http://www.dow.com/polyolefins/about/pptechctr/primer/typical.htm

2. L. Valentini, J. Biagiotti, J.M. Kenny and M.A. Lopez Manchado, "Physical and Mechanical Behavior of Single-Walled Carbon Nanotube/Polypropylene/Ethylene-Propylene-Diene Rubber Nanocomposites", Journal of Applied Polymer Science, 89, 2657 (2003)
3. http://www.basell.com/portal/site/basell/

4. H. Fukushima, "Graphite Nanoreinforcements in Polymer Nanocomposites", PhD Thesis, Michigan State University, 2003

5. W.N. Reynolds, "Physical Properties of Graphite" Elsevier Publishing Co. Ltd, pp 1- (1968)

6. J-W. Shen, X-M. Chen and W-Y. Huang, "Structure and Electrical Properties of Grafted polypropylene/Graphite Nanocomposites Prepared by Solution Intercalation", *Journal of Applied Polymer Science*, **88** 1864 (2003)

CHAPTER 3

DETERMINATION OF OPTIMIZED CONDITIONS DURING MELT-MIXING AND INJECTION MOLDING OF NANOCOMPOSITES USING FACTORIAL DESIGN OF EXPERIMENTS

3.1 Introduction

One of the objectives of this project is to use experimental design to determine the optimum operating conditions of the twin-screw microextruder-injection molder system, which is used for the fabrication of xGnP-PP nanocomposites. The goal is to seek the combination of values of the various processing conditions i.e., mixing time, screw speed, barrel temperature, temperature of the mold, and gap distance between the screws and the bottom of the barrel that will result in composites with the maximum flexural strength and modulus of elasticity.

Factorial design experiments are more efficient than performing one-factor-at-a-time experiments because they allow for evaluation of the effects of several variables simultaneously minimizing thus the total number of necessary experiments. Additionally, the use of factorial designs can prevent the misinterpretation of data that can occur when interaction effects are present in an experiment. Another advantage of using factorial design is that it provides a good prediction of the response over the range of the experiments since the effect of a change in the level of each factor is estimated at several levels of the other factors [1]. By using factorial design, it's possible to determine the effect that each factor (processing parameter) has on the system (PP and xGnP-PP composites) by calculating a single value to quantify the system's performance (flexural strength and modulus of elasticity).

The simplest class of factorial design is the two-level factorial design referred to as 2^k factorial because k factors are considered at two levels each. In this project with $k=3$, eight factor-level combinations are indicated. For each combination three observations (n) were made. The factorial design employed in this project is presented as a two-step process (i) evaluate the effect of the factors on the variable under consideration by using analysis of variance and (ii) predict the response of the system over the range defined by the low and high values of each factor by a regression model.

3.1.1 Analysis of Variances

In order to separate and evaluate the effects of the factors (i.e., temperature of the mold, barrel temperature and screw speed) on the observed variable (flexural properties) a three-way analysis of variances is used. This statistical method, which is the "structure" of factorial experiments, allows for evaluating the statistical significance of data and the conclusions derived from them within a defined limit of confidence [1,2].

The analysis of variances (ANOVA) was performed using Microsoft Excel 2000. The F statistic test was used. Both the F-statistical table and the analytical calculations for ANOVA can be found in *Appendix A* and *Appendix B* respectively. The algorithm for the analysis of variance computations is presented in Table 3.1. Once all the entries in Table 3.1 are computed, the F_o value for each effect is compared to the F^* value obtained using the F-statistics table for the given degrees of freedom and a confidence level of 5%.

Any effect for which $F_o/F^* > 1$ is significant. If $F_o/F^* < 1$ it means that there is insufficient statistical evidence for the particular effect.

Table 3.1: The Analysis of Variance Table for a 2^3 factorial design [3]

Effect (Source of Variance)	Degrees of freedom (df)	Sum of Squares	Mean Square (SS/df)	F_o
Factor A	a-1	SS_A	MS_A	MS_A/MS_E
Factor B	b-1	SS_B	MS_B	MS_B/MS_E
Factor C	c-1	SS_C	MS_C	MS_C/MS_E
AxB	(a-1)(b-1)	SS_{AB}	MS_{AB}	MS_{AB}/MS_E
AxC	(a-1)(c-1)	SS_{AC}	MS_{AC}	MS_{AC}/MS_E
BxC	(b-1)(c-1)	SS_{BC}	MS_{BC}	MS_{BC}/MS_E
AxBxC	(a-1)(b-1)(c-1)	SS_{ABC}	MS_{ABC}	MS_{ABC}/MS_E
Error	$abc(n$-1)	SS_E	MS_E	
Total	(abn-1)	SS_{TOTAL}		

where

A, B and C represent the three factors (main effects)

AB, BC, AC: two-factor interaction

ABC: three-factor interaction

$a=b=c=2$ number of levels of A, B and C factors respectively

$n=3$ observations per factor level combination.

The sums of squares for the main effects are calculated as follows

$$SS_A = \frac{1}{bnc}\sum_{i=1}^{a} y_{i...}^2 - \frac{y_{....}^2}{abnc} \tag{3.1}$$

$$SS_B = \frac{1}{anc}\sum_{j=1}^{b} y_{j...}^2 - \frac{y_{....}^2}{abnc} \tag{3.2}$$

$$SS_C = \frac{1}{abn}\sum_{k=1}^{c} y_{k...}^2 - \frac{y_{....}^2}{abnc} \tag{3.3}$$

where $y_{i...}$, $y_{j...}$, and $y_{k...}$ are the total of all observations under the *i*th, *j*th and *k*th level of factor *A*, *B* and *C* respectively and $y_{....}$ is the overall total of all observations.

The two-factor interaction sums of squares are calculated from

$$SS_{AB} = \frac{1}{nc}\sum_{i=1}^{a}\sum_{j=1}^{b} y_{ij..}^2 - \frac{y_{....}^2}{abnc} - SS_A - SS_B \tag{3.4}$$

$$SS_{AC} = \frac{1}{nb}\sum_{i=1}^{a}\sum_{k=1}^{c} y_{i.k.}^2 - \frac{y_{....}^2}{abnc} - SS_A - SS_C \tag{3.5}$$

$$SS_{BC} = \frac{1}{na}\sum_{j=1}^{b}\sum_{k=1}^{c} y_{.jk.}^2 - \frac{y_{....}^2}{abnc} - SS_B - SS_C \tag{3.6}$$

The three-factor interaction sum of squares is computed as follows

$$SS_{ABC} = \frac{1}{n}\sum_{i=1}^{a}\sum_{j=1}^{b}\sum_{k=1}^{c} y_{ijk.}^2 - \frac{y_{....}^2}{abnc} - SS_A - SS_B - SS_C - SS_{AB} - SS_{AC} - SS_{BC} \tag{3.7}$$

Finally the total sum of squares is defined as

$$SS_T = \sum_{i=1}^{a}\sum_{j=1}^{b}\sum_{k=1}^{c}\sum_{l=1}^{n} y_{ijkl}^2 - \frac{y_{....}^2}{abnc} \tag{3.8}$$

3.1.2 Regression Model

In a 2^3 factorial design the results of the experiments can be expressed in terms of a regression model as follows

$$Y = \beta_0 + \beta_A x_A + \beta_B x_B + \beta_{AB} x_A x_B + \beta_C x_C + \beta_{AC} x_A x_C + \beta_{BC} x_B x_C + \beta_{ABC} x_A x_B x_C \quad (3.9)$$

where

β_0 the overall mean

β*'s* are the regression coefficients

x*'s* are coded variables, one for each main effect

The coded variables are calculated based on the real variable as follows

$$x_A = \frac{A - (A_{low} + A_{high})/2}{(A_{high} - A_{low})/2} \quad (3.10)$$

x_B and x_C are defined by Equation (3.10) as well, with the difference that A is substituted by B and C respectively.

In order to calculate the regression coefficients β's, the various effects main and secondary are needed. To calculate the effects and also keep the analysis simple the eight experimental runs in the design are labeled using lower case letters as shown in Table 3.2. The high level of a factor is denoted by the corresponding lowercase letter and the low level by the absence of the corresponding letter i.e., the treatment combination labeled as *a* means that factor *A* was at its high level (+) while *B* and *C* at their low level (-). By convention (*1*) is used to denote all three factors at the low level.

Table 3.2: Notation of Treatment Combinations and Signs for Calculating Effects in the 2^3 Design[3]

Experimental run #	Treatment Combination	Factorial Design Effects						
		A	*B*	*C*	*AB*	*AC*	*BC*	*ABC*
1	*1*	-	-	-	+	+	+	-
2	*a*	+	-	-	-	-	+	+
3	*b*	-	+	-	-	+	-	+
4	*c*	-	-	+	+	-	-	+
5	*ab*	+	+	-	+	-	-	-
6	*ac*	+	-	+	-	+	-	-
7	*bc*	-	+	+	-	-	+	-
8	*abc*	+	+	+	+	+	+	+

The main effect A is calculated as follows

$$A = \bar{y}_{A^+} - \bar{y}_{A^-} \tag{3.11}$$

where

$\bar{y}_{A^+}$ is the average response of the four runs where A is at the high level (+)

$\bar{y}_{A^-}$ is the average response of the four runs where A is at the low level (-)

Using the notation for the experimental runs presented in Table 3.2 Equation (3.11) can be written as

$$A = \frac{1}{4n}[a + ab + ac + abc - (1) - b - c - bc] \tag{3.12}$$

Similarly, the effect of B is the difference in the average responses between the four treatment combinations with B at the high level (+) and the four combinations with

B at the low level (-). Applying the same concept for the rest of the effects C, AB, AC, BC and ABC the resulted equations are

$$B = \frac{1}{4n}[b + ab + bc + abc - (1) - a - c - ac] \tag{3.13}$$

$$C = \frac{1}{4n}[c + ac + bc + abc - (1) - a - b - ab] \tag{3.14}$$

$$AB = \frac{1}{4n}[abc + ab + (1) + c - ac - bc - a - b] \tag{3.15}$$

$$AC = \frac{1}{4n}[abc + ac + (1) + b - ab - bc - a - c] \tag{3.16}$$

$$BC = \frac{1}{4n}[abc + bc + (1) + a - ac - ab - c - b] \tag{3.17}$$

$$ABC = \frac{1}{4n}[abc + a + b + c - (1) - ac - bc - ab] \tag{3.18}$$

Once the effects are calculated the regression coefficients can be determined as follows

$$\beta_A = A/2,\ \beta_B = B/2, \text{etc.} \tag{3.19}$$

The error or residual sum of squares of the regression model is composed of a "pure error" component due to replication and a "lack of fit" component due to the interactions that were dropped from the model. The error introduced by the model, given in Equation (20), measures the proportion of the total variability explained by the model

$$R^2 = \frac{SS_{Model}}{SS_{Total}} \tag{3.20}$$

3.2. Selection of Factors and Factor Levels for the 2^3 Design

The processing parameters of the twin-screw microextruder-injection molder that can be controlled by the operator and are considered as the "factors" in the design are: (i) the temperature of the barrel, (ii) the temperature of the mold, (iii) the rotation screw speed, (iv) the mixing time and (v) the gap distance between the screws and the bottom of the barrel.

If all five parameters are considered simultaneously a 2^5 factorial design has to be used which complicates the analysis of the data. For reasons of simplicity the project is divided into two parts keeping the screw-barrel gap distance constant each time i.e., small gap distance (SG) in the first part and large gap distance (LG) in the second. In addition, preliminary experiments (results are presented in Appendix C) using the LG screw configuration were performed that showed that mixing time has no effect, at least in the range of values used, on the flexural strength and modulus of elasticity of the xGnP-PP nanocomposites. These mechanical properties, which are determined experimentally, are the dependent variables of the factorial design and the goal is to find the right combination of operating conditions, single point or operating window, which will maximize these properties.

The factors and the two levels at which each factor was tested are shown in Table 3.3 and Table 3.4 for the SG and LG screw configuration respectively. It is noted that in the second part i.e., experiments using LG screw configuration the low and high level of the barrel temperature and the screw speed are different than those used in the first part of the project in an effort to cover a wider range of values for these factors.

Table 3.3: Processing Conditions Used in Factorial Design for SG Screw Configuration

FACTORS	LEVELS	
	Low Value	High Value
Temperature of the barrel (°C)	170	180
Temperature of the mold (°C)	40	80
Screw Speed (rpm)	150	245

Table 3.4: Processing Conditions Used in Factorial Design for LG Screw Configuration

FACTORS	LEVELS	
	Low Value	High Value
Temperature of the barrel (°C)	180	200
Temperature of the mold (°C)	40	80
Screw Speed (rpm)	100	245
Mixing time (min)	3	6

As mentioned, the mixing time has no significant effect at least in the range of values (3 to 6min) used in the project. There is not enough flexibility in extending this range because shorter mixing times are not sufficient for mixing for the particular micro-extruder and longer times result in material degradation and increase the time of the process cycle.

Upper and lower limits exist also for the mold temperature. The higher the mold temperature the better in terms of flexural properties since fast cooling (low mold temperature, large temperature gradient) will result in smaller and less perfect spherulites. For mold temperatures above 80°C the composite's temperature after demolding was so high that the part is deformed due to thermal residual stresses.

The lower value for the barrel temperature used is T_{barrel}=170°C. This limitation is imposed by polypropylene's melting point. Higher temperatures are preferable especially at higher graphite loadings in order to decrease the viscosity of the melt. However, a barrel temperature above 200°C will lead to material degradation. Finally, the maximum screw rotation speed of 245rpm allowed by the microextruder was used as the upper level of this factor.

3.3. Results of Factorial Design for Optimum Processing Conditions

The dependent variables in the factorial design were the flexural strength and modulus of elasticity of both the neat PP and the 3vol% xGnP-1/PP nanocomposites that were determined by three point bending test using UTS machine [United Calibration Corp.] with a strain rate of 0.05 in/minute at room temperature following ASTM D790 standard. As mentioned the project is divided into two parts keeping the screw-barrel gap distance constant each time i.e., small gap distance (SG) in the first part and large gap distance (LG) in the second.

3.3.1 Composites Made Using Small-Gap Screw Configuration

In the first part of the project, (small screw-barrel gap size and mixing time of t=3min) samples were made for eight different combinations of processing conditions described in Table 3.3. The flexural strength of neat PP and 3vol% 1um EGF-PP nanocomposites are presented in Figures 3.1 and 3.2 respectively.

Increasing the screw speed from 150rpm to 245rpm does not affect the flexural strength of neat PP. This is expected because the screw speed is related to the dispersion of the reinforcement within the polymer matrix so changing screw speed in case of neat polymer should not make any difference. Increase of the barrel temperature from 170°C to 180 °C also does not affect the flex strength of the neat PP since due to absence of reinforcement the viscosity is kept low even at low barrel temperatures. However, increasing the mold temperature from 40 °C to 80 °C results in a significant increase of PP's flexural strength in the order of ~12%.

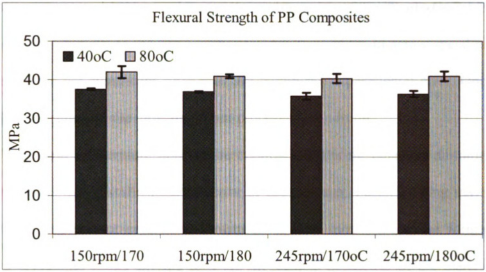

Figure 3.1. Flexural strength of PP made by melt mixing at various processing conditions for SG screw configuration and processing time of t=3min

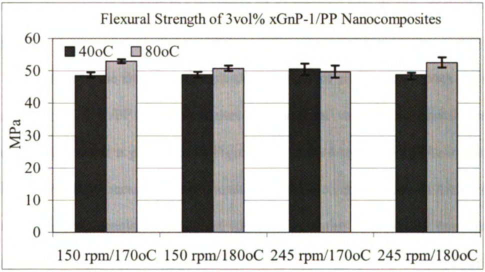

Figure3.2. Flexural strength of 3vol% xGnP-1/PP made by melt mixing at various processing conditions for SG screw configuration and processing time of t=3min

The same trend is observed in the flexural strength of 3vol% of xGnP-1/PP. Any changes in the strength of the nanocomposites due to changes in screw speed or barrel temperature are not significant since they are within the experimental error. Once more the mold temperature is the most important processing condition.

The mold temperature defines the cooling rate during injection molding which strongly affects the crystallization behavior of the polymer. Faster cooling may lead to thinner and less perfect crystalline structures or may even induce the formation of different crystalline forms altering thus the mechanical properties of the material. It is noted that in case of the nanocomposite the effect of T_{mold} on the strength is not as strong as in the case of the neat polymer. This may be due to the fact that the reinforcing effect is stronger and dominates over any effect due to differences in the crystallization behavior of the polymer or that the presence of xGnP also affects the crystallization of the polymer.

In addition to the flexural strength the modulus of elasticity for both the neat PP and the 3vol% xGnP-1/PP nanocomposites fabricated at various processing conditions was also recorded and it is presented in Figures 3.3 and 3.4 respectively. As in the case of flexural strength the processing condition that has the strongest effect on the modulus is the temperature of the mold. The highest values of modulus of elasticity were measured for samples made at a mold temperature of 80°C. The effect of mold temperature is stronger for the neat PP where the modulus is increased by ~11% by increasing the T_{mold} from 40°C to 80°C compared to ~7% increase of modulus for the xGnP-1/PP nanocomposites. Any changes in the temperature of the barrel and/or the screw rotation speed do not affect the modulus of neither the neat PP nor the xGnP-1/PP nanocomposites. It is speculated that both of these processing conditions will affect the modulus of the nanocomposites that have higher graphite content by altering the dispersion conditions and the viscosity of the melt.

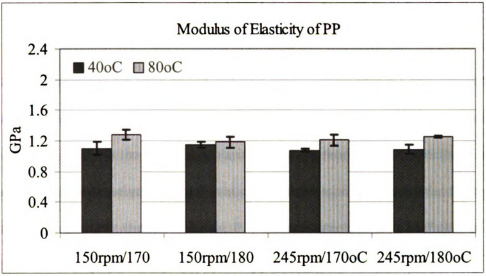

Figure 3.3. Modulus of elasticity of PP made by meltmixing at various processing conditions for SG screw configuration and processing time of t=3min

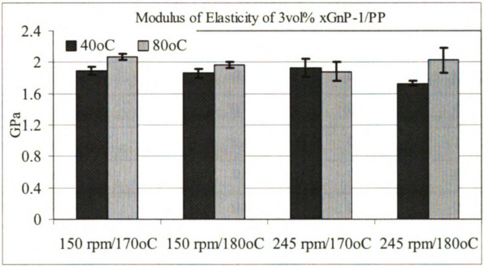

Figure3.4: Modulus of elasticity of 3vol% xGnP-1/PP made by melt mixing at various processing conditions for SG screw configuration and processing time of t=3min

An important conclusion that can be draw by comparing Figures 3.1 to 3.2 and Figures 3.3 to 3.4 is that addition of only 3vol% of xGnP-1 in PP results in an increase of the flexural strength by ~26% and of modulus by ~62% compare to the flexural strength and modulus of the neat polymer.

Based on the flexural strength and modulus of elasticity results of both the neat PP and the 3vol% xGnP-1/PP composites, presented in Figures 3.1 to 3.4, the analysis of variance was performed for each one of the four cases using Table 3.1 and calculating the degrees of freedom, the sum of squares and the mean square values from Equations (3.1) to (3.8). Table 3.5 shows the analysis of variance for the modulus of elasticity of neat PP. This case is presented analytically here while the analysis of variance tables for the other three cases i.e., flexural strength of neat PP, flexural strength and modulus of 3vol% xGnP-1/PP nanocomposites are presented in *Appendix B.*

Table 3.5: The Analysis of Variance Table for the modulus of elasticity of neat PP

Effect/Factor	df	Sum of Squares	Mean Square	F_o
T_{barrel}	1	7.61E-05	7.61E-05	0.0277
T_{mold}	1	0.0983	0.0983	35.8244
Screw Speed	1	0.0009	0.0009	0.3185
T_{barrel} x T_{mold}	1	0.0042	0.0042	1.5199
T_{barrel} x Screw Speed	1	0.0023	0.0023	0.8352
T_{mold} x Screw Speed	1	0.0056	0.0056	2.0245
T_{barrel} x T_{mold} x Screw Speed	1	0.0085	0.0085	3.1153
Error	16	0.0439	0.0027	1
Total	23	0.1637		

The F statistic method is used to determine the effect of each factor. According to this method all mean squares are tested against the error mean square. The result is the last column of Table 3.5 denoted as F_o. This is compared to the F^* value obtained from the F-statistic table [2] given also in *Appendix A*, using a significant level of 5%, $v_1=1$ and $v_2=16$ where v_1 and v_2 are the degrees of freedom of the factor under consideration and the "error" factor respectively. All factors besides the "error" factor have $v=1$ and thus have the same F^*, that is $F^*=4.54$. The only factor for which F_o/F^* is the mold temperature which means that this is the only factor that has significant effect on the modulus of elasticity. No conclusion can be draw for the effect of the other factors.

The results of the analysis of variance for the strength and modulus of neat PP and of 3vol% xGnP-1/PP nanocomposites are summarized and presented in Table 3.6, which is formed by using the F_o column of Table 3.5 and Tables B6 to B8 presented in *Appendix B*. The F^* value for all of them is $F^*=4.54$. The table entries for which $F_o/F^*>1$ are underlined.

Table 3.6. The F_o values based on the Analysis of Variance for four 2^3 Factorial Designs

Effect/Factor	Strength of PP	Strength of xGnP-1/PP	Modulus of PP	Modulus of xGnP-1/PP
T_{barrel}	0.08	0.07	0.03	1.36
T_{mold}	150.28	19.58	35.82	11.20
Screw Speed	7.06	0.03	0.32	2.30
T_{barrel} x T_{mold}	0.01	0.58	1.52	2.58
T_{barrel} x Screw Speed	3.59	1.93	0.84	0.16
T_{mold} x Screw Speed	0.50	2.13	2.02	0.00
T_{barrel} x T_{mold} x Screw Speed	0.00	15.47	3.12	9.83

As shown in Table 3.6 the processing factors that have a significant effect on the strength of neat PP are the temperature of the mold and the screw speed. There is also effect of mold temperature on the modulus of neat PP as indicated in Figure 3.3 while both the strength and modulus of elasticity of the 3vol% xGnP-1/PP nanocomposites are influenced by the temperature of the mold and by the three-factor interaction which reveals the existence of a synergistic effect.

A regression model of the form described in Equation (3.9) is proposed for each of the four cases presented in Table 3.6. In order to calculate the regression coefficients defined by Equation (3.19) one needs to estimate the effects using Equations (3.12) to (3.18). The factors that have a large effect value are included in the model. The regression coefficient values are shown in Table 3.7.

Table 3.7. Regression Coefficients for four 2^3 Factorial Designs

Effect/Factor		Strength of PP	Strength of xGnP-PP	MOE of PP	MOE of xGnP-PP
A	T_{barrel}	-0.017	-0.022	0.001	-0.007
B	T_{mold}	0.722	0.362	0.021	0.020
C	Screw Speed	-0.156	0.014	-0.002	-0.009
AB	T_{barrel} x T_{mold}	-0.005	0.062	-0.004	0.010
AC	T_{barrel} x Screw Speed	0.112	0.113	0.003	0.002
BC	T_{mold} x Screw Speed	0.041	-0.119	0.005	0.000
ABC	T_{barrel} x T_{mold} x Screw Speed	0.193	0.396	0.010	0.028

Recall Equation (3.9) that defines the regression model for a 2^3 factorial design. Taking into consideration only the significant terms the regression models for the strength of neat PP and of 3vol% xGnP-1/PP nanocomposites and their modulus of elasticity is given by Equations (3.21)-(3.24) respectively.

Strength of PP:

$$Y = 38.768 + 0.722x_B - 0.156x_C + 0.112x_A x_C + 0.193x_A x_B x_C \tag{3.21}$$

Strength of 3vol% 1um EGF-PP Nanocomposite:

$$Y = 50.392 + 0.362x_B + 0.113x_A x_C - 0.119x_b x_c + 0.396x_A x_B x_C \tag{3.22}$$

Modulus of Elasticity of PP:

$$Y = 1.166 + 0.021x_B + 0.010x_A x_B x_C \tag{3.23}$$

Modulus of Elasticity of 3vol% 1um EGF-PP Nanocomposite:

$$Y = 1.919 + 0.020x_B + 0.010x_A x_B - 0.09x_C + 0.028x_A x_B x_C \tag{3.24}$$

x_A, x_B and x_c are coded variables defined by Equation (3.10) and are calculated using Table 3.3 that shows the low and high levels of each factor for the case of small gap screw configuration. The final expressions for the coded variable are given in Equations (3.25)-(3.27).

$$x_A = \frac{A - (180 + 170)/2}{(180 - 170)/2} \tag{3.25}$$

$$x_B = \frac{B - (80 + 40)/2}{(80 - 40)/2} \tag{3.26}$$

$$x_C = \frac{C - (245 + 150)/2}{(245 - 150)/2} \tag{3.27}$$

where A, B, and C are the barrel temperature, the mold temperature and the screw speed respectively. The error introduced by the regression models is calculated using Equation (3.20). The values are presented in Table 3.8.

Table 3.8:Residuals of the Regression Models used for the 2^3 Factorial Designs

Dependent Variable of Regression	$R^2 = \frac{SS_{Model}}{SS_{Total}}$
Strength of PP	0.907
Strength of xGnP-1/PP	0.701
MOE of PP	0.869
MOE of xGnP-1/PP	0.597

It is concluded that from the four regression models proposed, the best one is for the strength of the neat PP which can model the experimental data introducing only an uncertainty of ~10%. The error is arising from the replication of the experimental runs (*n*=3) and the lack of fit due to the fact that not all the effects i.e., *A*, *AC et al* were included in the model.

3.3.2 Composites Made Using Large-Gap Screw Configuration

As mentioned in the introduction for reasons of simplicity the project was divided into two parts keeping the screw-barrel gap distance constant each time i.e., small gap distance (SG) in the first part (Section 3.3.1) and large gap distance (LG) in the second part which is presented in this section. A processing time of 3min was used in all experiments.

The flexural strength of neat PP and 3vol% xGnP-1/PP nanocomposites are presented in Figures 3.5 and 3.6 respectively. It is indicated that the most critical processing parameter is the temperature of the mold with the higher value of T_{mold}=80°C yielding the larger strength.

In particular, increasing the screw speed from 100rpm to 245rpm and/or the barrel temperature from 180°C to 200°C does not seem to affect the flexural strength of neat PP. However, increasing the mold temperature from 40°C to 80°C results in significant increase, in the order of ~16%, of PP's flexural strength. The same trend is observed in the flexural strength of 3vol% xGnP-1/PP as shown in Figure 3.6. Once more the mold temperature is the most important processing condition.

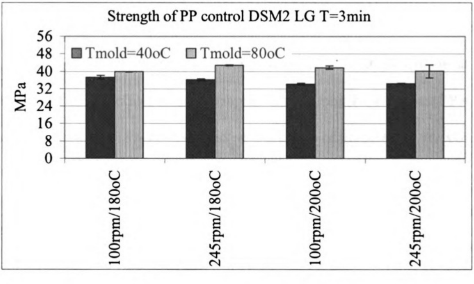

Figure 3.5: Flexural strength of PP made by melt mixing at various processing conditions for LG screw configuration and processing time of t=3min

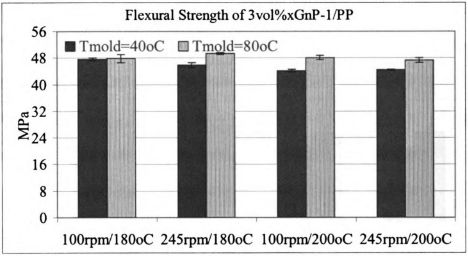

Figure 3.6. Flexural strength of 3vol% xGnP-1/PP made by melt mixing at various processing conditions for LG screw configuration and processing time of t=3min

The modulus of elasticity for both the neat PP and the 3vol% xGnP-1/PP for the various processing conditions is presented in Figures 3.7 and 3.8 respectively. The highest values of modulus of elasticity were measured for samples made at a mold temperature of 80°C. The effect of mold temperature is stronger for the neat PP where the modulus is increased by ~18% compared to ~6% increase of modulus for the xGnP-1/PP.

An important conclusion that can be draw by comparing Figures 3.5 to 3.6 and Figures 3.7 to 3.8 is that addition of only 3vol% of xGnP-1 in polypropylene results in an increase of the flexural strength by ~22% and of modulus of elasticity by ~40% compare to the flexural strength and modulus of the neat polymer.

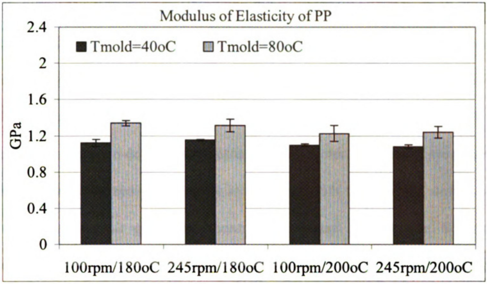

Figure 3.7. Modulus of elasticity of PP made by melt mixing at various processing conditions for LG screw configuration and processing time of t=3min

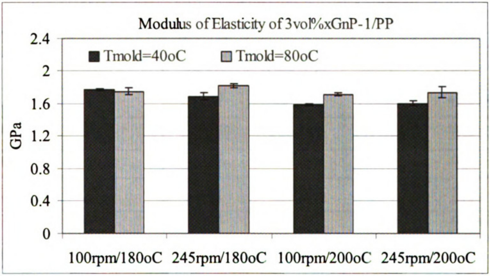

Figure 3.8. Modulus of elasticity of 3vol% xGnP-1/PP made by melt mixing at various processing conditions for LG screw configuration and processing time of t=3min

Based on the flexural strength and modulus of elasticity results for both the neat PP and the 3vol% xGnP-1/PP composites, presented in Figures 3.5-3.8, the analysis of variance is performed for each one of the four cases using Table 3.1 and Equations (3.1)-(3.8). The detailed tables of analysis of variance can be found in *Appendix B*. The *F* statistic method is used to determine the effect of each factor. The results are presented in Table 3.9 in a summarized format since is the same with the factorial design analysis performed for the small gap screw configuration case presented in Section 3.3.1 (significant level of 5%, v_1=1 and v_2=16 and F^*=4.54). Table 3.9 contains the F_o values for each factor for the four 2^3 factorial designs. The table entries for which $F_o/F^*>1$ are underlined.

Table 3.9: The F_o values based on the Aanalysis of Variance for four 2^3 Factorial Designs

Effect/Factor	Strength of PP	Strength of xGnP-1/PP	Modulus of PP	Modulus of XGnP-1/PP
T_{barrel}	8.609	40.391	15.061	43.134
T_{mold}	139.269	100.386	133.421	39.212
Screw Speed	0.047	0.584	0.293	0.122
T_{barrel} x T_{mold}	4.661	9.072	0.015	7.312
T_{barrel} x Screw Speed	2.883	0.069	0.299	0.896
T_{mold} x Screw Speed	1.244	4.736	0.001	7.678
T_{barrel} x T_{mold} x Screw Speed	10.193	17.411	0.911	5.523

By comparing Tables 3.6 and 3.9 it is concluded that in the case of large gap screw configuration the effect of processing conditions on the flexural properties of both PP and xGnP nanocomposites is stronger since more factors have a $F_o>F^*$. Besides the mold temperature another important factor is the temperature of the barrel. In most cases two factor and three-factor interactions are important indicating existence of synergistic effects.

A regression model of the form described in Equation 9 is proposed for each of the four cases presented in Table 9. As in the case of small gap screw configuration, the effects are estimated using Equations (12)-(18) and the regression coefficients using Equation (19), the values are shown in Table 3.10.

Table 3.10. Regression Coefficients for four 2^3 Factorial Designs

Effect/Factor		Strength of PP	Strength of xGnP-1/PP	MOE of PP	MOE of xGnP-1/PP
A	T_{barrel}	-0.230	-0.281	-0.011	-0.016
B	T_{mold}	0.927	0.443	0.033	0.015
C	Screw Speed	0.017	-0.034	0.002	0.001
AB	T_{barrel} x T_{mold}	0.170	0.133	0.000	0.007
AC	T_{barrel} x Screw Speed	-0.133	-0.012	0.002	0.002
BC	T_{mold} x Screw Speed	0.088	0.096	0.000	0.007
ABC	T_{barrel} x T_{mold} x Screw Speed	0.052	-0.029	0.005	-0.001

Taking into consideration only the significant terms and using Equation (3.9) the regression models for the strength modulus of elasticity of neat PP and of 3vol% xGnP-1 nanocomposites is given by Equations (3.27)-(3.30) respectively.

Strength of PP:

$$Y = 38.29 - 0.230x_A + 0.927x_B + 0.170x_A x_B - 0.133x_A x_C + 0.052x_A x_B x_C \quad (3.\ 27)$$

Strength of 3vol% 1um EGF-PP Nanocomposite:

$$Y = 46.829 - 0.281x_A + 0.443x_B + 0.133x_A x_B + 0.096x_B x_C - 0.029x_A x_B x_C \qquad (3.28)$$

Modulus of Elasticity of PP:

$$Y = 1.214 - 0.011x_A + 0.033x_B \qquad (3.29)$$

Modulus of Elasticity of 3vol% 1um EGF-PP Nanocomposite:

$$Y = 1.711 - 0.016x_A + 0.015x_B + 0.007x_A x_B + 0.007x_B x_C - 0.001x_A x_B x_C \qquad (3.30)$$

The coded variables x_A, x_B and x_c are given in Equations (31)-(33).

$$x_A = \frac{A-(200+180)/2}{(200-180)/2} \qquad (3.31)$$

$$x_B = \frac{B-(80+40)/2}{(80-40)/2} \qquad (3.32)$$

$$x_C = \frac{C-(245+100)/2}{(245-100)/2} \qquad (3.33)$$

where A, B, and C are the barrel temperature, the mold temperature and the screw speed respectively. The error introduced by the regression models is calculated using Equation (3.20). The values are presented in Table 3.11.

Table 3.11. Residuals of the Regression Models used for the 2^3 Factorial Designs

Dependent Variable of Regression	$R^2 = \frac{SS_{Model}}{SS_{Total}}$
Strength of PP	0.91
Strength of EGF-PP	0.91
MOE of PP	0.89
MOE of EGF-PP	0.86

3.3.3 Effect of Screw Gap Distance on The Flexural Properties of xGnP-1/PP Nanocomposites

Samples were made using T_{barrel}=180°C, mold temperature of T_{mold}=80°C, screw speed of 245rpm and mixing time t=3min. The effect of the screw gap distance on the flexural strength and modulus of PP and 3vol% xGnP-1/PP is shown in Figures 9 and 10 respectively. The small gap case seems to result in higher strength and modulus for both the neat PP and the xGnP-1/PP nanocomposites but due to overlapping of the error bars no solid conclusion can be made.

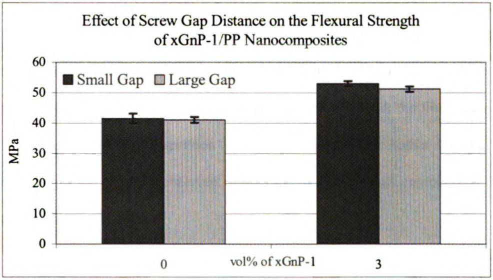

Figure 3. 9: Flexural strength of neat PP and 3vol% xGnP-1/PP Nanocomposites at small and large screw gap distance (T_{barrel}=180°C, T_{mold}=80°C, 245rpm and t=3min)

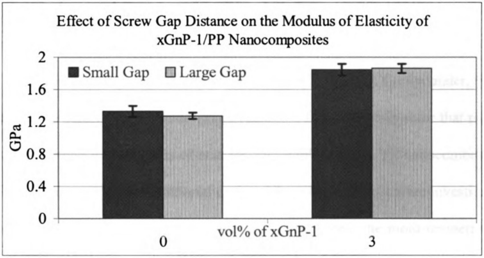

Figure 3.10. Modulus of elasticity of neat PP and 3vol% xGnP-1/PP nanocomposites at small and large screw gap distance(T_{barrel}=180°C, T_{mold}=80°C, 245rpm and t=3min)

The gap distance between the screws and the bottom of the barrel is expected to be an important parameter for micro-size reinforcements and/or fibers. In such cases the smaller gap distance will impose a higher shear which might break the fibers decrease of aspect ratio) or change the dispersion conditions especially at higher loading levels. However none of the above is observed in the case of xGnP-1 and especially at the low loading of 3vol% used here.

3.4 Conclusions and Comments

The optimum operating conditions of the DSM Micro15cc Compounder, (vertical, co-rotating twin-screw microextruder) connected to a Daca Micro Injector that maximize the flexural strength and modulus of neat PP and 3vol% xGnP-1/PP nanocomposites are determined using a series of 2^3 factorial design. The conditions that were investigated are the barrel temperature, the processing time, the screw speed, the mold temperature and the gap between the screw bottom and the barrel.

The setting points used for each condition were presented in Tables 3.4 and 3.5. Based on the analysis of variables the coefficients of the regression model were calculated using Equations (3.9) to (3.20) and presented in Tables 3.7 and 3.10 for the case of small and large screw-barrel gap distance respectively. A summary of the results is provided in Table 3.12. Based on the "F statistics" there are variables that have no effect on the flex strength and modulus and other that have positive or negative effect. These are denoted with "N", "+" and (-) respectively.

The most important parameter (larger magnitude of the regression coefficient) is the temperature of the mold. The suggested processing conditions are presented in Table 3.13. It is noted that the processing conditions have been optimized for polypropylene (profax 6301) as a matrix and xGnP-1 as reinforcement at a loading of 3vol%. For higher loadings or different type of reinforcements some modifications need to be made i.e., at loadings of 20vol% or higher the barrel temperature needs to be increased in order to maintain the viscosity at low levels.

Table 3.12. A Summary of the Effect Each Variable has on the Flexural Properties of PP and 3vol% xGnP-1/PP

Effect/Factor		Strength of PP		Strength xGnP-PP		MOE of PP		MOE of xGnP-PP	
		SG	LG	SG	LG	SG	LG	SG	LG
A	T_{barrel}	N	-	N	-	N	-	N	-
B	T_{mold}	+	+	+	+	+	+	+	+
C	Screw Speed	-	N	N	N	N	N	N	N
AB	T_{barrel} x T_{mold}	N	+	N	+	N	N	N	+
AC	T_{barrel} x Screw Speed	+	N	+	N	N	N	N	N
BC	T_{mold} x Screw Speed	N	N	-	+	N	N	N	+
ABC	T_{barrel} x T_{mold} x Screw Speed	+	+	+	-	+	N	+	-

Table 3.13. Optimum Processing Conditions based on Factorial Design Experiments

Processing Time (3min)	3
Screw Speed (rpm)	200-245
Barrel Temperature (°C)	180
Mold Temperature (°C)	80
Screw-barrel Gap (mm)	Any

3.5 References

1. N.P. Cheremisinoff, "Practical Statistics for Engineers and Scientists", Technomic Publishing AG, Pennsylvania, 1987

2. C.R. Hicks, "Fundamental Concepts in the Design of Experiments", 4th Edition, Saunders College Publishing, 1993

3. D.C. Montgomery, "Design and Analysis of Experiments", John Wiley & Sons, New York, 1997

CHAPTER 4

MECHANICAL PROPERTIES AND MORPHOLOGICAL CHARACTERIZATION OF EXFOLIATED GRAPHITE POLYPROPYLENE NANOCOMPOSITES

4.1 Introduction

The advantages of using nanosize reinforcements in composites were analytically presented in Chapter 1 and are briefly summarized here.

(i) Based on the work reported Griffith in 1920's [1,2] and confirmed also by Weibull in 1950's [3] the smaller a material is, the stronger it becomes assuming that the failure of macroscopic specimens is due to the existence of defects i.e., cracks and that materials that are smaller than a critical crack length are able to reach their theoretical maximum strength. Thus, as Piggott [4] concluded, nanomaterials are more effective reinforcements than their conventional counterparts because smaller amounts of nanomaterials causes a larger improvement of the matrix properties leading to lightweight composites with lower cost and easy processability.

(ii) The stress transfer from the matrix to the reinforcements is more efficient in case of nanocomposites due to the increased surface area, assuming good adhesion at the interface. Also, the crack propagation length at the interface becomes longer, improving the strength and toughness.

(iii) Energy absorbing mechanisms that have a positive effect on toughness i.e., increased plastic deformation of the matrix along the matrix-reinforcement interface, crack branching due to hindrance by reinforcements, creation of voids and crazes at the reinforcement edges are more dominant when nanoreinforcements are used.

(iv) As the size of the reinforcement decreases, the average dispersion distance becomes shorter which reduces the stress at the reinforcement edges due to the presence of other reinforcements located nearby.

The objectives of the work presented in this chapter are to:

- Determine the mechanical properties i.e., flexural strength and modulus, tensile modulus and impact strength of xGnP-PP nanocomposites
- Compare the reinforcing effect of xGnP to commercially available clays and carbon reinforcements such as carbon black, vapor grown and pan based carbon fibers
- Investigate the morphology of the nanocomposites in order to assess the dispersion and orientation of the reinforcement in the polymer matrix which provides information on how the processing relates to the mechanical properties of the nanocomposites
- Improve reinforcement dispersion by altering the compounding method
- Compare the experimental data of the modulus to theoretical predictions such as rule of mixtures, Halpin-Tsai and the Tandon and Weng model for the effective moduli of randomly oriented composites.

4.2 Experimental Conditions and Characterization Techniques

Flexural tests were performed with a UTS SFM-20 machine [United Calibration Corp.] at room temperature by following the ASTM D790 standard test method (3-point bending mode). The samples were made in standard bar shape and the span was set to 2 inches. The test was performed at flexural rate of 0.05 in/min.

The tensile modulus was determined by a tensile test using a UTS SFM-20 machine [United Calibration Corp.] at room temperature. The ASTM D638 standard test method conditions were not used since the DSM mold used during injection molding has different dimensions that the mold mentioned in the ASTM standard. However, the test method used is sufficient for screening experiments and the results are consistent since all the samples were made and tested under the same conditions. In particular, the samples had 1 inch gauge length. A preloading of 0.5lb was initially applied at a rate of 0.05in/min to assure perfect alignment of the samples with the grips. The test was performed at an elongation rate of 0.1 in/min up to a displacement of 0.025, which is the upper limit of the linear regime. Though recorded, the tensile strength is not reported because many samples failed outside of the gauge area. Impact resistance tests (Izod type) were performed following the ASTM D256 standard test method.

The morphology of the nanocomposites was investigated by Environmental Scanning Electron Microscopy (Electroscan 2020). The samples were gold coated to avoid charging and the voltage used was 20-30kV. The composites were made by the DSM microextruder injection molding system at the optimum processing conditions (3min, T_{barrel}=180°C, T_{mold}=80°C and 245rpm) resulting from the Design of Experiments study reported in Chapter 3.

4.3 Experimental Results and Discussion

4.3.1 Flexural Properties and Impact Strength of xGnP-PP Nancomposites

The flexural strength and modulus of elasticity of both the 1 and 15μm xGnP-PP nanocomposites at low loading levels (from 0 to 3 vol%) are shown in Figures 4.1 and 4.2 respectively. The values reported are the average of testing three samples.

It is noted that xGnP-1 improves the properties of PP even at very low loadings. The xGnP-15 also increases both the strength and modulus but is not as effective as the 1 micron xGnP at higher content (>1 vol%). It is obvious that xGnP-1 is more effective than xGnP-15 and their difference becomes greater as the xGnP loading increases.

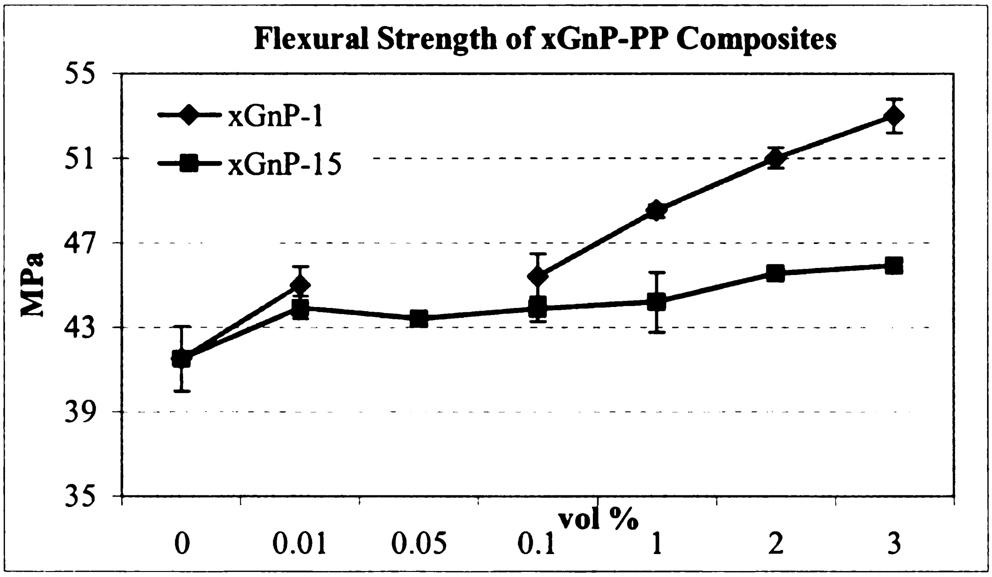

Figure 4.1. Flexural strength of xGnP-1/PP and xGnP-15/PP nanocomposites

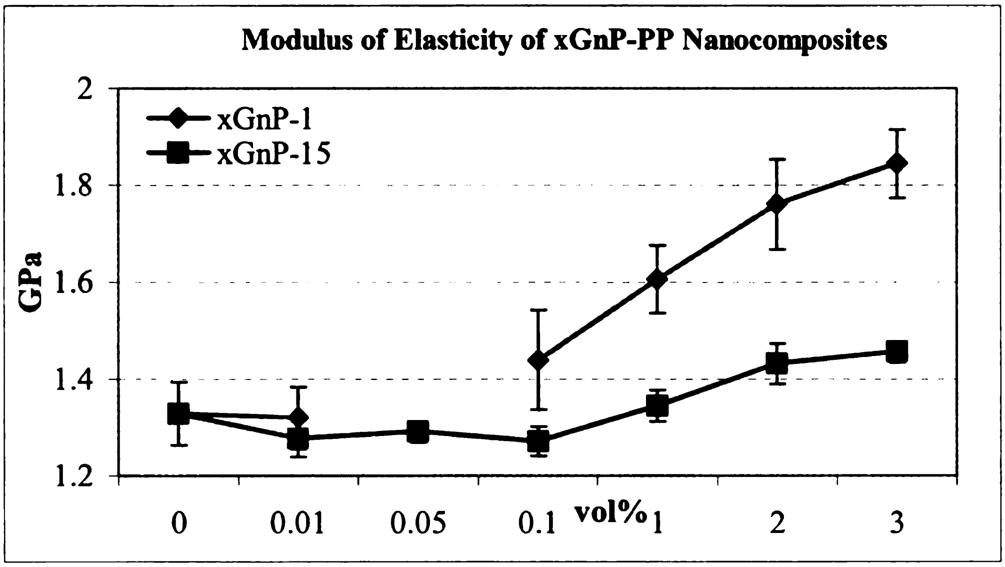

Figure 4.2. Modulus of elasticity of xGnP-1/PP and xGnP-15/PP nanocomposites

The impact strength of xGnP-PP nanocomposites with the same xGnP content made by DSM operating at the optimum conditions is presented in Figure 4.3. Although the error bars do overlap to some degree, the general trend is that the impact strength increases with xGnP-1 content whereas in case of xGnP-15 it reaches a maximum at 0.1-1vol%.

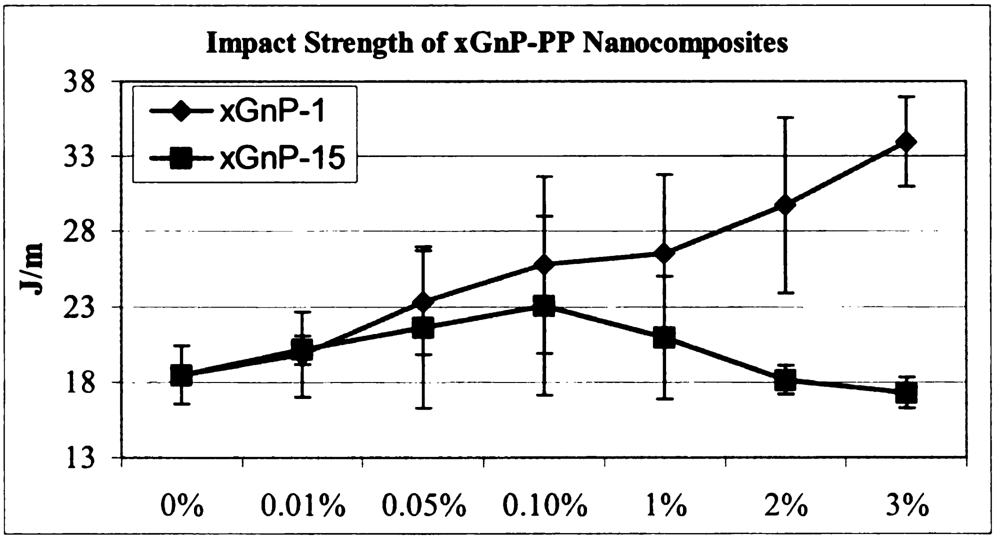

Figure 4.3. Impact strength of xGnP-1/PP and xGnP-15/PP nanocomposites

The differences in flexural properties and impact strength of the xGnP-1/PP and xGnP-15/PP composites reflect the difference in the aspect ratio of the two xGnP types, the differences in the absolute number of reinforcing elements per unit volume and indicate that xGnP dispersion and orientation in these composites may be different. In addition, differences in impact strength may indicate differences in crystallization behavior of the polymer i.e., presence of xGnP may alter the spherulite size and polymorphism that affect the impact strength of PP [5] or the presence or absence of bridging across the crack due to xGnP size. The effect of xGnP on the crystallization behavior of PP is analytically discussed in Chapter 7. The orientation and dispersion of xGnP in the polymer matrix, accessed by ESEM, as well as a qualitative evaluation of how the morphology affects the mechanical properties of the nanocomposites is presented in the following.

Flexural Specimen xGnP Morphology.

The surfaces that were studied were obtained by fracture in liquid N_2. The fracture surface of the neat PP, shown in Figure 4.4a, is more homogeneous and smooth compared to the fracture surface of xGnP-15/PP, shown in Figure 4.4b. Addition of an amount of xGnP as small as 0.01vol% is sufficient to significantly alter the surface and increase the roughness, which indicates an increase in the energy required to fracture the composite.

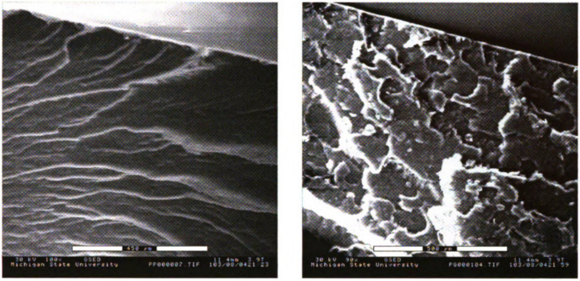

Figure 4.4. ESEM images of fracture surface of a) control PP (scale bar 450μm) and b) 0.01vol% xGnP-15/PP nanocomposite (scale bar 500 μm)

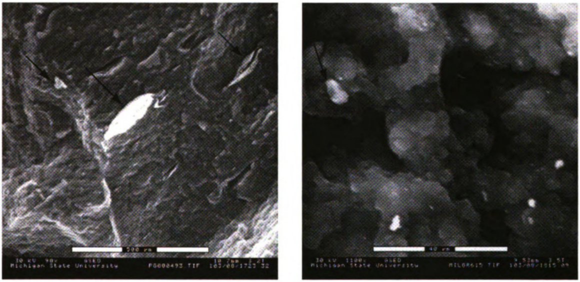

Figure 4.5. ESEM images of fracture surface of a) 1vol% xGnP-15/PP (scale bar 500μm) and b) 1vol% xGnP-1/PP (scale bar 40 μm)

Agglomeration of the xGnP-15 particles was observed at all xGnP-15 loadings used whereas the xGnP-1 was better dispersed in the PP matrix as shown in Figures 4.5a and 4.5b respectively. Theoretically, xGnP-15 is a round shape platelet with an average diameter of 15μm and thickness of <10nm however, as shown by the arrows in Figure 4.5a the xGnP-15 during the nanocomposite fabrication loses its layered structure and forms agglomerates that can be as large as 200-300μm. In case of xGnP-1 although there is agglomeration as well the graphite agglomerates are fewer and smaller (compared to the theoretically expected xGnP-1 dimensions) as indicated by the arrows in Figure 4.5b.

Since the affinity between the non-polar polymer and the graphite platelets is unaffected by reinforcement size and since similar processing conditions are used for both reinforcements, the difference in dispersion and agglomeration is contributed to the larger size of xGnP-15 which are more flexible compared to the stiffer smaller xGnP-1. As mentioned xGnP-15 do not maintain the platelet morphology within the polymer matrix. According to morphological investigation by ESEM it was found that xGnP-15 can bend/buckle as shown in Figure 4.6a, roll up as shown in Figure 4.6b, or agglomerate in response to the shear conditions they experience in the extruder during melt mixing. In addition, due to their high aspect ratio, xGnP-15 particles are better aligned than xGnP-1 during injection molding as indicated in Figure 4.7. The agglomeration of xGnP-15 and orientation along the flow direction is a common feature observed almost always during the morphological investigation of the xGnP/PP nanocomposites whereas the other structural features i.e., buckling and "roll-up" are less common but still they are indicative of morphological changes occurring to xGnP-15.

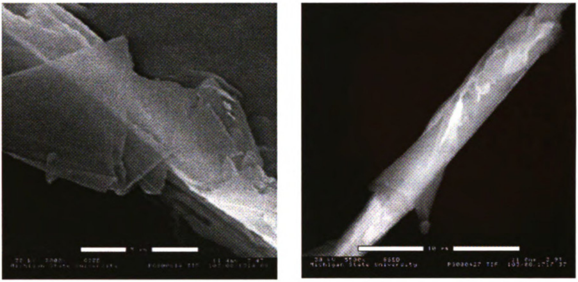

Figure 4.6. ESEM images of fracture surface of 1vol% xGnP-15/PP nanocomposite a) xGnP-15 particle buckled (scale bar 5μm) and b) xGnP-15 rolled-up (scale bar 10 μm)

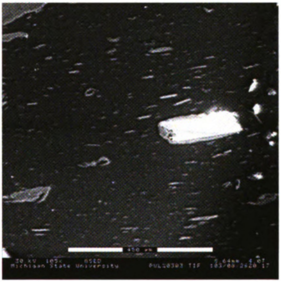

Figure 4.7. ESEM images of polished surface (parallel to the flow plane) of 3vol% xGnP-15/PP showing agglomeration and alignment of xGnP-15 along the flow direction (scale bar 450μm)

4.3.2 Flexural Properties and Impact Strength of PP Composites -Comparison of xGnP to other Reinforcements

Flexural Strength

Figure 4.8 shows the flexural strength of various polypropylene composites up to a loading level of 20vol%. At the given processing conditions it was not possible to make samples with carbon black content higher than 5vol%. The viscosity increased to levels where the extruder could not generate sufficient pressure to extrude the mix properly. However, this was not a problem with the other reinforcements.

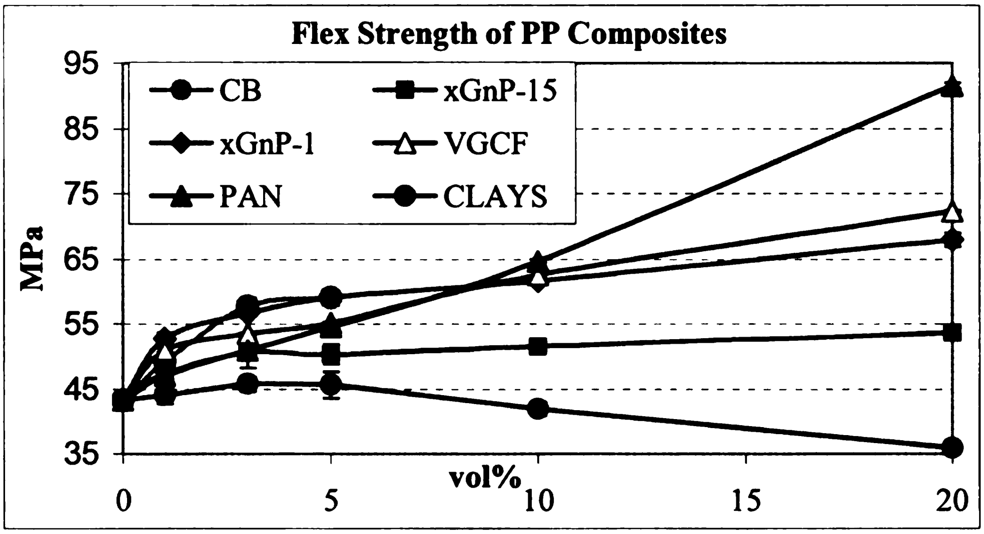

Figure 4.8. Flexural strength of various PP composites

The carbon black and xGnP-1 exhibit the greatest flexural strength improvement up to a loading of 5 vol% followed by the VGCF, PAN carbon fibers and xGnP-15. The highly aggregated structure of the carbon black allows excellent polymer penetration at low concentrations which makes it a more effective reinforcement by reducing its size and thereby reducing concentrations in the composite which contribute to stress concentrations and reduction in strength. [6].

At loadings higher that 3vol% of the nanoclay a reduction of strength was measured with the 20vol% clay-PP composite having 10% lower strength than the neat PP. The reason is that the clays used are modified with octadecylamine (25-30 wt% of octadecylamine on the clay surface as determined by TGA) and are specifically designed for a polyplropylene matrix but require the presence of a coupling agent i.e., maleic anhydride-co-polypropylene [7]. In the absence of the coupling agent there is weak adhesion of the modified clays with the non-polar PP matrix, poor dispersion and agglomeration of the clay particles that leads to poor mechanical properties.

The flexural strength for both types of xGnP increases rapidly at lower loadings but the rate of increase slows at xGnP content above 10 vol%. The xGnP-1 is a better reinforcement than xGnP-15 mainly due to the more homogeneous dispersion and less agglomeration of the xGnP-1. The plateau of the xGnP strength curves at ~10 vol% indicates that poor adhesion and insufficient dispersion of xGnP in the polymer matrix may be limiting the effectiveness of the xGnP.

At the highest loading used i.e., 20vol% both VGCF and PAN carbon fibers show significant improvement in the strength. In particular, the addition of PAN carbon fibers results in a ~100% improvement in the strength of PP. As indicated by ESEM (Figure 4.9), the rigid PAN fibers are aligned parallel to the flow direction during injection molding while the more flexible VGCF are not as aligned and form two dimensional networks. Figure 4.10a shows a surface normal to the flow of 10vol% PAN-PP composite prepared by polishing and etching using O_2 plasma. Figure 4.10b shows the fracture surface created during flexural testing of 10vol% PAN-PP. In both cases the PAN carbon fibers are parallel to the flow direction and the appearance of a few holes and short pull-out lengths in Figure 4.10b indicates that adhesion between the CF and PP is adequate.

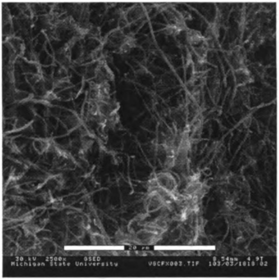

Figure 4.9. ESEM images of fracture surface of 10vol% VGCF/PP showing the two dimensional alignment of VGCF (scale bar 100 µm)

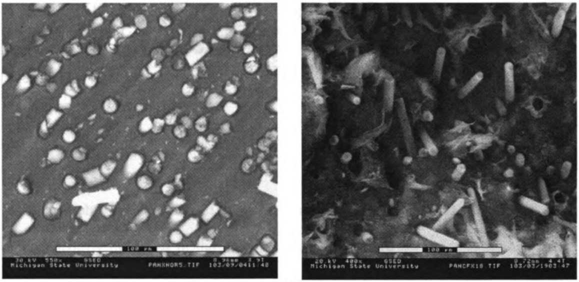

Figure 4.10. ESEM images of 10vol% PAN/PP a) surface normal to the flow (scale bar 100µm) and b) fracture surface showing fiber "pull outs" (scale bar 100 µm)

Flexural Modulus

Figure 4.11 shows the flexural moduli of various PP composites up to reinforcement content of 20vol%. The best reinforcing effect is obtained with xGnP-1 increasing the modulus ~900% at a loading of 20vol% followed by carbon black (at low loadings), PAN carbon fibers, VGCF and xGnP-15. Clays as in the case of flex strength prove to be the worst reinforcement resulting in a less than 2 fold increase of the modulus even at 20vol%. The results reflect the dispersion condition, the presence or absence of agglomerations and the degree of alignment that are different for the various reinforcements.

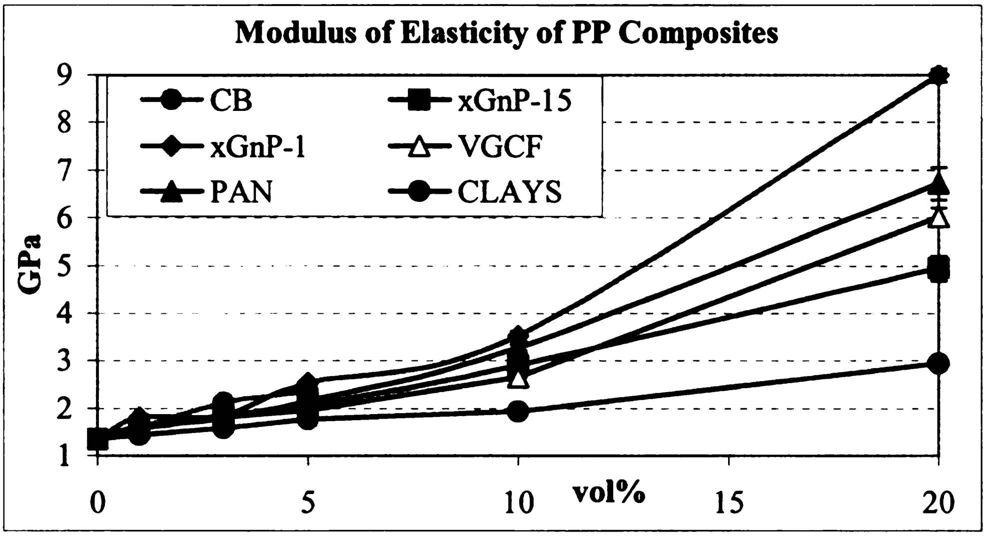

Figure 4.11. Modulus of Elasticity of various PP nanocomposites

Morphological studies of xGnP-1/PP nanocomposites indicated that xGnP-1 are homogeneously dispersed in the polymer matrix, there are no agglomerates even at a loading of 25 vol% and that at this content xGnP-1 are well embedded in the matrix as shown in Figure 4.12. The surface was obtained by fracture in liquid N_2. The fracture surface of neat PP prepared the same way is also shown for comparison in Figure 4.12a.

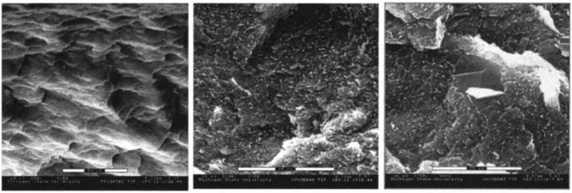

Figure 4.12. ESEM images of fracture surface a) neat PP (scale bar 50μm), b) 25vol% xGnP-1/PP (scale bar 40 μm) and c) 25vol% xGnP-1/PP (scale bar 25 μm)

Tensile Modulus

The tensile modulus of various PP composites with reinforcement content up to 20vol% is shown in Figure 4.13. At loadings up to 3vol% all materials besides the nanoclays result in a 3-fold increase of the modulus. At higher loadings i.e., above 5vol% PAN carbon fibers was the best reinforcement followed by xGnP-1.

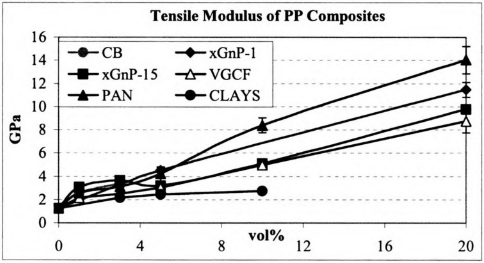

Figure 4.13. Tensile Modulus of various PP composites up to filler content of 20vol%

In general the flexural and tensile modulus are closely related and the trend observed in both is the same. However, in this particular case the DSM molds that are used are smaller compared to the molds described by the ASTM standards. Thus the difference in deformation mode (three point bending in flexural testing vs failure under extension in tensile), geometry and dimensions of the samples (flex bars vs dog-bone shape samples) are probably the reasons for the difference in the magnitude of the moduli between the flexural and tensile results as shown in Figures 4.11 and Figure 4.13 respectively. In particular, while xGnP-1 produces a larger improvement in flex modulus, PAN carbon fibers are the best reinforcement with respect to the tensile modulus. The main reason is that the tensile specimens are thinner compared to the flex bars so the degree of alignment along the flow direction during injection molding is higher. In addition, pulling the fibers along their axial direction produces, as expected, a higher modulus than bending the fibers during flexural testing.

Morphology of Flexural and Tensile Specimens.

The alignment of PAN carbon fibers in PP in a flexural bar away from the edges and near the sample edge is shown in Figures 4.14 and 4.15 respectively. The sample contains 5 vol% of PAN carbon fibers and the surface was prepared by polishing and acid etching followed by O_2 plasma.

The schematic of the flex bars in Figure 4.14 and 4.15 indicate which part of the surface is shown in the ESEM images. The arrow shows the direction of the flow. It can been seen that away from the edges the PAN fibers are aligned in plane but not necessarily along the flow direction. However, near the edges, Figure 4.15, the fibers are normal to the flow direction. Based on the ESEM study it is estimated that the in-plane morphology of the fibers covers 70-80% of the surface while the normal to the plane fiber morphology the 20-30%. The fibers that are oriented normal to the flow direction do not substantially contribute to the flexural modulus since during the testing they are subjected to bending force normal to their axis.

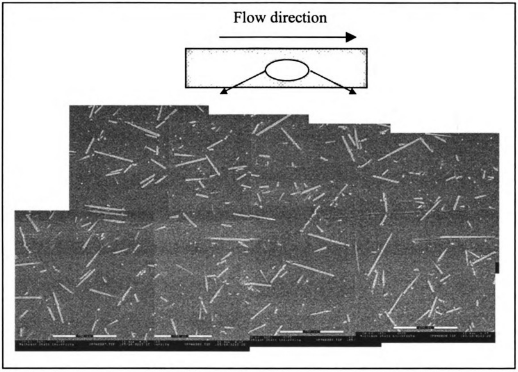

Figure 4.14. ESEM images of 5vol% PAN/PP flex bar showing the in plane orientation of fibers away from the specimen edges (scale bar 250 μm)

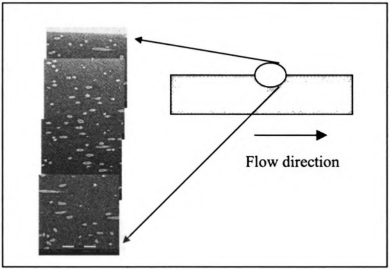

Figure 4.15. ESEM images of 5vol% PAN/PP flex bar showing the normal to the flow orientation of fibers near the specimen edges (scale bar 100 μm)

The alignment of PAN carbon fibers in PP in the tensile specimen away from the edges and near the sample edge is shown for both cases in Figures 4.16. The sample contains 5vol% of PAN carbon fibers and the surface was prepared by polishing and acid etching followed by treatment with O_2 plasma.

Away from the edges the PAN fibers are aligned mainly along the flow direction and not in plane as in the case of the flex bar, shown in Figure 4.14. As in the case of the flex bar the fibers near the edges are normal to the flow direction. Based on the ESEM study it is estimated that the in-plane morphology of the fibers covers 80-90% of the surface while the normal to the plane fiber morphology the 10-20%. Thus it is concluded that in the case of tensile specimens the concentration of fibers oriented along the flow direction, which contribute to the tensile modulus, is larger and the degree of orientation higher than in the case of a flex bar.

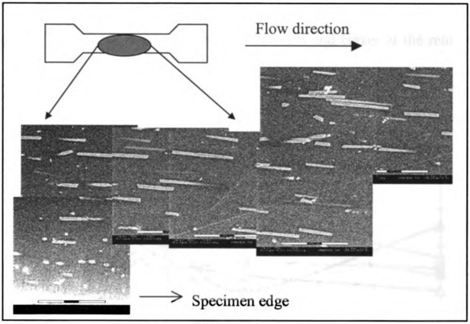

Figure 4.16. ESEM images of 5vol% PAN/PP tensile bar (scale bar 150 μm)

Impact Strength

The impact strength of various PP composites up to 10vol% of reinforcement is shown in Figure 4.17. There is an optimum concentration, different for each reinforcement, for which the impact strength is maximum. Increases in reinforcement loading decrease the impact strength. The highest impact properties are obtained with xGnP-1 at an optimum concentration of 3vol% where the impact strength of PP is increased by a factor of two. Carbon black has a negative effect i.e., at 5vol% the impact strength of neat PP is reduced by 50%.

Differences in impact strength may be due to differences in the crystalline morphology of the polymer [8], as discussed in more detail in Chapter 7, or due to changes in the energy absorbing mechanisms i.e., increased plastic deformation of the matrix along the matrix-reinforcement interface, crack branching due to hindrance by reinforcements, bridging of the crack, creation of voids and crazes at the reinforcement edges.

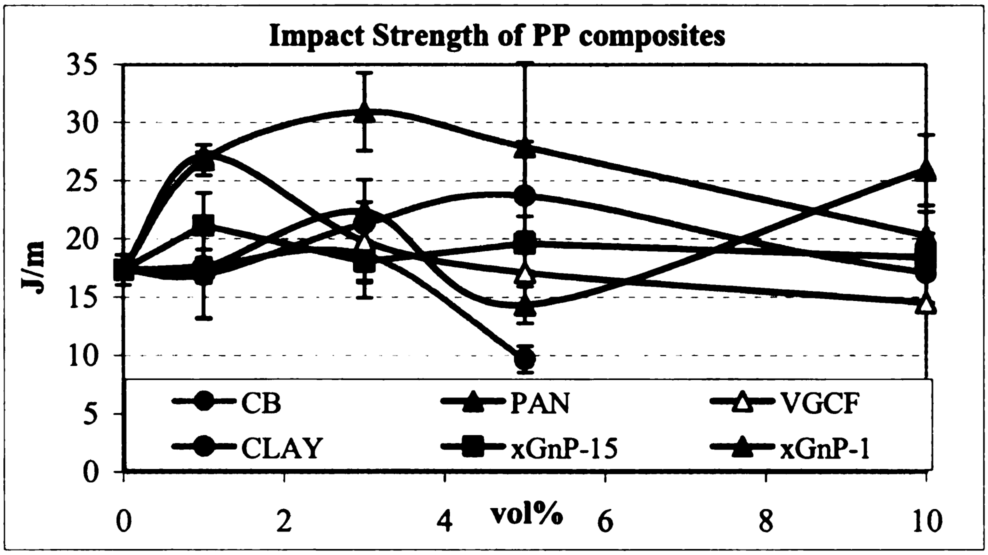

Figure 4.17. Impact strength of various PP composites

4.3.3 Effect of Compounding on Flexural Properties of xGnP-PP Nanocomposites

As indicated by the ESEM study presented in Figures 4.5-4.7 the melt mixing compounding of xGgnP-15 and PP in the DSM microextruder results in composites with agglomerates and poor dispersion of xGnP-15 and as consequence poor mechanical properties. In order to improve dispersion, xGnP-15 and PP were premixed in presence of isopropyl alcohol prior to melt mixing.

This premixed compounding method that is analytically described in Chapter 2 is time and cost effective and environmentally friendly since the solvent used is not toxic and can be recycled once the mixing is completed. The xGnP-15 is dispersed by sonication in isopropyl alcohol and the PP powder is added to the thick solution. The alcohol is removed by filtering or heating and the xGnP-15 cover PP powder is fed into the extruder.

The flexural strength and modulus of elasticity of xGnP-15/PP nanocomposites at 3, 5 and 10vol% made by (i) melt mixing using the DSM and injection molding and (ii) premixing followed by melt mixing in the DSM and injection molding are shown in Figures 4.18 and 4.19.

The premixed samples show 8% higher strength at 5 and 10 vol% and an improved modulus up to 60% at a loading of 10 vol% compared to the samples made by melt mixing. It is expected that premixing will not have such a strong effect or any effect at higher xGnP-15 contents because the number of graphite platelets will be so large that the amount of polymer present will not be sufficient to prevent agglomeration.

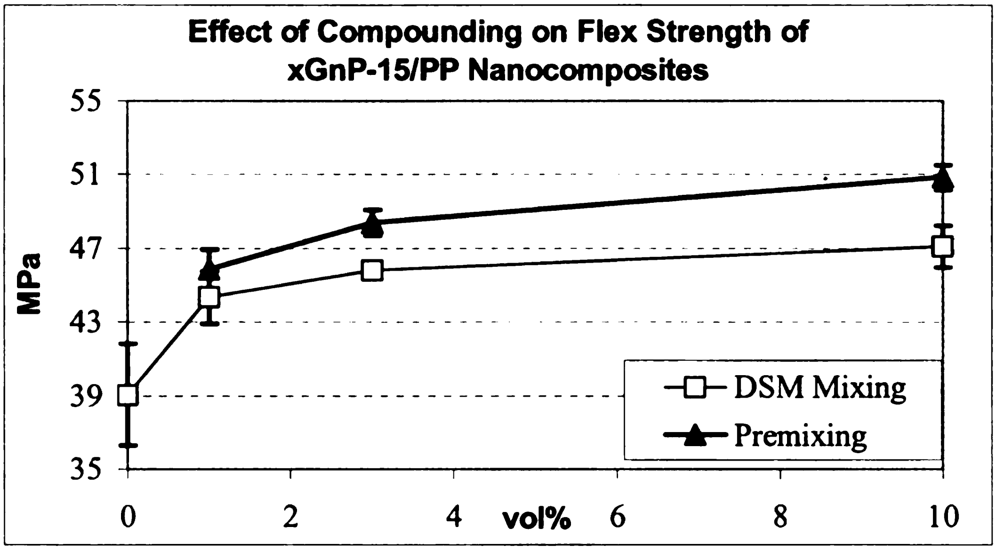

Figure 4.18. Effect of compounding on the flex strength of xGnP-15/PP composites

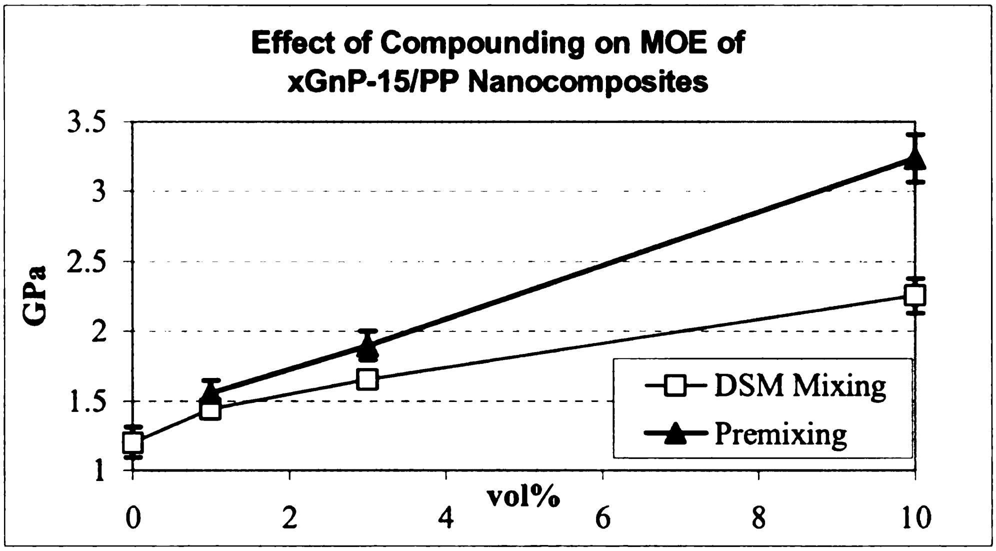

Figure 4.19. Effect of compounding on flex modulus of xGnP-15/PP composites

The morphology of the premixed and melt mixed samples at 10vol% of xGnP-15 was studied by ESEM. The fracture surfaces examined were obtained during flexural testing. Agglomerates of xGnP-15 are present in the samples made by melt mixing as shown by the arrows in Figure 4.20a whereas premixing by coating the PP powder with xGnP-15 using sonication breaks the graphite agglomerates and results in a well dispersed system free of particle agglomerations with the graphite platelets being well embedded in the PP matrix as shown in Figure 4.20b.

In addition, the surface of the melt mixed samples shows two distinguished types of morphology, a) areas with big xGnP-15 agglomerates shown in Figure 4.20a and large flat graphite platelets buckled and deformed that are shown in Figure 4.21 and b) areas that away from the specimen edges where no xGnP-15 or only very small graphite particles can be seen on the surface as indicated by the arrows in Figure 4.22. Based on Figures 4.20a, 4.21 and 4.22 which are typical ESEM images of melt mixed xGnP-15/PP morphology it is concluded that during melt mixing there is not enough shear to break down the xGnP-15 agglomerates and homogeneously disperse the graphite platelets.

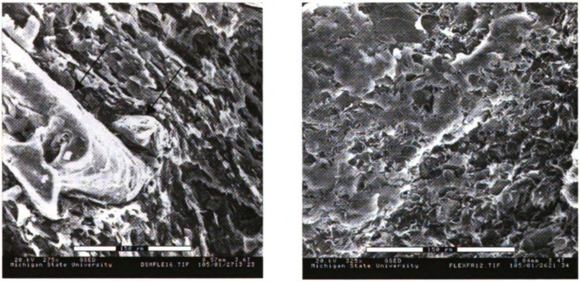

Figure 4.20. ESEM of fracture surface of 10vol% xGnP-15/PP composites made by a) melt mixing and b) premixing and melt mixing (scale bar 150μm)

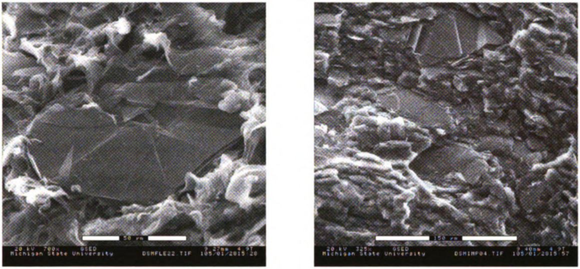

Figure 4.21. ESEM of fracture surface of 10vol% xGnP-15/PP composites made by melt mixing a) scale bar 50μm and b) scale bar 150μm

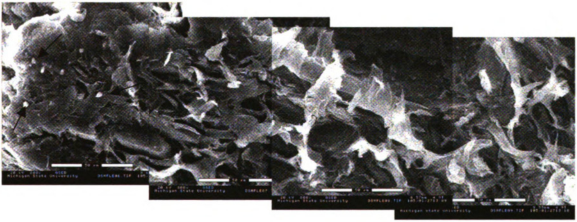

Figure 4.22. ESEM of fracture surface of 10vol% xGnP-15/PP composites made by melt mixing (scale bar 150μm)

4.4 Theoretical Models vs. Experimental Data

The theoretical models used for the prediction of modulus in nanocomposites such as the rule of mixtures and Halpin-Tsai are adequate for composites with macro-scale size reinforcements but there is a huge discrepancy between the predictions and experimental data when applied to composites with nanoreinforcements. The reason is that the models are built on the assumption that the bonding between the matrix-reinforcement interface is perfect. This is not a realistic assumption in the case of nanocomposites where as the reinforcement size decreases the interface increases significantly and consequently the effect of the imperfect bonding and weak adhesion on the strength and modulus of the composites dominates and cannot be ignored.

A more realistic approach is proposed by Shia *et al* [9] who used a simple interface model to quantify the imperfect interfacial bonding and introduced the concept of effective aspect ratio and effective aspect volume fraction of the platelets. These effective quantities depend on a single material parameter, the constant interfacial shear stress, which was determined by fitting the theory to experimental data obtained for elastomer-silicate nanocomposite systems by Burnside and Giannelis [10]. The concept of effective aspect ratio and volume fraction is used to account for the fact that an imperfect interface reduces the reinforcing efficiency of the platelet since a greater portion of its width is not fully loaded.

The difference between the predicted value of modulus calculated using the Halpin-Tsai and the Tandon-Weng model and the modulus determined experimentally for xGnP-1/PP, xGnP-15/PP and PAN/PP composites is shown in Figure 4.23.

The Halpin-Tsai equation [11] for the tensile, longitudinal modulus of unidirectional fiber-reinforced composites is given in Equation (4.1)

$$E = E_M \frac{1+\eta\xi V_f}{1-\eta V_f}, \quad \eta = \frac{\frac{E_f}{E_M} - 1}{\frac{E_f}{E_M} + \xi} \tag{4.1}$$

where E_M is the matrix Young's modulus, E_f is the longitudinal (E_{11}) modulus of the fibers, V_f is the fiber volume fraction. The parameter ξ is a function of the filler's aspect ratio, a, i.e., $\xi=2/3a$ for case of platelets and $\xi=2a$ for fibers.

The Tandon-Weng model for both the randomly oriented [12] and the inidirectionally aligned composites [13] was also used to predict the modulus of xGnP/PP and PAN/PP composites. In addition, the effective aspect ration of xGnP-1 was calculated by fitting the experimental data using the Tandon-Weng for the random case. It is noted that theTandon-Weng equation assumes that the fillers are isotropic.

As shown in Figure 4.23 there is a good agreement between the Tandon-Weng (aligned), the Halpin-Tsai and the experimental data for the case of the PAN/PP composites. The Tandon-Weng overpredicts the modulus at higher PAN loadings, which maybe attributed to the assumptions of the isotropy and perfect alignment.

In case of xGnP-15/PP composites both the Halpin-Tsai and Tandon-Weng models predict the same value for the modulus, which is however much larger compared to the experimental value. The main reason is that the theoretical aspect ratio of xGnP-15 used for the calculations is 1500. However, due to agglomeration and change of the platelet morphology during processing the effective aspect ratio of xGnP-15 is at least an order of magnitude smaller.

Finally, in case of xGnP-1/PP nanocomposites there is no difference between the moduli predicted by the Tandon-Weng (aligned) and the Halpin-Tsai models, which is in good agreement with the experimental data for low xGnP-1 loadings. At higher loadings however, the various models overpredict the modulus. As in the case of xGnP-15 the main reason is that the effective aspect ratio of xGnP-1 is smaller than the theoretical value i.e.100 used in the calculations.

This was confirmed by calculating the aspect ratio for which the Tandon-Weng model fitted better the experimental results (shown by the orange line in Figure 4.23). The calculated value of the aspect ratio is ~60 which is 40% smaller than the theoretical one.

In addition the deviation between the theoretical predictions and the experimental data at higher xGnP contents is also due to the fact that at these xGnP concentrations the interface becomes really important and thus the weak adhesion along the interface, which means not efficient load transfer from the matrix to the reinforcement, dominates.

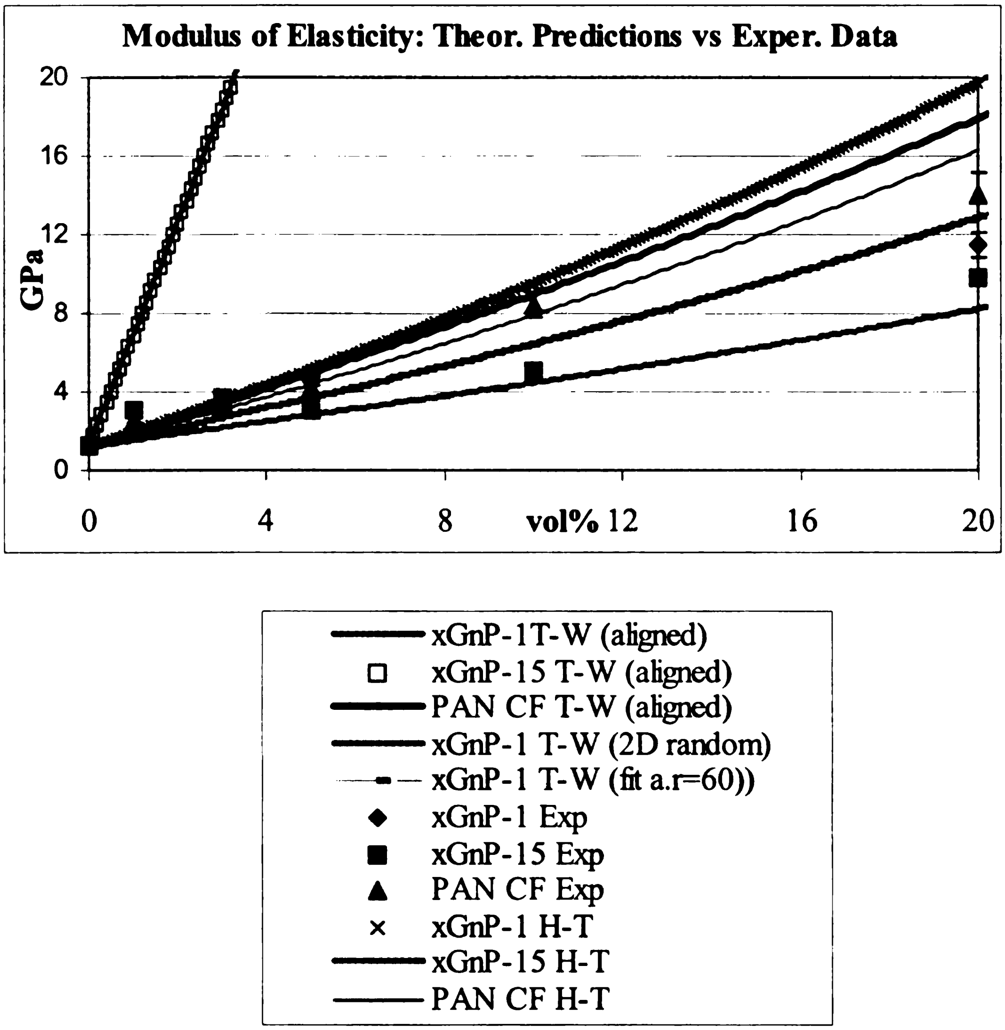

Figure 4.23. Modulus of Elasticity: Comparison of Halpin-Tsai and Tandon-Weng theoretical models to Experimental Data

4.5 Summary of Results

The addition of xGnP-1 to PP produced a greater improvement in flexural modulus and impact strength than the commercially available carbon materials i.e., carbon black, VGCF and PAN carbon fibers that were used for comparison. Octadecylamine surface treated clays that are specifically used as reinforcement in PP were also used, however, due to absence of compatibilizer no significant improvement on the mechanical properties of the clay-PP nanocomposites was observed. The superior properties of xGnP-1/PP system are an indication that the exfoliated graphite nanoplatelets have properties similar to highly crystalline graphite.

In case of xGnP-15 the small enhancement of mechanical properties combined with the results of the morphological study lead to the conclusion that xGnP-15 forms agglomerates that are aligned along the flow direction and can buckle or roll-up and thus xGnP-15 is not well dispersed in the polymer matrix resulting in non-homogeneous structures and poor mechanical properties.

Based on the morphological study of the xGnP-1, xGnP-15, PAN and VGCF reinforced composites it is concluded that the small aspect ratio reinforcements i.e., xGnP-1 and PAN carbon fibers behave similarly i.e., no buckling or roll-up of xGnP-1 was observed and the carbon fibers were almost unidirectional aligned along the flow direction. On the other hand the higher aspect ratio reinforcements such as the xGnP-15 and VGCF were more prone to the stress field present during processing and they either changed their morphology/shape (xGnP-15), or formed two-dimensional networks (VGCF), in response to the shear conditions they experience in the extruder during melt mixing. This is expected since the smaller aspect ratio reinforcements are stiffer (larger value of the weight/deflection ratio) which indicates that the deflection that a material undergoes under the same applied stress increases with its aspect ratio.

The flexural strength of both xGnP-1 and xGnP-15 reinforced PP composites increases at low concentrations of xGnP but reaches a plateau value at higher loadings. This result is interpreted as indicating the need for a better mixing/dispersion process and/or surface treatment of xGnP in order to improve dispersion within the polymer matrix and improve adhesion. It is noted that the processing conditions for the DSM microextruder injection molding system used were optimized for 3vol% of xGnP-1. Higher loadings might require higher barrel or mold temperatures or longer mixing time. Also high screw speed (high shear) or change in the barrel gap distance might result in reduction of the aspect ratio in case of fibers.

A new compounding method, the premixing of xGnP in isopropyl alcohol using sonication followed by xGnP coating of the PP powder at room temperature was found to improve the flexural properties of xGnP-15/PP nanocomposites made by melt mixing. In particular, due to premixing there was an improvement of the flexural strength of ~8% at 5 and 10 vol% and increase of the modulus up to 60% at 10 vol% compared to the samples made just by melt mixing. The enhancement of the flexural properties is attributed to the fact that sonication breaks the graphite agglomerates and results in a homogeneous graphite-coated PP powder which is used as the feedstock in the extruder.

Finally, the comparison of the experimental data of tensile modulus with values predicted based on the Halpin-Tsai equation indicates that

(i) There is good agreement for low reinforcement loading but as the content increases the models overestimate the modulus. This is expected since the agglomeration of the particles observed by ESEM is not taken into account in the theoretical models. In addition, the effect of the imperfect bonding at the interface and the weak adhesion becomes more dominant at higher reinforcement loadings.

(ii) In case of xGnP-15 where the aspect ratio of a platelet is assumed to be 1500 the models overestimate the modulus even for low xGnP-15 contents. This is anticipated since based on the ESEM morphological study of the xGnP-15/PP nanocomposites xGnP-15 platelets tend to form big agglomerates, and even change geometry i.e., buckle and roll-up reducing thus the aspect ratio.

4.6 References

1. A.A. Griffith, "The Theory of Rapture" Proceedings of the 1st International Congress on Applied Mechanics 55, (1924)

2. A. A. Griffith, " The phenomena of Rapture and Flaw in Solids" *Phil. Tans. Roy. Soc.*, **A221**, 163 (1920)

3. W. J. Weibull, " A Statistical Distribution Function of Wide Applicability" *J. Appl Mech.*, Sep 293, (1951)

4. M.R. Piggott, "Load Bearing Fibre Composites", Pergamon Press, Chapter 8, p141 (1980)

5. T. Huy, R. Adhikari, T. Lupke, S. Henning and G. Michler, "Molecular Deformation Mechanisms of Isotactic Polypropylene in α- and β-Crystal Forms by FTIR Spectroscopy" *Journal of Polymer Science: Part B: Polymer Physics* **42**, 4478-4488 (2004)

6. http://www.nanocor.com/tech_papers/ANTEC2002.pdf

7. P. Banerjee and B.M. Mandal, "Conducting polyaniline Nanoparticle Blends with Extremely Low Percolation Thresholds", *Macromolecules* **28**, 3940, (1995)

8. T. Huy, R. Adhikari, T. Lupke, S. Henning and G. Michler, "Molecular Deformation Mechanisms of Isotactic Polypropylene in α- and β-Crystal Forms by FTIR Spectroscopy" *Journal of Polymer Science: Part B: Polymer Physics* **42**, 4478-4488 (2004)

9. D. Shia, C.Y. Hui, S.D. Burnside and E.P. Giannelis, "An Interface model for the Prediction of Young's Modulus of Layered Silicate-Elastomer Nanocomposites", *Polymer Composites*, **19** 5, 608 (1998)

10. S.D. Burniside and E.P. Giannelis, "Synthesis and properties of new poly(dimethylsiloxane) nanocomposites" ***Chem.*** *Mater.*, **7** 1597 (1996)

11. J.C. Halpin and S.W. Tsai, "Effect of Environmental Factors on Composite Materials" Air Force Technical Report AFML-TR 67-423, wright Aeronautical Labs, Dayton, OH, (1967)

12. G.P. Tandon and G.J. Weng, "Average Stress in the Matrix and Effective Moduli of Randomly Oriented Composites", *Composites Science and Technology* **27**, 111-132 (1986)

13. G.P. Tandon and G.J. Weng, "The effect of Aspect Ratio of Inclusion on the Elastic Properties of Unidirectionally Aligned Composites", *Polymer Composites* **5**, (4) 327-333 (1984)

MICHIGAN STATE UNIVERSITY LIBRARIES
3 1293 02845 4779

THESIS
4
2007
V.2

139
724
THS

LIBRARY
Michigan State
University

PLACE IN RETURN BOX to remove this checkout from your record.
TO AVOID FINES return on or before date due.
MAY BE RECALLED with earlier due date if requested.

DATE DUE	DATE DUE	DATE DUE
MAY 1 3 2008 1 1 1 8 0 8		
AUG 2 9 2009		
06 28 12		

2/05 p:/CIRC/DateDue.indd-p.1

EXFOLIATED GRAPHITE NANOPLATELETS AS REINOFORCEMENT FOR MULTIFUNCTIONAL POLYPROPYLENE NANOCOMPOSITES

VOLUME II

By

Kyriaki Kalaitzidou

A DISSERTATION

Submitted to
Michigan State University
In partial fulfillment of the requirements
for the degree of

DOCTOR OF PHILOSOPHY

Department of Chemical Engineering and Materials Science

2006

CHAPTER 5

THERMAL, VISCOELASTIC AND BARRIER PROPERTIES OF EXFOLIATED GRAPHITE POLYPROPYLENE NANOCOMPOSITES

5.1 Introduction

Since xGnP is thermally conductive and has a low coefficient of thermal expansion, the addition of xGnP to a polymer matrix is expected to improve its thermal conductivity as well as its mechanical properties. A thermally conductive material is useful in applications such as lighting ballasts, transformer housings, microchip cooling, fuses, radiators, and fins [1]. In addition if the reinforcement has an aspect ratio greater than 1, then composites can be designed with strategically oriented fibers/particles to produce desired combinations of thermal conductivity and coefficient of thermal expansion. The reduction of coefficient of thermal expansion is a desirable property for composite structural applications.

From the processing and application point of view, the rheological properties of nanocomposites are also very important. They are related to the materials' microstructure, reinforcement's aspect ratio, dispersion, and orientation and the interactions between the reinforcement and the polymer chains. The rheological behavior of nanocomposites can correlate to the various nanocomposite properties such as mechanical, thermal and electrical. A common feature observed in the rheological properties of various nanocomposite systems i.e., polymer reinforced with layered silicates [2, 3], carbon fibers or carbon nanotubes [4, 5, 6] is nonterminal, solidlike behavior at low frequencies that has been attributed to a filler network formed in the nanocomposites.

Last but not less important, xGnP due to its platelet structure has the potential to improve the polymer barrier properties to small gas molecules such as O_2, CO_2 and H_2O by increasing the tortuous path the molecules have to follow in order to penetrate the polymer composite film. Such an improvement in barrier properties will allow the use of nanocomposites in packaging for electronics, food or beverages thereby increasing the range of the potential applications of xGnP-polymer nanocomposites.

5.1.1 Thermal Conductivity of Nanocomposites: Theory vs. Experimental Data

The existing understanding of the effective thermal conductivity of composites is based on continuum level micro-scale models. The basic models incorporate only factors like the conductivity of the constituents and the particle volume fraction, i.e, Maxwell-Eucken model [7], whereas, more advanced models account also for the particle size and shape i.e., the model proposed by Nielsen [8] and the one by Agari et al [7] also consider the effect of formation of a conductive path of particles on the thermal conductivity of the composite.

Agari *et al* [7, 9, 10, 11, 12, 13] provided basic knowledge about the factors that affect thermal conductivity in composites and their model could accurately predict conductivity values for a significant number of polymer systems such as PE, PVC, PS and polyamide with fillers such as graphite, carbon black and copper and aluminum oxides.

However, none of the existing models incorporates the fact that as the size of the reinforcement decreases, thermal transport will be dominated by the thermal contact resistance at the interface formed between the nanoreinforcement and the polymer matrix. In addition to the effect of the interface, the ballistic nature of heat transport also needs to be taken into account. The reason is that the temperature gradient which is the driving force for diffusion, vanishes as particle size decreases and thus diffusion does not contribute significantly to heat transfer.[14, 15].

Thermal energy is carried by phonons through lattice vibrations or by electrons in the case of metals. In conventional composites the main heat transfer mechanism is diffusion since the mean free path of phonons is much smaller than the size of the particle. However, in case of nanoreinforcements the mean free path of phonons is comparable or even larger than the particle size and for high reinforcement loadings can also be equal or larger than the mean particle distance, which means that ballistic heat transfer dominates over the diffusion mechanism [14, 15].

A good approximation for the heat transfer resistance across an interface, which is commonly used in analytical models or molecular simulation studies of thermal transport in nanoscale [14], is provided in Equation (5.1)

$$R_C = R_{CD} + R_{CB} \tag{5.1}$$

where R_C, R_{CD}, and R_{CB} are the overall heat resistances at the constriction/interface, the heat resistance at the interface due to diffusion and due to ballistic heat transfer respectively.

R_{CD} decreases with the Knudsen number, Kn, given by Equation (5.2) whereas R_{CB} is proportional to the Biot number, Bi, which is defined by Equation (5.3)

$$Kn = \frac{l}{a} \tag{5.2}$$

$$Bi = \frac{R_b k}{a} \tag{5.3}$$

where a is the length of the contact/interface between the reinforcement and the matrix, l is the phonon mean free path, k is a function of the conductivities of the constituents and R_b is the thermal boundary resistance.

Based on Equations (5.1)-(5.3) it becomes clear that as the size of the reinforcement decreases the contact length decreases as well while R_b increases. Thus both the Knudsen and Biot numbers increase indicating that the interfacial resistance in heat transfer is dominated by the ballistic mechanism.

Besides the ballistic transport in heat transfer, the thermal conductivity in composites can be enhanced by (i) ordered structures at the interface, i.e., crystalline interface vs amorphous [15]; (ii) lower interfacial resistance i.e, increase the size of the conductive particles or decrease the interface [15, 16], (iii) clustering effects [10], and (iv) by enhancing the chemical bonding or interactions between filler and matrix [16] which all result in reduction of phonon scattering.

Furthermore, the shape of the reinforcement is a very critical factor. Based on an experimental study on thermally conductive composites filled with platelet-shaped boron nitride particles it was suggested that fillers with platelet shape might offer advantages over other morphologies [17]. The same study concluded that the filler's thermal conductivity has little effect on the composite's conductivity in case of hard/stiff platelets i.e., aluminum oxide and silicon carbide. In case of more ductile materials of similar size and shape i.e., boron nitride that are able to deform changing thus shape and orientation, and permitting much closer contact between adjacent platelets; the intrinsic filler conductivity is very important and it is possible to reach high filler loading levels with good inter-particle contact and thus composites with higher thermal conductivities.

5.1.2 Objectives

The goal of the work presented in this chapter is to explore the effect of xGnP on the thermal i.e., coefficient of thermal expansion and thermal conductivity, viscoelastic i.e., viscosity, storage and loss modulus and barrier properties of polypropylene. The objectives are to:

- Compare the coefficient of thermal expansion (CTE) of xGnP-1/PP nanocomposites to the CTE of PP composites reinforced with commercially available carbon materials such as carbon black; vapor grown and pan based carbon fibers.
- Determine the coefficient of thermal conductivity of xGnP-PP nanocomposites as a function of xGnP loading and aspect ratio.
- Investigate the effect of xGnP and the other reinforcements on the rheological properties of PP i.e., viscosity, storage and loss modulus, as a way to assess the particle dispersion and the interconnected particle structures formed at high loadings and in order to determine the effect of the reinforcement in the processing of the matrix.
- Explore the possibility of using xGnP for the improvement of the gas barrier of PP by measuring the O2 permeability of xGnP-PP nanocomposite films and comparing to the barrier properties of PP films reinforced with carbon materials and clays.

5.2 Experimental Conditions and Characterization Techniques

The CTE of PP composites was determined by TMA 2940 (TA Instrument) for two regimes below and above the glass transition temperature (T_g). The samples made by the DSM were cut into small pieces, approximately 10 x 5 x 5 mm, and the dimension change was measured during heating process. The temperature range used was -25°C to 150 °C and the ramp rate was 2°C per minute.

The thermal conductivity of xGnP-PP composites was measured using dynamic scanning calorimetry (DSC). The samples made by DSM were disks (diameter of 5mm, and thickness~0.5mm) and the through plane conductivity was determined, i.e., the heat flow was normal to the flow direction induced during injection molding.

The rheological properties were measured with an Advanced Rheometrics Expansion System at 175°C using a 25mm parallel-plate fixture at a constant strain of 1%, which up to the maximum reinforcement loading used (20vol%) was within the linear viscoelastic regime determined by strain sweep at an oscillatory angular frequency of 1Hertz (2π rad/s). The samples made by DSM were discs with a diameter of 25mm.

The O_2 permeability of PP composite films at a reinforcement loading of 3vol% was measured based on ASTM method D3985 using Ox-Tran (Moden Controls Inc., Minneapolis, MN). The composite films were made by compression molding of flexural bars made by the DSM extruder injection molding system. The conditions used are 20 min at 220°C and no pressure applied followed by a second period of 20min at 220°C and a pressure of 30000 psi. The composite films were cooled to room temperature by air-cooling.

5.3 Results and Discussion

5.3.1 Effect of Reinforcements on Coefficient of Thermal Expansion

CTE was measured along two directions, the longitudinal, which is the direction along the flow of the melt during injection molding, and the transverse, which is the direction perpendicular to the flow. The CTE along each direction was measured for two temperature regimes i.e., for $T<T_g$ and $T>T_g$ shown in Figures 5.1 and 5.2 respectively.

Decrease of the CTE along the longitudinal direction was observed for all the fillers at both below and above T_g. In particular, for the regime below T_g, the xGnP-1 had the same effect with VGCF and PAN based carbon fibers, i.e., reduction of CTE by ~25%.

For the above T_g regime, graphite had the same effect as carbon black and VGCF (~20% decrease of CTE) but PAN based carbon fibers had a more dramatic effect reducing the CTE by ~65%. This reflects the high degree of alignment of the PAN carbon fibers along the flow direction (Figure 4.10 and 4.14) and the fact that these fibers are stiffer compared to the more flexible VGCF as discussed analytically in session 4.3.2.

The effect of reinforcements on CTE along the transverse direction for both temperature regimes was less dramatic. In the T>Tg area the xGnP-1 resulted in a 15-20% decrease of CTE followed by VGCF, carbon black and PAN carbon fibers which actually caused no reduction in the CTE of the neat polymer. This underlines the importance of using platelet-type reinforcement which when oriented properly can stiffen the composite in two directions rather than in one as in the case of aligned fibers [18]. The inherent CTE of graphite is 0.4-0.6μm/m for temperature range 30-100°C [19].

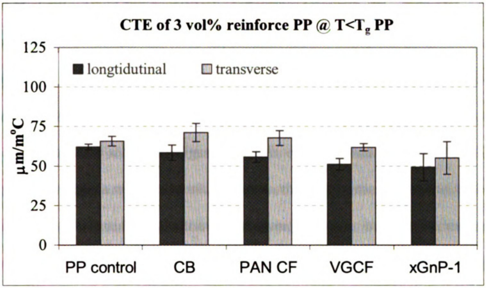

Figure 5.1. CTE of carbon reinforced PP nanocomposites for $T<T_g$

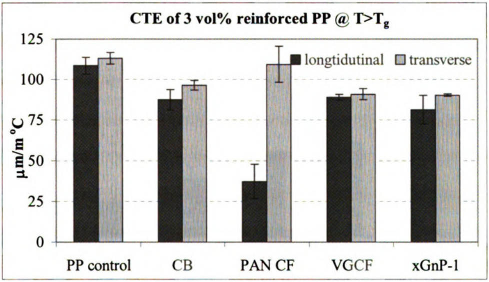

Figure 5.2. CTE of carbon reinforced PP nanocomposites for $T>T_g$

5.3.2 Thermal Conductivity of xGnP-PP Nanocomposites

The thermal conductivity of xGnP/PP nanocomposites was measured as a function of xGnP loading and concentration. Samples tested had a loading of 3, 10 and 25 vol% of xGnP-1 while the effect of aspect ratio i.e., xGnP-1 vs. xGnP-15 was only investigated in composites with 10 vol% xGnP loading. The thermal conductivity reported is the average value of three samples cut from a different flex bar.

The results are shown in Figure 5.3. It is expected that xGnP-15 due to higher aspect ratio and hence a smaller contribution from thermal contact resistance, will cause a larger increase in thermal conductivity. However, the error bars in the measurement overlapped at the 10vol% xGnP loading preventing this assessment from being made. More repetitions for each data point and at various xGnP contents are needed especially in case of xGnP-15 in order to determine the effect of the aspect ratio on the thermal conductivity.

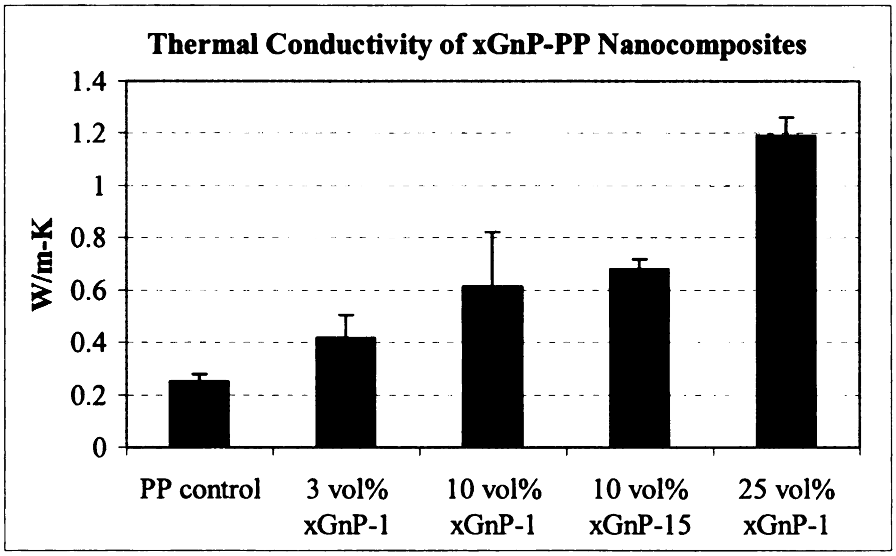

Figure 5.3. Thermal conductivity of xGnP-1 and xGnP-15um -PP composites

The conductivity measured is the through-plane conductivity. The in-plane thermal conductivity of xGnP-PP is expected to be much higher due to the orientation during injection molding and the anisotropy of xGnP as reported also by King's group [20]. Their work on thermally conductive graphite-nylon 6,6 composites indicated that the in-plane thermal conductivity is ~3 times larger than the through plane conductivity.

Theoretically the thermal conductivity of xGnP/PP composites at graphite contents should be much higher taking into account that the in-plane thermal conductivity of graphite is 210-230 W/m°C [19]. However, the results should be evaluated with respect to the morphology of xGnP-15/PP nanocomposites as presented in Chapter 4, i.e., poor dispersion and agglomeration of xGnP-15 in the PP matrix, buckle/bending and roll-up of xGnP-15 that result in reduction of the aspect ratio and change of the assumed platelet geometry.

Finally it should be noted that the method used i.e., use the slope of a heat flux vs. temperature plot obtained by DSC imposes an upper limit on the value for thermal conductivity. Though the method is sufficient for screening experiments and low filler contents it should not be used for materials where the thermal conductivity is expected to be larger than 1.2-1.5 W/m-K.

5.3.3 Rheological Characterization

Viscoelastic measurements of xGnP-PP nanocomposites as a function of xGnP's aspect ratio and loading as well as of VGCF and CB reinforced PP composites were performed at the temperature used during the fabrication of nanocomposites i.e., 175 °C, in order to investigate the effect of reinforcement on processing and assess the structure/morphology of the composites i.e., formation of interconnected particle network, which can also be related to the composite's percolation threshold for electrical conductivity [4, 5, 6].

Figures 5.4-5.8 show the increase of viscosity with reinforcement loading at various frequencies for xGnP-1/PP, xGnP-15/PP, VGCF/PP and CB/PP composites respectively. A common feature in these plots is that the viscosity increases with loading especially at lower frequencies. In addition, an abrupt increase of the viscosity in the low frequency regime is observed at a specific loading which is different for each reinforcement i.e., ~10vol% for xGnP-1 and xGnP-15, 3-5vol% for VGCF and 1-3vol% for CB. This is the loading at which a continuous particle network is formed in the composite that imposes a restraint on the long-range molecular motions of the polymer melt [21] and can be considered a rough estimation of the composite's percolation threshold.

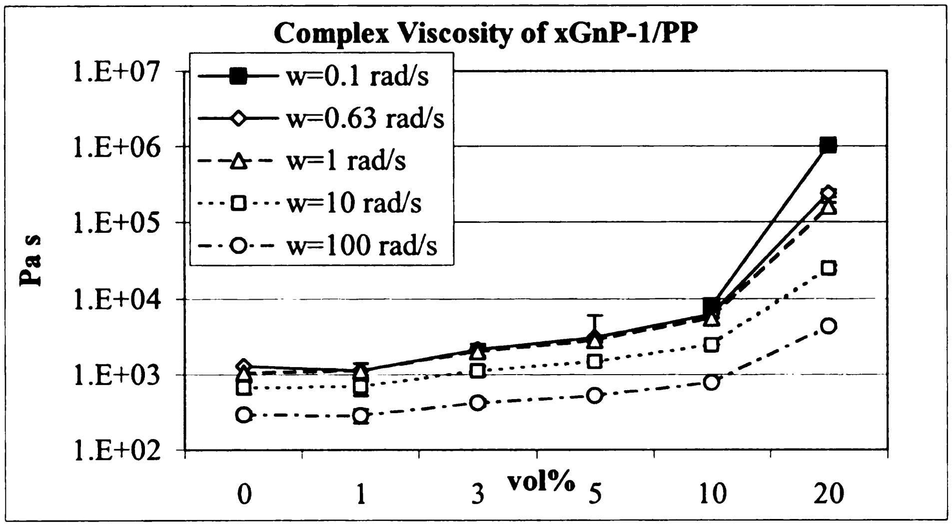

Figure 5.4: Complex viscosity of xGnP-1/PP at 1% strain and T=175°C

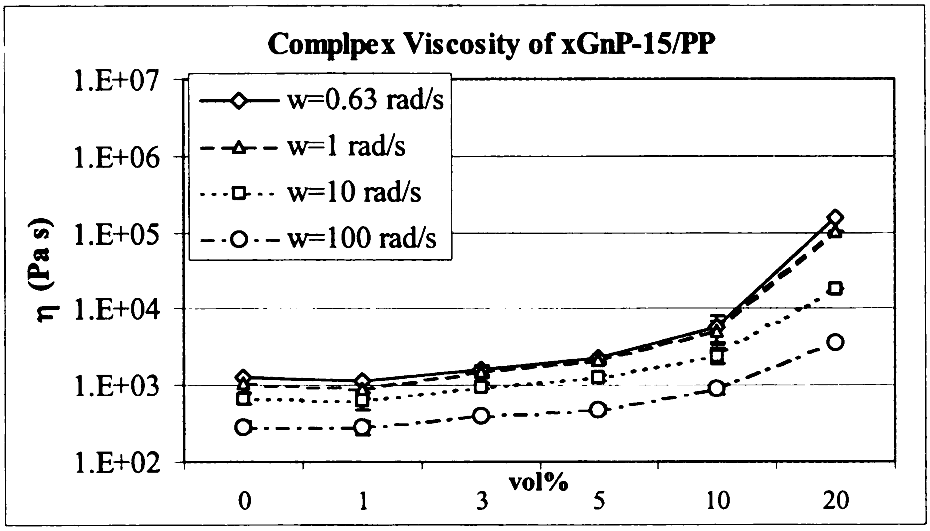

Figure 5.5: Complex viscosity of xGnP-15/PP at 1% strain and T=175°C

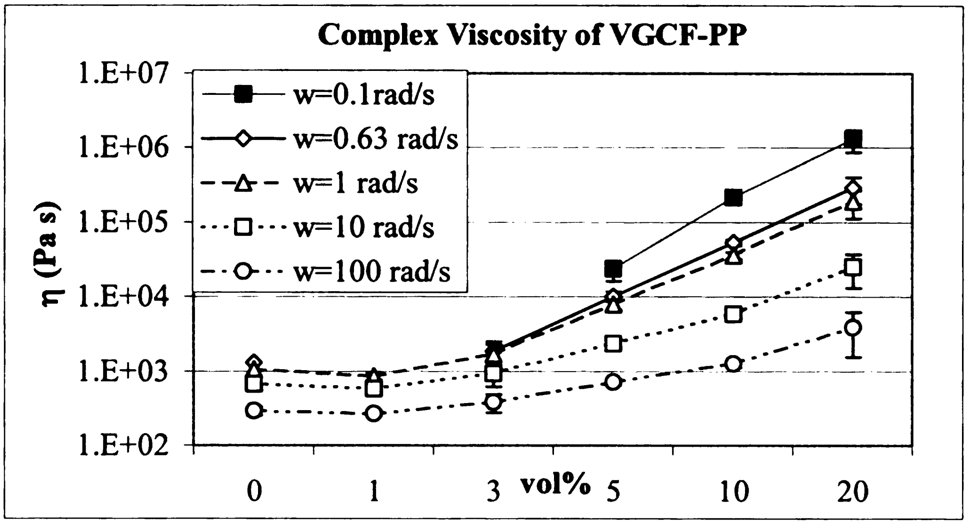

Figure 5.6: Complex viscosity of VGCF/PP at 1% strain and T=175°C

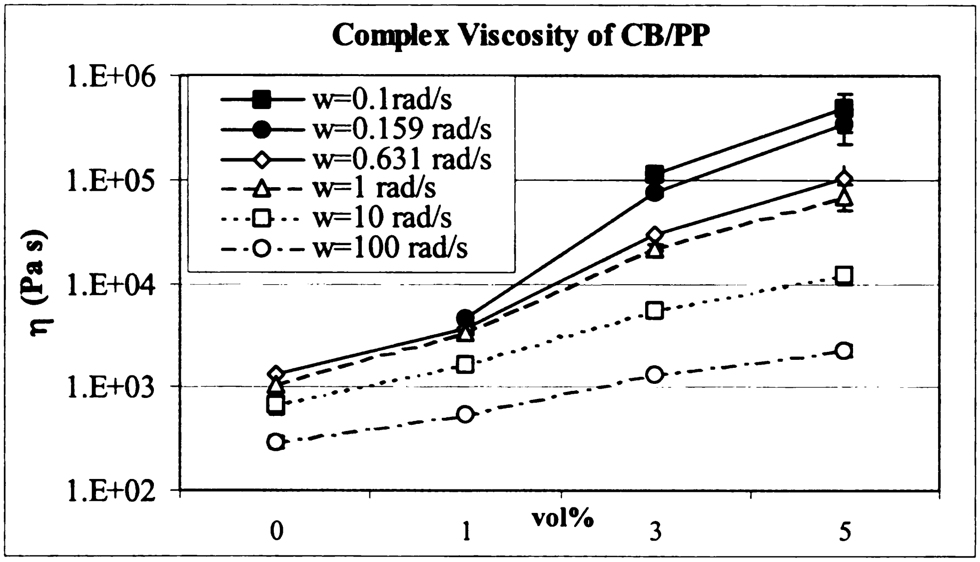

Figure 5.7: Complex viscosity of CB/PP at 1% strain and T=175°C

The viscoelastic behavior i.e., viscosity, elastic and storage modulus at low frequencies reveals information about the interactions between particles which for high reinforcement content result in formation of a rigid particle network, whereas the rheological behavior at high frequencies reflects the motions of the short molecular chains and is rarely affected by the presence of fillers [21]. As shown in Figures 5.4-5.6 at high frequencies i.e., ω=10 rad/s and ω=100rad/s addition of up to 20vol% of xGnP-1, xGnP-15 and VGCF results in a small increase of the viscosity while as shown in Figure 4.7 addition of only 5 vol% of CB causes a larger increase. This is because, as described in Chapter 2 the carbon black used is highly structured and thus, capable of forming a network even at low loading i.e., 2 vol%, which constrains the motions of even the short molecular chains. This increase in viscosity due to presence of carbon black defines the maximum content of CB that can be used as reinforcement in PP, which for the DSM microextruder used in this study is 5 vol% as described in Chapter 4.

A more common way to present the rheological data shown above is to provide the viscosity as a function of frequency for various reinforcement contents. However, in the viscosity–frequency plots, which for xGnP-1, xGnP-15, VGCF and CB reinforced PP composites are shown in Appendix D, the correlation of viscosity and percolation threshold for conductivity is not that obvious since the point at which the continuous path is formed does not appear as a step increase in the viscosity in the viscosity-frequency plots.

The storage modulus *G'* represents the elastic melt properties and provides a measure of nanocomposite 'stiffness' and its frequency dependence characterizes whether the material is in a liquid-like or solid-like state [5, 6, 22]. Figures 5.8, 5.9, 5.10 and 5.11 show the frequency dependence of *G'* for various reinforcement loadings for xGnP-1, xGnP-15, VGCF and CB reinforced PP composites respectively.

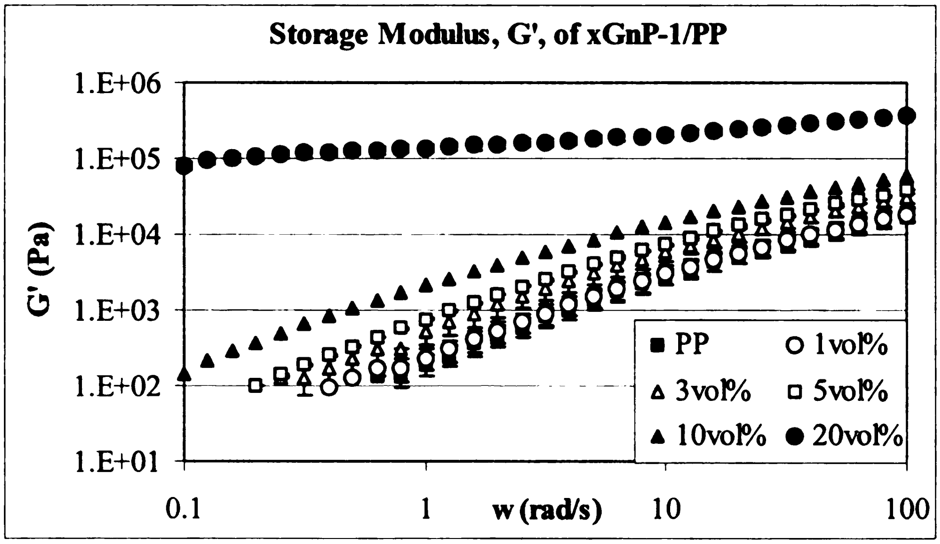

Figure 5.8: Storage modulus of xGnP-1/PP at 1% strain and T=175°C

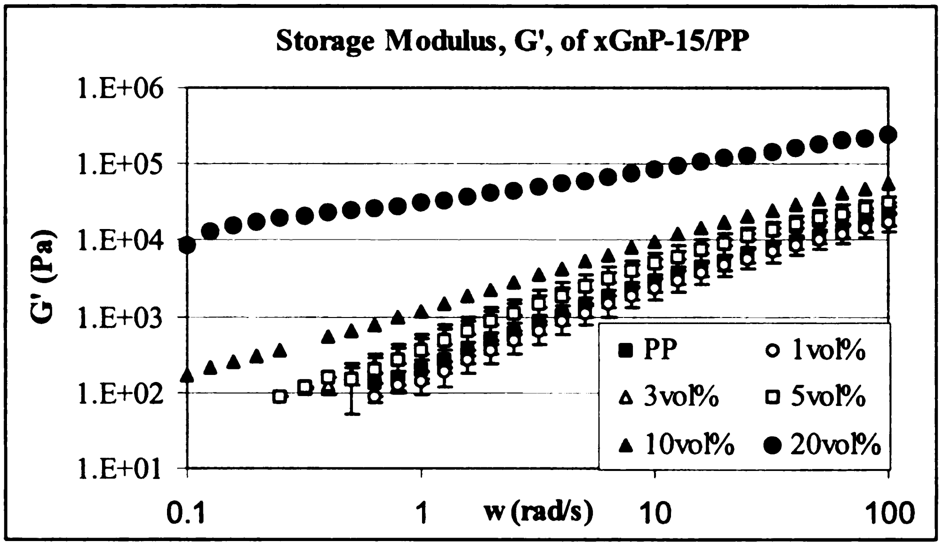

Figure 5.9: Storage modulus of xGnP-15/PP at 1% strain and T=175°C

Comparison between Figures 5.8 and 5.9 indicates that there is not any effect of xGnP's aspect ratio on the storage modulus of xGnP-PP nanocomposites. Only at the maximum loading used i.e., 20vol% xGnP-1 causes a larger increase in *G'* resulting in stiffer composites which may be due to the larger number of xGnP-1 particles compared to the number of particles contained in the same volume of xGnP-15.

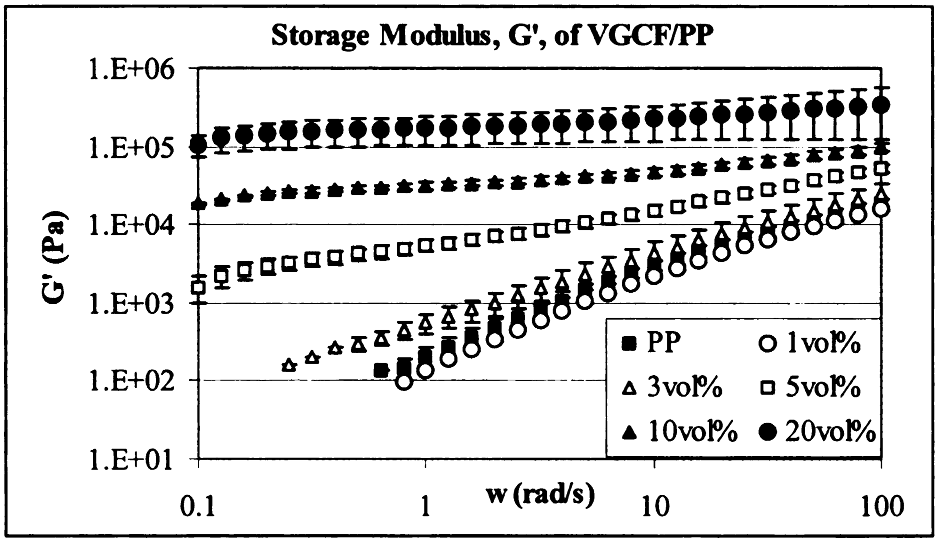

Figure 5.10: Storage modulus of VGCF/PP at 1% strain and T=175°C

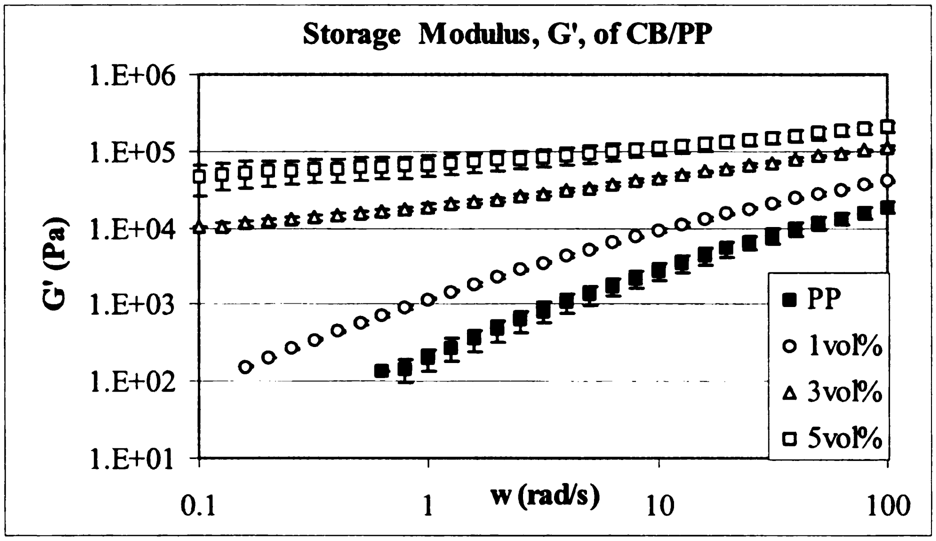

Figure 5.11: Storage modulus of CB/PP at 1% strain and T=175°C

A common feature in Figures 5.8-5.11 is that at the low frequency regime and for low reinforcement loadings the PP composites show the same rheological response as neat PP i.e., the typical newtonian liquid behavior with $G' \sim \omega^2$. However, as the reinforcement content increases, the elastic modulus becomes independent of frequency. This indicates a transition from a newtonian liquid to an ideal hookean solid, which accompanies the formation of a mechanically stable network structure [6]. Again, as in the case of the viscosity-concentration plots the concentration at which this transition occurs is different for each reinforcement and can be related to the composite's percolation threshold for electrical conductivity.

The loss modulus G", provides a measurement of viscous resistance to deformation and it follows the same trend as the elastic storage modulus G', i.e., increases with reinforcement loading at low frequencies and becomes independent of frequency at high reinforcement contents. The plots of storage modulus as well as of $tan\delta$ defined as the ratio of the loss over the storage modulus as a function of frequency at various reinforcement loadings for xGnP-1, xGnP-15, VGCF and CB reinforced PP composites are shown in *Appendix D.*

The viscoelastic properties of xGnP-polymer nanocomposites i.e., viscosity, loss and storage modulus are closely related to the percolation threshold for electrical conductivity and can be significantly modified by the flow conditions during processing. From application point of view this is very important since it allows for design and fabrication of nanocomposites with desired properties. For example this knowledge can be used for fabrication of "smart" materials i.e., pressure sensitive switches that will utilize these property changes.

5.3.4 O_2 Permeability of PP Reinforced Composites

One goal of this research is to explore the potential of using xGnP as an alternative to nanoclays which lack thermal and electrical conductivity and carbon nanotubes whose high cost limits their applications at least as reinforcements in composites. In addition to the enhancement of mechanical properties as discussed in Chapter 4, the reduction of CTE and the improvement of thermal conductivity of neat PP as presented in this chapter, xGnP also needs to improve the barrier properties of the neat polymer to small molecules i.e., O_2 in order to be competitive to clays. Addition of clays in polymers results in significant reduction of water adsorption as demonstrated in clay/nylon 6 systems [23-24] and the barrier properties improve dramatically as the silicate content increases [25].

From a theoretical point of view the improved barrier properties are the result of the presence of impenetrable platelets with high aspect ratio that are homogeneously dispersed in the penetrable polymer matrix leading to an increase of the diffusant path length (tortuosity) and consequently, a decrease of the gas permeability [26]. Factors that strongly affect the barrier properties of nanocomposites are the aspect ratio, dispersion and orientation of the platelets, the platelet/polymer interface and the crystallinity of the polymer matrix. All these factors can be optimized by choosing the proper processing method so it becomes evident that the barrier properties are closely related to other nanocomposite properties.

The effect of xGnP on the O_2 permeability of PP as a function of aspect ratio as well as comparison to the barrier properties of various PP composites at a reinforcement loading of 3vol% is shown in Figure 5.12.

CB does not improve the PP barrier to O_2 due mainly to its highly agglomerated structure, the irregular shape of the agglomerates and the high degree of porosity possibly promote the diffusion of the gas molecules. Both xGnP-1 and VGCF cause similar decrease in the O_2 permeability i.e., 10% at a reinforcement loading of 3vol%. The effect of aspect ratio was evident in case of xGnP-15 that caused the largest improvement in PP's barrier to oxygen i.e., ~20% followed by clays.

Based on the morphological study presented in Chapter 4, xGnP-15 forms large agglomerates and due to its high aspect ratio tends to strongly orient along the flow direction. It is possible that the agglomerates are destroyed during the compression molding used for the fabrication of the film and the platelets may slide against each other and align parallel to the mold plates, therefore xGnP-15 improves the barrier property of PP. In addition, taking into account the weak adhesion in the interface, as indicated in Chapter 4 based on the flexural strength data, the interface may provide a path for the gas molecules and thus xGnP-1 (small aspect ratio, large interface) causes less improvement in barrier properties than xGnP-15. Finally, the crystal structure of the matrix also affects the permeability of small molecules. Addition of xGnP-1 results in fewer but thinner crystals compared to crystals formed in presence of xGnp-15 as it will be discussed analytically in Chapter 7, and so it is easier for gas molecules to pass through.

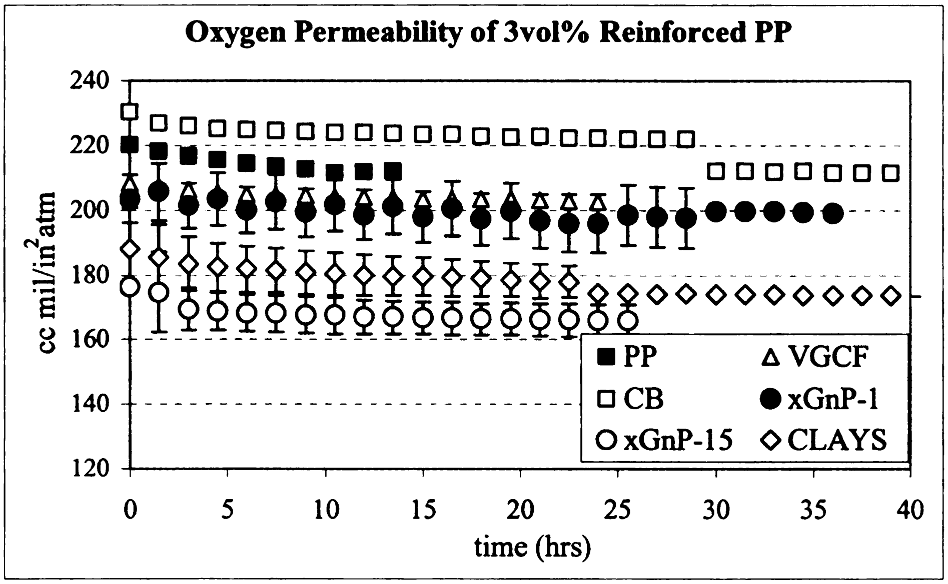

Figure 5.12: O_2 Permeability of 3vol% reinforced PP composites (T=25°C)

5.4 Conclusions

The coefficient of thermal expansion of xGnP-PP nanocomposites was determined and compared to the CTE of carbon reinforced PP. It is concluded that due to its platelet morphology xGnP can result in reduction of CTE in two dimensions i.e., in the graphite plane, while carbon fibers such as VGCF and PAN cause similar reduction in CTE but mainly in the direction parallel to their axis. Thus, xGnP can effectively be used as reinforcement in polymers for applications that require overall thermal stability of the part since graphite has a CTE of ~0.4-0.6 μ/m and as shown only at a loading of 3vol% can reduce the CTE of PP by ~20-25% in both the transverse and longitudinal direction..

The effect of xGnP concentration and aspect ratio on the thermal conductivity of PP was investigated. Addition of just 3vol% xGnP-1 increases the conductivity of the neat PP by a factor of two. The maximum conductivity value measured for 25vol% xGnP-1/PP composites was six times higher than that of PP.

Although no experimental data are provided in this study to allow for comparison of xGnP to other carbon reinforcements in terms of the composite's thermal conductivity; results reported in literature indicate that fillers with platelet geometry are more effective in increasing the thermal conductivity of composites because platelets can be more flexible and ductile and can deform during processing achieving good interparticle contact thus xGnP has an extra advantage over other carbon fillers used for thermally conductive composites.

The rheological behavior of xGnP-1, xGnP-15, VGCF and CB reinforced PP composites made by melt mixing and injection molding as a function of reinforcement content and frequency was investigated. In all the cases studied the viscosity increases with loading especially at lower frequencies. For the same loading the viscosity drops with frequency indicating shear-thinning behavior of these composites. An abrupt increase of viscosity as the reinforcement content increases is apparent in low frequencies. The reinforcement loading at which this transition occurs is different for each reinforcement used and is related to the percolation threshold for electrical conductivity.

The viscoelastic properties of xGnP-polymer nanocomposites i.e., viscosity, loss and storage modulus are closely related to the percolation threshold for electrical conductivity and can be significantly modified by the flow conditions during processing. Finally, it has been demonstrated that xGnP can effectively reduce the permeability of small molecules i.e., oxygen, in polymers even at low loadings i.e., 3vol% and that xGnP-15 is at least as effective as clays which are commonly used in polymers in order to improve the barrier properties. These results can be optimized by enhancing the adhesion at the xGnP-PP interface, as it will be discussed analytically in Chapter 8, and by improving the dispersion and preferential orientation of the platelets which can be accomplished by choosing the right processing method and conditions.

5.5 References

1. http://www.pittstate.edu/services/nsfreu/ResearchReports2004/dweberfuelcellicce11submit.pdffgh

2. R. Krishnamoorti and E.P. Giannelis, "Rheology of End-Tethered Polymer Layered Silicate Nanocomposites", *Macromolecules*, **30**, 4097-4102 (1997)

3. Q. Zhang and L.A. Archer, "Poly(ethylene oxide)/Silica Nanocomposites:Structure and Rheology", *Langmuir*, **18**, 10435-10442 (2002)

4. K. Lozano, J. Bonilla-Rios, and E.V. Barrera, "A study on Nanofiber-reinforced Thermoplastic composites (II): Investigation of the Mixing Rheology and Conduction Properties", *Journal of Applied Polymer Science,* **80,** 1162-1172 (2001)

5. P. Potscke, T.D. Fornes and D.R. Paul, "Rheological Bahavior of Multiwalled Carbon Nanotube/Polycarbonate Composites", *Polymer* **43** 3247-3255 (2002)

6. F. Du, R.C. Scogna, W. Zhou, S. Brand, J.E. Fischer and K.I. Winey, "Nanotube Networks in Polymer Nanocomposites: Rheology and Electrical Conductivity", Macromolecules **37**, 9048-9055 (2004)

7. Y. Agari, and T. Uno, "Thermal Conductivity of Polymer Filled with Carbon Materials: Effect of Conductive Particle Chains on Thermal Conductivity", *Journal of Applied Polymer Science*, **30** 2225 (1985)

8. L.E. Nielsen, "Thermal Conductivity of Particulate Filled Polymers", *Journal of Applied Polymer Science,* **17** 3819 (1973)

9. Y. Agari, T. Uno, "Estimation on Thermal Conductivities of Filled polymers", *Journal of Applied Polymer Science*, **32** 5705 (1986)

10. Y. Agari, M. Tanaka and S. Nagai, "Thermal Conductivity of a Polymer Composite Filled with Mixtures of Particles", *Journal of Applied Polymer Science*, **34** 1429, (1987)

11. Y. Agari, A. Ueda, M. Tanaka and S. Nagai, "Thermal Conductivity of a Polymer Filled with particles in the Wide Range from Low to Super-High Volume Content", *Journal of Applied Polymer Science*, **40** 929, (1990)

12. Y. Agari, A. Ueda and S. Nagai, "Thermal Conductivities of Composites in Several Types of Dispersion Systems", *Journal of Applied Polymer Science*, **42** 1665, (1991)

13. Y. Agari, A. Ueda and S. Nagai, "Thermal Conductivity of a Polyethylene Filled with Disoriented Short-Cut Carbon Fibers", *Journal of Applied Polymer Science*, **43** 1117 (1991)

14. R. Prasher, "Predicting the Thermal Resistance of Nanosided Constrictions", Nanoletters, **5**, 11, 2155 (2005)

15. P. Keblinski, S Phillpot, S. Choi and J. Eastman, "Mechanics of heat flow in suspensions of nano-sized particles (nanofluids), *International Journal of Heat and Mass Transfer* **45,** 855-863, 2002

16. E. Weber, M. Clingerman and J. King, "Thermally Conductive Nylon 6,6 and Polycarbonate Based Resins. I. Synergistic Effects of Carbon Fillers", *Journal of Applied Polymer Science,* **88**, 112 (2003)

17. R.F. Hill, "Thermal Conductivity of Platelet-filled Polymer-Ceramic Composites" Ph.D Dissertation, Institut für Struktur- und Funktionskeramik, Montanuniversität Leoben, Austria (2002)

18. M.R. Piggott, "Load Bearing Fibre Composites", Pergamon Press, Chapter 8, p141 (1980)

19. http://www.graftech.com/

20. J. King, K. Tucker, B. Vogt, E. Weber and C. Quan, "Electrically and Thermally Conductive Nylon 6,6", *Polymer Composites* **20**, 5, 643 (1999)

21. J. D. Ferry, "Viscoelastic Properties of Polymers" , Wiley, new York, p.356, (1980)

22. Kharchenko, S. B., Douglas, J. F., Obrzut, J., Grulke, E. A. & Milger, K. B. Flow-induced properties of nanotube-filled polymer materials. *Nature Mater.* **3,** 564–568 (2004)

23. Y.Kojima, A.Usuki, M.Kawasumi, A.Okada, T.Kurauchi, and O.Kamigaito, "Sorption of Water in Nylon 6-Clay Hybrid" *Journal of Applied Polymer Science*, **49**, 1259 (1993)

24. K. Yano, A. Usuki, A. Okada, T. Kurauchi and O. Kamigaito, "Synthesis and Properties of polyimide-Clay Hybrid", *J. Polym Sci.: Part A:Polym. Chem.*, **31** 2493, (1993)

25. P.B. Messersmith and E.P. Giannelis, "Synthesis and Barrier Properties of Poly(å-Caprolactone)-Layered Silicate Nanocomposites", *Journal of Polymer Science, Part A:Polymer Chemistry*, **33**, 1047-57 (1995)

26. L.E. Nielsen, "Models for the permeability of filled polymer system", *J. Macromol Sci Chem* **A1**, 929-942 (1967)

CHAPTER 6

EXPERIMENTAL STUDY OF THE FACTORS AFFECTING THE ELECTRICAL CONDUCTIVITY AND PERCOLATION THRESHOLD OF CONDUCTIVE POLYMER NANOCOMPOSITES

6.1 Introduction

Recently, there is an increased interest of using conductive materials such as carbon black [1], vapor grown carbon fibers [2-3], carbon nanotubes [4-7], as well as graphite [8-12], as reinforcements for polymers due mainly to their superior thermal and electrical properties.

Conductive composites can be used in place of metals when properties such as weight, toughness and corrosion resistance are required. An electrically conductive material can be used in static dissipative, slightly electrically conductive (e.g., fuel gages, etc.), or electromagnetic interference and radio frequency interference shielding applications as well as aircraft structural materials for protection against lightning. They can also be used for battery components and electric power cables. Finally, they have found applications as membrane in fuel cells [13].

The two important properties in electrically conductive composites are the electrical conductivity, which depends mainly on the filler volume fraction, and the percolation threshold, defined as the minimum volume content of the filler, above which the filler particles form a continuous network, as described by percolation theory and the composite becomes electrically conductive [14]. It is desirable for the conductive filler content to be as low as possible in order to achieve good processability, low cost and satisfactory mechanical performance.

As shown in Chapter 5 there is an abrupt change in the viscoelastic properties of PP composites at a specific reinforcement content that is different for the various reinforcements used. At this transition concentration, the electrically conductive xGnP particles are close enough to form a continuous network and the polymer composite changes from insulator to conductor.

6.1.1 Factors affecting the percolation threshold and electrical conductivity of composites

In order to utilize xGnP as conductive filler, it is necessary to identify each one of the factors that affect the percolation threshold and conductivity of composites, study them independently, and fully understand the mechanisms and interactions or synergistic phenomena at the nanoscale. These factors, which were analytically discussed in Chapter 1 and are briefly presented here, are [15-17]:

- Conductivities of constituents. The conductivity of the filler defines the upper limit for the electrical conductivity of the composite.
- Volume fraction and filler characteristics such as size, shape, surface area and morphology.
- Distribution and orientation of the filler as well as the interparticle filler spacing within the polymer matrix.

- Fabrication method and processing conditions. For example, extensive mixing can destroy the conductive network [1, 12], reduce the aspect ratio of the fillers [17] and induce filler orientation and alignment along the flow direction [17], resulting in composites with increased percolation threshold. On the other hand, solution intercalation [18, 19] reduces the percolation threshold because during the polymer dissolution the polymer chains get disentangled and can be physical adsorpted into the pores and interplanar spaces of the filler supporting the conductive network.
- The crystallinity of the matrix may also affect the conductivity of the composites since in a highly crystalline matrix the formation of the continuous conductive path is easier compared to a less crystalline polymer where the higher amorphous portion may result in more homogeneous particle distribution [20].

6.1.2 Objectives

A simple approach for the efficient design of electrically conductive composites is to use models that will take into account all the factors affecting the percolation threshold and conductivity of the composites. A review of the models that have been proposed for the calculation of the percolation threshold and the electrical conductivity of composites is given by King et al [21] and was analytically presented in Chapter 1. These models have limitations because they either do not consider all the key factors that affect the conductivity and/or they contain empirical parameters that cannot be measured experimentally and need to be assumed or calculated for each filler-polymer system.

The objective of the work presented in this chapter is to investigate the enhancement in electrical conductivity that can be produced in PP through the addition of xGnP. This includes determination of the electrical conductivity experimental data as well as the characterization information to both evaluate the enhancement and to identify shortcomings if models of electrical conductivity especially for particles having platelet type of morphology.

In particular, the percolation threshold and the electrical conductivity of carbon reinforced PP nanocomposites are determined for

- Different filler characteristics such as size, shape aspect ratio and surface area
- Various compounding methods i.e., melt-mixing, polymer solution and premixing
- Different conditions of filler orientation/alignment i.e., injection vs compression molding

6.2 Experimental Conditions and Characterization Techniques

The resistivity of carbon reinforced PP composites i.e., xGnP-1/PP, xGnP-15/PP, CB/PP, VGCF/PP and PAN/PP, was measured along the flow direction, in case of the injection-molded samples, using impedance spectroscopy by applying the two-probe method at room temperature. Samples with dimensions of 5x3x12 mm^3 were cut from the middle portion of flexural bars, and the resistivity was measured along the thickness direction (5mm). In this way, the conductivity could be measured in various directions. The two surfaces that were connected to the electrodes were first treated with O_2 plasma (10min, 550W) in order to remove the top surface layers which are rich in polymer and then gold coated to a thickness of 1-2nm to ensure good contact of the sample surface with the electrodes. The resistance of samples was measured in frequency range of 0.1 to 100,000Hz and converted to conductivity by taking into account the sample dimensions.

The composites were mainly fabricated by the DSM microextruder, injection molding system operating at the optimum processing conditions. Besides the melt mixing two other compounding methods were used in order to understand the effect of compounding on the electrical conductivity and percolation threshold of composites. These are i) a polymer solution method i.e., dissolution of PP in xylene at elevated temperature as proposed by Shen *et al* [18] and ii) a premixing method in which xGnP is added to PP powder in an organic non-solvent in order to coat the PP with the xGnP particles. Details are described in Chapter 2. The composite pellets/powder was used for injection or compression molding at conditions also described in Chapter 2.

6.3 Results and Discussion

6.3.1 Effect of Filler Characteristics

The electrical conductivity of carbon reinforced PP composites, made by melt mixing and injection molding, as a function of the filler content is shown in Figure 6.1. The percolation threshold varies with filler composition starting at under 2 vol% for carbon black, 5-8 vol% for VGCF, 8-9 vol% for xGnP-1 and xGnP-15, followed by 8-10 vol% for PAN based carbon fibers.

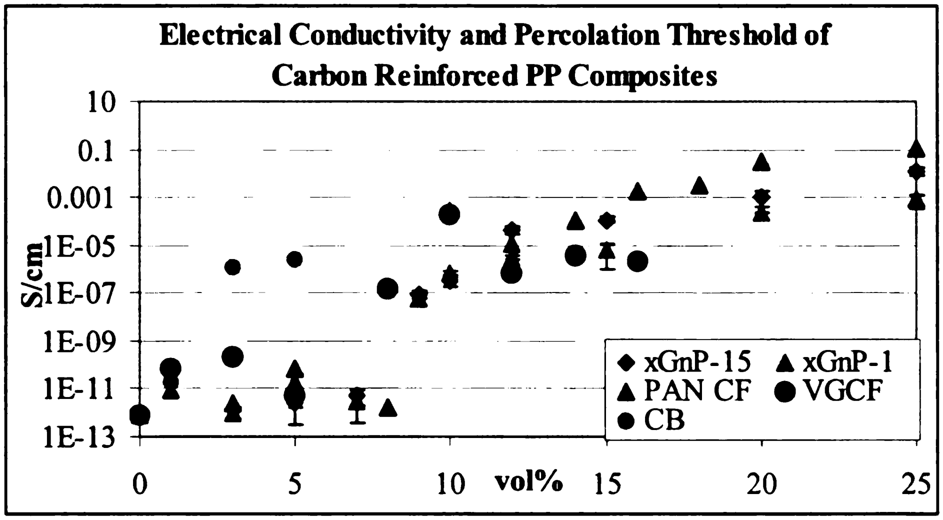

Figure 6.1: Effect of Filler's Geometry and Conductivity on Percolation Threshold and Conductivity of Carbon Reinforced PP Composites

With spherical particles (e.g. carbon black), the interparticle distance increases with increasing diameter such that it becomes more difficult to form a conductive pathway [15, 16]. Thus, it was anticipated that the carbon black should have a higher percolation threshold than observed. However, the carbon black used in this study does not consist of individual spherical particles but it is highly agglomerated (‘highly structured’) carbon black with a high degree of porosity having a surface area of 1400 m^2/g [22], that allows for polymer penetration. It can create a conductive network by occupying a large occluded volume at low concentrations [23] and by eliminating many of the particle-polymer interfaces through its aggregated structure.

For non-spherical particles (e.g., fibers, platelets), as the aspect ratio of the conductive fillers increases the critical concentration to induce bulk conductivity in the composite decreases significantly [4]. That is, the large aspect ratio particles can still maintain point-to-point contact at low concentrations which allows electron tunneling thus decreasing the percolation threshold. Based on Figure 6.1 the effect of aspect ratio on lowering the percolation threshold can be seen in case of carbon fibers i.e., VGCF with an aspect ratio of ~350-650 have a percolation threshold of 5-8 vol% while the corresponding value for the shorter PAN carbon fibers (aspect ratio of ~24) is in the range of 8-10 vol%. It is noted that the lower percolation threshold of VGCF-PP nanocomposites is a result of the synergistic effect of the high aspect ratio, the highly non-linear, entangled morphology, and the lower electrical resistivity of VGCF of ~55 μmohm cm [24] which is lower than that of PAN (1400 μmohm cm) [22] and xGnP (100 μmohm cm) [25].

According to Figure 6.1 it seems that there is no effect of xGnP’s aspect ratio on the percolation threshold since both the 1 um (aspect ratio ~100) and the 15 um (aspect ratio ~1500) graphite nanoplatelets percolate at 8-9 vol%. This result is in agreement with the results presented in Chapter 4 about the small enhancement of the mechanical properties of neat PP with the addition of xGnP-15. The minimal aspect ratio effect on the percolation threshold results from the low shear force in the extruder during melt mixing which is incapable of optimally disbursing the xGnP-15 agglomerates, thus reducing the effective aspect ratio. ESEM micrographs of the morphology of the of xGnP-15/PP nanocomposites, presented also in Chapter 4, show that a large fraction of the xGnP-15 platelets do not maintain the platelet geometry but they often have bent, buckled and "rolled-up" morphology which reduces their aspect ratio. Representative ESEM images of xGnP-15/PP microstructures illustrating the agglomerated and "roll-up" structures are shown in Figure 6.2a and 6.2b respectively.

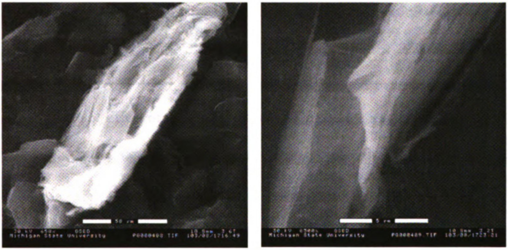

Figure 6.2: ESEM image of fracture surface of 1vol% xGnP-15/PP a) xGnP-15 agglomerates (scale bar 50 μm) and b) xGnP-15 "roll-up" (scale bar 5 μm)

6.3.2 Effect of Filler Orientation

The xGnP filler orientation in the polymer matrix is another factor affecting the percolation threshold and electrical conductivity of the composites. In order to investigate this effect and alter the orientation conditions during processing, xGnP-PP composites were fabricated by (i) melt mixing and injection molding (IM) and (ii) by melt mixing and compression molding (CM). The reinforcements used were xGnP-1 and xGnP-15. The electrical conductivity data are shown in Figure 6.3.

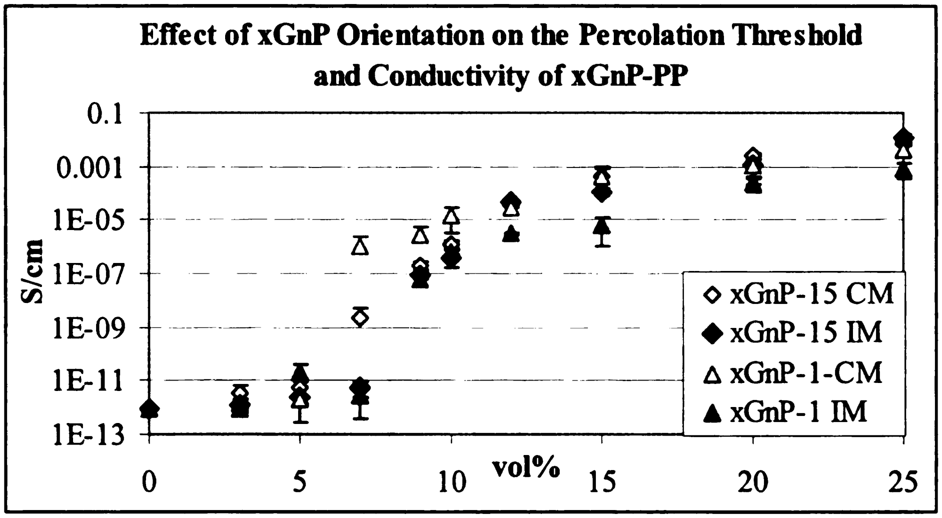

Figure 6.3: Effect of filler orientation on the percolation threshold and conductivity of xGnP-PP nanocomposites

As discussed earlier the xGnP aspect ratio has no effect on the composites conductivity. The electrical conductivity of both the xGnP-15 and the xGnP-1 IM samples begins to increase at ~7 vol%, while the corresponding value for the CM samples is ~5 vol% for both types of xGnP. Injection molding introduces filler alignment along the flow direction, as confirmed by ESEM (Figure 4.7). Initially the platelets are aligned parallel to each other along the flow direction and only at higher loading levels will they start intersecting with each other and form a conductive path as shown schematically in Figure 6.4. The result is that the injection molded specimens have a higher percolation threshold compared to the compression-molded ones where the random orientation of the filler facilitates the formation of the conductive network.

It is noted also that the xGnP-15-PP composites show a slightly higher conductivity than the xGnP-1-PP composites at higher loadings (>12vol%). This can be attributed to the presence of fewer but larger xGnP platelets for the xGnP-15 as compared to the xGnP-1, thus reducing the number of xGnP-PP interfaces and therefore reducing the number of instances of contact resistance.

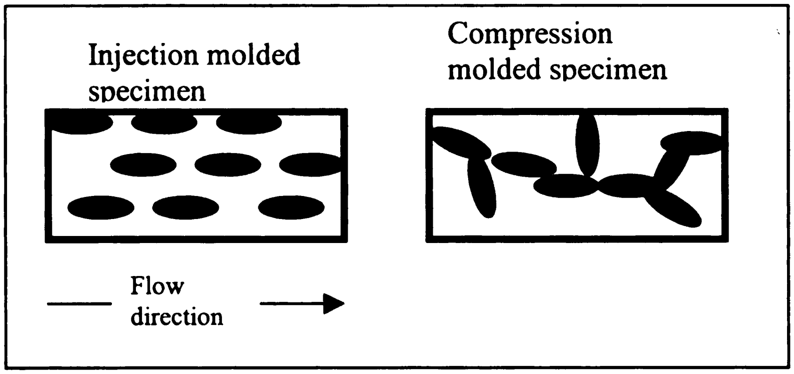

Figure 6.4: Schematic representation of filler distribution in the polymer matrix: a) filler orientation along the flow direction in injection-molded specimen, and b) random filler orientation in a compression-molded specimen

6.3.3 Effect of Filler Anisotropy

When asymmetrical conductive fillers such as fibers or platelets are used, it is expected that both the percolation threshold and the conductivity of the composites will vary directionally. In all of the above cases, the conductivity was measured along the flow direction i.e., along the fiber axis or parallel to the graphite plane.

In order to investigate how the percolation threshold and conductivity vary due to filler anisotropy, samples were fabricated by melt mixing and injection molding using molds of different geometry. One mold has a rectangular geometry with an end gate along the length direction and the other mold has a disk geometry with the gate placed at the periphery as shown in Figure 6.5.

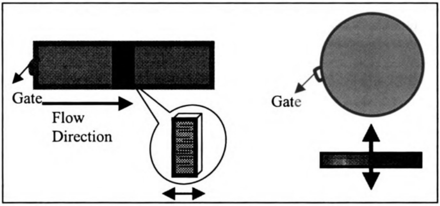

Figure 6.5: Schematic of molds used to explore the effect of xGnP anisotropy. The red arrow shows the direction of measurement a) along the flow direction, parallel to the graphite plane and b) normal to the flow, parallel to graphite c-axis

The electrical conductivity results are shown in Figure 6.6. The disk shape samples show higher percolation threshold (9 vol% for xGnP-1 and 10-12 vol% for xGnP-15) and lower conductivity, which is expected since in these samples the conductivity is measured through the plane, i.e., along the c-axis of the graphite plane, indicated by the arrow in Figure 6.5. The orientation of xGnP normal to the direction of the measurement is shown in Figure 6.7. The platelets are parallel to each other along the direction of the sample's thickness and at low concentrations the distance between them is large especially in the case of xGnP-15; since due to their large size the number of platelets contained in a given xGnP volume is smaller compared to xGnP-1. This also explains the higher percolation threshold of xGnP-15 in the disk samples. Only at higher loadings the distance between the platelets will be small enough to allow electron tunneling or the platelets will start touching forming a conductive network. It is noted that the electrical conductivity of graphite along the plane is ~10^4 $\text{ohm}^{-1}\text{cm}^{-1}$ and along the c-axis ~1 $\text{ohm}^{-1}\text{cm}^{-1}$ [25].

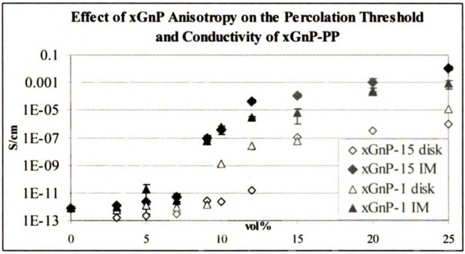

Figure 6.6: Effect of filler anisotropy on the percolation threshold and conductivity of xGnP-PP nanocomposites

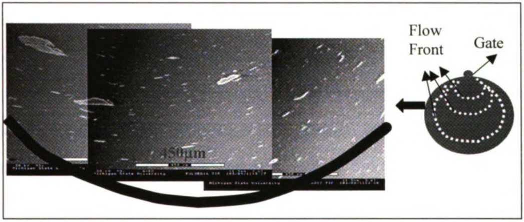

Figure 6.7: Orientation of xGnp-1 a disk shape xGnP-15/PP, a) ESEM image (scale bar 450 µm) b) schematic representation of the xGnP orientation along the flow front

6.3.4 Effect of Compounding

The fabrication method and processing conditions of the composites play an important role in the percolation threshold and conductivity since they affect the orientation, dispersion and interparticle spacing within the polymer matrix and they may alter the filler's aspect ratio or enhance the interactions between filler and matrix.

The effect of the three compounding methods; (i) melt mixing, (ii) polymer dissolution and (iii) premixing by coating the PP powder with xGnP-1, on the percolation threshold and electrical conductivity of xGnP-1-PP nanocomposites is shown in Figure 6.8. All the samples were compression molded and the electrical conductivity was measured in the direction parallel to the sample's length. As shown the conductivity of xGnP-1/PP nanocomposites made by the premix compounding method is as high as 10^{-4} S/cm at a loading of 3vol%, indicating that the percolation threshold is much lower. In case of composites with 5 vol% xGnP-1 the proposed compounding method results in conductivity higher than the conductivity of the solution processed samples. This indicates that the premixing method is at least as efficient in facilitating the formation of conductive network as the commonly used solution method.

The reason is that in case of premixing there are no agglomerates of xGnP due to the use of sonication and the PP powder is homogeneously coated by xGnP. When the polymer melts in the mold the xGnP platelets move along with the melt but they always remain out of polymer chain entanglements. However during the solution process xGnP agglomerates may exist and in addition, based on the fact that the composite powder obtained after the polymer precipitates has a non homogeneous gray color it is possible that some xGnP may be trapped inside chain entanglements and therefore these xGnP is not available to form the conductive network.

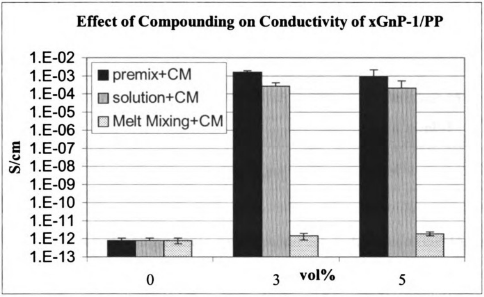

Figure 6.8: Effect of compounding on the percolation threshold and conductivity of xGnP-1-PP nanocomposites made by compression molding

Composites with lower xGnP content were made by premixing and compression molding using both 1 and 15 μm xGnP in order to determine the percolation threshold. As indicated in Figure 6.9 xGnP-1 has a percolation threshold of 0.1 vol% while the corresponding value for xGnP-15 is 0.3 vol%. The results although contradict the expected outcome i.e., the larger the aspect ratio the lower the percolation threshold, can be explained by considering that same volume of xGnP will contain more platelets in case of xGnP-1 so the possibility that the PP powder will be coated more effective during premixing is higher for the smaller platelets.

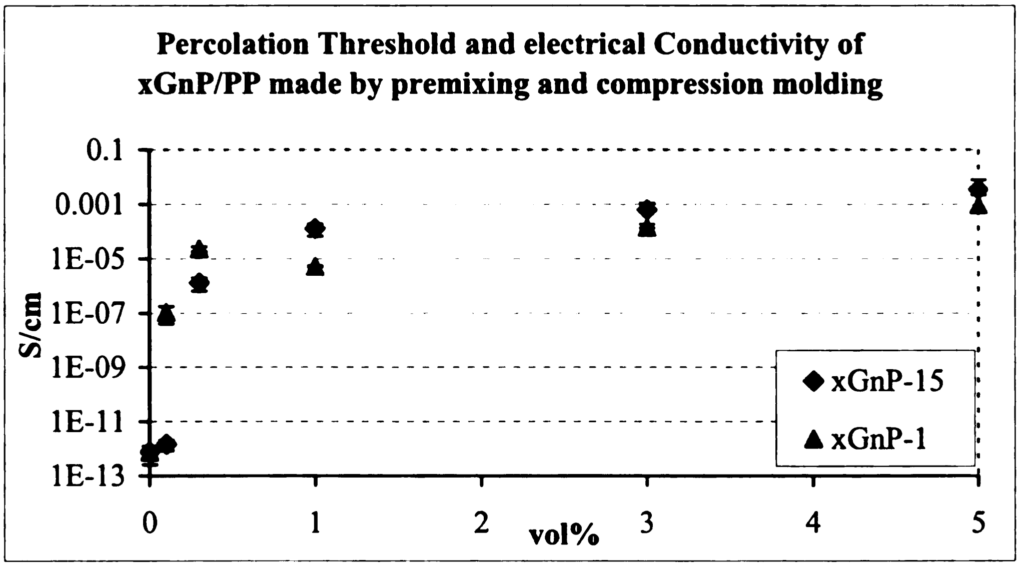

Figure 6.9: Percolation threshold and electrical conductivity of xGnP-15/PP

It is evident that combination of the premixing and compression molding yields composites with lower percolation threshold and higher conductivity. However, it is of practical interest to explore what is the effect of premixing in case of injection molded samples since injection molding is widely used both in research labs and large scale production. Composites were made using (i) melt mixing and injection molding and (ii) premixing, melt mixing and injection molding, since it is not practical to injection mold the premixed composite powder without passing it first through the extruder.

As indicated in Figure 6.10, the premixed samples have a percolation threshold less than 5 vol% while the melt mixed ones ~7 vol%. As the xGnP content increases the difference in electrical conductivity of the composites made with the two methods decreases. The reason is that premixing breaks down the xGnP agglomerates and allows for formation of a continuous network at lower loadings, however, as the graphite concentration increases the platelets agglomerate back together. The significant effect of filler orientation during injection molding on the percolation threshold is outlined by comparing Figures 6.9 and 6.10. The premixed and compression molded xGnP-15/PP have a percolation threshold of ~0.3vol% (Figure 6.9), whereas the premixed injection molded composites have a percolation threshold of ~5vol%.

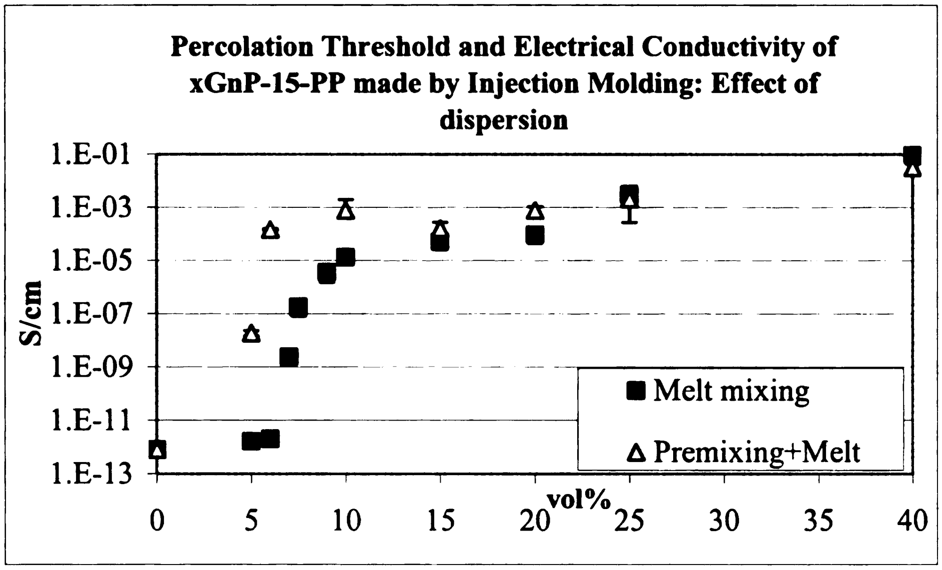

Figure 6.10: Effect of compounding on the percolation threshold and conductivity of xGnP-15-PP made by injection molding

6.3.5 Effect of Matrix's Crystallization Behavior

The crystallinity of the matrix may also affect the conductivity of the composites since in a highly crystalline matrix the formation of the continuous conductive path is easier compared to a less crystalline polymer where the higher amorphous portion may result in more homogeneous particle distribution [20]. However, in addition to the degree of crystallinity other crystallization characteristics of the polymer matrix such as type of crystal forms, number and size distribution of spherulites might also affect the electrical conductivity and percolation threshold. In order to understand how the crystallization of PP affects the electrical conductivity and percolation threshold of xGnP/PP composites, samples were made by premixing the xGnP with the PP powder and compression molding. The crystallization of the matrix was altered by using different cooling rates after the molding was completed. Two extreme cases were used i) fast cooling (fc) at a rate of ~20^{o}C/min and ii) slow cooling (sc) at a rate of ~0.3^{o}C/min.

The reinforcements used in this study are xGnP-1 and xGnP-15. In both cases the slowly cooled composites had lower percolation threshold (~0.1 vol% for xGnP-1 and between 0.3 and 0.5 vol% for xGnP-15). The reason that xGnP-1 which has smaller aspect ratio than xGnP-15 resulted in lower percolation threshold is that in the premixing method used for compounding the number of graphite platelets is more important than their size.

DSC and XRD and optical microscopy were employed in order to understand the mechanism behind the cooling rate effect. Since this work is also part of the crystallization study on how xGnP alters the crystallization behavior of PP, which is presented in Chapter 7 the experimental conditions used and the results obtained will be analytically discussed in the proceeding chapter. Only a brief description of the proposed mechanism responsible for the lower percolation threshold of slow cooled composites is presented here.

As indicated by DSC and optical microscopy xGnP is a nucleating agent for PP and the crystals are growing around the platelets. In the case of fast cooling it was found, by DSC and XRD, that there are more crystals so a larger number of graphite platelets are located in the center of the crystals and fewer are available to form the continuous network necessary for providing electrical conductivity as compared to the slow cooled samples. In addition, the conductive path of xGnP can be disrupted by the presence of many small spherulites that exist in the fast cooled composites. Thus a higher loading of xGnP, which means higher percolation threshold, is required to impart the electrical conductivity of the composites in case of fast cooling.

6.4 Comparison between Existing Models and Experimental Data

A review of the theoretical models proposed for the prediction of the electrical conductivity of composites was presented in Chapter 1. The limitations of these models are emphasized by comparison with the experimental data. Representative data on electrical conductivity of xGnP/PP composites presented above are compared to the conductivity values predicted using (i) the statistical model proposed by Kirkpatric [26] i.e., a power law model which has its foundation of the percolation theory, and (ii) the thermodynamic model proposed by Mamunya *et al* [27] that accounts for the filler and polymer surface energies, and the polymer melt viscosity.

The statistical model is described by Equation (6.1)

$$\sigma = \sigma_o (V - V_C)^S \tag{6.1}$$

where σ is the conductivity of the composite, σ_o the conductivity of the filler, V the filler volume fraction, V_C the percolation threshold, and S the critical exponent that depends on the dimension of the lattice. Reported values for the exponent are in the range of 1.1-3.8 as presented in a review by Fukushima [28].

The thermodynamic model is given in Equations (6.2)-(6.5)

$$\log\sigma = \log\sigma_c + (\log\sigma_m - \log\sigma_c)\left(\frac{\phi - \phi_c}{F - \phi_c}\right)^k \tag{6.2}$$

$$k = \frac{K\phi_c}{(\phi - \phi_c)^{0.75}} \quad K = A - B\gamma_{pf} \tag{6.3}$$

where σ_c the conductivity at the percolation threshold; σ_m the conductivity at F; F is the maximum packing fraction, ϕ the volume fraction, AR is the aspect ratio; ϕ_c the percolation threshold, γ_{pf} the interfacial tension and A and B, are constants. The exponent k depends on the filler volume fraction, percolation threshold and interfacial tension. The maximum packing fraction can be determined using the Equation (6.4):

$$F = \frac{5}{\frac{75}{10 + AR} + AR} \tag{6.4}$$

Equations (6.1) and (6.2) can be rewritten in a log-log form as shown in Equations (6.5) and (6.6) respectively

$$\log\sigma = \log\sigma_o + S\log(V - V_C) \tag{6.5}$$

$$\log(\log\frac{\sigma}{\sigma_c}) = k\log(\frac{\phi - \phi_c}{F - \phi_c}) + \log(\log\frac{\sigma_m}{\sigma_c}) \tag{6.6}$$

The experimental data on the conductivity of xGnP-1/PP and xGnP-15/PP composites for both cases of injection and compression molding were fitted linearly using Equations (6.5) and (6.6). The values obtained for the various empirical parameters involved in the models as well as the R^2 values that indicate how accurate the equations fit the data are presented in Tables 6.1 and 6.2 for the statistical and the thermodynamic model respectively.

In case of the statistical model the slope in the log-log plot is the exponent S and the intercept provides the conductivity of the reinforcement. Based on Table 6.1 the best fitting i.e., R^2=0.9843, is for xGnP-15/PP composites made by compression molding and the xGnP-15 conductivity calculated based on the intercept is 1012.978 S/cm which is very similar to the conductivity of graphite along the c-axis, that is ~10^4 S/cm [25]. However, the value obtained for the critical exponent S is much larger than the values reported and can not be explained or predicted based on the dimensionality of the lattice.

Table 6.1: Fitting Experimental Data to the Statistical/Percolation Model

	R^2	Exponent *S*	Electrical Conductivity of XGnP (S/cm)
xGnP-1 IM	0.9696	4.16	0.782
xGnP-1 CM	0.9517	3.72	1.094
xGnP-15 IM	0.9731	5.29	88.654
xGnP-15 CM	0.9843	6.8	1012.978

Table 6.2: Fitting Experimental Data to Mamunya's Model

			Intercept	Experimental	Intercept/Experimental
	R^2	slope, k	σ_m/σ_c	σ_m/σ_c	
xGnP-1 IM	0.9713	0.2887	5.727×10^8	2.919×10^8	1.961
xGnP-1 CM	0.9622	0.2013	5.45×10^9	9.524×10^9	0.572
xGnP-15 IM	0.953	0.3576	9.434×10^9	2.203×10^9	4.282
xGnP-15 CM	0.9386	0.5362	1.602×10^{10}	1.396×10^9	11.479

In the thermodynamic model the slope is the parameter *k* defined in Equation 6.3 and the intercept provides the value of the conductivity ratio σ_m/σ_c that can also be estimated experimentally. As shown in Table 6.2 based on the R^2 value, the best fit is for the case of xGnP-1 IM followed by the xGnP-1 CM. In both cases however; there is a large difference between the value of σ_m/σ_c determined experimentally and the one calculated based on the intercept.

The above comparison is a demonstration that there is discrepancy between the experimental data and the predictive theoretical models mainly due to the fact that the existing models do not account for all the factors that affect the percolation and electrical conductivity of composites such as the orientation of the fillers within the polymer matrix and the filler anisotropy just to mention a few. Also these models treat the reinforcements as stiff and rigid bodies that do not agglomerate and are homogeneous dispersed which as shown in case of xGnP-15 is not true. As discussed in Chapter 4, xGnP-15 are very flexible and tend to bend, buckle or roll up in response to the shear field in the extruder and as result they are losing their platelet morphology. Finally, polymer characteristics such as the degree of crystallinity, crystal type, number and size distribution, which also as shown affect the percolation threshold and conductivity, are not being considered in the models. An additional reason for the discrepancy between the particular experimental data and the two models presented above is that the value for the percolation threshold had not been accurately determined.

6.5 Conclusions

The percolation threshold and electrical conductivity of carbon reinforced PP composites were determined for various fabrication methods, fillers i.e., CB, VGCF, PAN and xGnP, and filler characteristics i.e., aspect ratio.

A new compounding process i.e., premixing by coating of PP powder with xGnP was identified as an alternative to the solvent intercalation method. This method results in composites with lower percolation threshold and higher conductivity and in addition does not require use of toxic solvents or high temperatures.

Composites made by melt mixing and injection molding show a higher percolation threshold because of limitations in the ability of the melt mixing equipment to disperse the xGnP and maintain their platelet type morphology. Furthermore, injection molding creates morphology with preferential alignment the platelets along the flow direction. As a result, no improvement in electrical conductivity resulting from the effect of larger xGnP aspect ratio was detected.

The lowest percolation threshold measured was less than 0.1 vol% for samples made by premixing and compression molding while composites with similar compositions made by melt mixing and injection molding had a percolation threshold of ~7 vol%.

6.6 References

1. D.M. Bigg, "The Effect of Compounding on the Conductive Properties of EMI Shielding Compounds", *Advances in Polymer Technology*, **4**, 255, (1984)

2. W. Brandl, G. Marginean, V. Chirila and W. Warschewski, "Production and Characterization of Vapour Grown Carbon Fiber/Polypropylene Composites", *Carbon*, **42**, 5 (2004)

3. F.W.J. Van Hattum and C.A. Bernardo, "A study of Thermomechanical Properties of Carbon Fiber-Polypropylene Composites", *Polymer Composites,* **20** 5, 683 (1999)

4. P. Calvert, "Nanotube Composites: A recipe for Strength", *Nature* **399**, 210 (1999)

5. W. Tang, M. Santare, and S. Advani, "Melt processing and mechanical property characterization of multi-walled carbon nanotube/high density polyethylene (MWNT/HDPE) composite films" *Carbon* **41**, 2779 (2003)

6. S. Kumar, H. Doshi and M. Srinivasarao, J.o. Park and D.A. Schiraldi, "Fibers from Polypropylene/Nano Carbon Fiber Composites", *Polymer,* **43** 1701 (2002)

7. S. Kumar, T.D. Dang, F.E. Arnold, A.R. Bhattacharyya. B.G. Min, X. Zhang, R.A. Vaia, C. Park, W.W. Adams, R.H. Hauge, R.E. Smalley, S. Ramesh, and P.A. Willis, "Synthesis, Structure, and Properties of PBO/SWNT Composites", *Macromolecules,* **35** 9039 (2002)

8. V.F. Lincoln and Z. Claude, "Organic Matrix Composites Reinoforced with Intercalated Graphite" US Patent 4,414,142 (1983)

9. D.D.L. Chung, "Composites of In-situ Exfoliated Graphite", US Patent, 4,946,892 (1990)

10. A. Celzard, E. McRae, J.F. Marache, G.Furdin, M, Dufort and C. Deleuze, "Composites based on Micron-Sized Exfoliated Graphite particles: Electrical Conduction, Critical Exponents and Anisotropy", *J. Phys. Chem Solid,* **57** 6-8, 715 (1996)

11. Y.S. Wang, M.A. O'Gurkis and J.T. Lindt, "Electrical Properties of Exfoliated-Graphite Filled Polyethylene Composites", *Polymer Composites*, **7**,5 349 (1996)

12. G-H. Chen, D-J. Wu, W-G Weng, and W-L Yan, "Preparation of Polymer/Graphite Conducting Nanocomposite by Intercalation Polymerization", *Journal of Applied Polymer Science*, **82** 2506, (2001)

13. http://www.pittstate.edu/services/nsfreu/ResearchReports2004/dweberfuelcellicce11submit.pdffgh

14. D. Stauffer, "Introduction of Percolation Theory", Taylor and Francis, London (1985)

15. X. Jing, W. Zhao, and L. Lan, "The Effect of Particle Size on Electric Conducting Percolation Threshold in Polymer/Conducting particle Composites", *Journal of Materials Science Letters* **19**, 377 (2000)

16. H. S. Gokturk, T. J. Fiske, and D. M. Kalyon, "Effects of Particle Shape and Size Distributions on the Electrical and Magnetic Properties of Nickel/Polyethylene composites", *Journal of Applied Polymer Science*, **50**, 1891 (1993)

17. M. Clingerman, E. Weber, J. King, and K. Schulz, " Development of an Additive Equation for Predicting the Electrical Conductivity of Carbon-Filled Composites", *Journal of Applied Polymer Science*, 88 2280-2299 (2003)

18. J-W. Shen, X-M. Chen and W-Y. Huang, "Structure and Electrical Properties of Grafted polypropylene/Graphite Nanocomposites Prepared by Solution Intercalation", *Journal of Applied Polymer Science*, **88** 1864 (2003)

19. X-M. Chen, J-W. Shen, W-I. Huang, 2002. "Novel Electrically Conductive Polypropylene/Graphite Nanocomposites", *Journal of Materials Science Letters*, 21: 213

20. I. Chodak and I. Krupa, "Percolation Effect and Mechanical Behavior of Carbon Black Filled Polyethylene", *Journal of Materials Science Letters*, **18** 1457, (1999)

21. M.L. Clingerman, J.A. King, K.H. Schulz and J.D. Meyers, "Evaluation of electrical Conductive models for Conductive polymer Composites", *Journal of Applied Polymer Science,* **83**, 1341 (2002)

22. J. King, K. Tucker, J. Meyers, E. Weber, M. Clingerman and K. Ambrosius, "Factorial Design Approach to Electrically and Thermally Conductive Nylon 6,6", *Polymer Composites* **22**, 1, 142 (2001)

23. P. Banerjee and B.M. Mandal, "Conducting polyaniline Nanoparticle Blends with Extremely Low Percolation Thresholds", *Macromolecules* **28**, 3940, (1995)

24. http://www.apsci.com/ngm-pyro1.html

25. D.D.L. Chung, "Review Graphite", *Journal of Materials Science* **37** 1475, (2002)

26. S. Kirkpatrick, "Percolation and Conduction", *Rev Mod Phys* **45** 574, (1973)

27. E. P. Mamunya, V.V. Davidenko, and E. V. Lebedev, *Compos Interf* **4** 169, (1997)

28. H. Fukushima, "Graphite Nanoreinforcements in Polymer Nanocomposites", PhD Thesis, Michigan State University, 2003

CHAPTER 7

EFFECT OF EXFOLIATED GRAPHITE NANOPLATELETS ON THE CRYSTALLIZATION BEHAVIOR OF POLYPROPYLENE

7.1 Introduction

As discussed in Chapters 4, 5 and 6, the mechanical, rheological and electrical properties of nanocomposites are strongly affected by the fabrication method and the processing conditions. In the case of polypropylene, which is a semicrystalline thermoplastic, crystallinity is an additional factor that has a significant impact on the composite's properties.

The crystallization behavior of a polymer, i.e., degree of crystallinity, crystallization temperature and rate, and size or type of crystallites is affected not only by the processing conditions but also by the presence of a second phase.

Any change in the crystallization behavior of the polymer will be reflected in the mechanical properties (impact strength) and electrical properties (percolation threshold and electrical conductivity). The barrier properties will also be affected since any change in crystallinity will influence the orientation of the polymer chains and may act as a constraint on their molecular freedom leading to a significant decline in permeation rates since the crystals are much less permeable and the mobility of the polymer chains is limited near the crystal boundaries [1, 2].

7.1.1 Nanoreinforcements as nucleating agents for polymers

It is well documented that nanoreinforcements i.e., clays or carbon nanotubes when added in polymers even at very small amounts act as nucleating agents. For example, addition of just 0.8 wt% of SWNT in polypropylene increases the crystallization rate by an order of magnitude as well as the crystallization temperature of the neat PP and results in smaller crystallites with a narrower size distribution [3].

In another crystallization study of a similar system it is reported that the crystallization rate and temperature increase with addition of SWNT and there is an indication of saturation of the nucleating action at higher [>5wt%] SWNT contents [4]. This was further explored by Raman spectroscopy and ESEM and it was concluded that at higher nanotube loadings there is not enough polymer to intercalate between the SWNTs, limiting dispersion and restricting the nanotube surface that is available for crystal nucleation.

Typically, thermoplastic polymers crystallize into a specific crystal form i.e., in case of isotactic PP there are different packing geometries of the PP helices that lead to four well-known crystal structures: monoclinic (α), trigonal (β), triclinic (γ), and smectic (δ) depending on the melting history, crystallization temperature, pressure and cooling rate as well as presence of a foreign material [5, 6]. The most common is the α-form structure. However, it has been reported that the less common occurring β-form has higher impact strength and toughness that are attributed to its peculiar lamellar morphology [7], the formation of an enlarged plastic zone [8] and the strain-induced β–α transition during mechanical deformation [9].

Based on TEM observations [10], the α-form crystals show a "crosshatched" lamellar arrangement in which the radial lamellae are slightly thicker than the tangential component and the angle between the two is ~80°. On the other hand, β crystals consist of thicker lamellae compared to those of a-form i.e., 20nm for b-form versus 10nm for the α-PP [11] that are locally parallel-stacked growing radially through the spherulite diameter revealing a sheaflike structure [5]. A schematic of the structure/alignment of the lamellae within the α- and β-form crystals of PP is shown in Figure 7.1

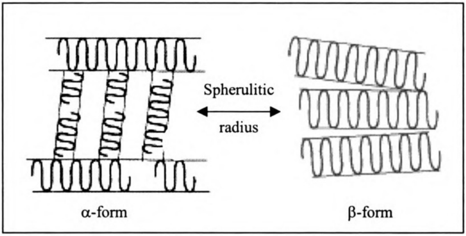

Figure 7.1: Alignment of lamellae within spherulites of a- and b-form PP [5]

As mentioned the presence of a second phase can promote the formation of the less common crystal forms. For example, addition of octadecylamine functionalized SWNTs in PP at a loading of 0.6 wt% promote the growth of the β-crystal form at the expense of α-form, along with an increase in the crystallization rate and temperature as indicated by DSC [12].

Similar results have been reported for a clay-Nylon,6 system where presence of clays favors the formation of the less common γ-form preferentially in the proximity of the silicate layers, whereas the α-form exists away from the polymer-silicate interphase and are more isotropic (not oriented with respect to clays) [13]. In addition in clay-PP nanocomposites, clays inhibit the formation of the β-phase and slightly promote the γ-phase. The clay acts as a nucleating agent in both cases. Considering that in the case of PP the β-form has higher impact strength and toughness [7-9] it is concluded that clays enhance the mechanical properties of PP not only due to the reinforcing effect but also because they induce polymorphism (more than one crystal-form).

Similar studies on the crystal polymorphism induced by clays in Nylon-6-clay indicate that the addition of clay orients the crystallites and acts as a template for epitaxial crystallization to the γ-phase, instead of the normally dominate α-phase, to the point where crystallization is not longer spherulitic [14-15].

Based on a study of PP-graphite nanocomposites where graphite oxide and maleated PP were used as interface modifiers, the graphite promotes the nucleation of β-form crystallites in PP [16]. However, due to the presence of the interface modifiers the role of graphite as a nucleating agent for the less common β-form crystals is not well established.

7.1.2 Objectives

It is evident that the properties of nanocomposites are strongly dependant on the fabrication method and processing conditions used as well as the crystallization behavior of the polymer matrix, which is also affected by the processing conditions and the reinforcement.

The goal of this chapter is to determine how xGnP affects the crystallinity of polypropylene, understand how the crystallinity relates to the mechanical properties and explore how altering the processing conditions (and thus the crystallization behavior of the matrix) it is possible to affect the electrical conductivity and the percolation threshold of the xGnP-PP nanocomposites. The objectives are:

- Determine the effect of xGnP on the crystallite size, crystallization temperature and rate and crystal polymorphism of neat PP as a function of xGnP's aspect ratio and concentration by means of DSC, optical microscopy and XRD.
- Revisit the impact strength results presented in Chapter 4 and discuss them in relation to the crystallization behavior of PP in the presence of xGnP.
- Investigate how compounding (melt-mixing vs. premixing by coating the PP powder with xGnP) affects the crystallinity of the nanocomposites.
- Explore the effect of the cooling rate during compression molding of xGnP-PP on the electrical conductivity and percolation threshold as a function of xGnP's aspect ratio and concentration and compare with the corresponding electrical properties of CB reinforced PP composites.

7.2 Experimental Conditions and Characterization Techniques

The degree of crystallinity, crystallization enthalpy (ΔH_c), crystallization temperature (T_c), melting enthalpy (ΔH_m) and melting temperature (T_m), were determined by DSC. The samples used were 5-10 mg and isothermal crystallization was studied using the following experimental conditions.

The sample was heated to 220°C at a rate of 30°C/min. The thermal history of the sample due to prior processing was erased by maintaining isothermal condition for 10min. Finally, the sample was cooled at 5°C/min to -40°C, held isothermally for 5min and reheated at 5°C/min to 220°C. The data on the melting behavior was collected along this second heat cycle whereas the crystallization data was collected during cooling the sample to room temperature at 5°C/min.

The degree of crystallinity was calculated using the following equation

$$\chi\% = \frac{1}{1 - wt\%}\frac{\Delta H_C}{\Delta H_f^o} \tag{7.1}$$

where $\chi\%$ is the percent crystallinity of the matrix, *wt%* is the content of xGnP, and ΔH_f^o is the theoretical crystallization enthalpy of the matrix if it was 100% crystalline.

Non-isothermal and isothermal crystallization of xGnP-PP nanocomposites were studied using an optical microscope. A hot stage was used to initially heat the sample above the melting point in order to erase the thermal history. The sample was heated up to 220°C at a rate of 20°C/min, held isothermally at 220 °C for 10min and then cooled to room temperature (for non isothermal crystallization) or to the desired crystallization temperature (for isothermal).

The X-ray diffraction patterns of the nanocomposites were obtained using a Rigaku Rotaflex 200B diffractometer employing Cu-Kα radiation (λ=1.54056 Å) with a curved graphite monochromator. The operating setting of the X-ray was 45kV and 100mA. The diffraction patterns were collected from 10° to 50° (2θ) at a scanning rate of 1°/min with divergence and scatter slit of 1/2°. Information obtained by the XRD pattern includes the types of crystals that are present and the crystal size (thickness of the crystallite along the direction perpendicular to the reflecting plane), which can be estimated using the Scherrer formula [17] described in equation (7.2):

$$Crystallite\ Size = K \times \lambda \,/\, FWHM \times \cos\theta \tag{7.2}$$

Where K is the crystal shape factor taken as 0.9, λ is the wavelength, and θ is the peak position.

The effect of processing conditions on crystallinity of xGnP-PP nanocomposites and consequently on the electrical conductivity and percolation threshold was investigated by altering the cooling conditions during the compression molding of the samples. Premixing by coating the PP powder with xGnP was used as the compounding method since as discussed in Chapter 6 it results in composites with the lowest percolation threshold. The composite powder was used for compression molding at conditions described in Chapter 2. Two extreme cases were used during cooling, fast cooling at a rate of ~20°C/min which was achieved by placing the mold between solid pieces of dry ice and slow cooling at a rate of ~0.3°C/min which was carried out by leaving the mold in the hot press and letting the samples slowly cool down to room temperature overnight.

7.3 Results and Discussion

7.3.1 Effect of xGnP-1 and Crystallization Conditions on Nucleation of PP

The crystallization of neat PP was monitored by optical microscopy and the results are shown in Figures 7.2a-c. The time intervals (t=0, 1 and 2 min) indicate how long the specimen was held at 130°C. At t=0 there are preexisting nuclei due to infusible heterogeneous particles (e.g., impurities or catalyst residues). As time proceeds spherulites form around these nucleating sites and keep growing. No secondary nucleation is observed.

Figures 7.2d-f track the crystallization of 0.01 vol% xGnP-1/PP at 130°C. The spherulites form and grow around the xGnP-1 particles, which is a first indication of the nucleating action of xGnP.

When comparing the neat PP crystallization to the filled system, several striking differences are observed. First the rate of crystallization, the length of time it takes for the spherulites to cover the micrograph area, is much faster for the xGnP-1/PP (completion in less than 3 min) than the neat PP (completion in 20 min) as observed in Figure 7.3. A more quantitative description of the crystallization rate is provided in Table 7.1. Figure 7.3 also reveals that the spherulites formed in the xGnP-1/PP system are almost 10x smaller than those formed in neat PP and have a more irregular shape.

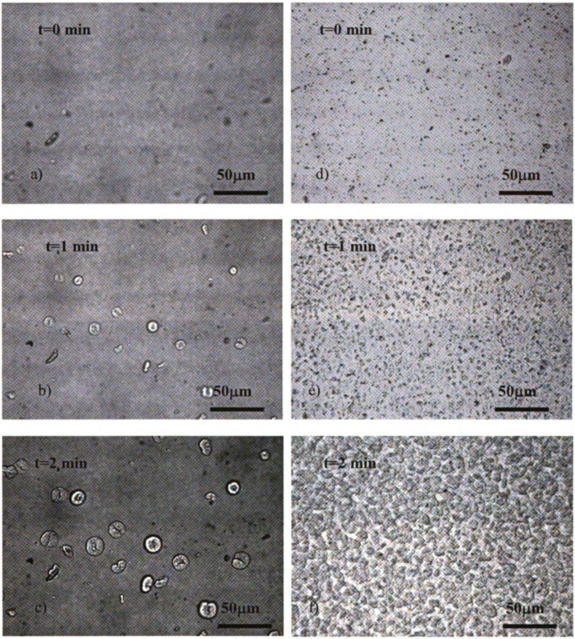

Figure 7.2: Isothermal crystallization at T=130°C of neat PP, images (a) through (c), and of 0.01 vol% xGnP-1/PP, images (d) through (f). Viewing the images from left to right shows the difference in crystallization between PP and xGnP/PP at a given time whereas viewing them from top to bottom shows how crystallization evolves with time for PP (left) and xGnP-1/PP (right).

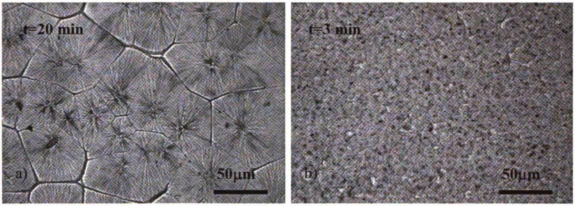

Figure 7.3: Isothermal crystallization at 130°C of a) neat PP at t=20min and

b) 0.01vol% xgnP-1/PP at t=3min

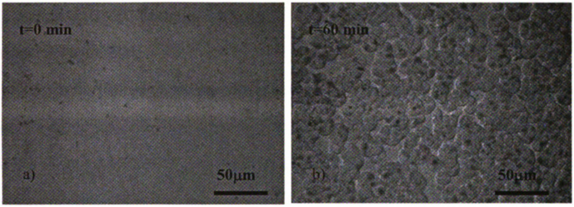

Figure 7.4: Isothermal crystallization of 0.01 vol% xGnP-1 at T_c=145°C

Table 7.1: Crystallization rate of xGnP/PP for isothermal crystallization at T_c=130°C

	xGnP-15	**xGnP-1**
vol%	(1/min)	(1/min)
0	0.060	0.060
0.01	0.164	0.193
0.1	0.226	0.299
1	0.535	0.381

The crystallization rate (1/min) calculated as the inverse of the time interval required for the completion of the crystallization during isothermal crystallization of xGnP/PP at T_c=130°C in DSC is presented in Table 7.1. The results are an average of three samples with a standard deviation less than 5%. Even at the low xGnP content of 0.01 vol% the crystallization rate of neat PP increase by a factor of ~3.

Besides the presence of xGnP the crystallization of PP can be affected also by the processing conditions. For example, increasing the temperature at which crystallization occurs i.e., from T_c=130°C to T_c=145 °C of xGnP-1 results in fewer but larger and more spherical spherulites and in lower crystallization rates i.e., the crystallization is completed in 3min at T_c=130°C as shown in Figure 7.3b, and in more than 60 min at T_c=145°C as shown in Figure 7.4b.

The crystallization temperature is not the only processing parameter that has an impact on the crystallization behavior and structure of the composites. The condition under which the crystallization occurs, for example isothermally or non isothermally, is equally important.

It was observed that in the case of isothermal crystallization, after the spherulites nucleate and grow at constant temperature they shrink during cooling to room temperature in order to accommodate thermal and residual stresses that were accumulated during the crystallization process as indicated by the black lines formed along the boundaries as shown in Figure 7.5. However, in the case of non isothermal crystallization where the spherulites nucleate and grow as the temperature decreases, no shrinkage was observed as shown in Figure 7.6, since the spherulites adjust their size/boundaries gradually during cooling. The non isothermal crystallization of 0.01 vol% xGnP-1/PP starts at ~T_c=120°C and is completed within few minutes at T_c=114°C.

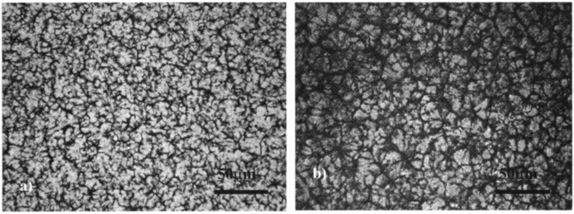

Figure 7.5: Optical micrograph of 0.01 vol% xGnP-1/PP at T=28°C, after isothermal crystallization at a) T_c=130°C for t=20min and b) T_c=145°C for t=60min

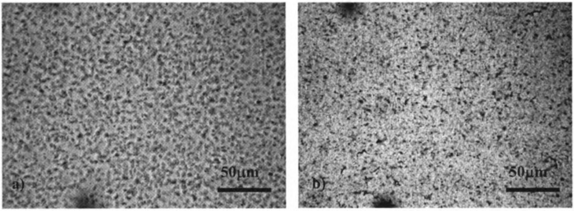

Figure 7.6: Optical micrograph of 0.01 vol% xGnP-1/PP crystallized non isothermally a) at T=120°C, beginning of crystallization and b) at T_c=28°C after cooling

Although optical microscopy can capture the crystal shrinkage this experimental technique is not capable to provide any deep understanding or quantitative results on the subject. However, this observation combined with a study on clay reinforced polyolefins [2] reporting that clays reduce the crystal shrinkage which is responsible for extensive cracking indicate that nanoreinforcements can enhance the composite's mechanical properties through an additional mechanism of reducing the residual stress from shrinkage besides the reinforcing and the nucleating effect.

In the case of neat polymer the shrinkage appears during recrystallization due to high degree of crystallinity and the large density difference between the amorphous melt and the crystal phase [2]. The nanoreinforcements have a much lower coefficient of thermal expansion compared to the polymer and based on the observation that spherulites grow around/on the nanoplatelets it can be concluded that the reduction of crystal shrinkage upon addition of nanoreinforcements is due to the constraint they impose on the polymer spherulites.

7.3.2 Effect of xGnP Concentration and Aspect Ratio on Nucleation of PP

In order to study the effect of xGnP concentration on the crystallization of PP, xGnP-15/PP samples at two different xGnP loadings of 0.01 and 0.1 vol% were crystallized isothermally at T_c=120°C in the hot stage under the optical microscope. The micrographs are shown in Figure 7.7. The crystallization rate as well as the number of nucleation sites and consequently the number of spherulites increases with the xGnP-15 concentration while their size is reduced and their shape becomes irregular.

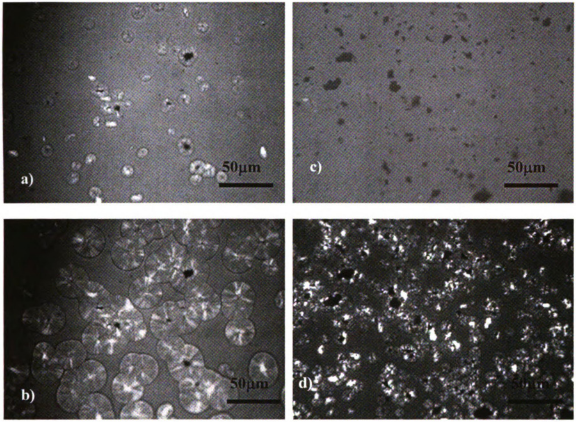

Figure 7.7: Isothermal crystallization at T=120°C of 0.01 vol% xGnP-15/PP at a) t=20sec and b) t=1min and of 0.1 vol% xGnP-15/PP at c) t=0sec and d) t=20sec

The nucleation starts around the graphite nanoplatelets as indicated in Figure 7.7a and 7.7d by the "bright" rings formed along the periphery of the xGnP-15. It is expected that this transcrystalline zone should also form in the case of xGnP-1 however; due to limitations imposed by the optical microscope it is difficult to be confirmed. Larger graphite platelets, xGnP-100 at a loading of 0.3 vol%, were used to verify the existence of the transcrystalline region. The sample was crystallized isothermally at T_c=130°C. Results are shown in Figure 7.8.

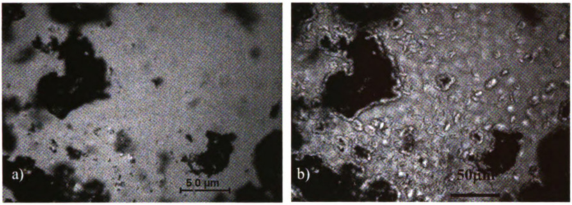

Figure 7.8: Isothermal crystallization of 0.3 vol5 xGnP-100/PP at T=130°C after a) t=0min and b) t=1min

As the aspect ratio of xGnP increases the number of particles contained at a given xGnP volume decreases which means fewer nucleation sites and thus fewer but larger spherulites. Increasing the xGnP concentration has a similar effect as shown in Figure 7.7. In addition, the xGnP concentration and aspect ratio effect on the crystallization of PP was studied by DSC and XRD. As the xGnP content increases the crystallization initiates at higher temperatures (Figure 7.9), which also confirms that xGnP acts as nucleating agent.

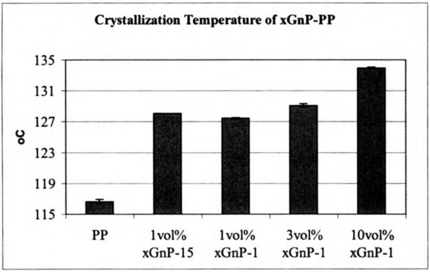

Figure 7.9: Crystallization temperature of xGnP-PP Nanocomposites

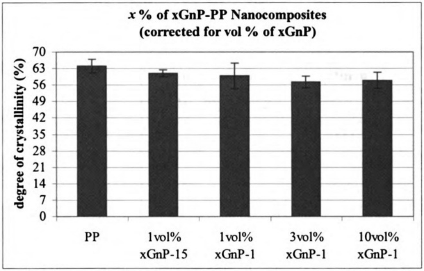

Figure 7.10: Degree of crystallinity of xGnP-PP nanocomposites

From Figure 7.10 it is concluded that the presence of xGnP does not have any significant effect on the total percent of crystallinity. The melting temperature, calculated as the minimum temperature of the exotherm melting peak provided by DSC, does not change, however, addition of xGnP alters the melting behavior i.e., the melting peak becomes narrower and taller compared to the melting peak of neat polypropylene indicating that the crystals becoming thinner and more homogeneous.

XRD was used to investigate the change in the crystal form of polypropylene due to addition of xGnP. The literature values for the characteristic XRD (Cu K$\alpha_{1,2}$) pattern of isotactic polypropylene and the corresponding crystallographic planes are summarized in Table 7.2. The crystalline forms of isotactic PP are α-monoclinic which is the most common, β-hexagonal (occurs under specific conditions i.e., temperature gradients, present of shearing forces or β-nucleating agents), and γ-triclinic, which is the least common observed in low molecular weight PP [18].

Table 7.2: Characteristic XRD peaks and corresponding crystallographic Planes of PP

2θ	**α-form** [18 19, 20]	**β-form** [20]	**γ-form** [18]
13.84			<111>
14.08	<110>		
15.05			<113)>
16		<300>	
16.95	<040>		
18.5	<130>		
20.07			<117>
21		<301>	
21.2	<111>		<202>
21.85	<041>		
21.88			<026>
25	<060>		
28	<220>		

The XRD pattern of melt mixed and injection molded xGnP-1/PP and xGnP-15/PP nanocomposites at various graphite loadings are shown in Figures 7.11 and 7.12 respectively. Four peaks are present in the XRD pattern of neat PP (0 vol%, black line) which correspond to α-form crystals. Addition of only 0.01vol% of xGnP-1 induces the formation of β-form crystals (at $2\theta=16^{\circ}$ and $2\theta=21^{\circ}$) shown by the arrows in Figure 7.11, which disappear at higher xGnP loadings (1vol%). It is also observed that the second PP peak at $2\theta=16.95^{\circ}$ that corresponds to the α <040)> plane dominates whereas in the case of neat PP all four peaks had similar height. Finally addition of xGnP gives rise to a fifth PP peak at $2\theta=25^{\circ}$ corresponding to the α <060> plane which is absent from the neat PP pattern.

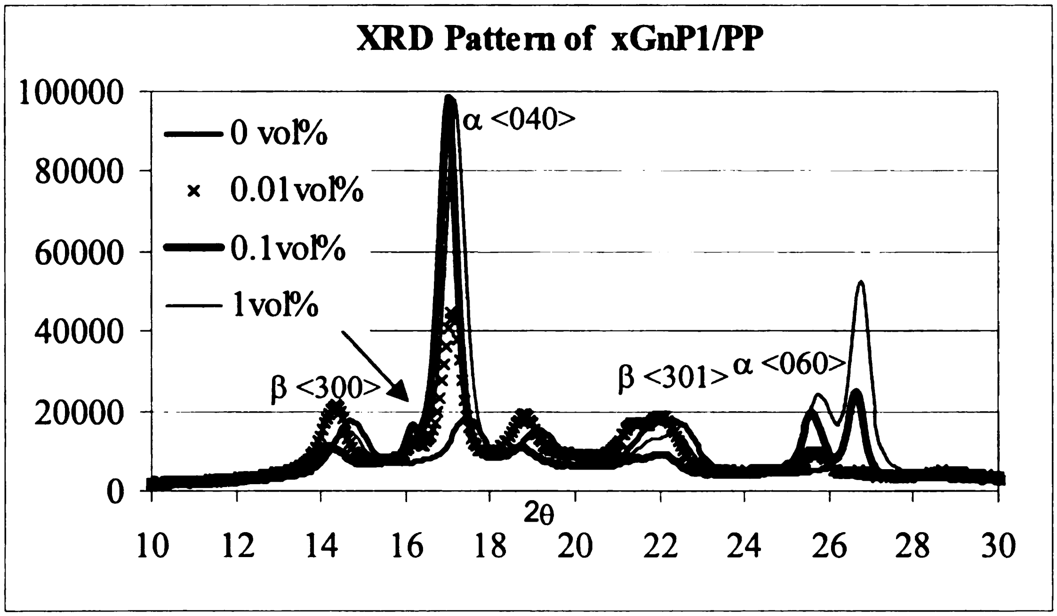

Figure 7.11: XRD of xGnP-1/PP made by melt mixing and injection molding

Similar features are observed in the XRD pattern of xGnP-15/PP nanocomposites as shown in Figure 7.12. Again, the second PP peak at $2\theta=16.95$ °, α <040> plane, becomes stronger and the PP peak at $2\theta=25^{\circ}$ corresponding to the α <060> plane, appears due to addition of xGnP-15. Presence of xGnP-15 also promotes the formation of β-form crystals with the β-form peak at $2\theta=16^{\circ}$ that corresponds to the <300> plane, dominating over the second β-form peak. It is noted that the three peaks that are strongly affected by xGnP correspond to the crystallographic planes of the general (00x) type, which also match crystallographically with the graphite's <002> plane.

Similar findings are reported in a study [21] about the nucleation effect of talc on the crystallization of PP. It was observed that there is oriented crystallization of PP in presence of talc as the mineral c-axis is merged with the PP b-axis (matching <001> plane of talc with the <010> plane of PP).

Based on the above it is concluded that in both the talc-PP and the xGnP-PP systems the nucleating efficiency of the reinforcement can be expressed as the change in the intensity ratio between the α <040> and α <110> reflections and that the onset of crystallization, which can be attributed to the alignment of few PP chains before the epitaxial growth, depends on the crystallographic nature of the substrate.

The differences between the XRD patterns of xGnP-1/PP and xGnP-15/PP are that in case of xGnP-15 the β-form peaks are present even at higher xGnP-15 loadings and that the xGnP peak at $2\theta=26.45^{\circ}$ that corresponds to the graphite's <002> plane [22, 23], is much stronger (with respect to the PP peaks) in case of xGnP-15 whereas similar loadings of xGnP-1 generate a smaller peak as shown in Figure 7.11. For example the β-form peaks are not present above 1 vol% of xGnP-1 but they can still be detected in PP reinforced with up to 10vol% of xGnP-15. This probably reflects the difference in size between the xGnP-1 and xGnP-15 and consequently, the number of graphite platelets that are present in each case for a given xGnP volume. It indicates saturation of the nucleating action at higher xGnP-1 content since there are not enough polymer chains to orient and align along all the graphite platelets that are present. Similar results of saturated nucleating effect were also reported in SWNT-PP system [4]. The stronger graphite peak in case of xGnP-15 is attributed to the presence of large oriented agglomerates due to poor dispersion and higher degree of alignment of xGnP-15 compare to xGnP-1, as discussed in Chapter 4.

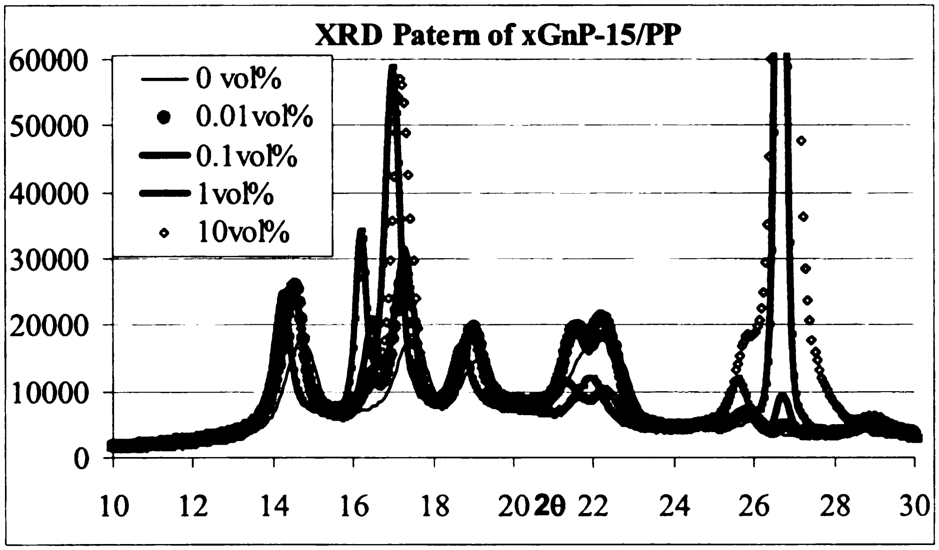

Figure 7.12: XRD of xGnP-15/PP made by melt mixing and injection molding

Taking into account that the β-form of PP has higher impact strength and toughness [5] and that xGnP up to a specific loading, ~1vol%, promotes the formation of β-form crystals it is theoretically expected that the impact strength of the neat PP will increase upon addition of xGnP and that it will reach a maximum at the xGnP loading that corresponds to the saturation of the nucleating effect which is different for the two types of xGnP used. Indeed such a trend can be seen in the impact strength data presented in Chapter 4. However, the impact strength does not only depend on the crystallization behavior of the polymer but also on changes in the energy absorbing mechanisms as discussed in Chapter 4.

7.3.3 Effect of Compounding on the Crystallization of PP

The effect of xGnP dispersion on the crystallization of PP was investigating by studying the XRD patterns of xGnP-PP nanocomposites made by i) melt mixing and injection molding and ii) premixing by coating the PP powder with xGnP, followed by melt mixing and injection molding. It is unavoidable to skip the melt mixing step since in order to do injection molding the premixed xGnP-PP powder has to go through the extruder. Both sizes of xGnP were used. It is noted that the pressure used during injection molding is 160psi compare to 100psi used in processing the composites discussed before.

The XRD of the neat PP, the xGnP-1/PP and xGnP-15/PP made by the two compounding methods are shown in Figures 7.13 to 7.15. The strong nucleating effect of the xGnP-1 and xGnP-15 can be seen by the increase of the three peaks that correspond to planes that match the crystallographic plane of graphite. These peaks are β <300> at $2\theta=16^{\circ}$, α <040> at $2\theta=16.95^{\circ}$, and α <060> at $2\theta=25^{\circ}$. These three peaks are stronger when premixing instead of melt mixing is used for the case of xGnP-1 as shown in Figure 7.14. This is probably due to a more homogeneous distribution of xGnP-1 and thus the number of available for nucleation graphite platelets is larger.

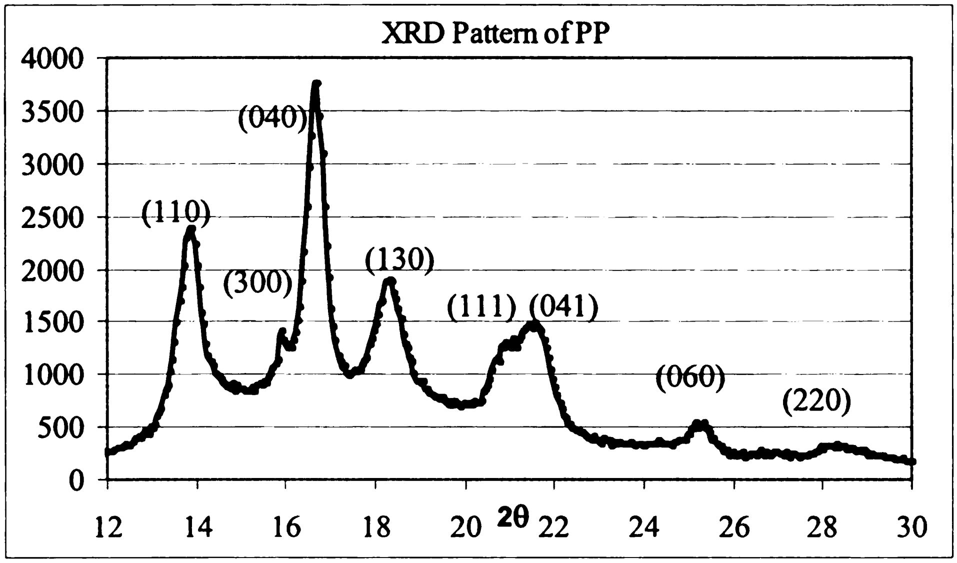

Figure 7.13. XRD Pattern of neat PP made by melt mixing and injection molding

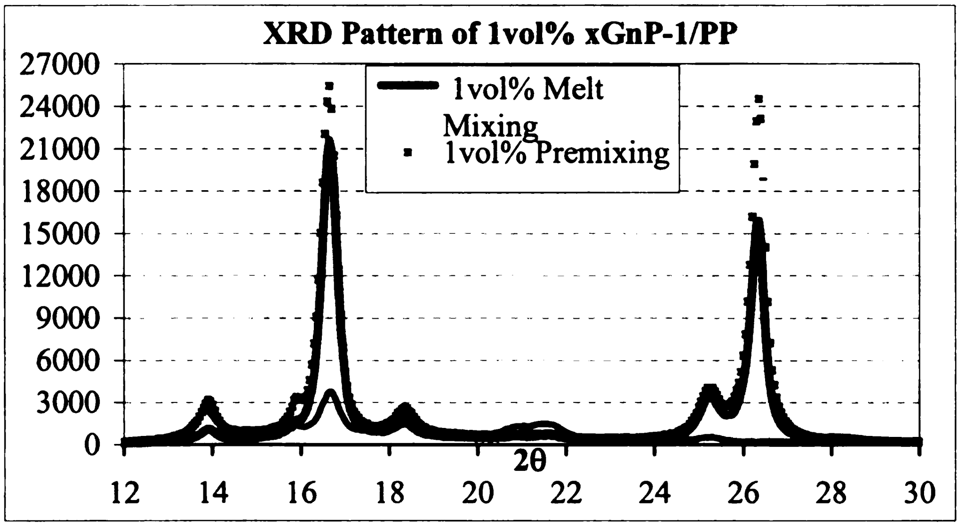

Figure 7.14. XRD Pattern of 1vol% xGnP-1/PP: Effect of Compounding

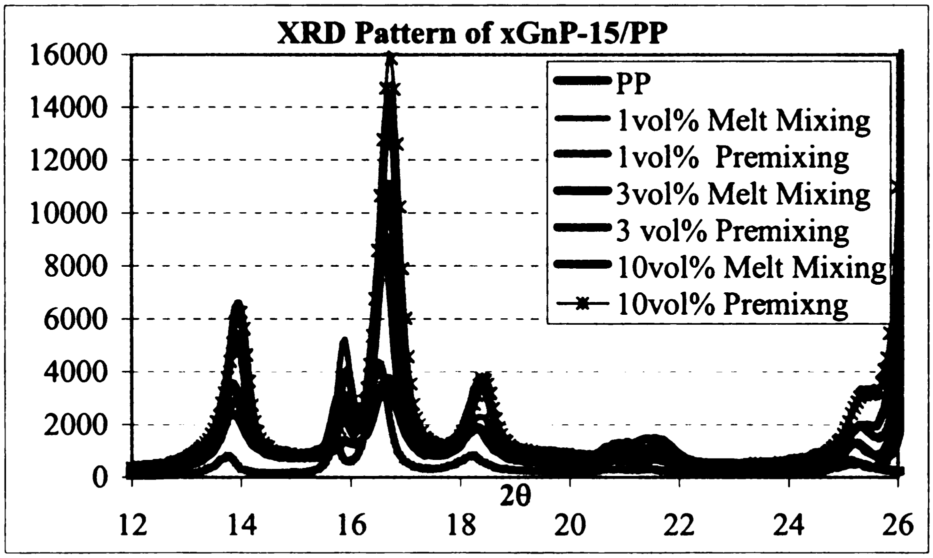

Figure 7.15. XRD Pattern of 1vol% xGnP-1/PP: Effect of Compounding

The trend is similar in case of xGnP-15. Again the three peaks that correspond to reflections of the general <00x> type become stronger upon addition of xGnP-15. Only the β-form peak at 2θ=16° reaches a maximum at ~ 1vol% xGnP-15 whereas the two α-form peaks keep increasing with xGnP-15 concentration. Based on Figure 7.15 it seems that the there is no significant difference in the XRD patterns due to the compounding method used.

7.3.4 Effect of Matrix Crystallization Behavior on Percolation Threshold

In an effort to understand how the crystallization of PP affects the electrical conductivity and percolation threshold of xGnP/PP composites, samples were made by premixing the xGnP with the PP powder and compression molding. The crystallization of the matrix was altered by using different cooling rates after the molding was completed.

Two extreme cases were used i) fast cooling (fc) at a rate of ~20oC/min and ii) slow cooling (sc) at a rate of ~0.3oC/min. The reinforcements used in this study were xGnP-1, xGnP-15 and CB. The electrical conductivity of the nanocomposites was determined using the experimental conditions and method described in Chapter 6. The effect of cooling rate on the crystallinity was investigated by DSC and XRD.

The electrical conductivity of xGnP-1/PP and xGnP-15/PP as a function of xGnP concentration and the cooling rate is shown in Figures 7.16 and 7.17 respectively. In both cases the slowly cooled composites have a lower percolation threshold (~0.1 vol% for xGnP-1 and between 0.3 and 0.5 vol% for xGnP-15). It is also observed that in case of xGnP-1 the effect of cooling rate decreases as the xGnP concentration increases.

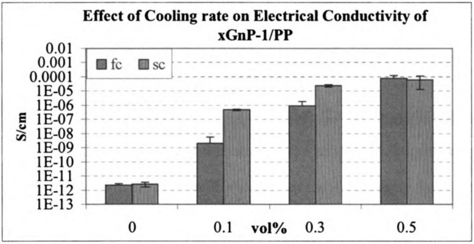

Figure 7.16. Effect of cooling rate on the electrical conductivity of xGnP-1/PP

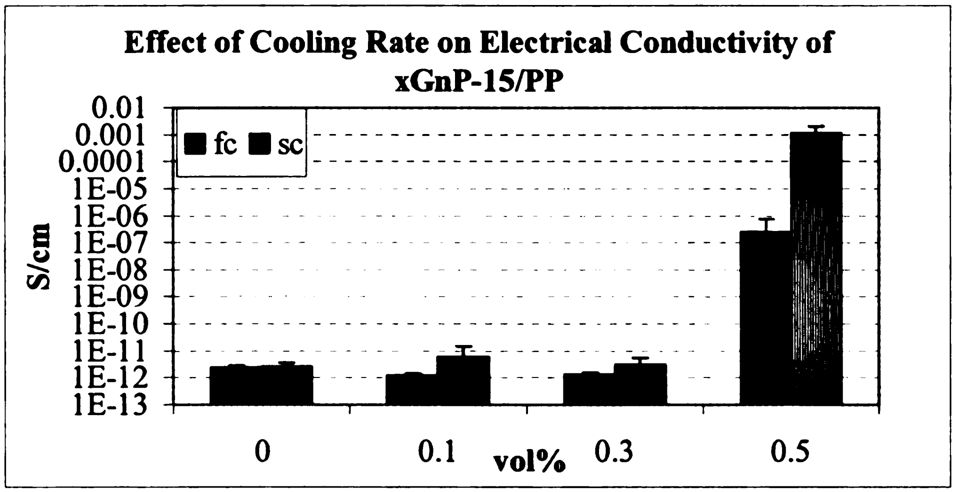

Figure 7.17. Effect of cooling rate on the electrical conductivity of xGnP-15/PP

It is know that increasing the conductive filler's aspect ratio lowers the percolation threshold [24], however, this is not observed with xGnP. The reason is that in the premixing method used for compounding, which results in PP powder coated by graphite platelets the number of graphite platelets is more important than their size. For example, assume that both xGnP-1 and xGnP-15 agglomerate, since it is difficult to achieve monolayer xGnP coverage of the PP powder, during the sonication used for premixing. Even if the extent of agglomeration is the same in both types of graphite, although there is indication that the larger platelets tend to agglomerate more, the area of PP left uncoated will be larger in case of xGnP-15 so a higher concentration of xGnP-15 is required to reach percolation. Once the PP powder is completely covered by graphite then xGnP-15 can result in higher values of electrical conductivity as shown by comparison of the 0.5 vol% data points of Figures 7.16 and 7.17.

The percolation threshold and electrical conductivity of CB/PP is shown in Figure 7.18. No conclusion can be made on how the cooling rate affects these properties since the percolation threshold is below 0.1vol%, which is the minimum concentration used in this study. This low percolation threshold is expected and the results are in agreement with the results presented in Chapter 6 where it was reported that the percolation threshold for CB/PP made my melt mixing and injection molding was below 2 vol% when the percolation for the other reinforcements was above 5 vol %.

Independent of how the CB/PP composites are made, they have a very low percolation threshold but the maximum conductivity measured is two orders of magnitude lower than the conductivity of xGnP/PP or carbon fiber reinforced PP composites. This is probably due to the highly agglomerated structure of CB and its high degree of porosity which results in a surface area of 1400 m^2/g [25] that enables CB to form a conductive network at lower concentrations [26]. However, the agglomerates consist of nanosize particles so it is likely that the conductive path formed has many discontinuities and higher resistance.

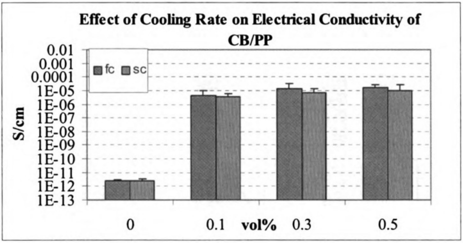

Figure 7.18. Effect of cooling rate on the electrical conductivity of CB/PP

Based on Figures 7.16 and 7.17 it is clear that use of slow cooling rate results in a lower percolation threshold and higher electrical conductivity for xGnP/PP nanocomposites. In order to understand the mechanism behind the cooling rate effect, the crystallization behavior of xGnP-1/PP and xGnP-15/PP at loadings of 0.1 and 0.3 vol% was studied by DSC using conditions that simulate the fast and slow cooling rates employed during compression molding.

As shown in Figures 7.19 the temperature at which the crystallization starts (during the cooling cycle) is higher by ~20 °C in the case of the slow cooled samples for both the neat PP and the xGnP/PP composites, which for each cooling rate have higher crystallization temperatures compared to the neat polymer due to the nucleating effect of xGnP as discussed above. The higher crystallization temperature leads to larger spherulite size as shown in Figures 7.3 and 7.4 where a comparison of the spherulites formed isothermally at T=130°C and T=145°C is provided. Thus it is concluded that the slow cooling rate leads to larger spherulites.

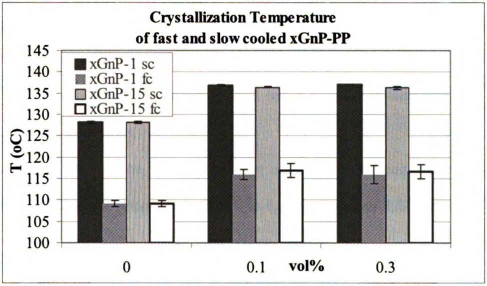

Figure 7.19. Effect of cooling rate on the crystallization temperature of xGnP/PP

The degree of crystallinity was calculated and is presented in Figure 7.20. For the neat polymer the slow cooling rate results in ~10% higher crystallinity compare to the fast cooled samples. However, the effect of cooling rate diminishes upon addition of any size of xGnP.

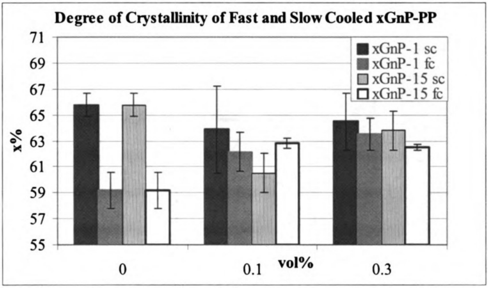

Figure 7.20. Effect of cooling rate on the degree of crystallinity of xGnP/PP

Since slow cooling results in larger spherulites and since the degree of crystallinity is the same for both the slow and the fast cooled samples it is concluded that the slow cooling rate yields composites with lower percolation threshold that contain larger but fewer spherulites.

Additional information about the melting enthalpy and melting temperature of the PP and xGnP/PP nanocomposites is shown in Figures 7.21 and 7.22 respectively. That the slowly cooled samples release more energy during melting compared to the fast cooled specimens indicate that the spherulites are thicker and larger which is in agreement with the observation made in a study on isotactic PP reported that higher crystallization temperatures lead to thicker crystals [14]. As shown in Figure 7.22 the fast cooled samples have slightly higher melting temperature, estimated as the maximum of the melting peak at the DSC runs. The high melting temperature is attributed to the melting of crystals formed by recrystallization during the reheating process [27].

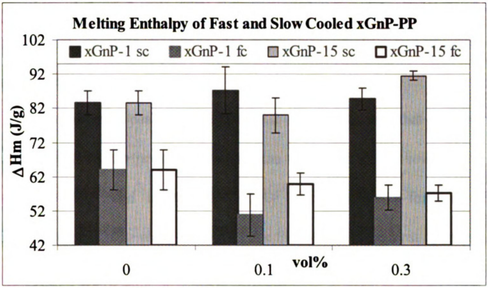

Figure 7.21. Effect of cooling rate on the melting enthalpy of xGnP/PP

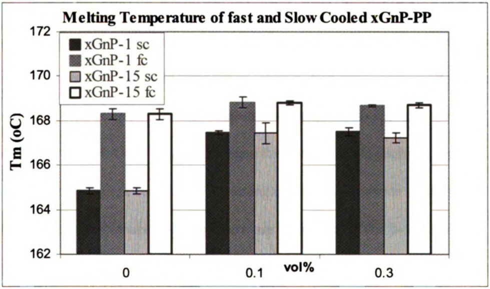

Figure 7.22. Effect of cooling rate on the melting temperature of xGnP/PP

XRD patterns of neat PP, xGnP-1/PP, xGnP-15/PP and CB/PP at reinforcement content of 0.1, 0.3 and 0.5 vol% made by premixing and compression molding using the slow and fast cooling rates were obtained in order to investigate any correlation between the diffraction peaks and the percolation threshold of the composites. Representative results are shown below whereas the rest are presented in Appendix E. Two and in some cases three samples were studied for each condition (type and loading of reinforcement and cooling rate).

There are six main peaks in all of the XRD patterns obtained that correspond to α-form crystals. One of the peaks, at $2\theta \sim 21^\circ$, can either reflect the α-form crystal that appears at $2\theta=21.2^\circ$ and reflects the <111> plane or the β-form at $2\theta=21.2^\circ$ corresponding to the <301> plane. However, due to absence of the most dominant β-form peak at $2\theta=16.8^\circ$ it is assumed that the peak corresponds to the α-form crystal.

Only in case of the neat polymer as shown in Figures 7.23 and 7.24 is there evidence of β-form crystals based on the weak peak at $2\theta=16.8^\circ$ which however disappears upon addition of xGnP. The reason is that since xGnP is a nucleating agent it increases the crystallization temperature as shown also in Figure 7.19. In addition, according to a time-temperature-crystallization diagram for iPP [6] it is expected that only α-phase crystallites will be present since they form first at higher temperatures and if they grow too much (in case of slow cooling) or the cooling rate is too high (case of fast cooling) there is no space or the temperature is too low so the β-form crystals cannot form.

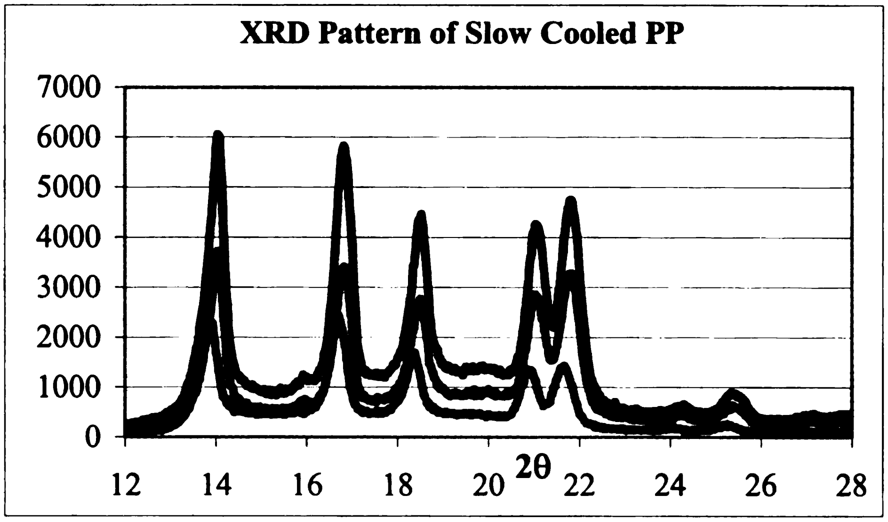

Figure 7.23. XRD pattern of slow cooled PP

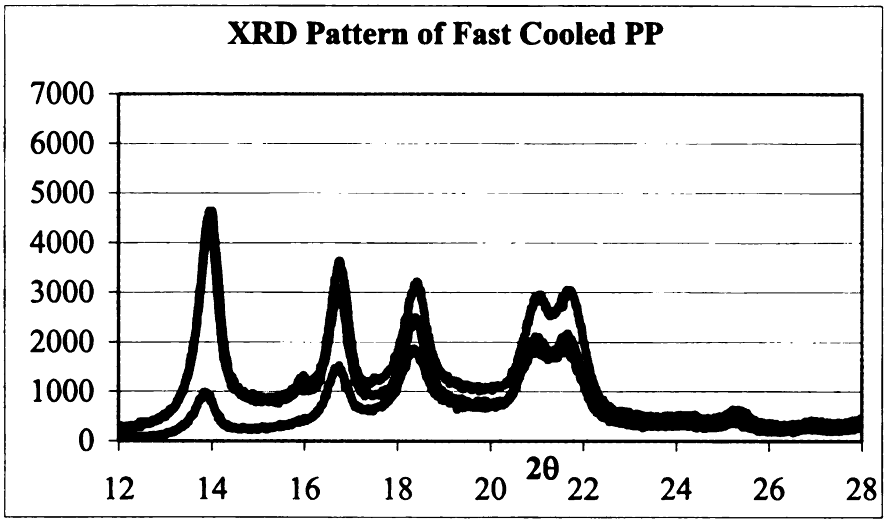

Figure 7.24. XRD pattern of fast cooled PP

The basic difference between the slow and fast cooled samples is that at slow cooling rate the XRD peaks are sharper and well defined whereas fast cooling rate results in samples with wider and weaker XRD peaks. In addition, as the xGnP content increases the peaks at $2\theta=16.95^{\circ}$ and $2\theta=25^{\circ}$, which correspond to the <040> and <060> crystallographic planes, are enhanced which is attributed to the nucleating effect of xGnP, <002> plane, as discussed previously.

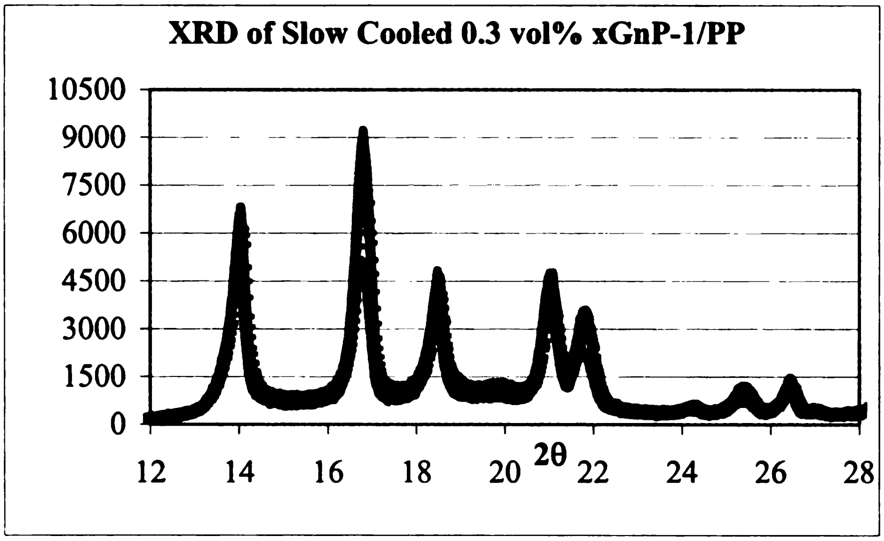

Figure 7.25. XRD pattern of slow cooled 0.3 vol% xGnP-1/PP

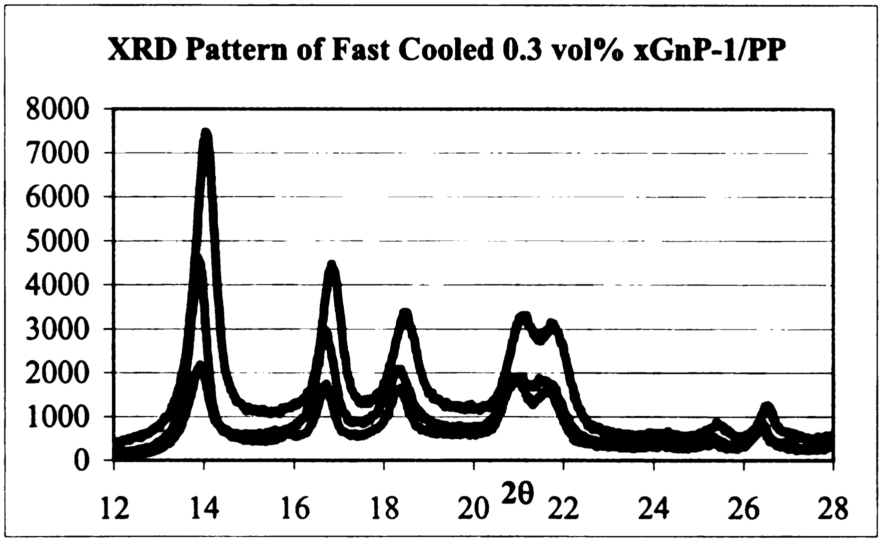

Figure 7.26. XRD pattern of fast cooled 0.3 vol% xGnP-1/PP

The observed increase in FWHM for the fast cooled samples indicates overall reduction of the crystallite size and as such it is concluded that the fast cooled samples have smaller crystallites as it was also indicated by DSC (Figure 7.21).

Representative results are presented in Figures 7.27, 7.28 and 7.29, which show the crystal thickness of neat PP, 0.1 vol% xGnP-15/PP and 0.5 vol% xGnP-15/PP respectively. Although there are only six main peaks in the XRD patterns the crystal size has been estimated for all the peaks that are present.

As mentioned above, β-form crystals exist only in case of neat polymer and in particular of those samples made by fast cooling as shown in Figure 7.27. The β-form crystals are twice as large as compared to the α-form, which is in agreement with a study reporting that the lamellae of β–form PP (20 nm) are thicker than those of α–form PP (10 nm) [28]. The difference in the absolute value of the crystal thickness between the experimental data and the literature may be due to processing method and conditions used to fabricate the samples and the value assumed for the shape factor used in Equation (7.2).

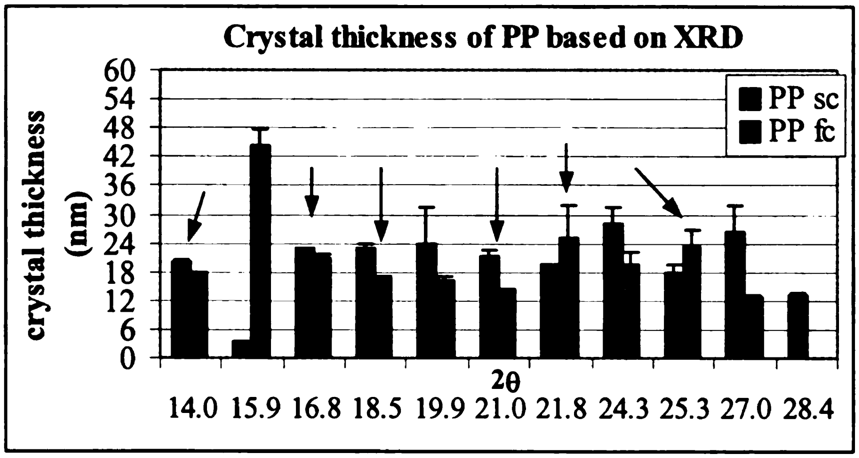

Figure 7.27. Crystal size of PP based on XRD

The arrows in Figure 7.27 indicate the crystal size corresponding to the six main XRD peaks. In most cases the slow cooling results in thicker crystals and the difference becomes larger upon addition of xGnP as shown in Figures 7.28 and 7.29.

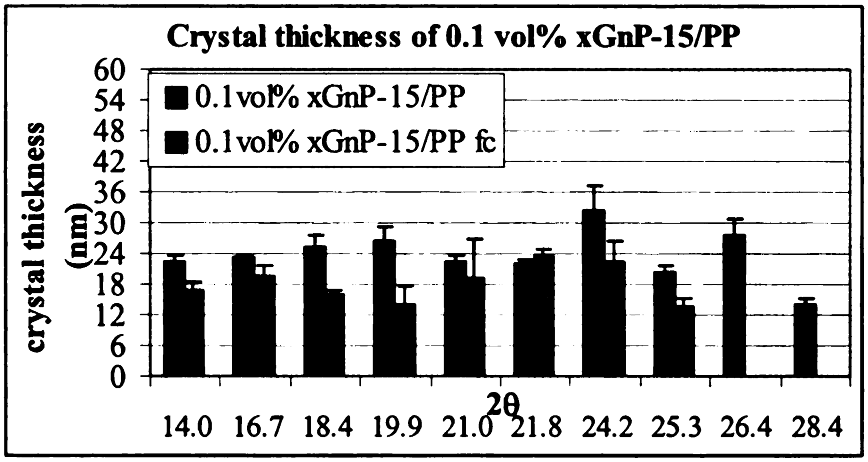

Figure 7.28. Crystal size of 0.1 vol% xGnP-15/PP based on XRD

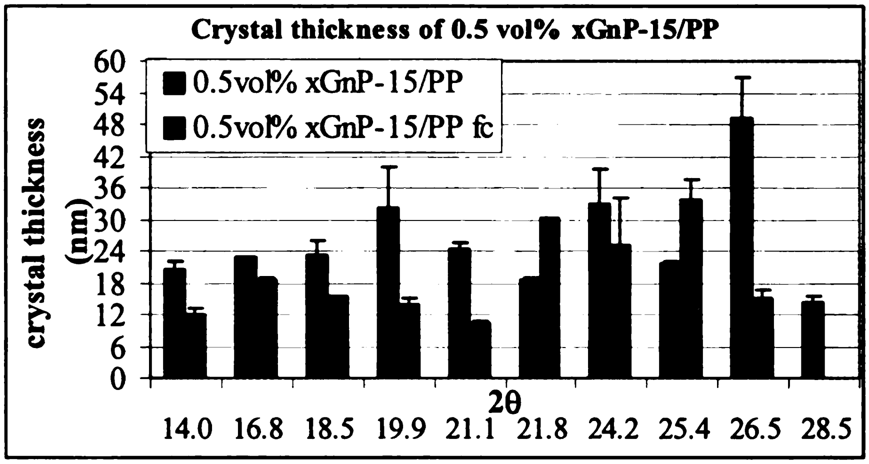

Figure 7.29. Crystal size of 0.5 vol% xGnP-15/PP based on XRD

The question why the slow cooling compared to fast cooling and the smaller aspect ratio graphite, xGnP-1, compared to xGnP-15 result in composites with lower percolation threshold can be answered by taking into consideration and combining all the results presented in this section. In more details:

Based on Figures 7.28 and 7.29 it is evident that fast cooling results in crystals that are ~20-30% thinner compared to the crystals formed during slow cooling of the composites. According to Figure 7.20 the degree of crystallinity is the same for both the slow and the fast cooled samples, thus it is concluded that slow cooling results in larger but fewer crystals.

As indicated by DSC and optical microscopy xGnP is a nucleating agent for PP and the crystals are growing around the platelets. In the case of fast cooling there are more crystals so a larger number of graphite platelets will be in the center of the crystals and fewer will be available to form the continuous network necessary for providing electrical conductivity as compared to the slow cooled samples. In addition, the conductive path of xGnP can be disrupted by the presence of many small spherulites that exist in the fast cooled composites. Thus a higher loading of xGnP, which means higher percolation threshold, is required to impart the electrical conductivity of the composites in case of fast cooling.

The same argument can also explain why xGnP-1 has lower percolation threshold since a specific volume loading of xGnP contains more xGnP-1 platelets. Additionally, xGnP-15 tends to agglomerate more and thus the number of platelets available to form the conductive path is further reduced. However, once the conductive path is formed then the electrical conductivity of xGnP-15/PP is higher (10^{-3} S/cm at 0.5 vol%) compared to xGnP-1/PP (10^{-4} S/cm at 0.5 vol%), which reflects the effect of the aspect ratio and size.

The mechanism described above is summarized schematically in Figure 7.30. Both the slow and the cooled samples shown in Figure 7.30a and 7.30b respectively contain the same amount of reinforcement (black spots). The PP crystals grow around the xGnP in both cases. The basic difference is that in the slow cooled sample there are fewer but (20-30%) larger crystals and the number of xGnP available to form the conductive path which is indicated by the red arrows, is higher.

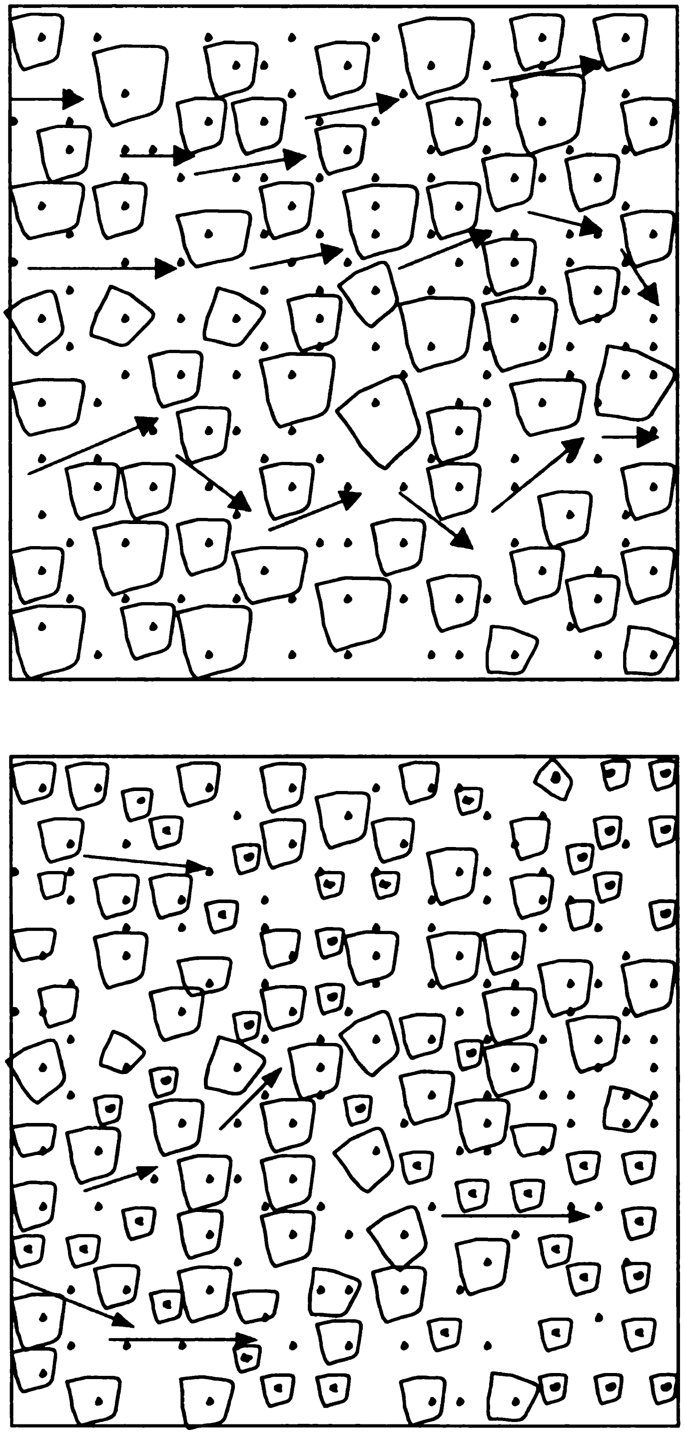

Figure 7.30. Schematic of the microstructure of premixed compression molded xGnP/PP a) slow cooled and b) fast cooled. The arrows indicate the formation of conductive network which can span the across the whole sample in case of slow cooling.

7.4 Conclusions

The effect of xGnP on the crystallization behavior of PP was investigated using optical microscopy, DSC and XRD.

It was found that xGnP, even at loadings as low as 0.01 vol%, is a nucleating agent for PP and increases the crystallization temperature (during the cooling cycle) and the crystallization rate. No effect on the degree of crystallinity was observed and the number of nucleation sites increases with the concentration of any type of xGnP.

Furthermore, it was demonstrated that xGnP can induce, under specific processing conditions (injection molding with T_{mold}=80°C and pressure of 100psi), the nucleation of the β-form PP crystals which have higher impact strength compared to the most common α-form PP crystals. A saturation effect on the nucleation of β-form crystals was observed at higher xGnP concentrations (1 vol% for xGnP-1 and ~10 vol% for xGnP-15) which is attributed to the fact that there is not enough polymer to penetrate between the platelets and keep them apart leading to a poor dispersion that does not utilize the xGnP surface that is available for crystal nucleation.

According to the XRD study presented, the nucleating efficiency of xGnP can be also expressed as the change in the intensity ratio between the α-form (040) and (110) reflections and/or as the enhancement of peaks that correspond to crystallographic planes of the general (00α) type which is attributed to the alignment of PP chains along the xGnP surface and epitaxial crystal growth due to crystallographic match between these PP planes and the graphite's (002) plane.

In addition to the effect of xGnP on the crystallization behavior of PP, the relation between crystallinity and percolation threshold/electrical conductivity of xGnP/PP nanocomposites was also investigated. The crystallization of the matrix was altered by cooling the composites at different rates once the molding was completed. It was found that fast cooling results in composites with higher percolation threshold. Based on the experimental data obtained this reflects mainly the difference in the number of xGnP that are available to form the conductive network. In the fast cooled composites there are more but smaller/thinner crystals, hence more graphite platelets are in the center of the crystals and thus fewer available to form the conductive path. In addition the more and smaller crystals may disrupt the formation of the conductive network increasing thus the percolation threshold. It was also found that xGnP-1 has lower percolation threshold (10^{-6} S/cm at 0.1 vol%) compared to xGnP-15 (10^{-3} S/cm at 0.5 vol%) which is also attributed to the larger number of xGnP-1 that are contained in a given xGnP loading and to the fact that xGnP-15 agglomerate more and thus the number of platelets available to form the conductive path is further reduced.

It is concluded that the presence of xGnP significantly alters the crystallization behavior of PP and by using the proper processing conditions the properties of xGnP/PP such as impact strength, percolation threshold and electrical conductivity can be strongly affected.

7.5 References

1. J G. Klijusuric, "Changes in polymer foils used in food packaging tested by using differential scanning calorimetry", Sadhana **28** (6) 991-998 (2003)

2. D.J. Chaiko and A.A. Leyva, "Thermal Transitions and barrier Properties of Olefinic Nanocomposites" *Chem. Mater* **17** (1), 13-19 (2005)

3. A.R. Bhattacharyya, T.V.Sreekumar, T. Liu, S. Kumar, L.M. ericson, R.H. Hauge and R.E. Smalley, "Crystallization and Orientation Studies in Polypropylene/Single wall Carbon Nanotube Composite" *Polymer* **44**, 2373-2377 (2003)

4. L. Valentini, J.Biagiotti, M.A. Lopez, Manchado, S. Santucci and J.M. Kenny "Efffects of Carbon Nanotubes on the Crystallization Behavior of Polypropylene", *Polymer Engineering and Science*, **44** 2, 303-311 (2004)

5. T. Huy, R. Adhikari, T. Lupke, S. Henning and G. Michler, "Molecular Deformation Mechanisms of Isotactic Polypropylene in α- and β-Crystal Forms by FTIR Spectroscopy" *Journal of Polymer Science: Part B: Polymer Physics* **42**, 4478-4488 (2004)

6. W. Zheng, X. Lu, C.L. Toh, T.H. Zheng and C. He, "Effects of Clay on Polymorphism of Polypropylene in Polypropylene/Clay Nanocomposites", *Journal of Polymer Science: Part B:Polymer Physics*, **42** 1810-1816 (2004)

7. J. Karger-Kocsis, J. Varga, and G.W. Ehrenstein, "Comparisonof the Fracture and Failure Behavior of Injection-Molded α- and β-Polypropylene in High-Speed Three-point Bending Tests", *Journal of Applied Polymer Science*, **64** 2057-2066 (1997)

8. J. Karger-Kocsis, "How Does "Phase Transformation Toughening" Work In Semicrystalline Polymers?", *Journal of Polymer Engineering and Science*, **36** 203–210 (1996)

9. J. Karger-Kocsis, and J. Varga, "Effects of b-a Transformation on the Static and Dynamic Tensile behavior of Isotactic Polypropylene" *Journal of Applied Polymer Science*, **62** 291–300 (1996)

10. F.J. Padden, and H.D. Keith, H. D. "Spherulitic Crystallization in Polypropylene", *Journal of Applied Physics* **30**, 1479–1484 (1959).

11. J.X. Li and W.L. Cheung, "On the Deformation Mechanisms of b-Polypropylene: 1. Effect of Necking on b-Phase PP Crystals", Oxford, UK, Elsevier, 39, pp. 6935-6940, (1998)

12. B.P. Grady, F. Pompeo, R.L. Shambaugh and D. E. Resasco, "Nucleation of Polypropylene Crystallization by Single-Wall Carbon Nanotubes" *J. Phys. Chem. B* **106** 5852-5858 (2002)

13. S-Y Park, Y-H Cho and R.A. Vaia, "3-D Structure of the Zone- Drawn Film of the Nylon-6/Layered Silicate Nanocomposites", *Macromolecules,* **38** (5), 1729-1735 (2005)

14. E. Devaux, S. Bourbigot and A-E. Achari, "Crystallization Behavior of PA-6 Clay Nanocomposite Hybrid", *Journal of Applied Polymer Science*, **86**, 2416 (2002)

15. S.S. Nair and C. Ramesh, "Studies on the Crystallization Behavior of Nylon-6 in the Presence of Layered Silicates Using Variable Temperature WAXS and FTIR", *Macromolecules* **38**, 454 (2005)

16. T.G. Gopakumar and D.J.Y.S. Page, "Polypropylene/Graphite Nanocomposites by Thermo-Kinetic Mixing", Polymer engineering and Science, 44 (6) 1162-1169 (2004)

17. E.W. Nuffield, "X-ray Diffraction Methods" Wiley: New York, (1966)

18. J-H Chen, F-C Tsai, Y-H Nien and P-H Yeh, Isothermal crystallization of isotactic polypropylene blended with low molecular weight atactic polypropylene. Part I. Thermal properties and morphology development, Polymer 46 (2005) 5680-5688

19. Q. Zheng, Y. Shangguan, S. Yan, Y. Song, M. Peng and Q. Zhang, "Structure, morphology and non-isothermal crystallization of polypropylene catalloys, Polymer, 46 (2005) 3163-3174

20. J. Isasi, R.Alamo and L. Mandelkern, The isothermal expansion of the monoclinic unit cell of isotactic polypropylene, Journal of Polymer Science: Part B: Polymer Physics 35 2945-2949 (1997)

21. E. Ferrage, F. Martin, A. Boudet, S.Petit, G. Fourty, F. Jouffret, P. Micoud, P. de Parseval, S. Salvi, C. Bourgerette, J.Ferret, Y. Saint-Gerard, S. Buratto, and J.P. Fortune, "Talc as nucleating agent of Polypropylene:Morphology Induced by Lamellar Particles Addition and Interface Mineral-Matrix Modelization", *Journal of Materials Science* **37** 1561 (2002)

22. D. Chung, Review Graphite, Journal of Materials Science, 37 (2002) 1475-1489

23. G-H. Chen, D-J. Wu, W-G Weng, and W-L Yan, "Preparation of Polymer/Graphite Conducting Nanocomposite by Intercalation Polymerization", *Journal of Applied Polymer Science*, **82** 2506, (2001)

24. P. Calvert, "Nanotube Composites: A recipe for Strength", *Nature* **399**, 210 (1999)

25. J. King, K. Tucker, J. Meyers, E. Weber, M. Clingerman and K. Ambrosius, "Factorial Design Approach to Electrically and Thermally Conductive Nylon 6,6", *Polymer Composites* **22**, 1, 142 (2001)

26. P. Banerjee and B.M. Mandal, "Conducting polyaniline Nanoparticle Blends with Extremely Low Percolation Thresholds", *Macromolecules* **28**, 3940, (1995)

27. P. Supaphol and J.E. Spruiell, "Thermal Properties and Isothermal Crystallization of Syndiotactic polypropylenes: Differential Scanning Calorimetry and Overall Crystallization Kinetics", Journal of Applied Polymer Science, 75 44-59 (2000)

28. J. X. Li and W.L. Cheung, "On the deformation mechanisms of β-polypropylene: Effects of necking on b-phase PP crystals", *Polymer* **39**, 6935–6940 (1998)

CHAPTER 8

SURFACE TREATMENT OF EXFOLIATED GRAPHITE NANOPLATELETS

8.1 Introduction

8.1.1 Rationale for Surface Treatment of xGnP

A basic advantage of using nanomaterials instead of conventional micro size reinforcements is that due to the increased surface area the stress transfer from the matrix to the reinforcements is more efficient and the crack propagation energy at the interface becomes greater resulting in improved strength and toughness.

This is true only if there is good adhesion at the polymer-reinforcement interface. However, based on the results presented in Chapter 4 in case of xGnP-PP nanocomposites, even for the well dispersed xGnP-1, the flexural strength reaches a maximum plateau value at 10 vol% of xGnP indicating that there is need to improve the adhesion at the interface.

The improvement of adhesion at the interface, mainly by surface modification of the reinforcement, is possible if there is a fundamental understanding of the bonding and interactions that are present between reinforcements and matrix, that is the type, quantity and reactivity of the functional groups on the surface of the reinforcements are known.

8.1.2 Surface Treatment of Carbon Fibers

As indicated by Drzal [1,2], the carbon-polymer interface includes a three-dimensional interphase region with thickness ranging from 0.5 to 500nm. Both the reinforcement and the polymer contained in the interphase are chemically and morphologically different than those found in the one phase, bulk regions. Based on the same study it is possible to microengineer the fiber-matrix interphase through the use of sizings and coatings to create an interphase with beneficial properties.

A common surface treatment for carbon/graphite materials is liquid phase chemical oxidation [3], where oxidizing agents such as nitric acid or hydrogen peroxide are employed to introduce acidic functionalities especially at less crystalline regions. However, such treatment can also introduce defects on the surface and thus may result in reduction of the material's tensile strength.

Plasma treatment is another method for modifying the surface of carbon materials. During the process various reactions including ionization, excitation and recombination can occur due to interactions/collisions of electrons and other species existing in the plasma chamber. The atmosphere used i.e., O_2, air, NH_3 or Ar defines the type of functionalities introduced on the carbon surface [4,5].

Furthermore, sizing of carbon materials has also been used to improve adhesion. It has been reported that epoxy sizing of carbon fibers resulted in enhancement of the tensile, compressive and flexural strength whereas no change was observed for the moduli. The improvement in strength is attributed to the strong interfacial bonding that alters the failure mechanism from the interface-initiated more to the matrix-initiated mode [6-9].

8.1.3 Funtionalization of Carbon Nanotubes

Recently due to the increased interest in CN reinforced polymer nanocomposites there is a plethora of studies reported on the surface modification of CN in order to enhance the adhesion to the polymer along the interface. The methods proposed, that can also be applied in xGnP since the two carbon materials have the same chemistry, can be summarized as follows:

(i) Functionalization of the SWCN end-caps with long aliphatic amines [10]. It is a two step process where initially carboxylic groups are introduced at the open ends of the CNs by treating with HCl followed by a reaction of the oxidized CNs with octadecylamine at ~100 °C for ~5 days.

(ii) Plasma activation of CNs for chemical modification [11]. A concentric layer of (acetaldehyde) plasma polymer film is homogeneously deposited onto each of the constituent aligned CNs by plasma polymerization (e.g., acetaldehyde). This method provides a novel approach for chemical modification of CNs through plasma activation and subsequent reactions characteristic of the plasma induced surface functionalities.

(iii) Functionalization of SWNTs by amine-rich polymers [12]. CNs are submerged in a 20 wt % solution of polyethylene imine (PEI) in methanol overnight, followed by thorough rinsing with methanol in order to remove nonspecifically adsorbed PEI resulting nearly in a monolayer of PEI irreversibly adsorbed on SWNTs.

(iv) Covalent modification of SWCNs [13]. Oxidative etching of SWNTs followed by treatment with thionyl chloride, and subsequent amidation. These oxidations also result in the introduction of moieties at defect sites along the sidewalls, and functionalities other than carboxylic acids can be formed.In case of CN and xGnP the oxidation is a necessary step before any other functionalization process can take place since both materials are highly crystalline, which means that there are no defects to act as active sites, and they are very inert i.e., there are no functional groups along the edges or on the graphite's basal plane that can participate/initiate a chemical reaction. The most common scheme for oxidation is sonication of the CNs in mixtures of sulfuric and nitric acids [14], treatment with piranha (sulfuric acid-hydrogen peroxide) [15] or with ozone [16,17]. Depending on the conditions used the oxidation can clean the CN by removing catalyst particles and amorphous carbon, open the CN ends, reduce their length and introduce oxygenated functionalities such as carboxylic acids, anhydrites, quinines, and esters [13-17].

8.1.4 Objectives

The goal of the work presented in this chapter is to explore possible methods for modifying the surface of xGnP in order to improve the adhesion with the PP matrix. A two-step approach was followed:

(i) Oxidation of xGnP-1. Various oxidizing agents and experimental conditions i.e., temperature and time were explored and evaluated according to the kind of oxygen functionalities they introduce.

(ii) Treatment of the oxidized xGnP-1 with silane coupling agent. Various organolisanes with different reactive and alkyl groups were used in order to determine the maximum % of silane that can be grafted on xGnP-1 and that could maximize the interactions with the PP matrix.

8.2 Experimental Conditions and Characterization Techniques

The surface composition of the untreated and surface modified xGnP-1 was determined by X-ray Photoelectron Spectroscopy (XPS). X-ray photoelectron spectra were obtained from a Physical electronics PHI 5400 ESCA system. A non-monochromatic Mg source (with a Ka1,2 wavelength at 1253.6 eV) was used with a take-off angle of 45 degrees. Data was collected by a multi-channel detector with an Omni VI lens assembly. The instrument was operated with a pass energy of 93.90 eV for survey scans and 29.35 eV for regional scans. All peaks were referenced to adventitious carbon at 284.6 eV. Semi quantitative atomic concentrations were calculated using pre-determined sensitivity factors. XPS samples were prepared by applying the sample in powder form directly to double-sided copper tape on a stainless steel stub.

The effect of graphite's surface treatment on the crystallization behavior of PP was determined by DSC and XRD. The DSC samples used were 5-10 mg and non-isothermal crystallization was studied using the following experimental conditions. The sample was heated to 220°C at a rate of 30°C/min. The thermal history of the sample due to prior processing was erased by maintaining isothermal condition for 10min. Finally, the sample was cooled at 10°C/min to 100°C, held isothermally for 2min and reheated at 10°C/min to 200°C. The crystallization data was collected during the first cooling cycle whereas the data on the melting behavior was collected along the second heat cycle. Details on the preparation of the samples for XRD characterization and the experimental conditions used were provided in Section 7.2.

It is expected that any change in the xGnP-PP adhesion due to surface modification of xGnP will be reflected in the flexural strength of the xGnP-1/PP nanocomposites. Flexural tests were performed with a UTS SFM-20 machine [United Calibration Corp.] at room temperature by following the ASTM D790 standard test method (3-point bending mode) as described in Section 4.2. The flexural samples were made by melt mixing and injection molding using the DSM microextruder operating at the optimum processing conditions.

A morphological study using optical microscope (reflected light) was performed to investigate how the oxidation of xGnP affects its dispersion within the polymer matrix. The samples used were flexural bars and the surface examined, which was parallel to the flow plane, was prepared by polishing using 1200 and 4000 grits at 150 rpm for 5min followed by 2min polishing using 1μm Al_2O_3 powder. The samples were washed with DI water and air dried. To assure a surface free of contaminants i.e., particles from the polishing media the samples were immersed in H_2SO_4 for 5min. An additional advantage of the chemical etching is that it removes a thin layer of the polymer matrix from the surface without affecting the xGnP.

A Cahn TG System 121 analyzer was used for thermogravimetric analysis (TGA) that provided the weight loss of xGnP-1 samples during heating up to 600°C at 10°C/min. The samples used are 10-20mg.

8.3 Results and Discussion

8.3.1 Oxidation of xGnP-1

xGnP-1 is chemically inert since it is highly crystalline and has no defects or functional groups except at the dedges of the graphene platelets (less than 6 atomic% of oxygen based on XPS) that are necessary for any surface modification. An easy way to introduce oxygen-contained functional groups on xGnP is oxidation. The oxidizing agents as well as the conditions used such as time and temperature are shown in Table 8.1. The quantities used are 2g of xGnP-1, 300ml of H_2SO_4 and 100ml of HNO_3. Sonication was used in all cases.

Table 8.1: Experimental Conditions for Oxidation of xGnP-1

Oxidizing Agent	Time (hrs)	Temperature (^oC)
H_2O_2/ H_2SO_4 (1:3)	0.5	25
HNO_3:H_2SO_4 (1:3)	8	70
HNO_3/ H_2SO_4 (1:3) + O_3	1	80-90

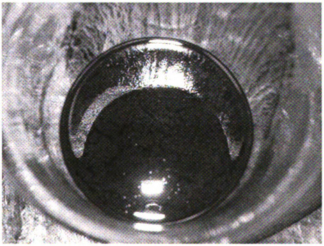

Figure 8.1: xGnP-1 in a solution of HNO_3/H_2SO_4

It is noted that in all cases the color of acid solution changes from black to metallic green as shown in Figure 8.1, within the first few minutes of the xGnP addition into the acidic solution indicating existence of stage I graphite i.e., the xGnP particles are further exfoliated into single graphene sheets.

Once the oxidation is completed the acids are removed by filtration using DI water as washing medium and the oxidized xGnP is dried overnight at 120°C. XPS was used to determine the surface concentration (atomic %) of xGnP before and after the oxidation and fitting of the carbon peak was used to evaluate the type of functional groups present. The results are shown in Table 8.2 and 8.3 respectively.

Table 8.2: XPS results of oxidized xGnP-1

Sample ID	**$C_{1}s$**	**$N_{1}s$**	**$O_{1}s$**	**$S_{2}p$**	**$Zr_{3}d$**	**O/C**
1. control xGnP-1	93.06		6.76		0.18	0.069
2. H_2O_2/H_2SO_4	87.89	1.36	9.33	1.2	0.21	0.101
3 HNO_3/H_2SO_4	90.26		9.4		0.33	0.097
4. H_2SO_4/HNO_3 +O_3	89.05		10.49		0.46	0.107

Table 8.3: Percent of surface carbon that participates on the specified functional groups

	Binding Energy (eV)	**Sample 1**	**Sample 2**	**Sample 3**	**Sample 4**
C-C	284.86	88.43	90.03	87.71	85.12
C-O	286.39	8.27	5.32	6.17	6.77
C=O	287.86	0	0.02	0.35	0.59
-COO	289.6	2.1	1.7	3.21	4.67

The presence of Zr on the surface of xGnP-1 is due to contamination of xGnP from the ZrO_2 milling media during the milling process. According to Table 8.2 the amount of atomic oxygen on the graphite surface, expressed as the ratio of O/C (corrected for the oxygen contained in ZrO_2), increased in all of the three cases studied from 0.069 (control xGnP-1) to ~0.1. The maximum increase was observed for oxidation using a (3:1) mixture of H_2SO_4/HNO_3 in presence of ozone. The same oxidation method (sample 4) resulted in higher % of surface carbon that forms bonds with oxygen based on Table 8.3. This information that is derived from fitting the carbon peak does not reveal the exact type of the functional group, i.e, for sample 4, 6.7% of the carbon forms a single oxygen bond that can be either ether or hydroxyl type. Fitting the oxygen peak, which for the purpose of this research was not necessary, can provide such information.

The oxidation of xGnP-1 by H_2SO_4/HNO_3 in presence of ozone that resulted in the maximum oxygen concentration is a method that has not been reported in literature. Ozonolysis has been used in case of SWCN to create carbonyl surface functionalities [16] or to determine the fraction of oxidized carbon sites introduced in SWNT by acidic oxidation (H_2SO_4/HNO_3). This has been done by measuring the evolution of CO and CO_2 on heating up to 1000°C followed by titration with O_3 [17]. However, combination of acids with ozone for oxidation of carbon materials has not been reported. Furthermore, the experimental set up is simple i.e., a glass beaker with the acids where the delivery tube for the O_3 and the sonication probe, are immersed; allows for scale up. Indeed, the process has been applied to 30g of xGnP-1 at once using 1200 ml of acids H_2SO_4/HNO_3 (3:1). Based on XPS the xGnP-1 was homogeneously oxidized.

8.3.2 Treatment of Oxidized xGnP-1 with Organosilanes

The introduction of functional groups mainly along the edges of the graphite platelets by oxidation allow for further surface modification of xGnP-1 by attaching various macromolecules through covalent bonding. Since the goal is to improve adhesion with the PP matrix, which does not show any direct opportunity for covalent coupling, a first approach is use organosilanes due to their well established coupling action.

Silane coupling agents are able to form a durable bond between organic and inorganic materials due to the existence of two types of functionality. A silane coupling agent can be described by the general formula $RSiX_3$ where R and X are organofunctional and hydrolysable groups respectively. Following hydrolysis of the X groups a reactive silanol group is formed, which can condense with other silanol groups and form hydrogen bonds with OH groups of the substrate. During drying or curing a covalent bond with the substrate is formed due to loss of water. The R group is a nonhydryzable organic radical, which possesses a functionality enabling the coupling agent to bond to organic resins and polymers [18-19].

Improvement of strength in polyolefin based composites through coupling with vinyl or methacryloxy groups and addition of a small amount of peroxide (0.15-0.25%) that introduces additional coupling sites into the polymer has been reported [18]. Silylsulfonylazides is another type of silanes that are suggested for coupling PP according to the following mechanism. Sulfonyl azides decompose above 150°C to form a molecule of nitrogen and a reactive nitrene that is capable of insertion into carbon-hydrogen bonds, carbon-carbon double bonds, and aromatic bonds [18].

Based on the above, the ability of the three silanes, shown in Figure 8.2, to couple xGnP-1 and PP was investigated. The third silane is not expected to improve the strength of the xGnP-1/PP composites and it is used as a control to validate the success coupling ability of the other two.

1. methacryloxypropyl triisopropoxysilane	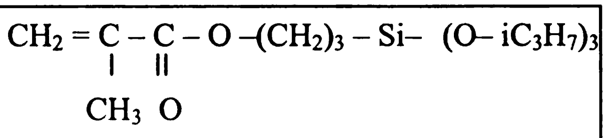 $CH_2=\underset{CH_3}{\underset{\vert}{C}}-\underset{O}{\underset{\Vert}{C}}-O-(CH_2)_3-Si-(O-iC_3H_7)_3$
2. 6-azidosuffonylhexyl thiethoxysilane	$N_3SO_2-(CH_2)_6-Si-(O-C_2H_5)_3$
3. 3 aminpropyl-triethoxysilane	$NH_2-C_3H_6-Si-(O-C_2H_5)_3$

Figure 8.2: First group of organosilanes used for treatment of oxidized xGnP-1

The silane treatment of oxidized xGnP-1 is performed as follows. The oxidized xGnP-1 was added in a solution consisted of silane, isopropyl alcohol and DI water at concentrations of 2, 95 and 3 vol% respectively. The solution was sonicated for 5hrs and the xGnP was retrieved by washing with acetone and dried overnight at 120°C. The ratio of xGnP-1 to silane used was 1 to 1 which is three times larger than the stoichiometric ratio, taking into account that the surface covered by silane is approximate $300m^2/g$ [18] and that xGnP-1 has a surface area of $\sim 100m^2/g$ [4].

The necessity of xGnP-1 oxidation as well as the importance of the oxidized xGnP-1/silane reaction time on the amount of silane bonded to graphite is demonstrated in Table 8.4. The amount of Si detected was double (0.34%) for the oxidized xGnP-1 compared to the standard xGnP-1 (0.17%). It is concluded that longer times increase the reaction yield, however, for practical reasons a reaction time of 5hrs was used.

Table 8.4: XPS results showing the importance of oxidation and reaction time for the silane treament of xGnP-1

	C_1s	**N_1s**	**O_1s**	**Zr_3d**	**Si**
xGnP-1	93.06		6.76	0.18	
Oxi xGnP-1	85.32	1.08	13.41	0.20	
Si-1 xGnP-1	94.18		5.52	0.20	0.17
Oxi+ Si-1 xGnP-1	89.24		10.32	0.11	0.34
Oxi+Si-1 xGnP-1 (12hr)	90.11		9.10	0.03	0.76

The oxidized and silane treated xGnP-1 was used at a loading of 3vol% to fabricate PP composites by melt mixing and injection molding using the DSM microextruder operating at the optimum conditions. Prior to the fabrication of nanocomposites the treated graphite was characterized by XPS. As shown in Table 8.5 the atomic % of O decreases upon reaction with silane. For the first two silanes i.e., the methacryloxypropyl- and the azidosuffonylhexyl- silane the oxygen contained on functional groups on the xGnP surface is actually less than the value reported in Table 8.5 since for every Si on the surface there are 2 O that belong to the silane. The atomic % of Si detected on the surface was less for the aminpropyl-triethoxysilane, which anyway is not expected to provide good coupling with the PP matrix.

Table 8.5: XPS results for oxidized xGnP-1treated with the silanes #1, 2 and 3

	C_1s	**N_1s**	**O_1s**	**Zr_3d**	**S_2p**	**Si_2p**
Oxi xGnP-1	85.32	1.08	13.41	0.20		
Oxi +Si-1 xGnP-1	88.69		10.85			0.47
Oxi +Si-2 xGnP-1	87.47	0.65	10.81		0.33	0.74
Oxi +Si-3 xGnP-1	87.52	0.91	11.27			0.29

The flexural properties of 3vol% oxidized and silane treated xGnP-1/PP nanocomposites are shown in Figure 8.3. A slight reduction in the order of ~5% was observed in both the strength and the modulus due to the oxidation and silane treatment of xGnP-1. The reduction in modulus in compositets containing equal amount of the same reinforcement is a strong indication for existence of agglomerates. All three silanes used regardless of their different functional groups and the different degree of grafting resulted in composites with the same flex properties.

Various factors can be responsible for this behavior. As mentioned the coupling between silane-PP requires presence of radicals in the PP chain. In absence of these radicals the organofunctional silane group may react or form hydrogen bonds either with the oxidized xGnP-1 or with other silane groups resulting in both cases in formation of graphite agglomerates. Another possible mechanism for improving adhesion even in the absence of radicals is by entanglement but this requires silanes with longer alkyl chains.

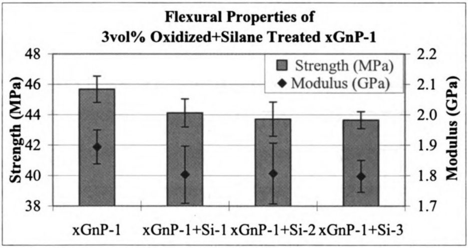

Figure 8.3 Flexural Properties of oxidized and silane treated xGnP-1. Si-1= methacryloxypropyl triisopropoxysilane, Si-2=6-azidosuffonylhexyl thiethoxysilane, and Si-3=3-aminpropyl-triethoxysilane

In the light of the above explanation two different silanes that have longer alkyl chains were employed for treatment of oxidized xGnP-1. These two silanes are shown in Figure 8.4. The conditions used are the same are mentioned above. Silane #1 was also used again for comparison. The corresponding XPS results are shown in Table 8.6. In case of silane #1 the difference in the atomic % of Si reported in Tables 8.5 and 8.6 is a result of the different batch of oxidized xGnP-1 that was used. The first time (Table 8.5) the oxidized xGnP-1 contained 13.41 atomic % of oxygen whereas there was only 10.88% of oxygen (Table 8.6) in the second oxidized xGnP-1 batch which means fewer OH groups to interact with the silane.

4. n-octadecylmethyldimethoxysilane

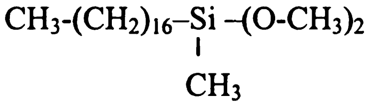

$$CH_3\text{-}(CH_2)_{16}\text{-}\underset{\overset{|}{CH_3}}{Si}\text{-}(O\text{-}CH_3)_2$$

5. 11-(triethoxysilyl)udecanal $O{=}CH\text{-}(CH_2)_{10}\text{-}Si\text{-}(OC_2H_5)_3$

Figure 8.4: Second group of organosilanes used for treatment of oxidized xGnP-1

Table 8.6: XPS results for oxidized xGnP-1treated with the silanes #1, 4 and 5

	C1s	**O1s**	**Zr3d**	**Si2p**
Oxi xGnP-1	89.09	10.88	0.03	
Oxi +Si-1 xGnP-1	91.97	7.74		0.29
Oxi +Si-4 xGnP-1	89.06	10.43		0.51
Oxi +Si-5 xGnP-1	90.29	9.29		0.42

PP nanocomposites containing 3vol% of oxidized and silane treated xGnP-1 were fabricated by melt mixing and injection molding using the optimum conditions as mentioned above. In addition 4 wt%, with respect to the PP, of maleated anhydrite PP was used expecting that this low molecular weight PP is more possible to form radicals and interact with the silane than the inert PP matrix and can also promote mechanical interlocking. However, as shown in Figure 8.5 a reduction in the order of ~5% for the strength and ~7% for the modulus was observed again for all the composites contained oxidized and silane treated xgnP-1 regardless of the type of silane used.

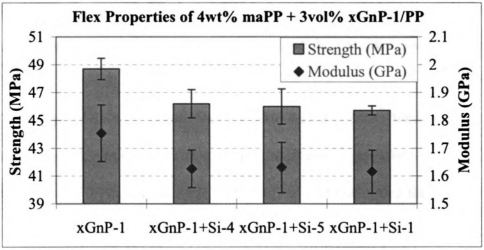

Figure 8.5 Flexural Properties of oxidized and silane treated xGnP-1.

Si-1= methacryloxypropyl triisopropoxysilane, Si-4= n-octadecylmethyldimethoxysilane, and Si-5=11-(triethoxysilyl)udecanal

8.3.3 xGnP-1 vs Oxidized xGnP-1: Effect on Flexural Properties and Crystallization of PP

In summary five different silanes were used to treat oxidized xGnP-1 and in all cases there was a reduction of the flexural strength and modulus of the treated xGnP-1/PP composites compared to the untreated xGnP-1/PP ones regardless of the silane's organofunctional group, degree of grafting and the presence of maleated PP. A possible reason might be that during the silane treatment the oxidized xGnP-1 is not well dispersed so that the silane enhances the formation of xGnP aggregates rather than assisting with the dispersion of the xGnP in the PP. It is also possible that during the oxidation there is formation of hydrogen bonds between the graphite platelets that leads to agglomeration and therefore to poor dispersion of the oxidized and treated xGnP-1 within the PP.

This hypothesis was investigated by (i) determining the flexural properties of oxidized xGnP-1/PP composites, (ii) studying the effect of graphite's oxidation on the crystallization of PP by means of XRD and DSC and (iii) examining the morphology of xGnP-1/PP and oxidized xGnP-1/PP by optical microscopy.

As shown in Figure 8.6 both the flexural strength and modulus of oxidized xGnP-1/PP composites are ~10% lower than the corresponding properties of xGnP/PP. The presence of ma PP although enhances the properties of xGnP-1/PP composites does not make any difference when the oxidized xGnP-1 is used which supports the hypothesis for existence of agglomerates and poor dispersion in case of oxidized xGnP-1.

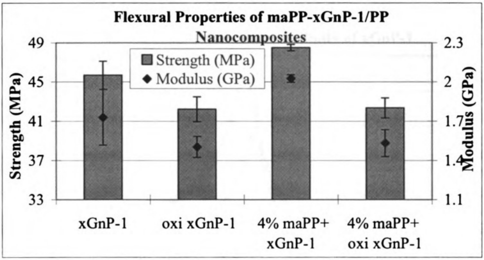

Figure 8.6: Effect of xGnP-1 oxidation and maPP on the flexural properties of xGnP-1/PP

It is possible that during the oxidation due to the severe conditions used i.e., combination of H_2SO_4/HNO_3 with O_3 and high temperature, in addition to the introduction of functional groups along the edges of the graphite platelets, defects on the surface may be created as well which disturb the crystalline structure of graphite and may alter its nucleating action which has been presented in Chapter 7.

The XRD pattern of xGnP-1 and oxidized xGnP-1 is shown in Figure 8.7. There is no significant change in the 2θ value that relates to the d-spacing. The most striking difference is that the oxidized xGnP-1 peak is wider and therefore the full width at half maximum (FWHM) is larger which means that the "crystal size" is smaller. The "crystal size" is defined as the effective thickness of the crystallite in a direction perpendicular to the reflecting planes [20]. Oxidation reduces this thickness by ~30% from 21nm to 14nm that may indicate that the amorphous content of graphite is increased.

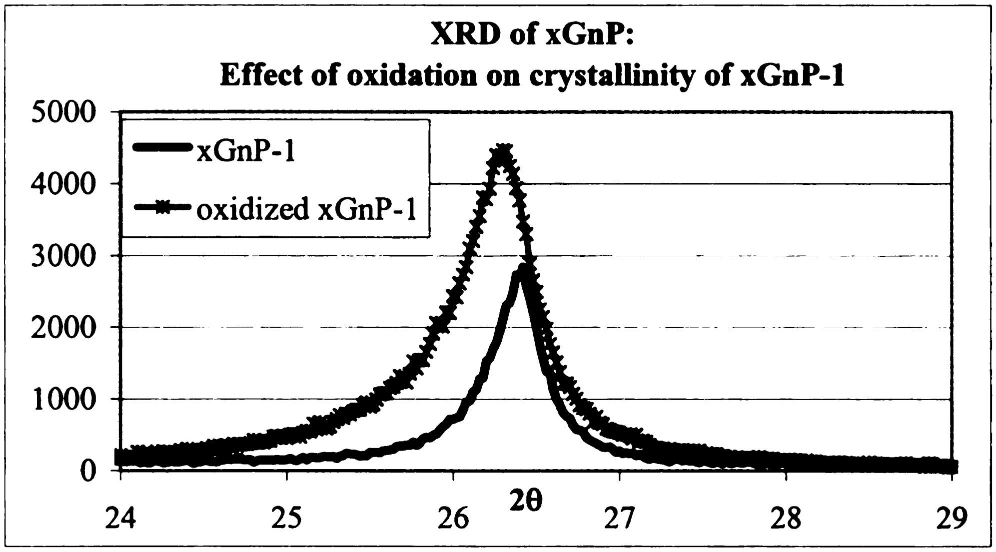

Figure 8.7: XRD pattern showing the effect of oxidation on the crystallinity of xGnP-1

XRD was employed to investigate the effect of xGnP-1 oxidation on the crystallinity of PP (types of peaks present and their relative intensity). Figures 8.8, 8.9 and 8.10 show the XRD pattern of neat PP, 3vol% oxidized xGnP-1/PP and 3vol% xGnP-1/PP respectively. Two samples were run for each. The corresponding crystallographic planes for the PP peaks [21-23], are shown if Figure 8.8. Oxidation of xGnP-1 does not change significantly the pattern of neat PP except that it enhances the signal of the <003> and the <060> planes. However, xGnP-1 strongly promotes the crystallization of PP along the <040> and <060> crystallographic planes whereas the signal of the other PP peaks is dramatically decreased.

It is also noted that although in both cases the concentration of graphite is the same i.e., 3vol%, the relative intensity of the graphite peak with respect to the PP peaks, in the case of oxidized xGnP-1 is much smaller. Since the degree of crystallinity of both the oxidized xGnP-1/PP and xGnP-1/PP based on DSC, is the same it is concluded that the oxidized xGnP-1 is less crystalline. Increase of the amorphous phase in xGnP-1 and reduction in the crystallite thickness due to oxidation alters it's the nucleating efficiency of xGnP-1 i.e., types of PP crystals formed, their number and size distribution which affect the impact strength and percolation threshold of xGnP-1/PP composites as discussed in Chapters 4 and 6 respectively. The difference in the crystallization behavior of PP due to oxidation of xGnP-1 is expected to affect also the flexural properties of the xGnP-1/PP.

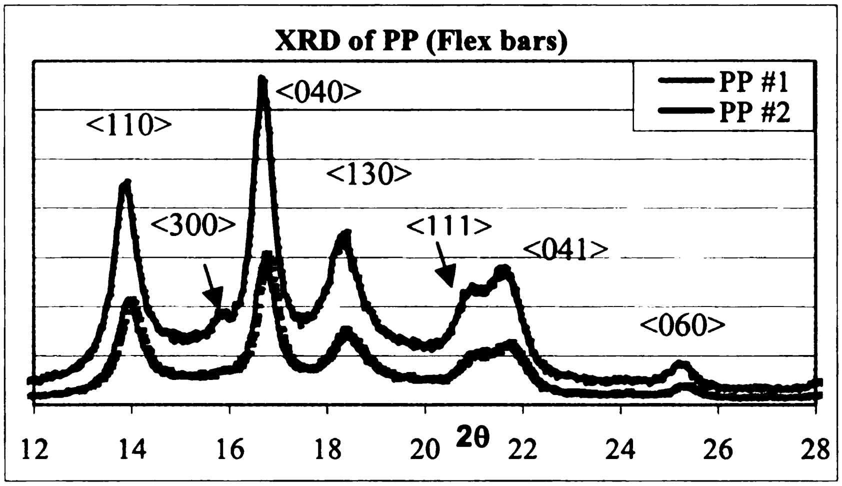

Figure 8.8: XRD of PP

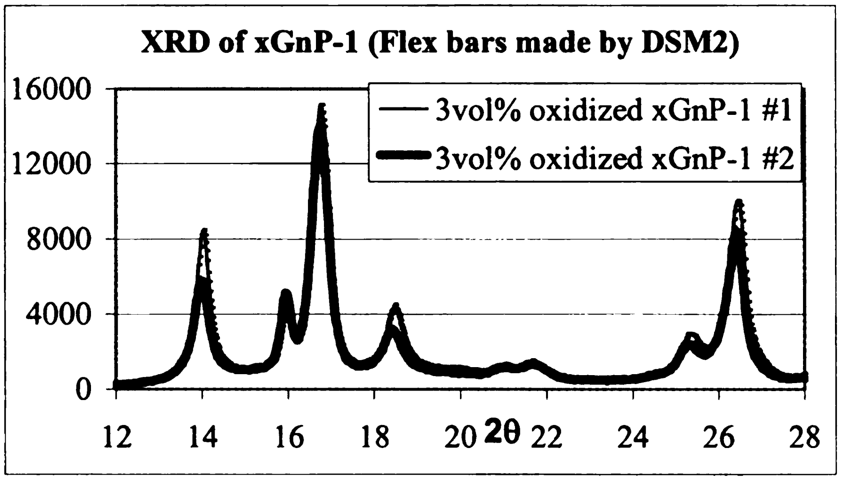

Figure 8.9: XRD of 3vol% oxidized xGnP-1/PP

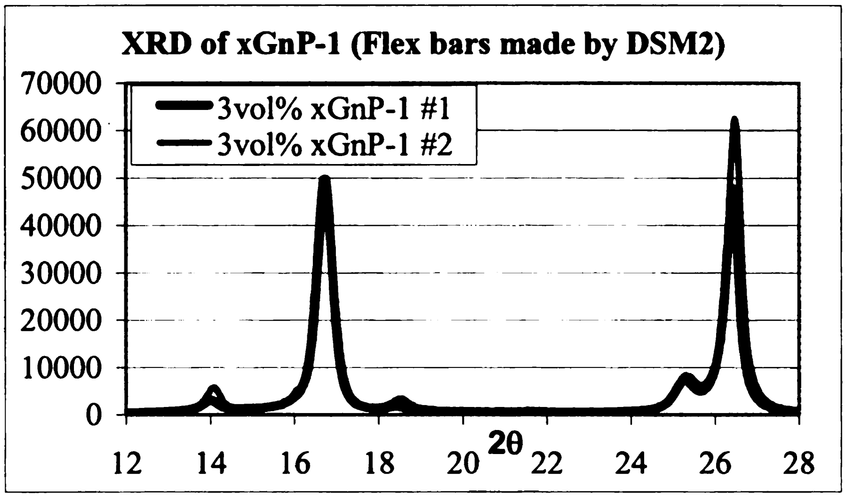

Figure 8.10: XRD of 3vol% oxidized xGnP-1/PP

The effect of xGnP-1 oxidation on the crystallization behavior of PP was also studied using DSC. The most striking difference is that oxidation resulted in a decrease of the crystallization temperature by ~2°C, as shown in Figure 8.11, which indicates that the oxidization reduces the nucleating action of xGnP-1. As small decrease on the melting temperature due to oxidation, shown in Figure 8.11, is also observed which combined with the fact that the melting peak for oxidized xGnP-1 is broader and melting initiates at temperature lower by ~5°C leads to the conclusion that the PP crystals form in presence of oxidized xGnP-1 are thinner and the crystal size distribution is wider. No difference in the degree of crystallization due to oxidation was observed.

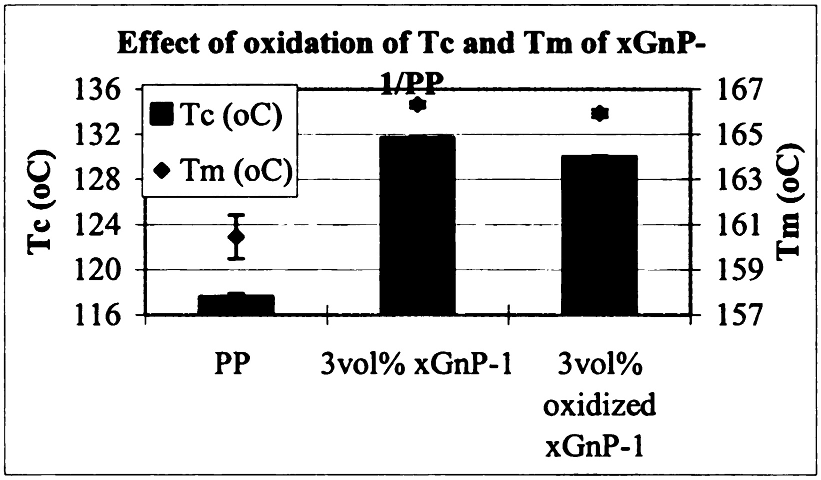

Figure 8.11: Effect of xGnP-1oxidation on the crystallization, T_c, and melting, T_m, temperature of 3vol% xGnP-1/PP based on DSC

The differences in the nucleating efficiency of xGnP and crystallization behavior of PP i.e., crystal thickness and distribution due to the oxidation of xGnP-1 are reflected also on the flexural properties of xGnP-1/PP nanocomposites. However, the morphology of the composites i.e., dispersion and possible existence of agglomerations is expected to be the main reason for the decrease in the flex strength and modulus of oxidized xGnP-1/PP. The morphology of 3vol% xGnP-1/PP and 3vol% oxidized xGnP-1/PP nanocomposites was investigated by optical microscope. The samples are prepared by polishing and etching as described in Section 8.2. Results are shown in Figures 8.12-8.13.

Comparison of Figures 8.12 and 8.13 confirms the hypothesis that oxidation leads to agglomerates of xGnP-1 which are responsible for the decrease in the strength and modulus of the oxidized xGnP-1/PP composites. The reason is that due to aggregation xGnP is removed from the matrix and therefore the modulus decreases whereas the decrease in flexural strength may be due to the stress concentrations created by the large aggregates.

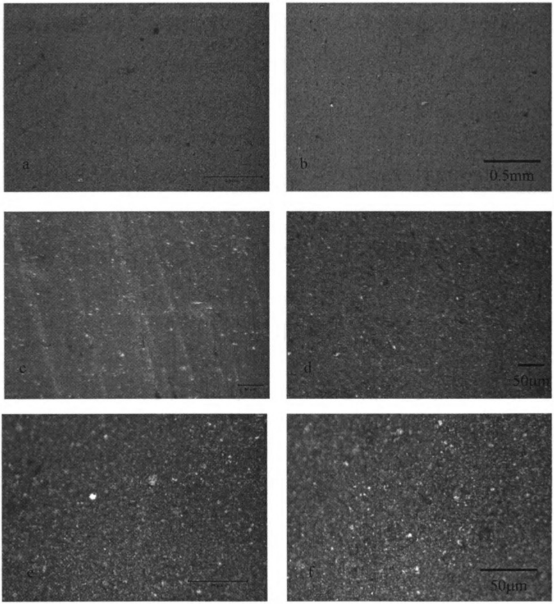

Figure 8.12: Optical micrographs of 3vol% xGnP-1/PP; plane shown is parallel to the flow direction; scale bars are 0.5mm for a) and b), 50μm for c) through f)

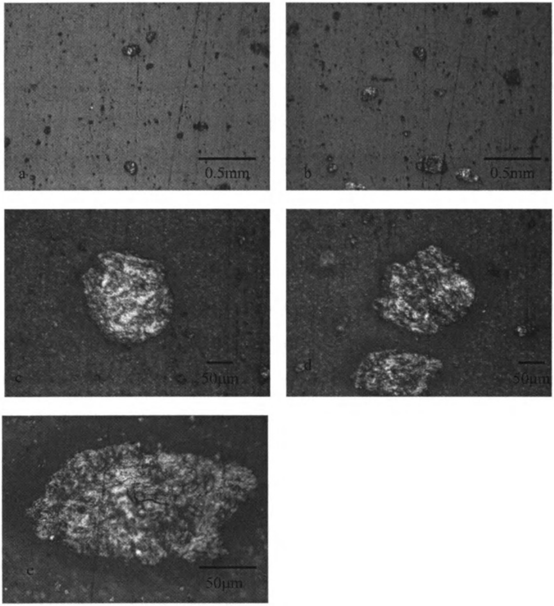

Figure 8.13: Optical micrographs of 3vol% xGnP-1/PP; plane shown is parallel to the flow direction; scale bars are 0.5mm for a) and b), 50μm for c) through e)

8.4 Conclusions

The objective of the work presented in this chapter was to enhance the adhesion between the xGnP-1 and the PP matrix in order to further improve the flexural strength of the xGnP-1/PP nanocomposites. The approach followed is a two-step process, i) oxidation of xGnP-1, which was based on methods proposed for the oxidation of CN, in order to introduce functional groups on the graphite and ii) treatment of the oxidized xGnP-1 with organosilanes to assure coupling with the PP matrix.

A new oxidation method, which consists of exposure of xGnP-1 to H_2SO_4/HNO_3 in presence of O3, is proposed that introduces 10-13% of oxygen on the graphite surface and due to the simple experimental set up it allows for scale up of the process. Based on XPS the oxidized xGnP-1 contains various oxygen based functional groups such as OH, C=O, and –COO that allows for further modification of the graphite surface.

Five silanes that differ in the organofunctional group and length of the alkyl chain were used to treat the oxidized xGnP-1. The atomic % of Si detected on the after the reaction was 0.3-0.8% depending on the silane used and the initial oxygen content of the oxidized xGnP-1.

PP composites were made with 3vol% of xGnP-1, oxidized xGnP-1 and oxidized and silane treated xGnP. Maleated anhydrite grafted PP was also used in some cases as compatibilizer. The flexural properties of composites containing oxidized and oxidized silane treated xGnP-1 reduced by ~5-10%. This reduction in properties was investigated by means of XRD and DSC which show that oxidation reduces the nucleating effect of xGnP-1 and results in PP crystals that are thinner and have wider size distribution. In addition to the changes in the crystallization of PP oxidation results also in formation of xGnP-1 agglomerates as shown by morphological study . Both phenomena, the change in crystallinity and the existence of agglomerations due to oxidation are responsible for the reduction in modulus and reduction in strength of the se composites.

It is concluded that although the oxidation was successful in terms of that it introduced a significant amount of functional groups mainly on the graphite edges it led to agglomeration of xGnP-1 destroying the good dispersion conditions of xGnP-1 in the PP matrix.

8.5 References

1. L.T. Drzal, "Advances in Polymer Science II' 75 (K. Dusek ed.), Spring-Verlag, (1985)

2. L.T. Drzal, "Fiber-Matrix Interphase", Copy right, Michigan State University, (1992)

3. L.G. Tang and J.L. Kardos, "A Review of Method for Improving the Interfacial Adhesion Between Carbon Fiber and Polymer Matrix", *Polymer Composites* **16**, 1 100 (1997)

4. H. Fukushima, "Graphite Nanoreinforcements in Polymer Nanocomposites", PhD Thesis, Michigan State University, (2003)

5. N. Dilsiz, N.K. Erinc, E. Bayramli and G. Akovali, "Surface Energy and Mechanical Properties of Plasma-Modified Carbon Fibers" *Carbon* **33**, 6 853 (1995)

6. M.S. Madhukar and L.T. Drzal, "Fiber-Matrix Adhesion and Its eEffect on Composite Mechanical Properties. I. Inplane and Interlaminar Shear behavior of Graphite Epoxy Composites" *Journal of Composite Materials* **25**, 932 (1991)

7. M.S. Madhukar and L.T. Drzal, "Fiber-Matrix Adhesion and Its eEffect on Composite Mechanical Properties. II. Longitudinal and Transverse Tensile and Flexure Behavior of Graphite Epoxy Composites" *Journal of Composite Materials* **25**, 958 (1991)

8. M.S. Madhukar and L.T. Drzal, "Fiber-Matrix Adhesion and Its eEffect on Composite Mechanical Properties. III. Longitudinal Compressive Properties of Graphite Epoxy Composites" *Journal of Composite Materials* **26**, 310 (1992)

9. M.S. Madhukar and L.T. Drzal, "Fiber-Matrix Adhesion and Its eEffect on Composite Mechanical Properties. IV. Mode I and Mode II Fracture Touhgness of Graphite Epoxy Composites" *Journal of Composite Materials* **26**, 936 (1992)

10. J. Chen, M. Hamon, H. Hu, Y. Chen, A. Rao, P. Eklund and R. Haddon, "Solution Properties of SWCNs" *Science* **282**, 95-98 (1998)

11. Q. Chen, L. Dai, M. Gao, S. Huang, and A. Mau, "Plasma Activation of Carbon Nanotubes for Chemical Modification", *J. Phys. Chem. B*, **105**, 618-622 (2001)

12. M. Shim, A. Javey, N. Wong, S. Kam, and H. Dai, "Polymer Functionalization for Air-Stable n-Type Carbon Nanotube Field-Effect Transistors", *J. Am. Chem. Soc.*, **123**, 11512-11513 (2001)

13. J. Bahr and J. Tour, "Covalent Chemistry of Single-Wall Carbon Nanotubes", *J. Mater. Chem.*, **12** 1952-1958 (2002)

14. J. Liu, A. G. Rinzler, H. Dai, J. H. Hafner, R. K. Bradley, P. J. Boul, A. Lu, T. Iverson, K. Shelimov, C. B. Huffman, F. Macias-Rodriguez, Y-S. Shon, T. R. Lee, D. T. Colbert and R. E. Smalley, "Fullerene Pipes" *Science* **280**, 1253-1256 (1998)

15. A. G. Rinzler, J. Liu, H. Dai, P. Nikolaev, C. B. Huffman, F. J. Rodriguez-Macias, P. J. Boul, A. H. Lu, D. Heymann, D. T. Colbert, R. S. Lee, J. E. Fischer, A. M. Rao, P. C. Eklund and R. E. Smalley, "Large-scale Purification of Single-Wall Carbon Nanotubes: Process, Product, and Pharacterization", *Applied Physics A: Materials Science and Processing*, **67**, 29-37 (1998)

16. D. B. Mawhinney, V. Naumenko, A. Kuznetsova, J. T. Yates Jr., J. Liu and R. E. Smalley, "Infrared Spectral Evidence for the Etching of Carbon Nanotubes: Ozone Oxidation at 298 K", *J. Am. Chem. Soc.* **122**, 2383-2384 (2000)

17. D. B. Mawhinney, V. Naumenko, A. Kuznetsova, J. T. Yates Jr., J. Liu and R. E. Smalley, "Surface Defect Site Density on Single Walled Carbon Nanotubes by Tritation", *Chemical Physics Letters* **324**, 213-216 (2000)

18. "Silanes and Silicones" Gelest Catalog 3000-A p 166

19. B. Arkles, "Silane Coupling Agent Chemistry" in Silicon Compounds:Register and Review, 5th Edition United Chemical Technologies, Inc.

20. E.W. Nuffield, "X-ray Diffraction Methods" Wiley: New York, (1966)

21. J-H Chen, F-C Tsai, Y-H Nien and P-H Yeh, Isothermal crystallization of isotactic polypropylene blended with low molecular weight atactic polypropylene. Part I. Thermal properties and morphology development, Polymer 46 (2005) 5680-5688

22. Q. Zheng, Y. Shangguan, S. Yan, Y. Song, M. Peng and Q. Zhang, "Structure, morphology and non-isothermal crystallization of polypropylene catalloys, Polymer, 46 (2005) 3163-3174

23. J. Isasi, R.Alamo and L. Mandelkern, The isothermal expansion of the monoclinic unit cell of isotactic polypropylene, Journal of Polymer Science: Part B: Polymer Physics 35 2945-2949 (1997)

CHAPTER 9

CONCLUSIONS AND SUGGESTIONS FOR FUTURE WORK

It has been demonstrated that xGnP due to its superior mechanical, thermal, barrier and electrical properties has great potential, as a nanoreinforcement for polypropylene nanocomposites that can be used in a plethora of applications such as structural, packaging, thermal management and applications that require not only an enhancement in mechanical properties but also gain electrostatic dissipation or EMI (Electromagnetic Interference)/RFI (Radio Frequency Interference) shielding.

This research provides an understanding about how the fabrication method and processing conditions used affect the properties of these xGnP/PP nanocomposites and therefore can lead to materials with desired properties. For example, for composites that will be used for structural applications, melt mixing followed by injection molding is the proper fabrication method whereas, if there is a need for electrical conductive materials with low percolation threshold then compounding by premixing of the polymer powder with the xGnP followed by compression molding is the optimum method to fabricate those composites.

An investigation of the processing conditions i.e., mixing time, screw speed, barrel and mold temperature in case of melt mixing and injection molding, resulted in the use of a factorial design of experiments to determine the optimum conditions. The compounding method and cooling rate used for compression molding were also optimized. Although the optimization is done for the specific materials used i.e., PP and xGnP, this work provides a general scheme that can be employed for any matrix-reinforcement system in order to optimize the processing conditions depending on the desired properties.

A significant contribution of this research is also the use of a new compounding method, i.e., premixing of xGnP and PP powder in isopropyl alcohol using sonication. The premixing method is more effective than the solution method widely used, in terms of lowering the percolation threshold of nanocomposites. It may result that this is one of the only methods to insure that the large platelet morphology of xGnP can be preserved in the final composite. Additional advantages of this method are that the experimental set up is very simple, no solvents are used, there is no need for high temperatures and the isopropyl alcohol can be recycled which make this method practical, safe, cost and time effective and environmentally friendly.

The feasibility of using xGnP-PP nanocomposites was investigated not only by evaluating the properties of this system but also by comparing the xGnP-PP with composites made with commercially available carbon reinforcements and clays. It is concluded that xGnP is superior to the other materials used for improving the impact strength, the flexural modulus and barrier properties with PP and due to its platelet morphology, xGnP is able to reduce the coefficient of thermal expansion in two dimensions rather than in one as in the case of aligned fibers.

In addition to the reinforcing ability of xGnP, it was found that xGnP can also be used in very low concentrations as a nucleating agent for the PP β-form crystals. The improvement in impact strength of PP upon addition of xGnP was found to be the result of the nucleating efficiency of xGnP and that under specific conditions i.e., cooling rate and mold temperature, promotes the formation of the β-form PP crystals, which have higher impact strength and toughness compared to the most commonly occurring α-form.

The xGnP-PP crystallization study revealed that the aspect ratio and concentration of xGnP are very important parameters that combined with the crystallization conditions which can, in addition to the formation of the less preferred β-form crystals, affect the size and number of spherulites formed. Taking into account that the type, population and size distribution of spherulites in a semicrystalline polymer is closely related to the mechanical and barrier properties, this result becomes of great practical importance because it provides a fundamental understanding of how the xGnP affects the crystallization behavior of PP and therefore how xGnP-PP composites can be engineered to have desired crystal structure.

In addition, the crystal structure of the polymer was also found to affect the percolation threshold. The presence of many small spherulites nucleated by the xGnP disrupts the continuous network formed by the conductive particles and thus increases the percolation threshold of the composite. Other factors such as the shape and aspect ratio of the conductive filler, its morphology, distribution and orientation which are dictated by the fabrication method and processing conditions as well as by the filler-matrix interactions were also explored and evaluated. This detailed experimental study offers systematic knowledge of how the various factors affect the electrical properties of the composites and the experimental data obtained can be the basis for developing a predictive type of theoretical model or can be used to provide more realistic assumptions for simulation studies on electrically conductive composites.

The morphological investigation of the PP nanocomposites indicated the presence of particle agglomerates and poor dispersion especially in the case of high aspect ratio xGnP and clays. In addition, the plateau observed in the flexural strength-xGnP loading curve points toward weak adhesion along the xGnP-PP interface who's role becomes more important as the filler size decreases and the loading gets higher. The problem of agglomeration was partially solved by using the premixing compounding method as an extra step prior to the melt mixing in the extruder. However, at high xGnP concentrations the amount of polymer present is not enough to separate the graphite platelets and prevent agglomeration. Oxidation of xGnP followed by silane treatment was employed in order to address the problem of weak adhesion along the xGnP-PP interface.

Although oxidation of xGnP-1 was successful in the sense that it resulted in introduction of a significant amount of oxygen based functional groups on the graphite surface, even when the oxidized xGnP was further treated by silanes, this approach failed to improve the flexural properties of the composites. Aggregation of surface treated xGnP occurred, judging from the existence of xGnP agglomerates, even at very low xGnP loadings which were not present in the case of non oxidized xGnP/PP nanocomposites.

In conclusion, this research provides systematic knowledge about the interactions between xGnP and polymer chains by understanding how the nanocomposite properties are related to xGnP's microstructure; state of dispersion, aspect ratio and orientation of the nanoplatelets within the PP polymer matrix. Therefore, xGnP-PP composite materials can be engineered to have a desired combination of mechanical, electrical and barrier properties.

Future Research. The importance of homogeneous dispersion of the fillers within the polymer matrix and strong adhesion along the filler-matrix interface was underlined during the course of this research. The microextruder used for the fabrication of composites does not provide sufficient shear during the melt mixing. An approach to overcome this limitation is to use a masterbatch or apply an extra mixing step and compounding method such as a mixer or a roller that can achieve shear stresses high enough to break the agglomerates and provide homogeneous filler distribution but without distorting the platelet morphology.

Alternative approaches should be taken to improve the adhesion at the interface. Oxidation can be used to introduce functionalities to the chemical inert and very stable xGnP but the conditions should be less severe and optimized to introduce specific oxygen groups that are necessary for the further xGnP treatment i.e., if silane is to be used then only OH should be present on the xGnP surface while reaction with amines would require COOH. This way there will be no extra oxygen on the surface of graphite available to form the hydrogen bonds that result in agglomerates.

Finally, one can further improve the properties of PP nanocomposites by taking advantage of synergistic effects that come into play when more than one type of filler is used. It has been reported that the percolation threshold can be lowered by using fillers with different shapes or that have wide size distribution i.e., combining xGnP-1 which contains a large number of platelets with xGnP-15 which are much larger and fewer in number, may lower the percolation threshold. Adding xGnP to fiber reinforced composites may reinforce the inter-fiber matrix and enhance the formation of the conductive network. Mechanical properties may also be improved due to synergy of fillers, whereas combination of a conductive i.e., xGnP with a non conductive i.e., glass fibers, reinforcement can make the conventional and widely used glass reinforced polymer composites conductive at a very small cost without compromising other properties or affecting their processing.

APPENDIX A
F DISTRIBUTION

Table A1: Cumulative F Distribution

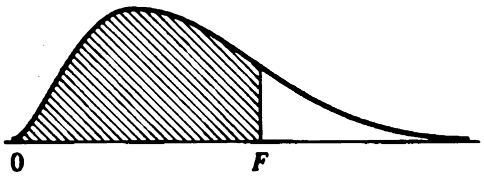

Table D Cumulative F Distribution

Tabled value is F_p where $p = P(F \le F_p)$ and $F \sim F_{(\nu_1,\nu_2)}$.

		ν_1									
ν_2	p	1	2	3	4	5	6	7	8	9	10
1	0.005	0.00006	0.0051	0.018	0.032	0.044	0.054	0.062	0.068	0.073	0.078
	0.01	0.00025	0.010	0.029	0.047	0.062	0.073	0.082	0.089	0.095	0.100
	0.025	0.0015	0.026	0.057	0.082	0.100	0.113	0.124	0.132	0.139	0.144
	0.05	0.0062	0.054	0.099	0.130	0.151	0.167	0.179	0.188	0.195	0.201
	0.10	0.025	0.117	0.181	0.220	0.246	0.265	0.279	0.289	0.298	0.304
	0.90	39.9	49.5	53.6	55.8	57.2	58.2	58.9	59.4	59.9	60.2
	0.95	161	200	216	225	230	234	237	239	241	242
	0.975	648	800	864	900	922	937	948	957	963	969
	0.99	4050	5000	5400	5620	5760	5860	5930	5980	6020	6060
	0.995	16200	20000	21600	22500	23100	23400	23700	23900	24100	24200
2	0.005	0.00005	0.0050	0.020	0.038	0.055	0.069	0.081	0.091	0.099	0.106
	0.01	0.00020	0.010	0.032	0.056	0.075	0.092	0.105	0.116	0.125	0.132
	0.025	0.0013	0.026	0.062	0.094	0.119	0.138	0.153	0.165	0.175	0.183
	0.05	0.0050	0.053	0.105	0.144	0.173	0.194	0.211	0.224	0.235	0.244
	0.10	0.020	0.111	0.183	0.231	0.265	0.289	0.307	0.321	0.333	0.342
	0.90	8.53	9.00	9.16	9.24	9.29	9.33	9.35	9.37	9.38	9.39
	0.95	18.5	19.0	19.2	19.2	19.3	19.3	19.4	19.4	19.4	19.4
	0.975	38.5	39.0	39.2	39.2	39.3	39.3	39.4	39.4	39.4	39.4
	0.99	98.5	99.0	99.2	99.2	99.3	99.3	99.4	99.4	99.4	99.4
	0.995	198	199	199	199	199	199	199	199	199	199
3	0.005	0.00005	0.0050	0.021	0.041	0.060	0.077	0.092	0.104	0.115	0.124
	0.01	0.00019	0.010	0.034	0.060	0.083	0.102	0.118	0.132	0.143	0.153
	0.025	0.0012	0.026	0.065	0.100	0.129	0.152	0.170	0.185	0.197	0.207
	0.05	0.0046	0.052	0.108	0.152	0.185	0.210	0.230	0.246	0.259	0.270
	0.10	0.019	0.109	0.185	0.239	0.276	0.304	0.325	0.342	0.356	0.367
	0.90	5.54	5.46	5.39	5.34	5.31	5.28	5.27	5.25	5.24	5.23
	0.95	10.1	9.55	9.28	9.12	9.01	8.94	8.89	8.85	8.81	8.79
	0.975	17.4	16.0	15.4	15.1	14.9	14.7	14.6	14.5	14.5	14.4
	0.99	34.1	30.8	29.5	28.7	28.2	27.9	27.7	27.5	27.3	27.2
	0.995	55.6	49.8	47.5	46.2	45.4	44.8	44.4	44.1	43.9	43.7

Table A1: Cumulative F Distribution (continued)

Table D *(Continued)*

ν_2	p	ν_1									
		1	2	3	4	5	6	7	8	9	10
12	0.005	0.00004	0.0050	0.023	0.048	0.075	0.100	0.122	0.143	0.161	0.177
	0.01	0.00016	0.010	0.037	0.070	0.101	0.130	0.155	0.176	0.196	0.212
	0.025	0.0010	0.025	0.070	0.114	0.153	0.186	0.214	0.238	0.259	0.276
	0.05	0.0041	0.052	0.114	0.169	0.214	0.250	0.280	0.305	0.325	0.343
	0.10	0.016	0.106	0.192	0.257	0.306	0.344	0.375	0.400	0.420	0.438
	0.90	3.18	2.81	2.61	2.48	2.39	2.33	2.28	2.24	2.21	2.19
	0.95	4.75	3.89	3.49	3.26	3.11	3.00	2.91	2.85	2.80	2.75
	0.975	6.55	5.10	4.47	4.12	3.89	3.73	3.61	3.51	3.44	3.37
	0.99	9.33	6.93	5.95	5.41	5.06	4.82	4.64	4.50	4.39	4.30
	0.995	11.8	8.51	7.23	6.52	6.07	5.76	5.52	5.35	5.20	5.09
15	0.005	0.00004	0.0050	0.023	0.049	0.076	0.102	0.125	0.147	0.166	0.183
	0.01	0.00016	0.010	0.037	0.070	0.103	0.132	0.158	0.181	0.202	0.219
	0.025	0.0010	0.025	0.070	0.116	0.156	0.190	0.219	0.244	0.265	0.284
	0.05	0.0041	0.051	0.115	0.170	0.216	0.254	0.285	0.311	0.333	0.351
	0.10	0.016	0.106	0.192	0.258	0.309	0.348	0.380	0.406	0.427	0.446
	0.90	3.07	2.70	2.49	2.36	2.27	2.21	2.16	2.12	2.09	2.06
	0.95	4.54	3.68	3.29	3.06	2.90	2.79	2.71	2.64	2.59	2.54
	0.975	6.20	4.76	4.15	3.80	3.58	3.41	3.29	3.20	3.12	3.06
	0.99	8.68	6.36	5.42	4.89	4.56	4.32	4.14	4.00	3.89	3.80
	0.995	10.8	7.70	6.48	5.80	5.37	5.07	4.85	4.67	4.54	4.42
20	0.005	0.00004	0.0050	0.023	0.050	0.077	0.104	0.129	0.151	0.171	0.190
	0.01	0.00016	0.010	0.037	0.071	0.105	0.135	0.162	0.187	0.208	0.227
	0.025	0.0010	0.025	0.071	0.117	0.158	0.193	0.224	0.250	0.273	0.292
	0.05	0.0040	0.051	0.115	0.172	0.219	0.258	0.290	0.318	0.340	0.360
	0.10	0.016	0.106	0.193	0.260	0.312	0.353	0.385	0.412	0.435	0.454
	0.90	2.97	2.59	2.38	2.25	2.16	2.09	2.04	2.00	1.96	1.94
	0.95	4.35	3.49	3.10	2.87	2.71	2.60	2.51	2.45	2.39	2.35
	0.975	5.87	4.46	3.86	3.51	3.29	3.13	3.01	2.91	2.81	2.77
	0.99	8.10	5.85	4.94	4.43	4.10	3.87	3.70	3.56	3.46	3.37
	0.995	9.94	6.99	5.82	5.17	4.76	4.47	4.26	4.09	3.96	3.85
24	0.005	0.00004	0.0050	0.023	0.050	0.078	0.106	0.131	0.154	0.175	0.193
	0.01	0.00016	0.010	0.038	0.072	0.106	0.137	0.165	0.189	0.211	0.231
	0.025	0.0010	0.025	0.071	0.117	0.159	0.195	0.227	0.253	0.277	0.297
	0.05	0.0040	0.051	0.116	0.173	0.221	0.260	0.293	0.321	0.345	0.365
	0.10	0.016	0.106	0.193	0.261	0.313	0.355	0.388	0.416	0.439	0.459
	0.90	2.93	2.54	2.33	2.19	2.10	2.04	1.98	1.94	1.91	1.88
	0.95	4.26	3.40	3.01	2.78	2.62	2.51	2.42	2.36	2.30	2.25
	0.975	5.72	4.32	3.72	3.38	3.15	2.99	2.87	2.78	2.70	2.64
	0.99	7.82	5.61	4.72	4.22	3.90	3.67	3.50	3.36	3.26	3.17
	0.995	9.55	6.66	5.52	4.89	4.49	4.20	3.99	3.83	3.69	3.59

APPENDIX B
ANALYSIS OF VARIANCE FOR 2^3 FACTORIAL DESIGN

Table B1: Excel Spreadsheet for the experimental lay out of the2^3 factorial design about the flexural strength of PP (Small gap, t=3min)

	T_{barrel}				TOTAL
	170°C		180 °C		
	T_{mold}		T_{mold}		
Screw Speed	40 °C	80 °C	40 °C	80 °C	
150rpm	37.58	40.86	37.08	40.35	
	37.76	43.09	36.78	41.35	
	37.34	41.11	36.65	40.91	
	SUM=112.67 SS=4231.91	SUM=125.06 SS=5216.09	SUM=110.51 SS=4070.86	SUM=122.61 SS=5011.5	470.85
245rpm	36.64	39.12	36.27	42.19	
	35.57	40.43	37.10	40.66	
	34.95	41.38	35.54	39.76	
	SUM=107.16 SS=3829.09	SUM=120.93 SS=4877.02	SUM=108.90 SS=3954.49	SUM=122.60 SS=5013.5	459.59
TOTAL	219.83	245.98	219.41	245.21	930.44

Table B2: Analysis of variance for PP's flexural strength (Small gap, t=3min)

Effect/Factor	SS	df	MS	F
T_{barrel}	0.06	1.00	0.06	0.08
T_{mold}	112.46	1.00	112.46	150.28
Screw Speed	5.28	1.00	5.28	7.06
T_{barrel} x T_{mold}	0.01	1.00	0.01	0.01
T_{barrel} x Screw Speed	2.69	1.00	2.69	3.59
T_{mold} x Screw Speed	0.37	1.00	0.37	0.50
T_{barrel} x T_{mold} x Screw Speed	0.00	1.00	0.00	0.00
Error	11.97	16.00	0.75	1.00
Total	132.84	23.00		

Table B3: Excel Spreadsheet for the experimental lay out of the2^3 factorial design about the flexural strength of 3vol% of xGnP-1/PP (Small gap, t=3min)

	T_{barrel}					TOTAL
	170°C		180°C			
	T_{mold}		T_{mold}			
Screw Speed	40°C	80°C	40°C	80°C		
150rpm	47.72	53.34	48.84	51.28	47.72	
	48.22	53.49	49.37	50.97	48.22	
	49.66	52.10	49.61	49.57	49.66	
	SUM=145.60 SS=7068.16	SUM=158.93 SS=8420.87	SUM=147.83 SS=7284.93	SUM=151.82 SS=7685.0		604.18
245rpm	48.99	51.86	49.29	52.50		
	52.26	48.46	48.08	54.19		
	50.51	48.88	49.12	51.08		
	SUM=151.75 SS=7681.73	SUM=149.21 SS=7428.02	SUM=146.49 SS=7154.24	SUM=157.77 SS=8301.6		605.22
TOTAL	297.35	308.14	294.32	309.59		1209.40

Table B4: Analysis of variance for the flexural strength of 3vol% of xGnP-1/PP (Small gap, t=3min)

Effect/Factor	SS	df	MS	F
T_{barrel}	0.104	1.000	0.104	0.072
T_{mold}	28.287	1.000	28.287	19.578
Screw Speed	0.045	1.000	0.045	0.031
T_{barrel} x T_{mold}	0.834	1.000	0.834	0.577
T_{barrel} x Screw Speed	2.781	1.000	2.781	1.925
T_{mold} x Screw Speed	3.080	1.000	3.080	2.132
T_{barrel} x T_{mold} x Screw Speed	22.348	1.000	22.348	15.468
Error	23.117	16.000	1.445	1.000
Total	80.597	23.000		

Table B5: Excel Spreadsheet for the experimental lay out of the2^3 factorial design about the modulus of elasticity of PP (Small gap, t=3min)

	T_{barrel}					TOTAL
	170°C		180 °C			
	T_{mold}		T_{mold}			
Screw Speed	40 °C	80 °C	40 °C	80 °C		
150rpm	1.01	1.32	1.19	1.10	1.01	
	1.16	1.23	1.12	1.23	1.16	
	1.13	1.23	1.13	1.22	1.13	
	SUM= 3.30	SUM= 3.78	SUM= 3.44	SUM= 3.54		14.06
	SS= 3.64	SS= 4.77	SS= 3.95	SS= 4.19		
245rpm	1.05	1.17	1.10	1.27	1.05	
	1.09	1.23	1.13	1.24	1.09	
	1.08	1.27	1.02	1.25	1.08	
	SUM= 3.22	SUM= 3.67	SUM= 3.26	SUM= 3.77		13.92
	SS= 3.47	SS= 4.48	SS= 3.55	SS= 4.74		
TOTAL	6.52	7.45	6.70	7.31		27.98

Table B6: Analysis of variance for the modulus of elasticity of PP (Small gap, t=3min)

Effect/Factor	SS	df	MS	F
T_{barrel}	7.61E-05	1	7.6E-05	0.03
T_{mold}	9.83E-02	1	9.8E-02	35.82
Screw Speed	8.74E-04	1	8.7E-04	0.32
T_{barrel} x T_{mold}	4.17E-03	1	4.2E-03	1.52
T_{barrel} x Screw Speed	2.29E-03	1	2.3E-03	0.84
T_{mold} x Screw Speed	5.55E-03	1	5.6E-03	2.02
T_{barrel} x T_{mold} x Screw Speed	8.55E-03	1	8.5E-03	3.12
Error	4.39E-02	16	2.7E-03	1.00
Total	1.64E-01	23		0.03

Table B7: Excel Spreadsheet for the experimental lay out of the2^3 factorial design about the modulus of elasticity of 3vol% xGnP-1/PP (Small gap, t=3min)

	T_{barrel}					TOTAL
	170°C		180°C			
	T_{mold}		T_{mold}			
Screw Speed	40°C	80°C	40°C	80°C		
150rpm	1.82	2.07	1.91	1.96	1.82	
	1.91	2.10	1.89	1.99	1.91	
	1.93	2.02	1.86	1.89	1.93	
	SUM= 5.66	SUM= 6.19	SUM= 5.66	SUM= 5.85		23.36
	SS= 10.69	SS= 12.77	SS= 10.68	SS= 11.41		
245rpm	1.81	2.01	1.71	2.07	1.81	
	2.04	1.84	1.71	2.16	2.04	
	1.93	1.79	1.77	1.84	1.93	
	SUM= 5.79	SUM= 5.64	SUM= 5.19	SUM= 6.08		22.70
	SS= 11.20	SS= 10.64	SS= 8.97	SS= 12.36		
TOTAL	11.45	11.83	10.84	11.93		46.05

Table B8: Analysis of variance for the modulus of elasticity of 3vol% xGnP-1/PP (Small gap, t=3min)

Effect/Factor	SS	df	MS	F
T_{barrel}	0.011	1	0.01	1.36
T_{mold}	0.089	1	0.09	11.20
Screw Speed	0.018	1	0.02	2.30
T_{barrel} x T_{mold}	0.021	1	0.02	2.58
T_{barrel} x Screw Speed	0.001	1	0.00	0.16
T_{mold} x Screw Speed	0.000	1	0.00	0.00
T_{barrel} x T_{mold} x Screw Speed	0.078	1	0.08	9.83
Error	0.127	16	0.01	1.00
Total	0.345	23		

Table B9: Excel Spreadsheet for the experimental lay out of the2^3 factorial design about the flexural strength of PP (Large gap, t=3min)

	A T_{barrel}				TOTAL
	180°C		200°C		
C	**B** T_{mold}		T_{mold}		
Screw Speed	40°C	80°C	40°C	80°C	
100rpm	36.31	39.61	33.78	42.04	
	37.66	40.01	34.02	42.23	
	37.87	39.77	34.74	40.93	
	SUM=111.85	SUM=119.39	SUM=102.53	SUM=125.21	458.98
	SS=4171.33	SS=4751.38	SS=3504.77	SS=5226.73	
245rpm	36.66	42.58	34.53	43.11	
	35.58	42.64	34.45	37.17	
	36.22	42.97	34.40	39.90	
	SUM=108.46	SUM=128.19	SUM=103.37	SUM=120.18	460.20
	SS=3921.88	SS=5477.42	SS=3562.01	SS=4831.72	
TOTAL	220.31	247.58	205.91	245.38	**919.17**

Table 10: Analysis of variance for PP's flexural strength (Large gap, t=3min)

Effect/Factor	SS	df	MS	F
T_{barrel}	11.476	1	11.476	8.609
T_{mold}	185.638	1	185.638	139.269
Screw Speed	0.062	1	0.062	0.047
T_{barrel} x T_{mold}	6.212	1	6.212	4.661
T_{barrel} x Screw Speed	3.844	1	3.844	2.883
T_{mold} x Screw Speed	1.658	1	1.658	1.244
T_{barrel} x T_{mold} x Screw Speed	13.586	1	13.586	10.193
Error	21.327	16	1.333	1
Total	243.804	23		

Table B11: Excel Spreadsheet for the experimental lay out of the2^3 factorial design about the flexural strength of 3vol% of xGnP-1/PP (large gap, t=3min)

	T_{barrel}				TOTAL
	180°C		200°C		
	T_{mold}		T_{mold}		
Scr Speed	40°C	80°C	40°C	80°C	
100rpm	47.28	49.01	44.55	47.39	
	47.55	47.79	43.75	48.36	
	48.12	46.68	44.08	48.60	
	SUM= 142.96 SS= 6812.50	SUM= 143.48 SS= 6864.90	SUM= 132.39 SS= 5842.37	SUM= 144.35 SS= 6946.34	563.17
245rpm	45.57	49.15	44.29	47.91	
	45.26	49.30	44.37	47.62	
	46.66	49.68	44.51	46.42	
	SUM= 137.50 SS= 6303.37	SUM= 148.13 SS= 7314.71	SUM= 133.16 SS= 5910.42	SUM= 141.94 SS= 6717.14	560.74
TOTAL	280.46	291.61	265.54	286.29	1123.91

Table B12: Analysis of variance for the flexural strength of 3vol% of xGnP-1/PP (large gap, t=3min)

Effect/Factor	SS	df	MS	F
T_{barrel}	17.063	1	17.063	40.391
T_{mold}	42.406	1	42.406	100.386
Screw Speed	0.247	1	0.247	0.584
T_{barrel} x T_{mold}	3.832	1	3.832	9.072
T_{barrel} x Screw Speed	0.029	1	0.029	0.069
T_{mold} x Screw Speed	2.001	1	2.001	4.736
T_{barrel} x T_{mold} x Screw Speed	7.355	1	7.355	17.411
Error	6.759	16	0.422	1
Total	79.691	23		

Table B13: Excel Spreadsheet for the experimental lay out of the2^3 factorial design about the modulus of elasticity of PP (large gap, t=3min)

	T_{barrel}				TOTAL
	180°C		200°C		
	T_{mold}		T_{mold}		
Screw Speed	40°C	80°C	40°C	80°C	
100rpm	1.06	1.36	1.04	1.28	
	1.19	1.32	1.07	1.29	
	1.22	1.35	1.09	1.26	
	SUM=3.47	SUM=4.02	SUM=3.20	SUM=3.83	14.52
	SS=4.02	SS=5.38	SS=3.41	SS=4.90	
245rpm	1.16	1.35	1.11	1.36	
	1.12	1.35	1.10	1.25	
	1.14	1.37	1.09	1.23	
	SUM=3.42	SUM=4.07	SUM=3.30	SUM=3.84	14.63
	SS=3.89	SS=5.52	SS=3.63	SS=4.93	
TOTAL	6.88	8.09	6.50	7.68	29.14

Table B14: Analysis of variance for the modulus of elasticity of PP (large gap, t=3min)

Effect/Factor	SS	df	MS	F
T_{barrel}	0.027	1	0.027	15.061
T_{mold}	0.237	1	0.237	133.421
Screw Speed	0.001	1	0.001	0.293
T_{barrel} x T_{mold}	0.000	1	0.000	0.015
T_{barrel} x Screw Speed	0.001	1	0.001	0.299
T_{mold} x Screw Speed	0.000	1	0.000	0.001
T_{barrel} x T_{mold} x Screw Speed	0.002	1	0.002	0.911
Error	0.028	16	0.002	1
Total	0.294	23		

Table B15: Excel Spreadsheet for the experimental lay out of the2^3 factorial design about the modulus of elasticity of 3vol% xGnP-1/PP (large gap, t=3min)

	T_{barrel}				TOTAL
	180°C		200°C		
Screw Speed	T_{mold}		T_{mold}		
	40°C	80°C	40°C	80°C	
100rpm	1.76	1.79	1.60	1.70	
	1.78	1.77	1.58	1.73	
	1.78	1.70	1.59	1.72	
	SUM= 5.33	SUM= 5.26	SUM= 4.77	SUM= 5.15	20.50
	SS= 9.45	SS= 9.22	SS= 7.59	SS= 8.84	
245rpm	1.64	1.81	1.57	1.79	
	1.71	1.85	1.63	1.76	
	1.73	1.80	1.61	1.67	
	SUM= 5.07	SUM= 5.46	SUM= 4.81	SUM= 5.22	20.56
	SS= 8.58	SS= 9.92	SS= 7.71	SS= 9.10	
TOTAL	10.40	10.71	9.58	10.37	41.07

Table B8: Analysis of variance for the modulus of elasticity of 3vol% xGnP-1 (large gap, t=3min)

Effect/Factor	SS	df	MS	F
T_{barrel}	0.056	1	0.056	43.134
T_{mold}	0.051	1	0.051	39.212
Screw Speed	0.000	1	0.000	0.122
T_{barrel} x T_{mold}	0.009	1	0.009	7.312
T_{barrel} x Screw Speed	0.001	1	0.001	0.896
T_{mold} x Screw Speed	0.010	1	0.010	7.678
T_{barrel} x T_{mold} x Screw Speed	0.007	1	0.007	5.523
Error	0.021	16	0.001	1
Total	0.155	23		

APPENDIX C

EFFECT OF PROCESSING TIME ON FLEXURAL PROPERTIES OF PP AND XGNP-1/PP NANOCOMPOSITES

The processing parameters that can be controlled by the operator during the extrusion-injection molding of EGF-PP nanocomposites are: (i) the temperature of the barrel, (ii) the temperature of the mold, (iii) the rotation screw speed, (iv) the mixing time and (iv) the gap distance between the screws and the bottom of the barrel.

In order to simplify the factorial design preliminary experiments were performed to explore the effect of processing time on the flexural properties of PP and EGF-PP nanocomposites. The samples were made using the large gap distance between the screws and the barrel and mold temperature of T_{mold}=80°C. The values of the other three processing conditions used are given in Table C1.

TableC1: Values of processing conditions used in fabrication of PP and 3vol% xGnP-1/PP Nanocomposites (LG and T_{mold}=80°C)

FACTORS	LEVELS	
	Low Value	High Value
Temperature of the barrel (°C)	180	200
Screw Speed (rpm)	100	245
Mixing time (min)	3	6

The flexural strength of PP and 3vol% xGnP-1/PP nanocomposites is shown in Figures C1 and C2 respectively. The effect of time on the modulus of elasticity of the neat PP and the 3vol% xGnP-1/PP nanocomposites is shown in Figures C5 and C6. In all four cases increasing the processing time from 3 to 6min does not affect the strength or the modulus since any observed variation is within the experimental error.

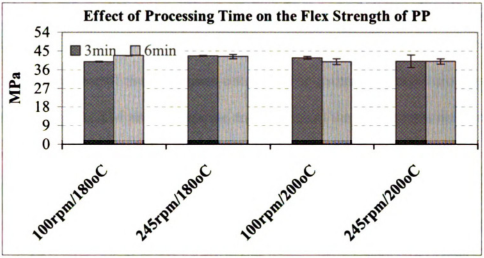

Figure C1: Flexural Strength of Polypropylene at various processing conditions for LG screw configuration and T_{mold}=80°C

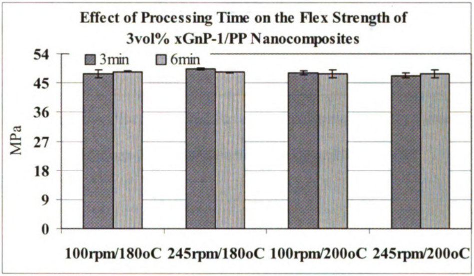

Figure C2: Flexural Strength of 3vol% xGnP-1/PP nanocomposites at various processing conditions for LG screw configuration and T_{mold}=80°C

An alternative way to plot the flex strength data in order to easily find if there is any effect of processing time is shown in Figures C3 and C4. The y-axis is expanded in order to highlight any differences. There are four lines in each figure, the slope of each line represents the change in flex strength by increasing the processing time from 3 to 6min keeping the rest of the conditions constant. The magnitude of the slope indicates how strong is the effect of processing time and the sign of the slope shows the trend i.e., a negative slope means that the strength drops as the processing time increases.

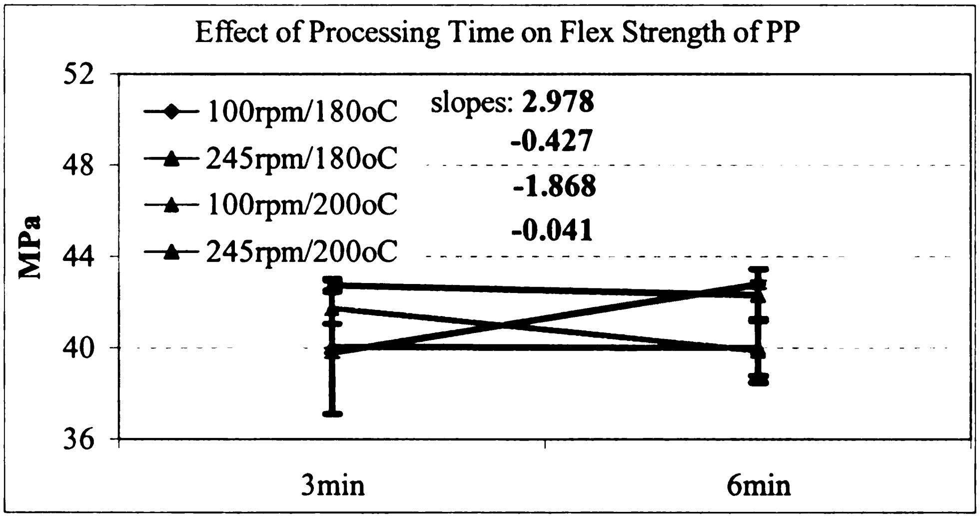

Figure C3: Alternative Plot of Flexural Strength of Polypropylene at various processing conditions for LG screw configuration and T_{mold}=80°C

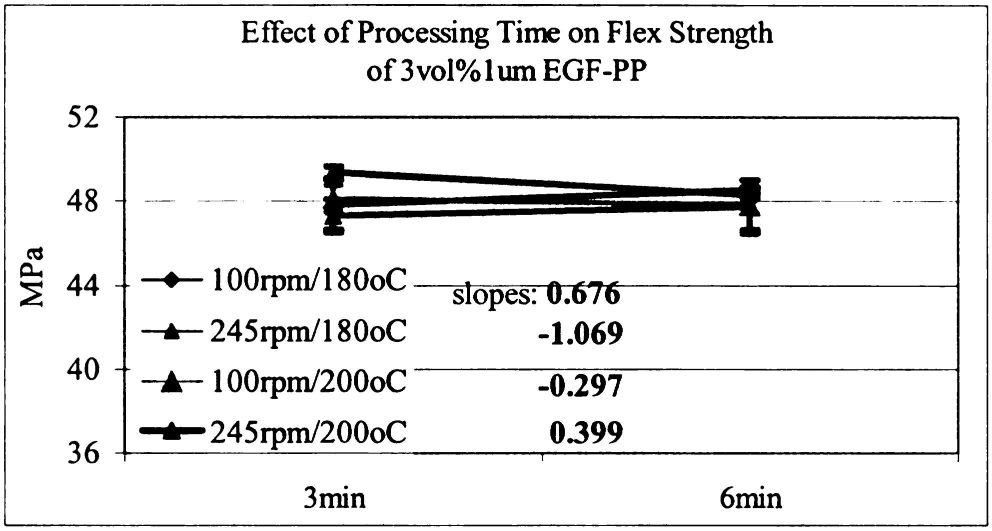

Figure C4: Flexural Strength of 3vol% xGnP-1/PP nanocomposites at various processing conditions for LG screw configuration and T_{mold}=80°C

Finally, the processing time has no effect of the modulus of elasticity of both the neat PP and the 3vol% xGnP-1/PP nanocomposites as shown in Figures C5 and C6 respectively. Only the alternative plots using the slopes are given.

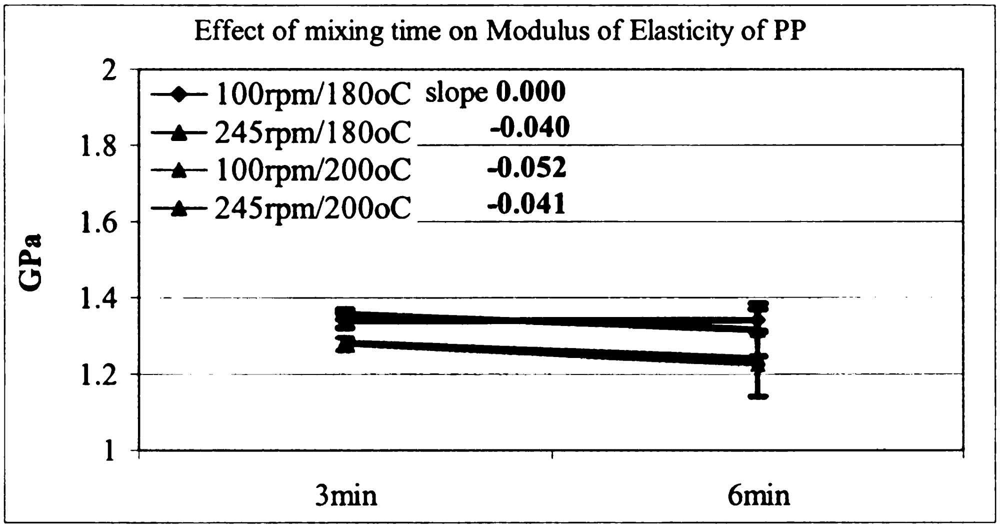

Figure C5: Modulus of Elasticity of PP at various processing conditions for LG screw configuration and T_{mold}=80°C

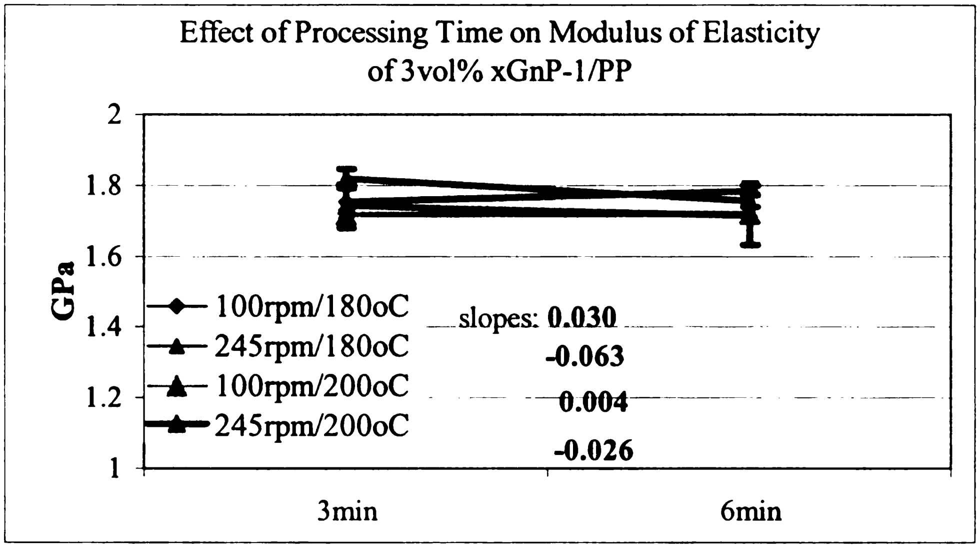

Figure C6: Modulus of Elasticity of 3vol% xGnP-1/PP nanocomposites at various processing conditions for LG screw configuration and T_{mold}=80°C

APPENDIX D

VISCOELASTIC PROPERTIES OF CARBON REINFORCED PP COMPOSITES

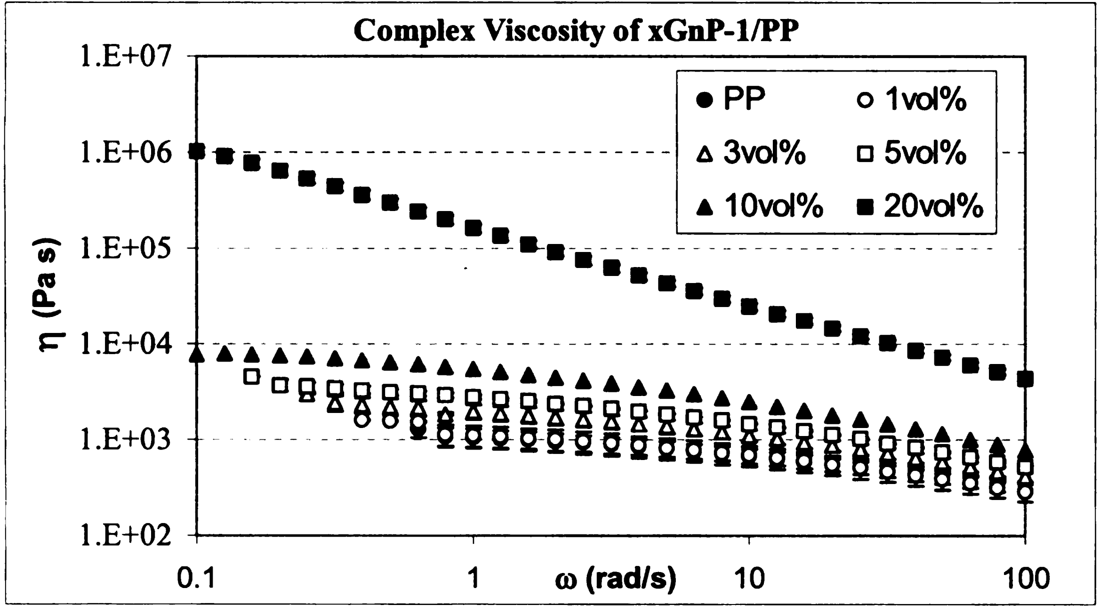

Figure D1: Complex Viscosity of xGnP-1/PP at 1% strain and T=175°C

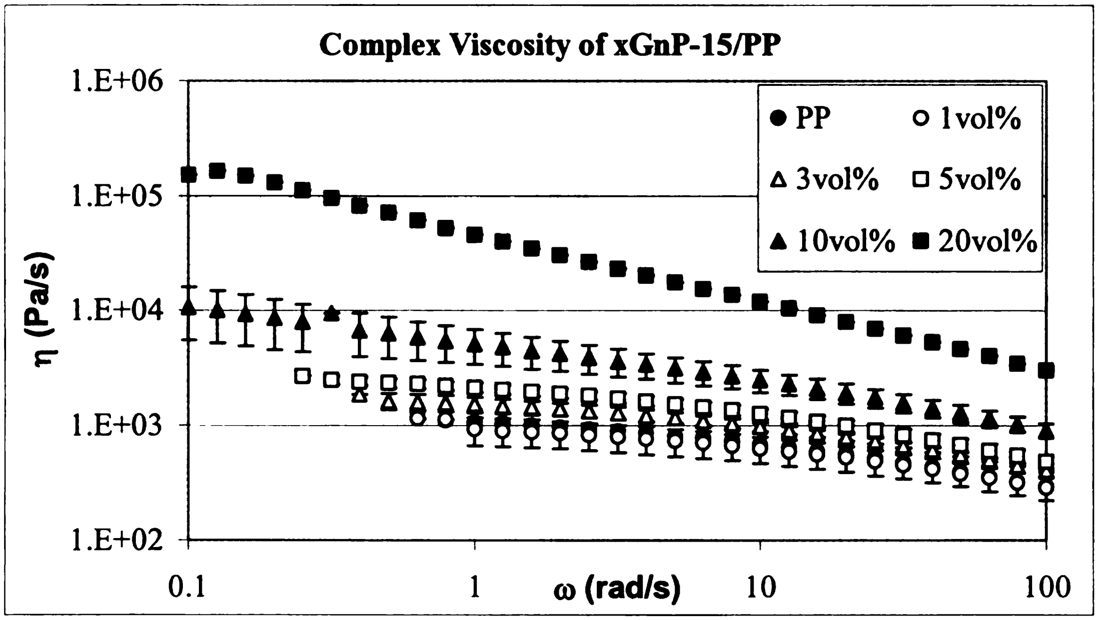

Figure D2: Complex Viscosity of xGnP-15/PP at 1% strain and T=175°C

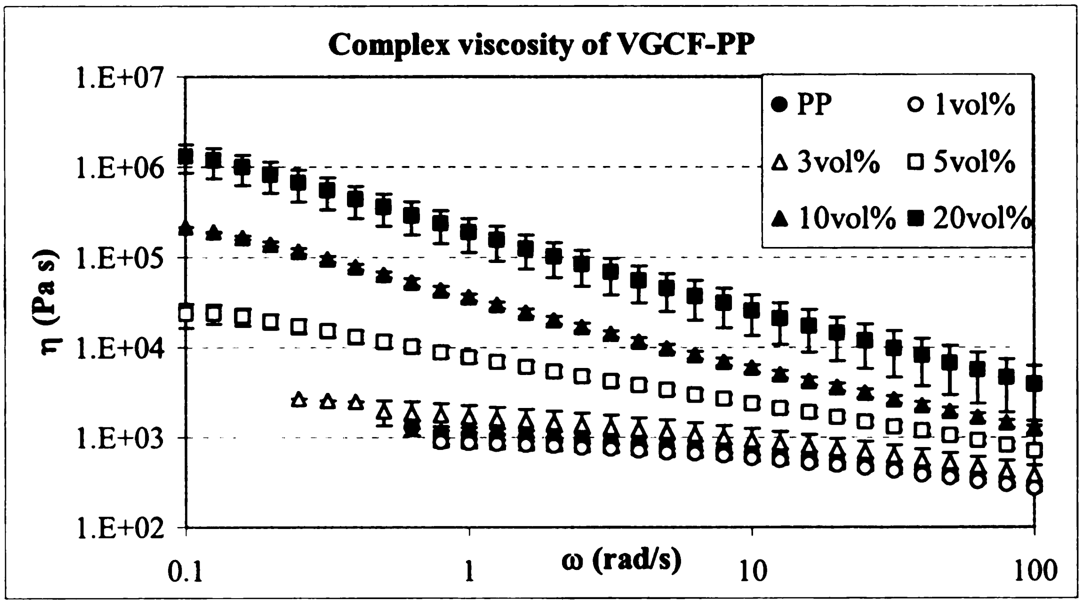

Figure D3: Complex Viscosity of VGCF/PP at 1% strain and T=175°C

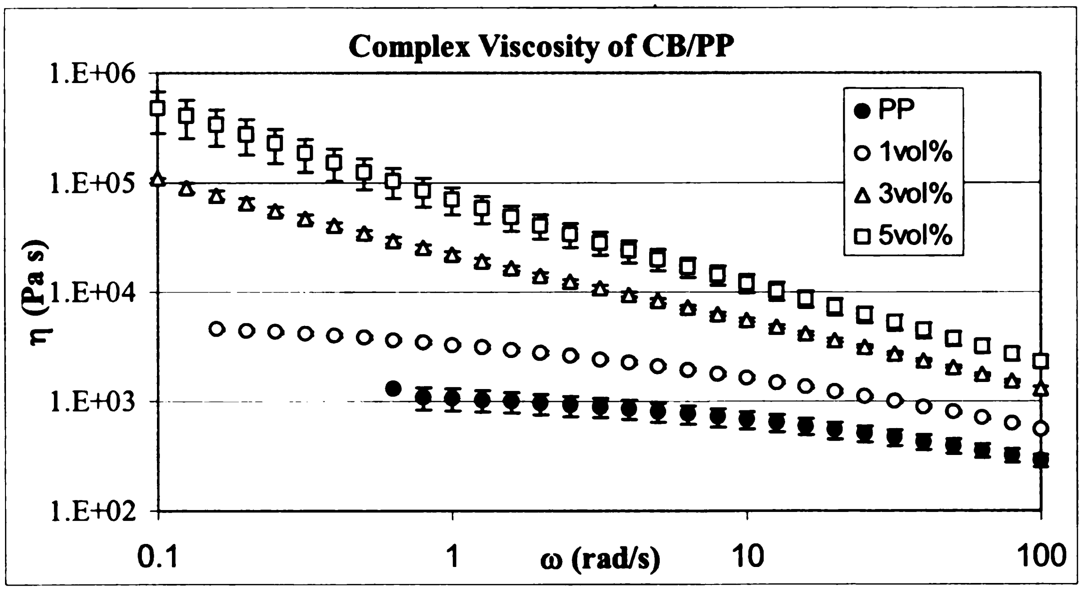

Figure D4: Complex Viscosity of CB/PP at 1% strain and T=175°C

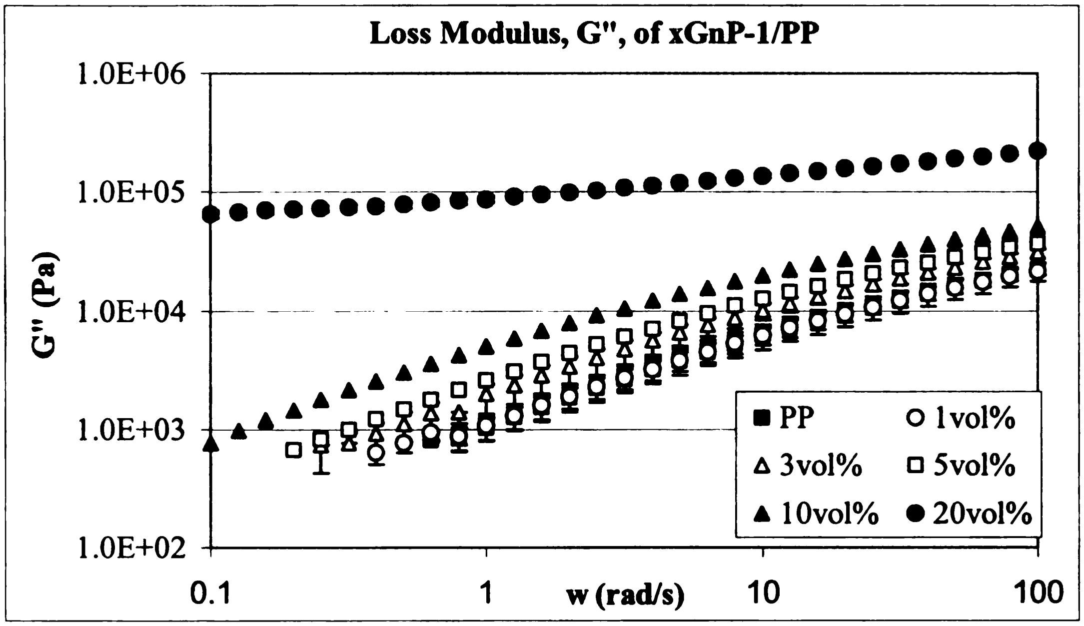

Figure D5: Loss Modulus of xGnP-1/PP at 1% strain and T=175°C

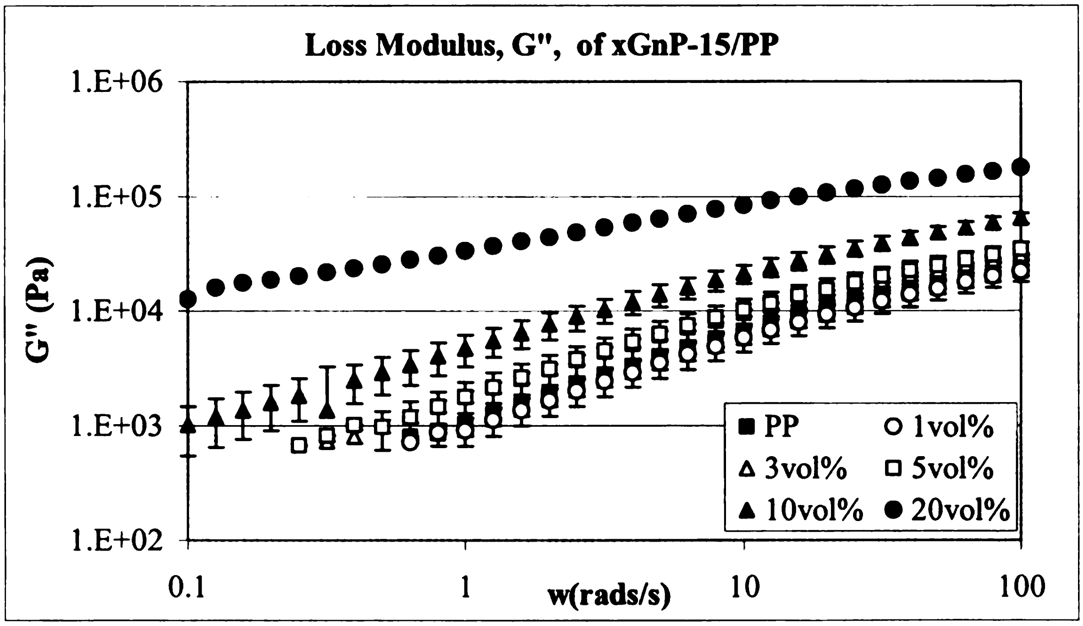

Figure D6: Loss Modulus of xGnP-15/PP at 1% strain and T=175°C

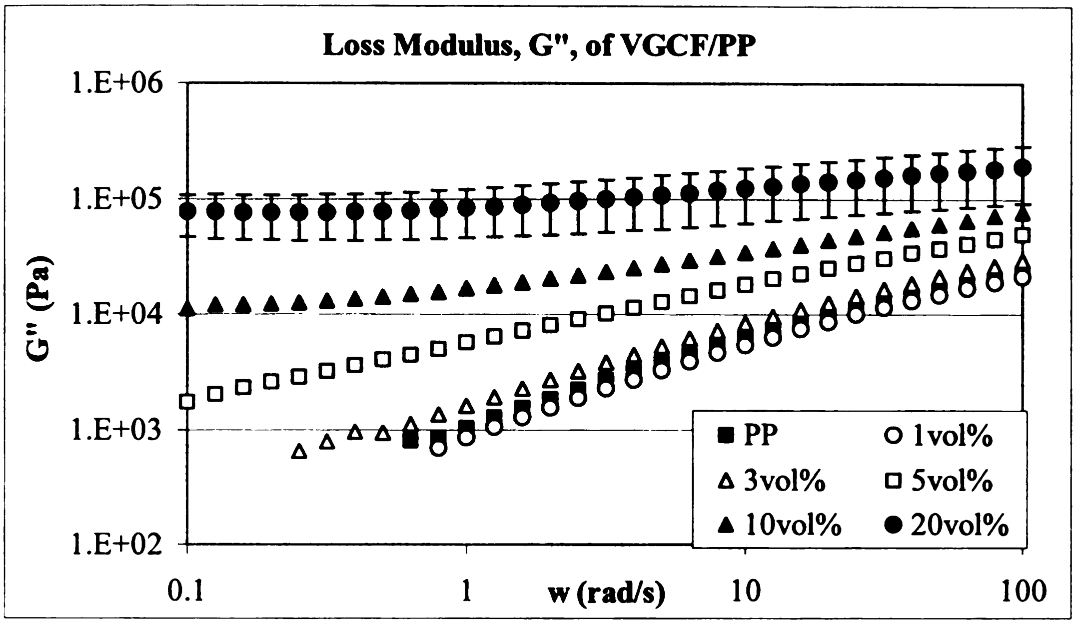

Figure D7: Loss Modulus of VGCF/PP at 1% strain and T=175°C

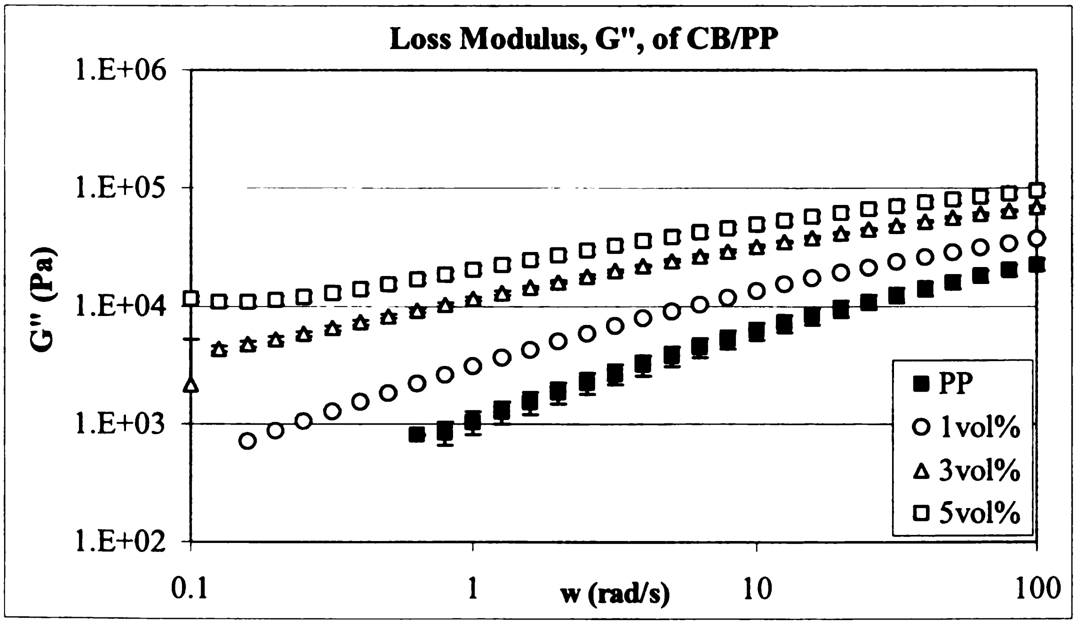

Figure D8: Loss Modulus of CB/PP at 1% strain and T=175°C

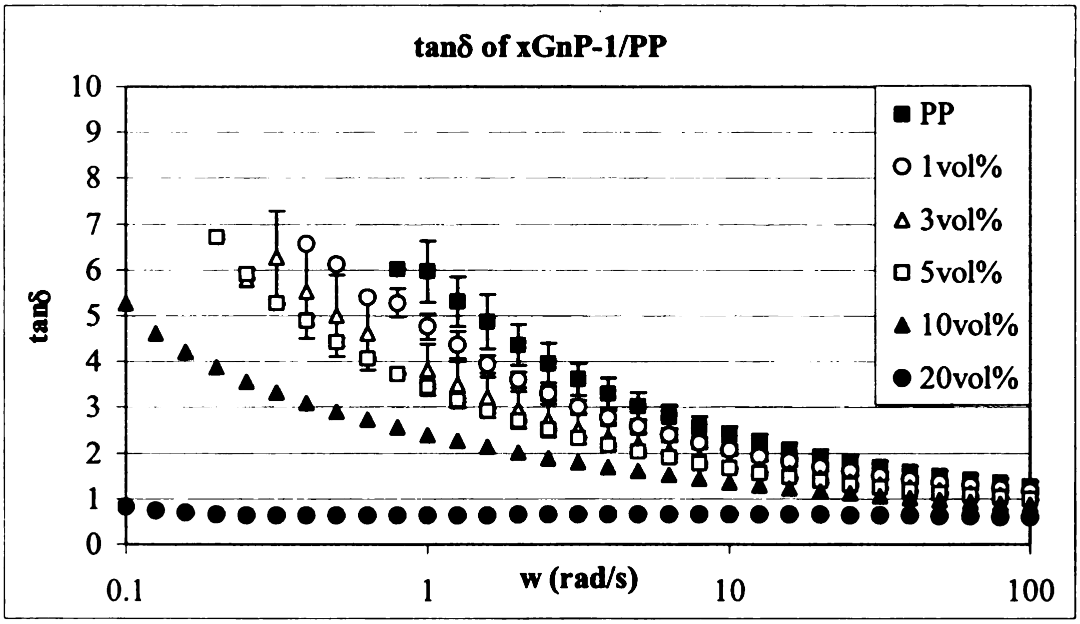

Figure D9: tanδ of xGnP-1/PP at 1% strain and T=175°C

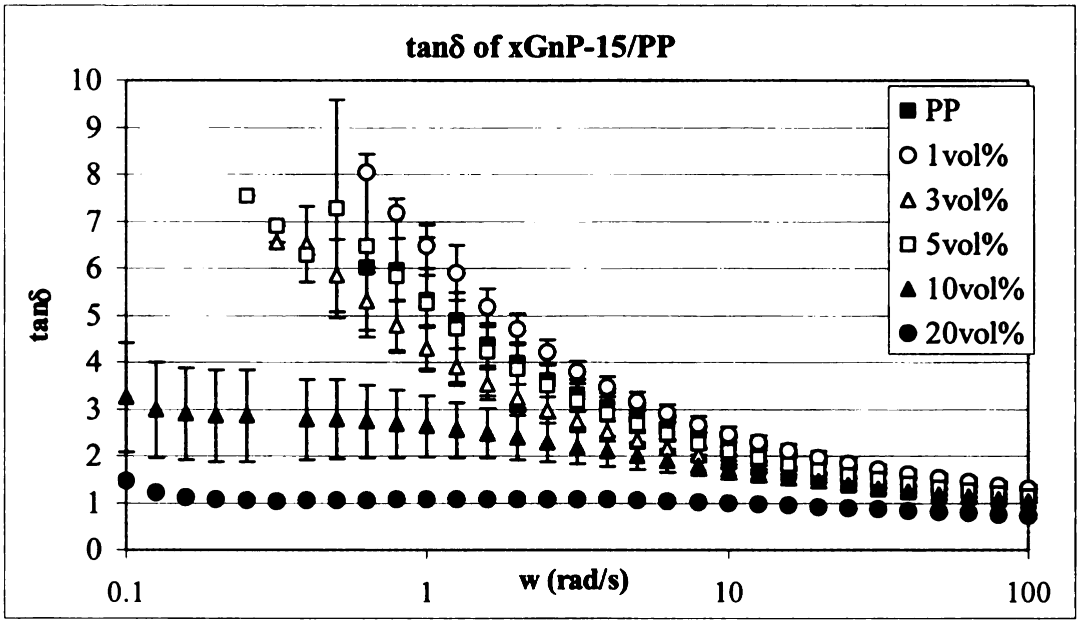

Figure D10: tanδ of xGnP-15/PP at 1% strain and T=175°C

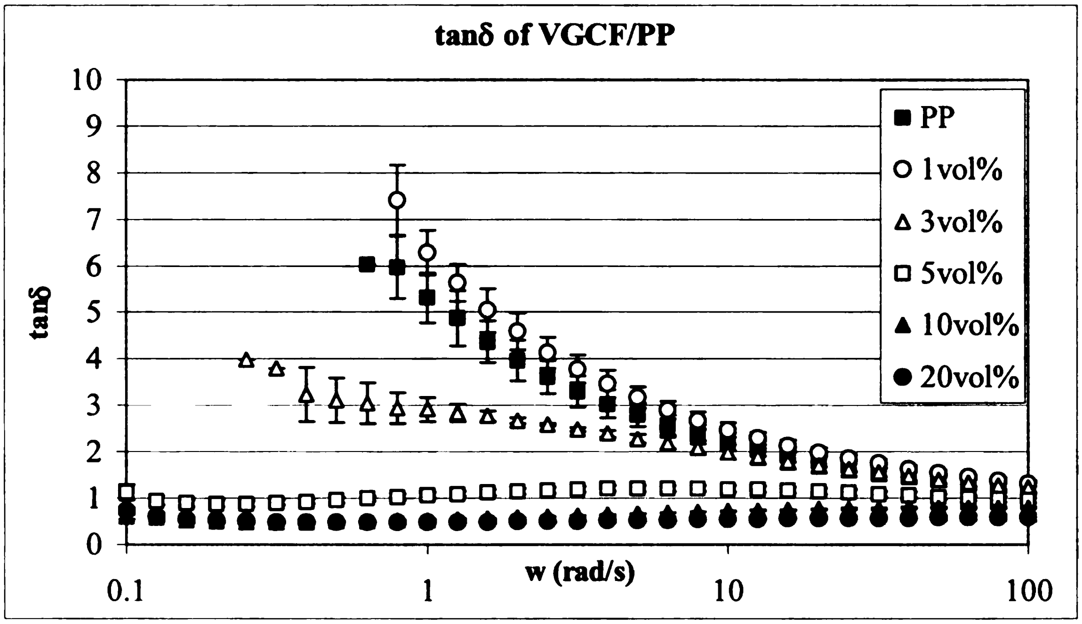

Figure D11: tanδ of VGCF/PP at 1% strain and T=175°C

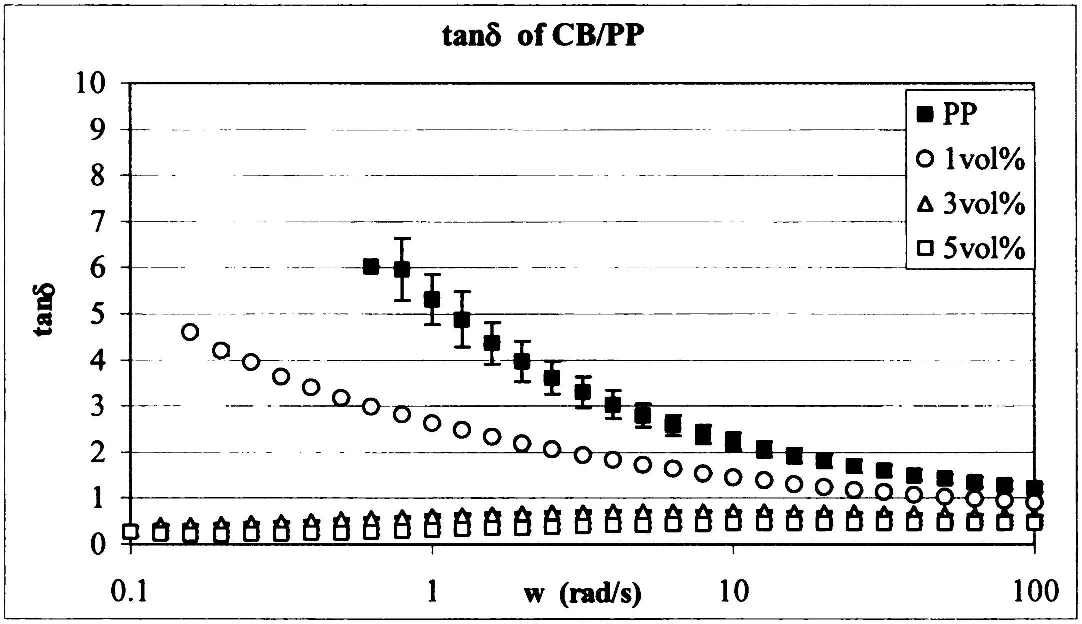

Figure D12: tanδ of CB/PP at 1% strain and T=175°C

APPENDIX E

EFFECT OF COOLING RATE ON THE XRD PATTERN OF PP NANOCOMPOSITES

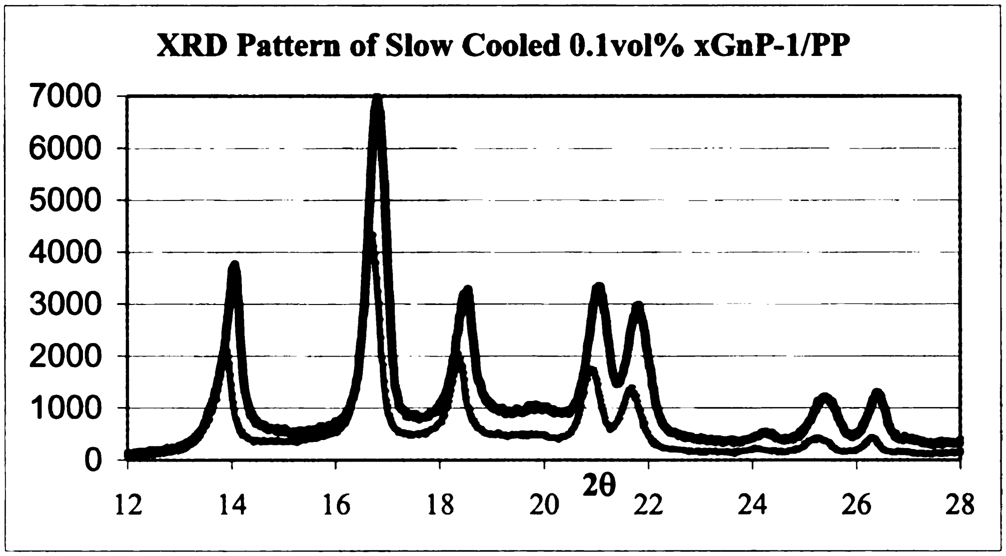

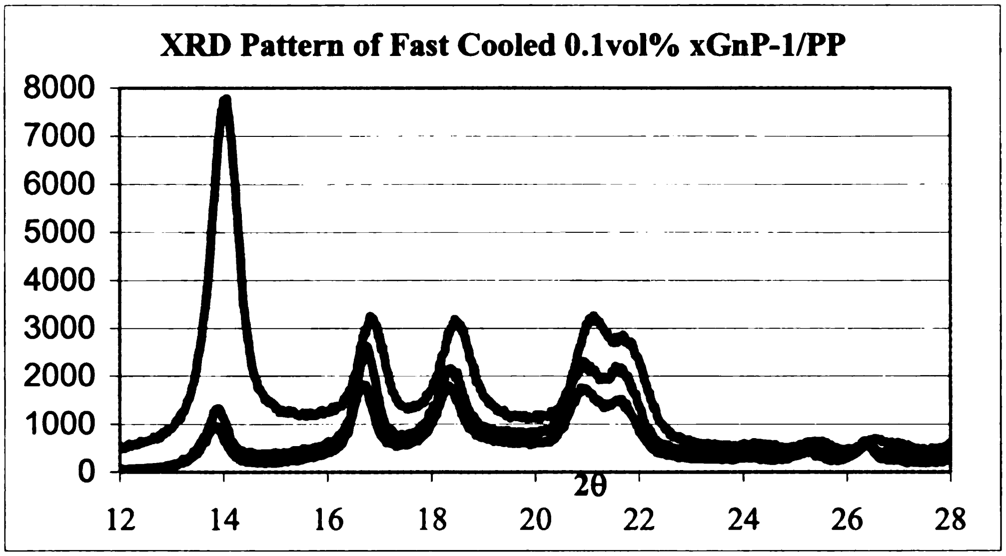

Figure E1: XRD patterns of slow and fast cooled 0.1 vol% xGnP-1/PP, made by premixing and compression molding

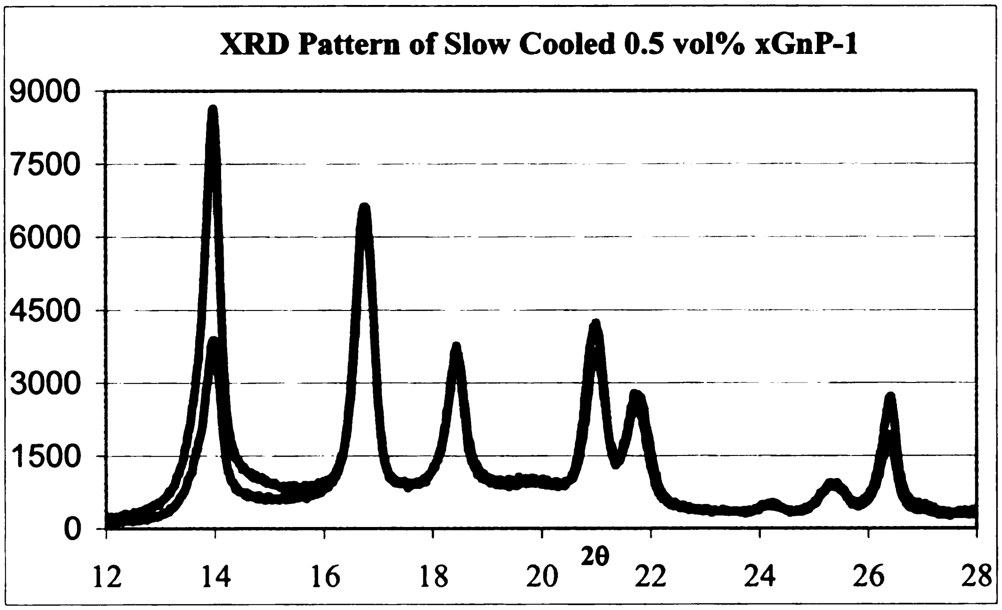

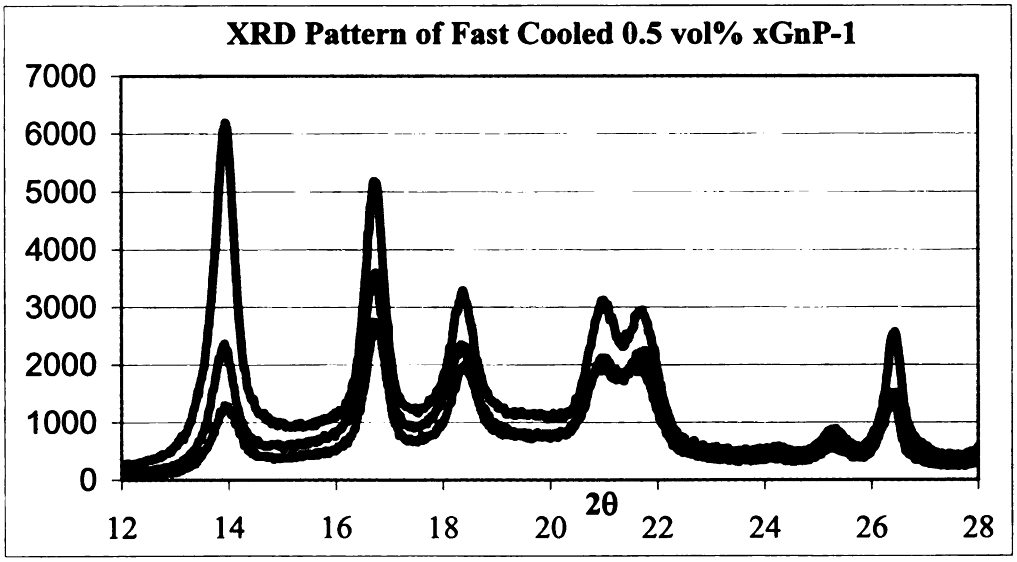

Figure E2: XRD patterns of slow and fast cooled 0.5 vol% xGnP-1/PP, made by premixing and compression molding

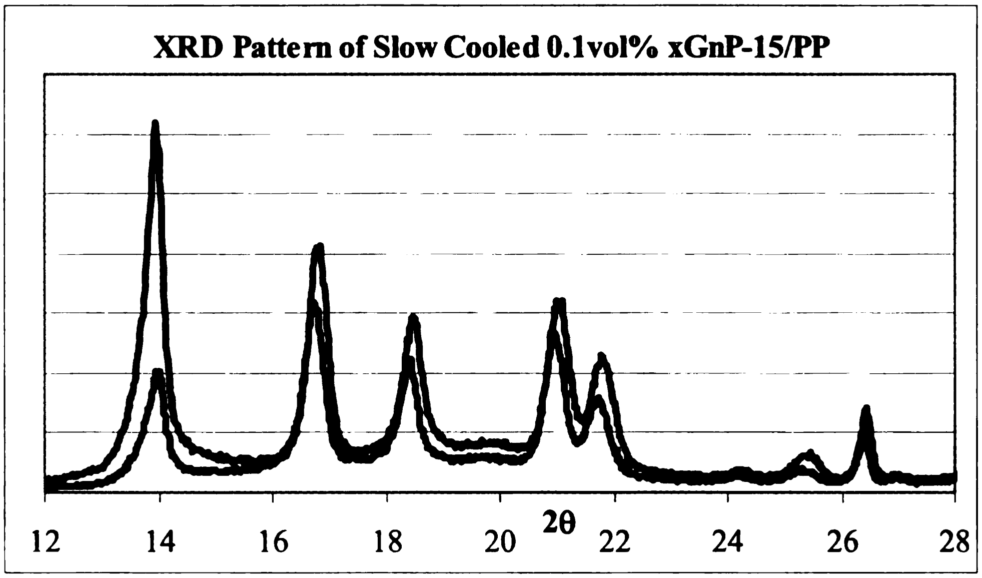

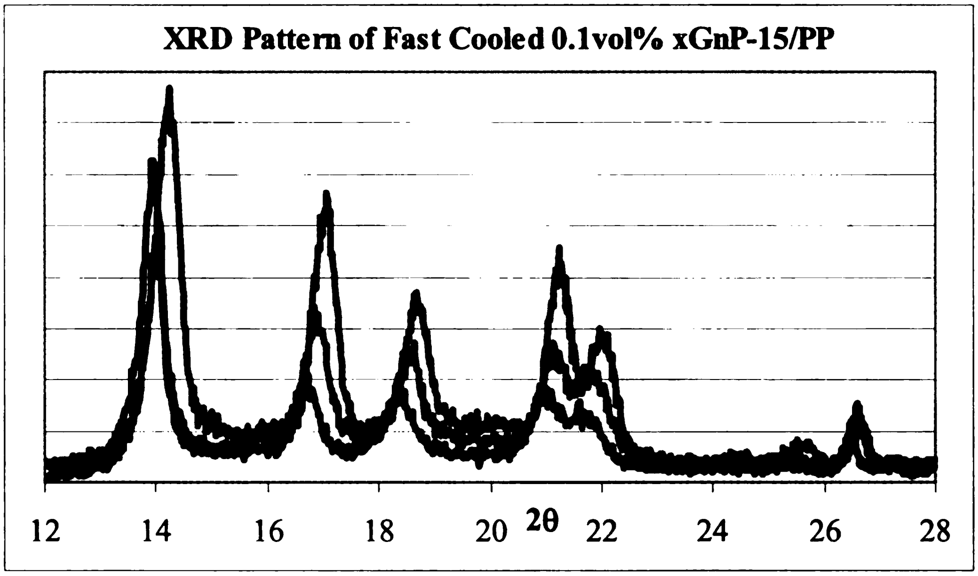

Figure E3: XRD patterns of slow and fast cooled 0.1 vol% xGnP-15/PP, made by premixing and compression molding

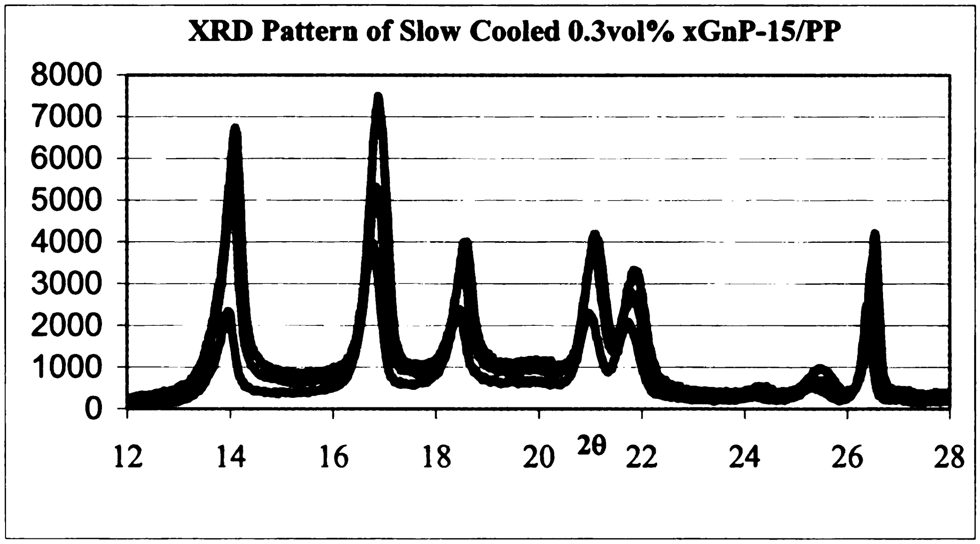

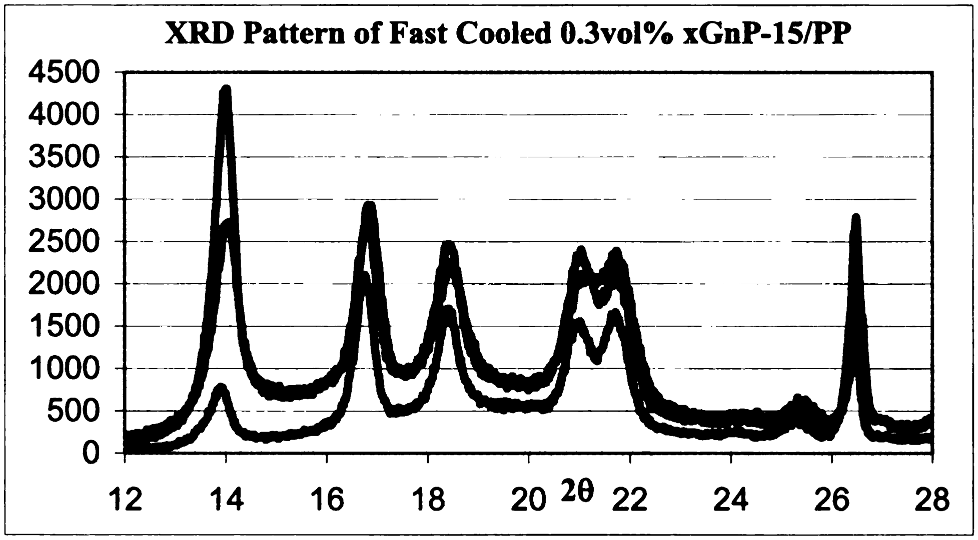

Figure E4: XRD patterns of slow and fast cooled 0.3 vol% xGnP-15/PP, made by premixing and compression molding

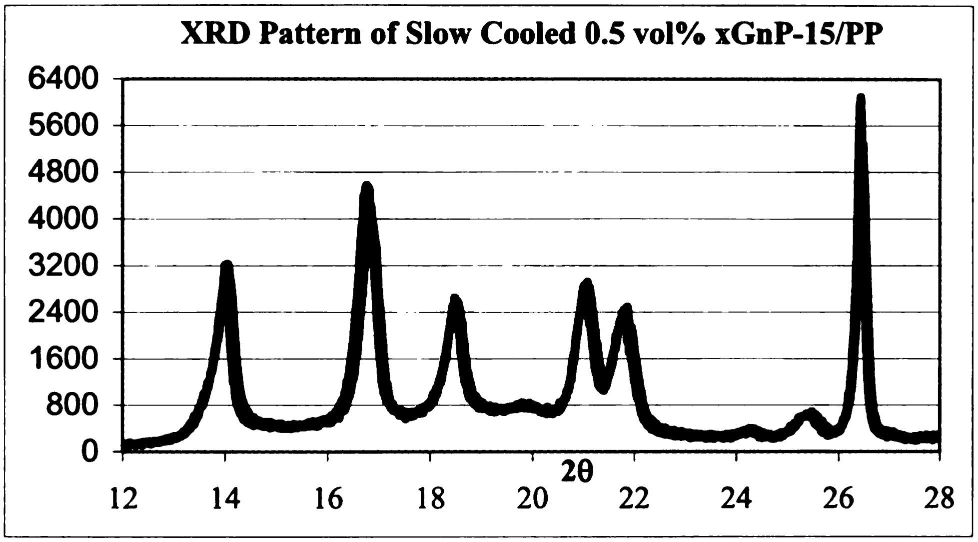

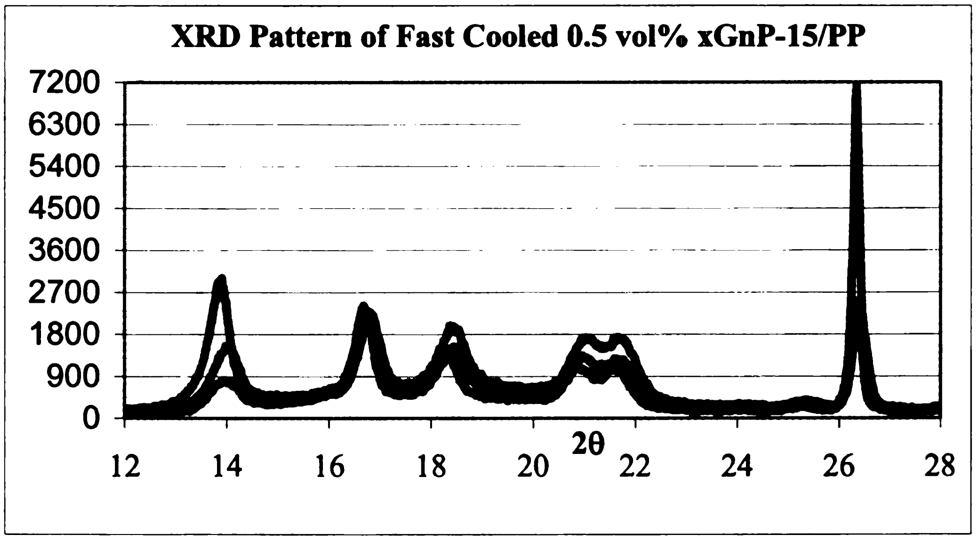

Figure E5: XRD patterns of slow and fast cooled 0.5 vol% xGnP-15/PP, made by premixing and compression molding

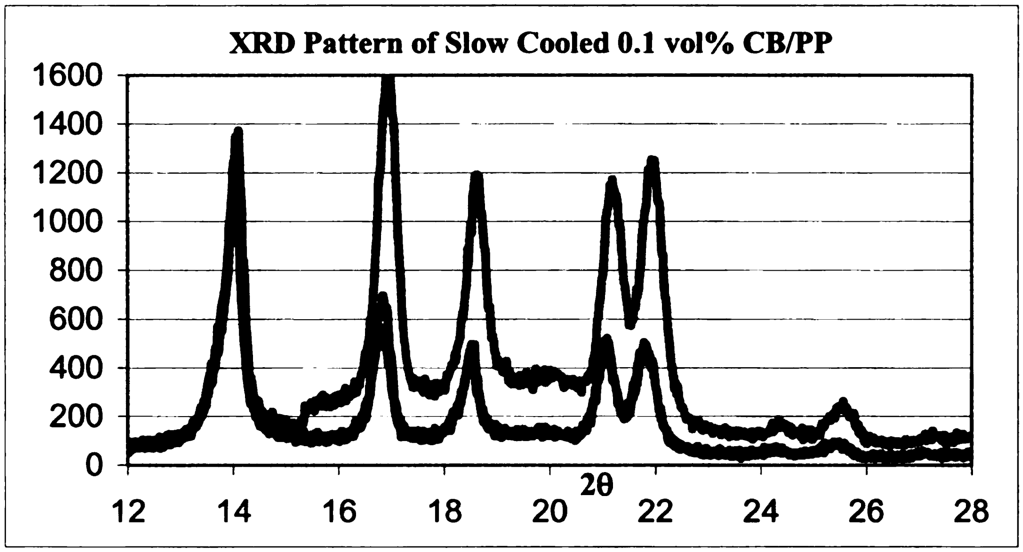

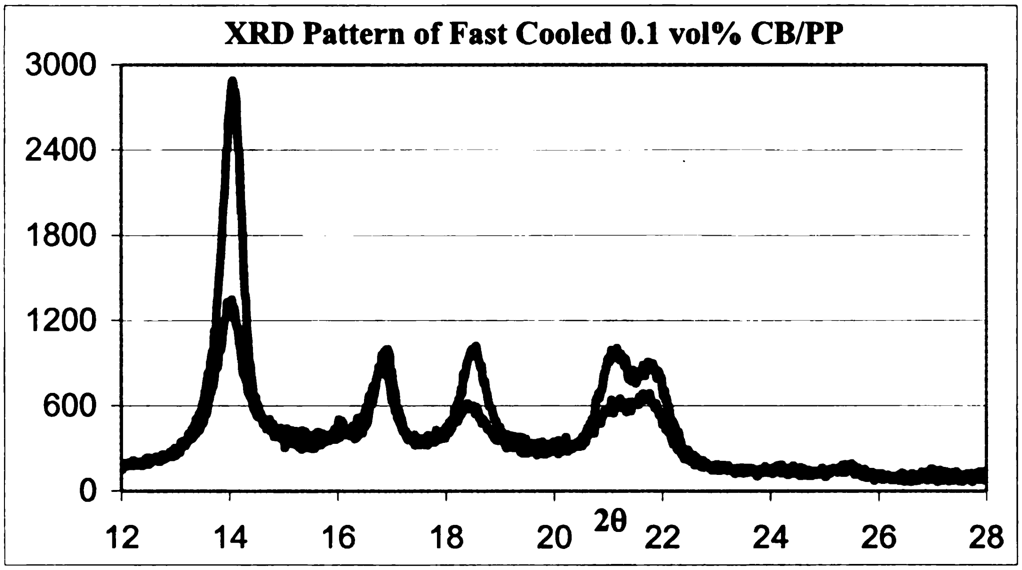

Figure E6: XRD patterns of slow and fast cooled 0.1 vol% CB/PP, made by premixing and compression molding

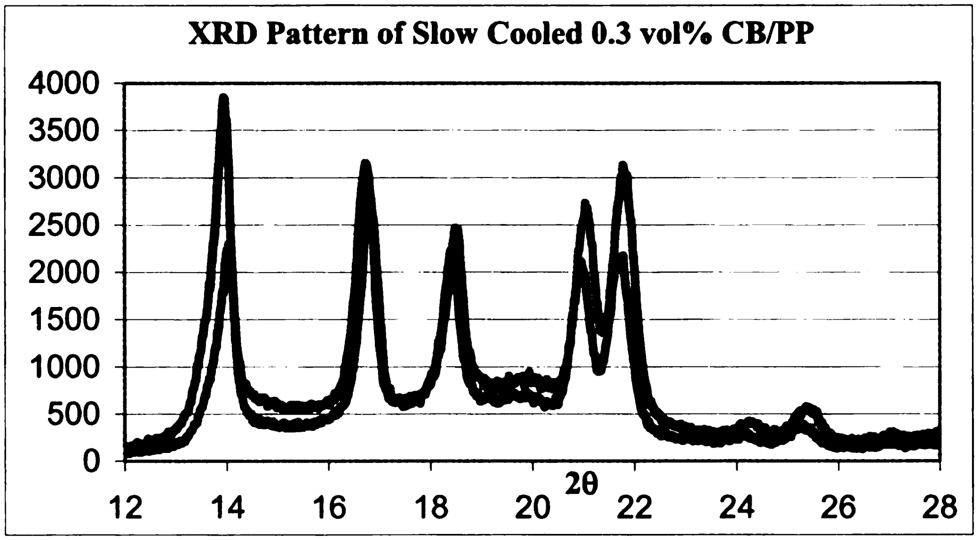

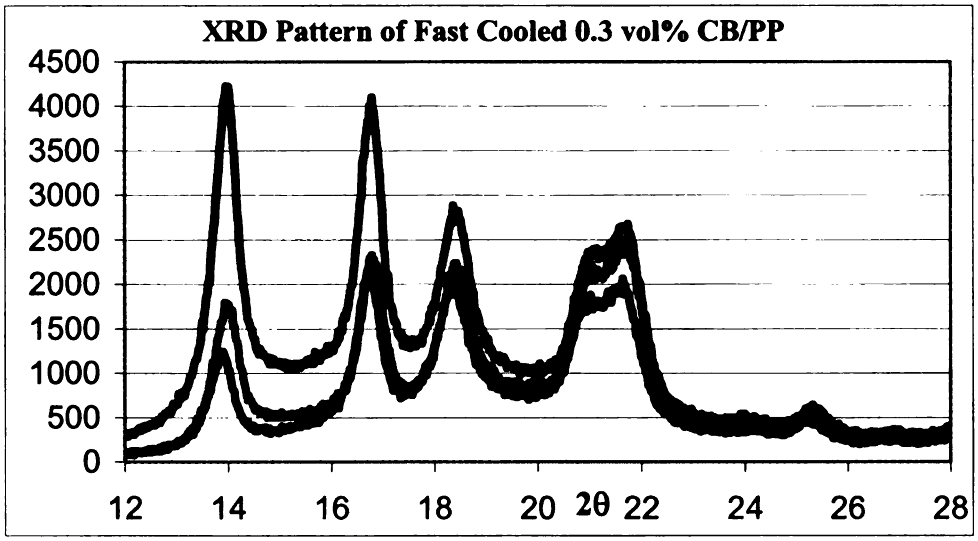

Figure E7: XRD patterns of slow and fast cooled 0.3 vol% CB/PP, made by premixing and compression molding

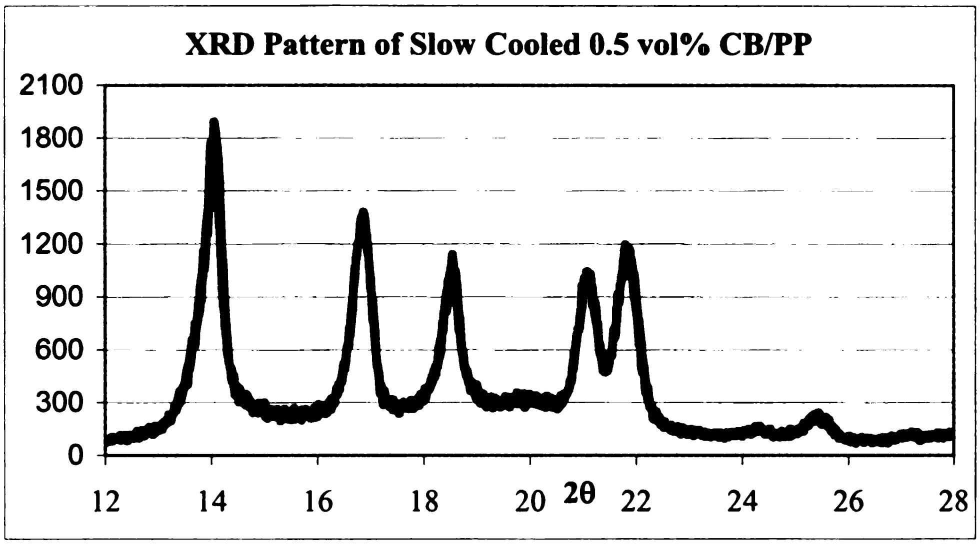

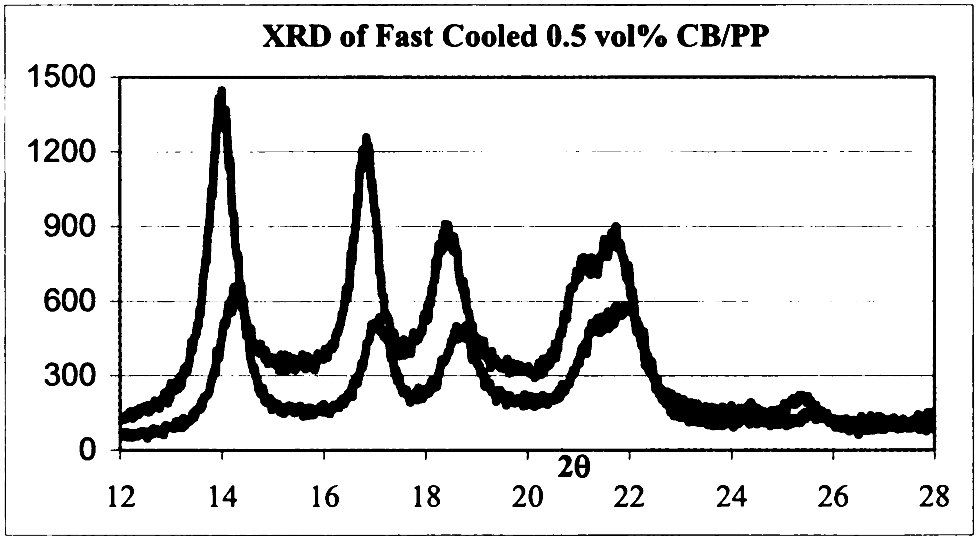

Figure E8: XRD patterns of slow and fast cooled 0.5 vol% CB/PP, made by premixing and compression molding

MICHIGAN STATE UNIVERSITY LIBRARIES
3 1293 02845 4787